UNIVERSITY OF CALIFORNIA,
IRVINE

Elucidating the Structures of Oligomers Formed by Macrocyclic β-Hairpin Mimics: Insights into Alzheimer's Disease

DISSERTATION

submitted in partial satisfaction of the requirements
for the degree of

DOCTOR OF PHILOSOPHY

in Chemistry

by

Adam G. Kreutzer

Dissertation Committee:
Professor James S. Nowick, Chair
Professor Jennifer A. Prescher
Professor Gregory A. Weiss

2017

DEDICATION

To my parents. Thank you for your unconditional love and support.

TABLE OF CONTENTS

LIST OF FIGURES

LIST OF TABLES

LIST OF CHARTS

LIST OF SCHEMES

ACKNOWLEDGMENTS

Thank you, James. Your invaluable mentorship has made me the scientist, writer, and friend that I am today. You are the epitome of the mentor I one day hope to become. You made me excited about doing science every day. Your empathy toward others is something I will strive to match throughout the remainder of my career and life.

Thank you, Labmates. You made coming to lab everyday fun. I want to especially thank Ryan Spencer for providing guidance through my first two years, Stan Yoo for helping me so much with synthesizing trimers and other peptides and setting up crystal trays, and my undergraduate Imane Hamza for sticking with me all of these years and helping on every project I worked on without hesitation.

Thank you, Mom and Dad. Your love, encouragement, and support have played an immeasurable role in getting me to this point.

CURRICULUM VITAE

ADAM G. KREUTZER

Department of Chemistry
1102 Natural Sciences 2
University of California Irvine
Irvine, CA 92697-2025

Tel: (801) 860-0811
Email: akreutze@uci.edu

EDUCATION

Ph.D., Chemistry, **University of California Irvine** 2012–2017
M.S., Oncological Sciences, **University of Utah**, 2006–2008
B.S., Biology (Chemistry minor), **University of Utah**, 2002–2006

RESEARCH EXPERIENCE

2012–2017 Graduate Student Researcher with Professor and Department Chair James Nowick. *University of California, Irvine*.
2008–2012 Laboratory Technician with Professor Anne Moon. *University of Utah*.
2006–2008 Graduate Student Researcher with Professor Susan Mango. *University of Utah*.
2004–2006 Undergraduate Researcher with Professor Elizabeth Leibold. *University of Utah*.
2003–2004 Undergraduate Researcher with Professor Raymond Gesteland. *University of Utah*.

AWARDS

2016 Regents Dissertation Fellowship. *University of California, Irvine*
2005 Undergraduate Research Opportunities Program Research Support ($1050). *University of Utah*.
2005 Certificate of Achievement for Excellence in Undergraduate Research. *University of Utah*.

PROFESSIONAL MEMBERSHIPS

2015– American Chemical Society

POSTERS AND TALKS

2017 Speaker at the 2017 National ACS Meeting, San Francisco, CA. *Stabilization, Assembly, and Toxicity of Trimers Derived from Aβ.* (paper number: ORGN 690).
2017 Poster presenter at the 2017 National ACS Meeting, San Francisco, CA. *X-ray crystallographic structures of a trimer, dodecamer, and annular pore formed by an $A\beta_{17–36}$ β-hairpin.* (paper number: ORGN 606).
2016 Poster presenter at the 2016 ISACS19: Challenges in Organic Chemistry meeting, Irvine, CA. *X-ray crystallographic structures of a trimer, dodecamer, and annular pore formed by an $A\beta_{17–36}$ β-hairpin* (poster number: P44).

2015 Speaker at the Postdoc and Graduate Student Colloquium, Irvine, CA. *Studying amyloid diseases using chemical model systems.*

2015 Speaker at the 2015 National ACS Meeting, Boston, MA. *X-ray crystallographic structures of amyloid oligomers: A dodecamer of $A\beta_{17–36}$ that forms an annular pore* (paper number: ORGN 73).

2015 Speaker at the 2015 National ACS Meeting, Boston, MA. *X-ray crystallographic structures of amyloid oligomers: A toxic crosslinked trimer of β-hairpins derived from $A\beta_{17-36}$* (paper number: ORGN74).

2015 Speaker at the 2015 AGS Symposium, Irvine, CA. *Using chemical model systems to gain atomic resolution insights into the structures of the Alzheimer's related peptide amyloid beta.*

2005 Speaker at the Undergraduate Research Symposium, Salt Lake City, UT. *The Nature of Disrupted Open Reading Frames in the S. oneidensis genome.*

PATENTS

1. "Synthetic Beta-Amyloid Peptides Capable of Stabilized, Cross-Linked Oligomerization", Nowick, J. S.; **Kreutzer, A. G.**; Spencer, R. K.; Salveson, P. J. Provisional Patent Application 62/414,326 filed October 28, 2016.

PUBLICATIONS

8. **Kreutzer, A. G.**; Spencer, R. K.; McKnelly, K. J.; Yoo, S.; Hamza, I. H.; Salveson, P.J.; Nowick, J. S. A Hexamer of a Peptide Derived from $A\beta_{16–36}$. *Biochemistry* **2017**, doi: 10.1021/acs.biochem.7b00831.

7. Suire, C.; Nainar, S.; Fazio, M.; **Kreutzer, A.**; Topper, C. L.; Thompson, C. R.; Leissring, M. A. Peptidic Inhibitors of Insulin-Degrading Enzyme Suitable for Dermatological Applications Discovered via Phage Display. Submitted to *J. Biol. Chem.*

6. Wang, Y.; **Kreutzer, A. G.**; Truex, N. L.; Nowick, J. S. A Tetramer Derived from Islet Amyloid Polypeptide. *J. Org. Chem.* **2017**, *82*, 7905–7912.

5. **Kreutzer, A. G.**;‡ Salveson, P. J.;‡ Spencer, R. K.;‡ Nowick, J. S. X-ray Crystallographic Structure of a Compact Dodecamer from a Peptide Derived from $A\beta_{16–36}$. *Org. Lett.* **2017**, *19*, 3462–3465. ‡These authors contributed equally to this work.

4. **Kreutzer, A. G.**; Yoo, S.; Spencer, R. K.; Nowick, J. S. Stabilization, Assembly, and Toxicity of Trimers Derived from Aβ. *J. Am. Chem. Soc.* **2017**, *139*, 966–975.

3. Yoo, S.; **Kreutzer, A. G.**; Truex, N. L.; Nowick, J. S. Square Channels Formed by a Peptide Derived from Transthyretin. *Chem. Sci.* **2016**, *7*, 6946–6951.

2. **Kreutzer, A. G.**, Hamza, I. H.; Spencer, R. K.; Nowick J. S. X-ray Crystallographic Structures of a Trimer, Dodecamer, and Annular Pore Formed by an $A\beta_{17–36}$ β-Hairpin. *J. Am. Chem. Soc.* **2016**, *138*, 4634–4642.

1. Spencer, R. K.; **Kreutzer, A. G**.; Salveson, P. J.; Li, H.; Nowick, J. S. X-ray Crystallographic Structures of Oligomers of Peptides Derived from β_2-Microglobulin. *J. Am. Chem. Soc.* **2015**, *137*, 6304–6311.

ABSTRACT OF THE DISSERTATION

Elucidating the Structures of Oligomers Formed by Macrocyclic β-Hairpin Mimics: Insights into Alzheimer's Disease

By

Adam G. Kreutzer

Doctor of Philosophy in Chemistry

University of California, Irvine

2017

Professor James S. Nowick, Chair

Chapter 1 provides an overview of the field of amyloid structural biology and provides context for the work described in this dissertation. In the more than a century since its identification, Alzheimer's disease has become the archetype of amyloid diseases. The first glimpses of the chemical basis of Alzheimer's disease began with the identification of "amyloid" plaques in the brain in 1892 and extended to the identification of proteinaceous fibrils with "cross-β" structure in 1968. Further efforts led to the discovery of the β-amyloid peptide Aβ as a 40- or 42-amino acid peptide that is responsible for the plaques and fibrils. At this point, a three-decade long marathon began to elucidate the structure of the fibrils and identify the molecular basis of Alzheimer's disease. Along the way, an alternative model began to emerge in which small aggregates of Aβ, called "oligomers", rather than fibrils, are the culprits that lead to neurodegeneration in Alzheimer's disease. This dissertation describes my efforts to understand the structural, biophysical, and biological properties of the oligomers in Alzheimer's disease.

β-Sheets are the building blocks of amyloid fibrils and oligomers. Amyloid fibrils generally consist of extended networks of parallel β-sheets. Amyloid oligomers appear to be more compact enclosed structures, some of which are thought to be composed of antiparallel β-sheets comprising β-hairpins. β-Hairpins are special because their twisted shape, hydrophobic surfaces, and exposed hydrogen-bonding edges impart a unique propensity to form compact assemblies. Our laboratory has developed macrocyclic β-sheets that are designed to mimic β-hairpins formed by amyloidogenic peptides and proteins. The β-hairpin mimics contain two β-strand peptide fragments linked together at their *N*- and *C*-termini by two δ-linked ornithine turn mimics to create a macrocycle. An *N*-methyl group is installed on one of the β-strands to prevent uncontrolled aggregation. These design features facilitate crystallization of the β-hairpin mimics and determination of the X-ray crystallographic structures of the oligomers that they form.

During the past few years, our laboratory has elucidated the X-ray crystallographic structures of oligomers formed by β-hairpin mimics derived from Aβ, α-synuclein, and β_2-microglobulin. Out of these three amyloidogenic peptides and proteins, the Aβ β-hairpin mimics have provided the most insight into amyloid oligomers. Our studies have revealed a previously undiscovered mode of self-assembly, whereby three Aβ β-hairpin mimics assemble to form a triangular trimer. The triangular trimers are remarkable, because they contain two largely hydrophobic surfaces that pack together with other triangular trimers to form higher-order oligomers, such as hexamers and dodecamers. Some of the dodecamers pack in the crystal lattice to form annular porelike assemblies. Some of the β-hairpin mimics and triangular trimers assemble in solution to form oligomers that recapitulate the crystallographically observed oligomers. These oligomers exhibit toxicity toward neuronally derived cells, recapitulating the toxicity of the oligomers formed by full-length amyloidogenic peptides and proteins. These

findings are significant, because they address a gap in understanding the molecular basis of amyloid diseases. We anticipate that these studies will pave the way for developing diagnostics and therapeutics to combat Alzheimer's disease, Parkinson's disease, and other amyloid diseases

Chapter 2 presents the X-ray crystallographic structures of oligomers formed by a 20-residue peptide segment derived from Aβ. The development of a peptide, in which $A\beta_{17–36}$ is stabilized as a β-hairpin is described and the X-ray crystallographic structures of oligomers it forms are reported. Two covalent constraints act in tandem to stabilize the $A\beta_{17–36}$ peptide in a hairpin conformation: a δ-linked ornithine turn connecting positions 17 and 36 to create a macrocycle, and an intramolecular disulfide linkage between positions 24 and 29. An *N*-methyl group at position 33 blocks uncontrolled aggregation. The peptide readily crystallizes as a folded β-hairpin, which assembles hierarchically in the crystal lattice. Three β-hairpin monomers assemble to form a triangular trimer, four trimers assemble in a tetrahedral arrangement to form a dodecamer, and five dodecamers pack together to form an annular pore. This hierarchical assembly provides a model, in which full-length Aβ transitions from an unfolded monomer to a folded β-hairpin, which assembles to form oligomers that further pack to form an annular pore. This model may provide a better understanding of the molecular basis of Alzheimer's disease at atomic resolution.

Chapter 3 describes the design, synthesis, X-ray crystallographic structures, and biophysical and biological properties of two stabilized trimers derived from $A\beta_{17–36}$. These triangular trimers are stabilized through three disulfide crosslinks between the monomer subunits. The X-ray crystallographic structures reveal that the stabilized trimers assemble hierarchically to form hexamers, dodecamers, and annular porelike structures. Solution-phase biophysical studies reveal that the stabilized trimers assemble in solution to form oligomers that

recapitulate some of the higher-order assemblies observed crystallographically. The stabilized trimers share many of the biological characteristics of oligomers of full-length Aβ, including toxicity toward a neuronally derived human cell line, activation of caspase-3 mediated apoptosis, and reactivity with the oligomer-specific antibody A11. These studies support the biological significance of the triangular trimer assembly of Aβ β-hairpins and may offer a deeper understanding of the molecular basis of Alzheimer's disease.

Chapter 4 describes the design and study of a macrocyclic β-hairpin peptide derived from $A\beta_{16–36}$. SDS-PAGE and size exclusion chromatography studies show that the $A\beta_{16–36}$ β-hairpin peptide assembles in solution to form hexamers, trimers, and dimers. X-ray crystallography reveals that the peptide assembles to form a hexamer in the crystal state and that the hexamer is composed of dimers and trimers. LDH release assays show that the oligomers formed by the $A\beta_{16–36}$ β-hairpin peptide are toxic toward neuronally derived SH-SY5Y cells. Replica exchange molecular dynamics (REMD) demonstrates that the hexamer can accommodate full-length Aβ. These findings expand our understanding of the structure, solution-phase behavior, and biological activity of Aβ oligomers, and may offer insights into the molecular basis of Alzheimer's disease.

Chapter 1

Structural Studies of Amyloidogenic Peptides and Proteins: Fibrils, Monomers, and Oligomers

Introduction

In amyloid diseases, amyloidogenic peptides and proteins self-assemble into oligomers and fibrils (Table 1.1). Amyloid oligomers have emerged as important contributors to the pathogenesis of amyloid diseases.[1,2] High-resolution structures of the toxic amyloid oligomers have eluded researchers since their discovery, constituting a significant gap in understanding amyloid diseases. Over the past few years, our laboratory has used X-ray crystallography to identify undiscovered modes of self-assembly of macrocyclic β-hairpin mimics containing sequences from amyloidogenic peptides and proteins. These assemblies provide insights into the

structures of the elusive amyloid oligomers and may help shed light on the molecular basis of amyloid diseases. This chapter summarizes the accomplishments thus far in elucidating the structures of amyloid fibrils, monomers, and oligomers at high resolution.

Table 1.1. Amyloidogenic peptides and proteins discussed in this chapter and their associated diseases.

disease	peptide/protein
Alzheimer's disease	β-amyloid peptide Aβ
Parkinson's disease	α-synuclein (α-Syn)
Huntington's disease	huntingtin
amyotrophic lateral sclerosis (ALS)	superoxide dismutase 1 (SOD1)
Creutzfeld-Jakob disease	human prion protein (hPrP)
type-2 diabetes	islet amyloid polypeptide (IAPP)
dialysis-related amyloidosis	β_2-microglobulin (B2M)

Structural Elucidation of Amyloid Fibrils

Aβ is the most extensively characterized of the more than thirty known amyloidogenic peptides and proteins and has served as the archetype for studying the structures of amyloid assemblies. X-ray diffraction measurements initially revealed that amyloid plaques produced a "cross-β" pattern, indicating that the proteinaceous components of the plaques have a "pleated sheet" conformation, providing a glimpse into the molecular structures of amyloid fibrils.[3,4,5] The determination of the sequences of the 40- and 42-amino acid alloforms of Aβ ($A\beta_{40}$ and $A\beta_{42}$) provided the next piece of the puzzle.[6,7] Solid-state NMR spectroscopy (ss-NMR) and X-ray diffraction of fibrils established that the fibrils are composed of an extended network of in-register parallel β-sheets, with the β-strands running perpendicular to the long axes of the fibrils and the hydrogen bonds running parallel.[8,9,10,11,12,13,14,15,16,17,18] These studies produced the first molecular models of amyloid fibrils.

Elucidating the full three-dimensional structures of $A\beta_{40}$ and $A\beta_{42}$ fibrils has required further effort over the course of decades, because the structures of amyloid fibrils are difficult to determine by traditional high-resolution structure determination techniques. ss-NMR has thus far proven the most fruitful technique in fibril structure determination. Extensive ss-NMR studies by Tycko and coworkers unlocked the molecular structures of $A\beta_{40}$ fibrils and revealed a rich structural polymorphism of the fibrils. ss-NMR studies by the research groups of Riek, Ishii, and Griffin elucidated the structure of a fibril polymorph of $A\beta_{42}$. Eisenberg and coworkers pioneered X-ray crystallography of single micro-crystals composed of peptide fragments from key regions of amyloidogenic peptides and proteins, providing additional insights into how amyloid fibrils pack. Recently, cryo-electron microscopy (cryo-EM) has begun to emerge as a promising new technique for amyloid fibril structure determination. The following sections present the structures of fibrils of full-length amyloidogenic peptides and proteins, with a focus on structures that have been deposited in the Protein Data Bank (PDB) and are publically available to download (Table 1.2).

Table 1.2. Amyloid fibril structures deposited in the PDB.

fibrils					
peptide/protein	disease	approach	PDB ID	technique	comments
$A\beta_{40}$	AD	D	2M4J, 2LMP, 2LMQ, 2LMN and 2LMO	ss-NMR	
$A\beta_{40}$	AD	D	2LNQ	ss-NMR	D23N (Iowa mutant)
$A\beta_{40}$	AD	D	2MVX	ss-NMR	E22Δ (Osaka mutant)
$A\beta_{42}$	AD	D	2NAO, 5KK3, 2MXU, 5AEF, 2BEG, and 5OQV	NMR, ss-NMR, c-EM	
$A\beta_{15-40}$	AD	A	2MPZ	ss-NMR	D23N (Iowa mutant)
$A\beta_{15-23}$	AD	B	4Q8D	X-ray	
$A\beta_{15-36}$	AD	C	5V64	X-ray	$F19F^{I}$, $A\beta_{22-29}$ omitted
$A\beta_{16-21}$	AD	A	2Y2A, 3OW9, and 2Y29	X-ray	
$A\beta_{27-32}$	AD	A	3Q2X	X-ray	
$A\beta_{29-34}$	AD	A	3PZZ	X-ray	
$A\beta_{35-40}$	AD	A	2OKZ and 2ONA	X-ray	
$A\beta_{35-42}$	AD	A	2Y3K and 2Y3L	X-ray	
$A\beta_{37-42}$	AD	A	2ONV	X-ray	
α-syn	PD	D	2N0A	ss-NMR	
α-syn_{47-56}	PD	A	4ZNN	EC	A53T
α-syn_{69-77}	PD	A	4RIK	X-ray	
α-syn_{68-78}	PD	A	4RIL	EC	
α-syn_{72-78}	PD	A	4R0U	X-ray	
α-syn_{70-76}	PD	A	4R0W	X-ray	
tau	AD	D	5O3O, 5O3T	c-EM	
tau_{VQIVYK}	AD	A	5K7N, 4NP8, and 2ON9	EC, X-ray	
$IAPP_{15-25}$	T2D	A	5KO0	EC	
$IAPP_{19-29}$	T2D	A	5KNZ	EC	S20G
$IAPP_{22-28}$	T2D	A	5E5V	X-ray	
$IAPP_{13-18}$	T2D	A	5E5X	X-ray	
$IAPP_{16-21}$	T2D	A	5E5Z	X-ray	
$IAPP_{23-29}$	T2D	A	5E61	X-ray	
$IAPP_{18-23}$	T2D	A	3FPO	X-ray	
$IAPP_{14-19}$	T2D	A	3FR1	X-ray	
$IAPP_{14-20}$	T2D	A	3FTH	X-ray	
$IAPP_{31-37}$	T2D	A	3FTK	X-ray	
$IAPP_{28-33}$	T2D	A	3DG1	X-ray	
$IAPP_{21-27}$	T2D	A	3DGJ	X-ray	
$TTR_{105-115}$	SSA, FAP, FAC	A	1RVS, 2M5K, 2M5M, 2M5N, and 3ZPK	ss-NMR, EM	
$TTR_{106-121}$	SSA, FAP, FAC	C	5HPP	X-ray	$TTR_{113-114}$ omitted
$TTR_{111-116}$	SSA, FAP, FAC	A	4XFN	X-ray	
$TTR_{139-144}$	SSA, FAP, FAC	A	4XFO	X-ray	
$hPrP_{170-175}$	CJD	A	2OL9	X-ray	
$B2M_{20-41}$	DRA	A	2E8D	ss-NMR	
$B2M_{74-79}$	DRA	A	3LOZ	X-ray	

disease: CJD = Creutzfeldt Jakob disease, AD = Alzheimer's disease, PD = Parkinson's disease, DRA = dialysis related amyloidosis, T2D = type 2 diabetes, SSA = senile systemic amyloidosis, FAP = familial amyloid polyneuropathy, FAC = familial amyloid cardiomyopathy, N/A = not applicable
approach: A = peptide fragment, B = macrocyclic β-sheet, C = β-hairpin mimic, D = full-length peptide, E = stabilized β-hairpin
technique: X-ray = X-ray crystallography, NMR = solution-state NMR, ss-NMR = solid-state NMR, EM = electron microscopy, c-EM = cryo-electron microscopy, EC = electron crystallography

$A\beta_{40}$ Fibrils. Tycko and coworkers are at the forefront of $A\beta_{40}$ fibril structure determination and have developed methods for generating homogeneous fibrils from chemically synthesized $A\beta_{40}$. These methods yielded two varieties of $A\beta_{40}$ fibrils that have been characterized thus far at high resolution: one contains three-fold symmetrical fibrils that have a

twisted morphology; the other contains two-fold symmetrical fibrils that have a striated ribbon morphology.[19,20] In the two-fold symmetrical fibrils, the two protofilament subunits stack on top of one another to create a four-layered β-sheet (Figure 1.1B). In the three-fold symmetrical fibrils, the three protofilament subunits arrange in a triangular fashion (Figure 1.1A). The structures of the protofilament subunits of both varieties are very similar, each being composed of extended networks of layered, in-register parallel β-sheets. Central residues 11–22 and *C*-terminal residues 30–39 comprise two β-strands connected by a loop containing residues 23–29. The *N*-terminal residues 1–10 are unstructured.

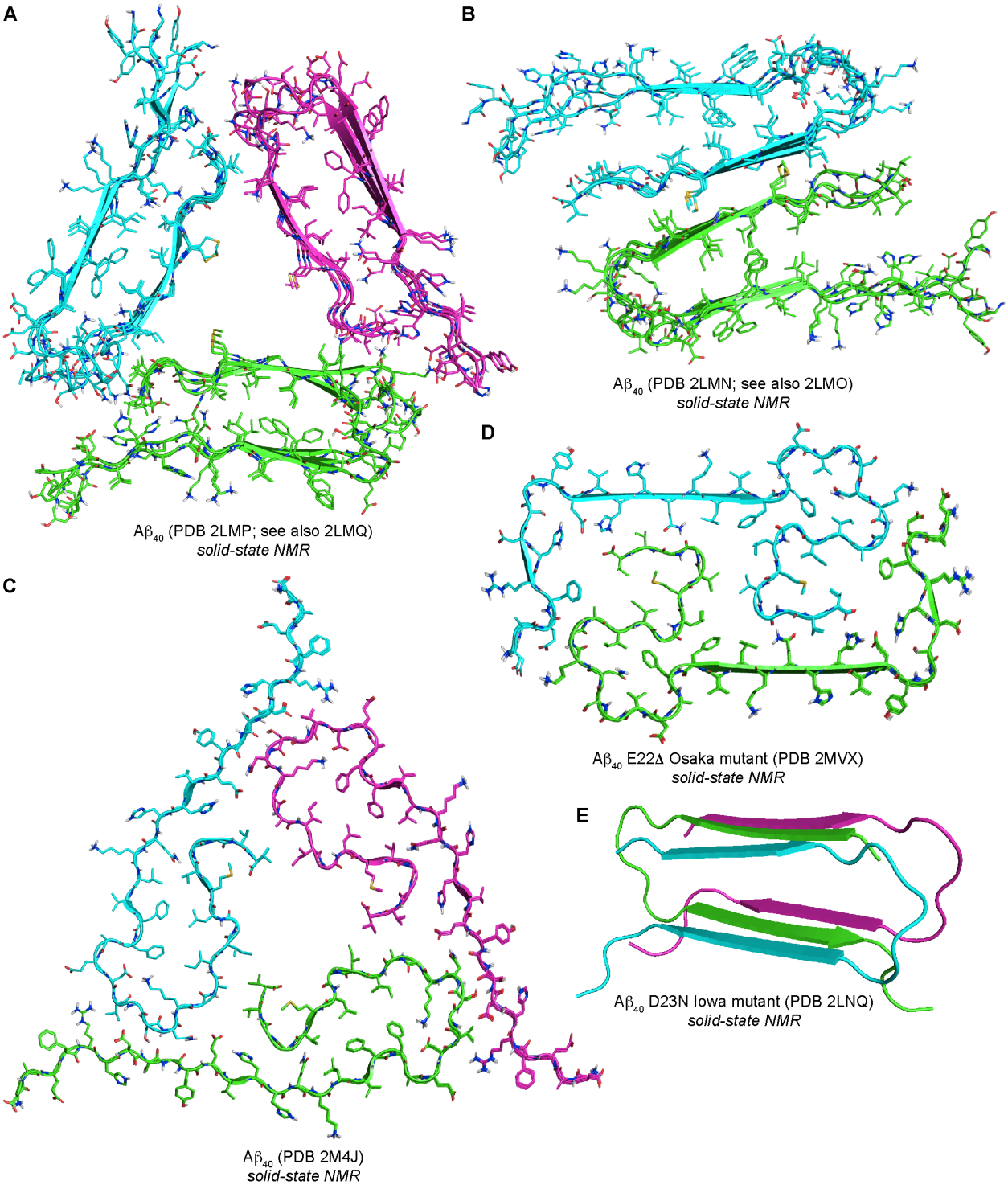

Figure 1.1. Structures of $A\beta_{40}$ fibrils.

Tycko and coworkers have extended these techniques to determine the structure of $A\beta_{40}$ fibrils from brain tissue using fibrils isolated from Alzheimer's disease brain to seed fibrils of isotopically labeled $A\beta_{40}$.[21] ss-NMR revealed a three-fold symmetrical fibril (Figure 1.1C), similar to the three-fold symmetrical fibrils prepared and studied previously. In this fibril structure, residues 12–19 form a β-strand connected to residues 30–40 by a loop comprising residues 21–29. Residues 30–40 are buried in the hydrophobic core of the fibril.

A small percentage of Alzheimer's disease cases are associated with mutations in the amyloid precursor protein that fall within the Aβ sequence.[22] Tycko and coworkers determined that the $A\beta_{40}$ D23N Iowa mutant forms metastable fibrils composed of antiparallel β-sheets that convert to fibrils composed of parallel β-sheets *in vitro*.[23] The structure of the antiparallel fibrils revealed a double-layer antiparallel β-sheet in a single cross-β protofilament with β-strands comprising residues 16–23 and 30–36 connected by a loop comprising residues 24–39 (Figure 1.1E). Meier and coworkers determined the structure of the $A\beta_{40}$ E22Δ Osaka mutant. This structure revealed two-fold symmetrical fibrils, with convoluted protofilament subunits that create a tightly packed core filled exclusively with hydrophobic residues (Figure 1.1D).[24]

$A\beta_{42}$ Fibrils. The research groups of Riek, Griffin, and Ishii have independently determined the structure an $A\beta_{42}$ fibril polymorph using solid-state NMR.[25,26,27] These structures revealed that $A\beta_{42}$ forms two-fold symmetrical fibrils (Figures 1.2A and 1.2B). The protofilament subunits of these $A\beta_{42}$ fibrils have a convoluted S shape, which differs substantially from the shape of the protofilament subunits in $A\beta_{40}$ fibrils. The inside of the protofilament subunits contain packed hydrophobic cores, while the solvent-exposed outside contains primarily charged and polar residues. A salt bridge between the *C*-terminal carboxylate group and the side chain of Lys_{28} provides additional stability, and may explain why $A\beta_{42}$ forms

different fibrils than $A\beta_{40}$, as the two additional amino acids in $A\beta_{42}$ likely allow this salt bridge to form. Schröder, Willbold and coworkers recently determined the structure of an $A\beta_{42}$ fibril polymorph at 4.0 Å resolution using cryo-electron microscopy (Figure 1.2C).[28] This structure revealed a two-fold symmetrical fibril composed of convoluted protofilaments. Unlike previous Aβ fibril structures, the *N*-terminus is ordered and part of the cross-β structure of the fibril. Amino acid side chains in the *N*-terminus form a network of salt bridges with residues in the central region of the peptide.

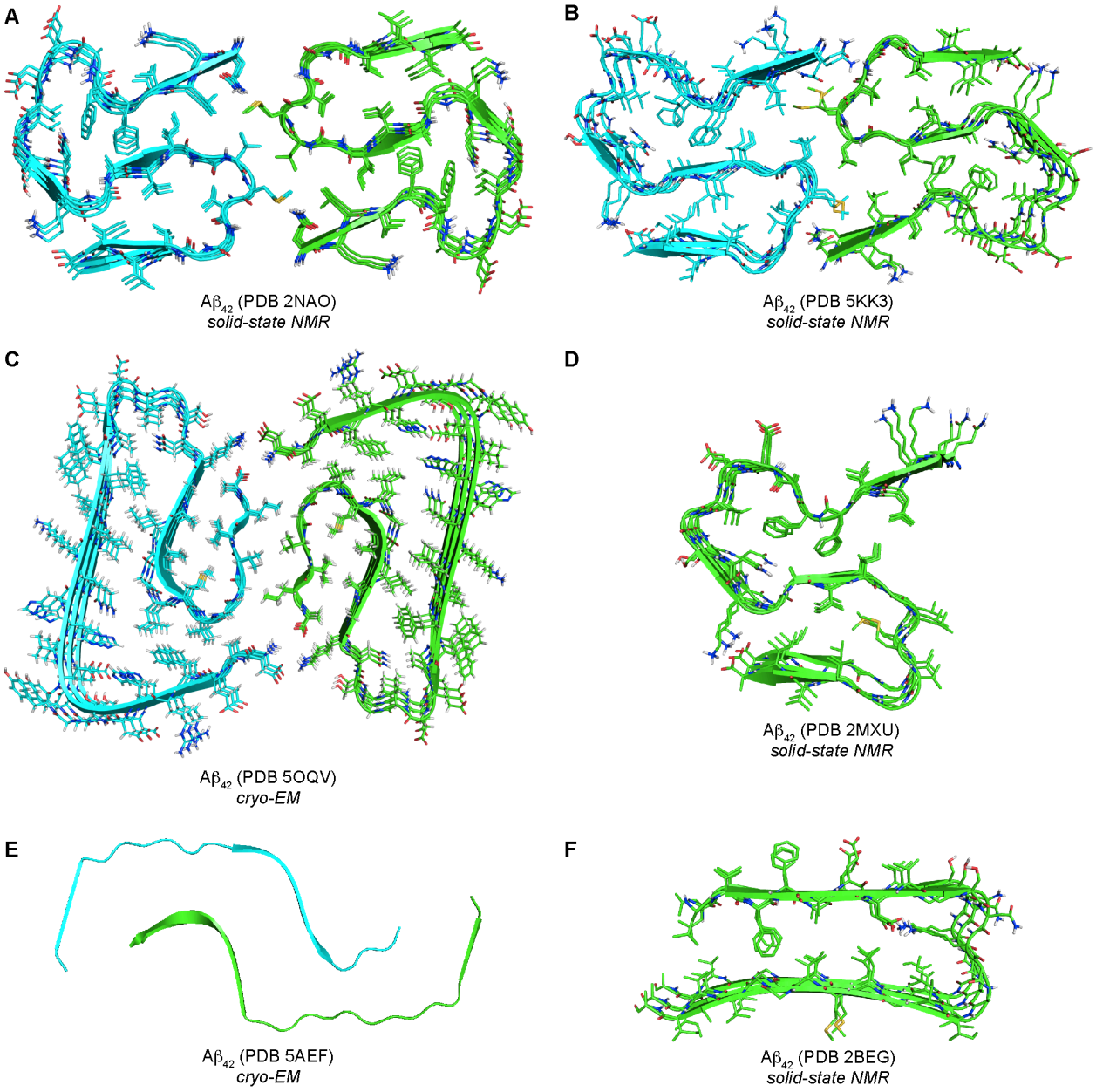

Figure 1.2. Structures of $A\beta_{42}$ fibrils.

α-Syn and Tau Fibrils. Rienstra and coworkers determined the structure of an α-Syn fibril generated from recombinantly expressed α-Syn.[29] This structure revealed a single protofilament in which the packed core is composed of in-register parallel β-sheets (Figure 1.3A). Scheres and coworkers used cryo-EM to determine the structures of two different paired filaments of the tau protein that were isolated from the brains of Alzheimer's disease patients.[30] The paired filaments

consist of two identical protofilament subunits comprising $tau_{306–378}$ and contain in-register parallel β-sheets (Figure 1.3B).

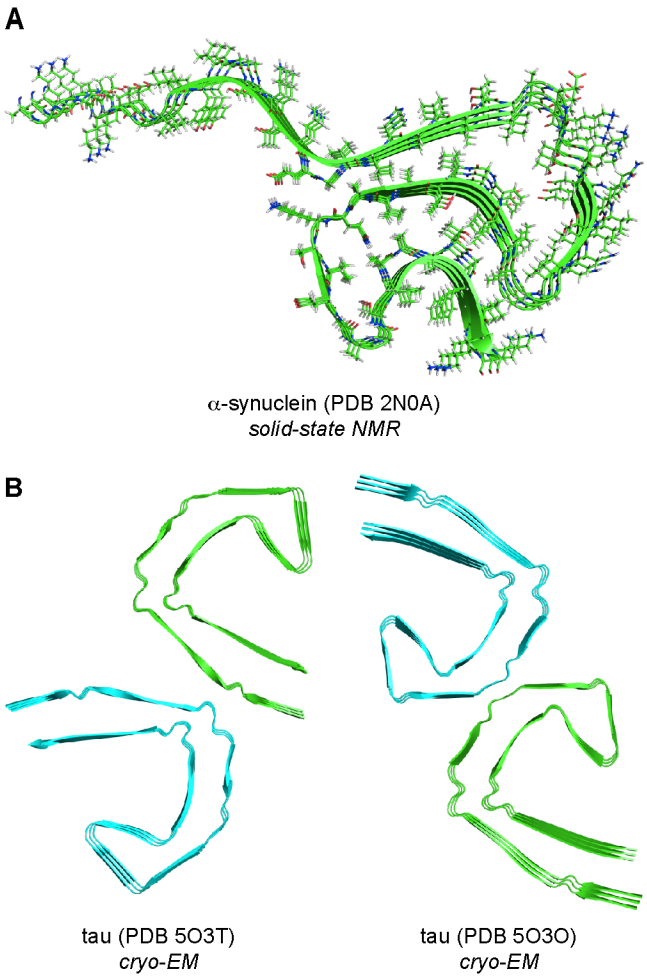

Figure 1.3. Structures of an α-synuclein fibril (A) and two different paired filaments of the tau protein (B).

Additional Insights into Amyloid Fibril Structures. Eisenberg and coworkers have determined the X-ray crystallographic structures of fibrils formed by peptide fragments from amyloidogenic peptides and proteins.[31,32,33] These structures revealed that the peptide fragments often form extended networks of in-register, parallel β-sheets, which pack together through hydrophobic interactions. Eisenberg and coworkers used these fibril structures composed of

peptide fragments to construct models of fibrils of full-length amyloidogenic peptides and proteins, providing a complementary approach to ss-NMR.

Over the last three decades, the structural studies of amyloid fibrils have provided insights into the molecular basis of amyloid diseases. Through these studies, two structural patterns have emerged. Early work revealed flat, extended networks of laminated, layered β-sheets. Subsequent studies have shown more complex structures with convoluted shapes and densely packed cores. The structures of amyloid fibrils are remarkable within the realm of structural biology, because they are composed of repeats of monomer subunits that extend in a single dimension. The extended networks of fibrils are in stark contrast with the enclosed structures of globular proteins, even though the same stabilizing forces that govern globular protein folding also direct the assembly of amyloid fibrils.

Structural Elucidation of Amyloid Monomers

Amyloidogenic peptide and protein monomers are often classified as "intrinsically disordered proteins", meaning that in their monomeric state the proteins lack stable secondary structural elements. Upon interaction with another entity, such as another monomer, oligomer, fibril, or lipid membrane, the monomer undergoes a structural transformation to adopt more stable secondary structural elements. The structures of monomers of smaller amyloidogenic peptides, such as Aβ, α-Syn, and IAPP are difficult to study under physiologically relevant conditions using NMR spectroscopy and X-ray crystallography, because the bulk of the solution is often composed of aggregates. Table 1.3 summarizes key structures of monomeric amyloidogenic peptides and proteins that have been deposited in the PDB.

Table 1.3. Amyloid monomer structures deposited in the PDB.

monomers					
peptide/protein	disease	approach	PDB ID	technique	comments
$A\beta_{40}$	AD	D	2LFM	NMR	
$A\beta_{40}$	AD	D	2OTK	NMR	$A\beta_{40}$/affibody complex
$A\beta_{17–34}$	AD	A	2MJ1	NMR	
α-syn	PD	A	4BXL	NMR	α-syn/affibody complex
IAPP	T2D	D	5MGQ	NMR	
IAPP	T2D	D	5K5G	NMR	IAPP/affibody complex
IAPP	T2D	D	2L86	NMR	

disease: AD = Alzheimer's disease, PD = Parkinson's disease, T2D = type 2 diabetes,
approach: A = peptide fragment, D = full-length peptide
technique: NMR = solution-state NMR

β-Hairpins are thought to have particular significance in the oligomerization of amyloidogenic peptides and proteins. β-Hairpins are special because their twisted shape, hydrophobic surfaces, and exposed hydrogen-bonding edges impart a unique propensity to form compact assemblies. Härd, Hoyer, and coworkers have reported structures of β-hairpins formed by monomeric $A\beta_{40}$, α-Syn, and IAPP (Figure 1.4).[34,35,36] In these studies, the monomeric peptide is bound to an affibody designed to stabilize the β-hairpin, and solution-phase NMR is used to elucidate the structure of the β-hairpin-affibody complex. The structures of these β-hairpins revealed the sequences of amino acids in Aβ, α-Syn, and IAPP that adopt β-strand conformations and the alignment of the β-strands that comprise the β-hairpin.

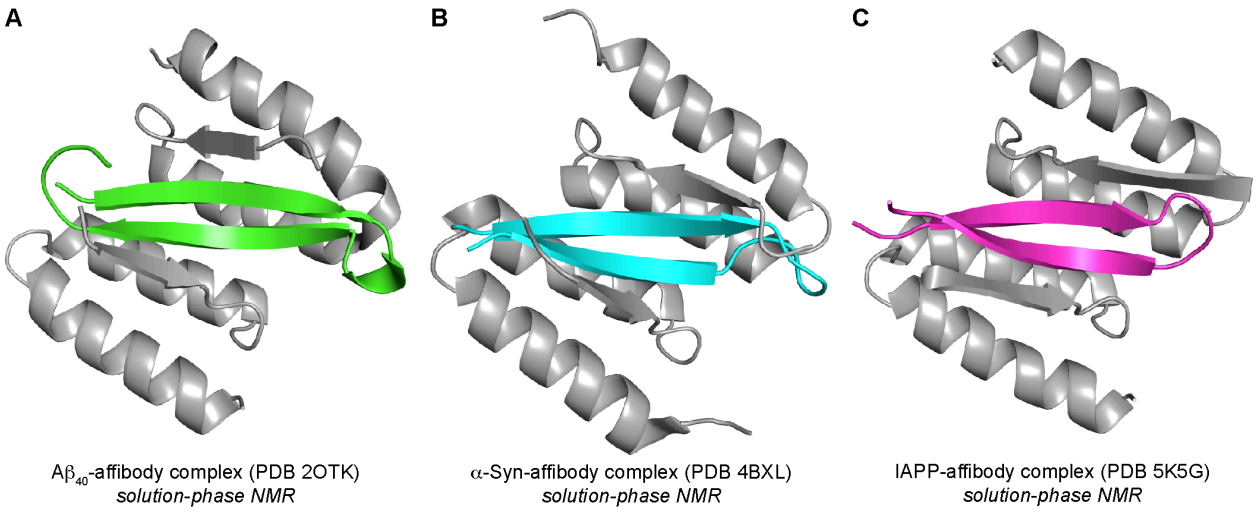

Figure 1.4. Structures of β-hairpin monomer-affibody complexes of Aβ (A), α-Syn (B), and IAPP (C).

Structural Elucidation of Amyloid Oligomers

As researchers worked to understand amyloid fibrils, increasing evidence began to emerge that other, smaller assemblies termed "oligomers" play a crucial role in the pathogenesis of amyloid diseases. Amyloid oligomers are heterogeneous and in structure, stability, and stoichiometry, making it challenging to elucidate their structures by NMR spectroscopy or X-ray crystallography. Some oligomers are thought to be composed of antiparallel β-sheets comprising β-hairpins.[37,38,39,40] Currently, no high-resolution structures of amyloid oligomers formed by full-length amyloidogenic peptides and proteins are available in the PDB. Excluding our own work, only three structures of amyloid oligomers composed of peptide fragments have been reported (Table 1.4).

Table 1.4. Amyloid oligomer structures deposited in the PDB.

oligomers					
peptide/protein	disease	approach	PDB ID	technique	comments
αB crystallin$_{90–100}$	N/A	A	3SGN, 3SGO, 3SGP, and 3SGR	X-ray	antiparallel β-sheet cylindrin
SOD1$_{28–38}$	ALS	A	5IIW	X-ray	antiparallel β-sheet corkscrew, P28K
hPrP$_{177–182}$	CJD	A	4E1I and 4E1H	X-ray	disulfide stabilized antiparallel β-sheet
Aβ$_{15–23}$	AD	B	4IVH	X-ray	
Aβ$_{16–36}$	AD	C	5V63	X-ray	
Aβ$_{16–36}$	AD	C	5W4H	X-ray	F19F$^{p\text{-iodo}}$, Aβ$_{23–29}$ omitted
Aβ$_{17–21}$	AD	B	3Q9H	X-ray	
Aβ$_{17–36}$	AD	C	4NTR and 4NW9	X-ray	M35Orn, Aβ$_{24–29}$ omitted
Aβ$_{17–36}$	AD	C	5SUT and 5SUR	X-ray	stabilized trimers, M35Orn, Aβ$_{24–29}$ omitted
Aβ$_{17–36}$	AD	C	5V65	X-ray	F19F$^{p\text{-iodo}}$, Aβ$_{24–29}$ omitted
Aβ$_{17–36}$	AD	E	5HOX	X-ray	V24C, G29C
Aβ$_{30–34}$	AD	B	3Q9J	X-ray	G33F
Aβ$_{30–36}$	AD	B	3T4G	X-ray	
α-syn$_{36–55}$	PD	C	5F1T	X-ray	G36A and Y39F$^{p\text{-iodo}}$, α-syn$_{42–49}$ omitted
tau$_{VQIVY}$	AD	B	3Q9G	X-ray	
tau$_{SVQIVYK}$	AD	B	4E0M, 4E0N, and 4E0O	X-ray	
B2M$_{58–63}$	DRA	B	4E0K	X-ray	
B2M$_{62–68}$	DRA	B	4E0L	X-ray	
B2M$_{63–69}$	DRA	C	4P4V, 4P4W, 4P4X, 4P4Y, 4P4Z, 4WC8, and 4X0S	X-ray	Y66F$^{p\text{-iodo}}$
IAPP$_{11–17}$	T2D	B	5UHR	X-ray	R11Cit

disease: CJD = Creutzfeldt Jakob disease, AD = Alzheimer's disease, PD = Parkinson's disease, DRA = dialysis related amyloidosis, T2D = type 2 diabetes, N/A = not applicable
approach: A = peptide fragment, B = macrocyclic β-sheet, C = β-hairpin mimic, E = stabilized β-hairpin
technique: X-ray = X-ray crystallography

To better understand the structures of amyloid oligomers, researchers have turned to studying peptide fragments from regions of amyloidogenic peptides and proteins that are important in assembly. Eisenberg and coworkers determined the X-ray crystallographic structure of a β-barrel-like oligomer, termed a *cylindrin*, formed by an 11-residue peptide fragment from αB crystallin (Figure 1.5A).[41] The cylindrin oligomer is composed of six β-strands that form a twisted antiparallel β-sheet that closes back on itself to form a cylinder. Recently, Eisenberg and coworkers determined the X-ray crystallographic structure of a corkscrew-like oligomer formed by an 11-residue peptide fragment derived from superoxide dismutase 1 (SOD1, Figure 1.5B).[42] Surewicz and coworkers determined the X-ray crystallographic structure of a hexameric oligomer formed by a disulfide-stabilized β-sheet fragment from human prion protein (hPrP, Figure 1.5C).[43] The hPrP oligomer is composed of three four-stranded antiparallel β-sheets that

pack to form a hydrophobic core. These three structures illustrate the role of antiparallel β-sheets in amyloid oligomers and demonstrate the importance of hydrogen bonding and packed hydrophobic cores in oligomer stabilization.

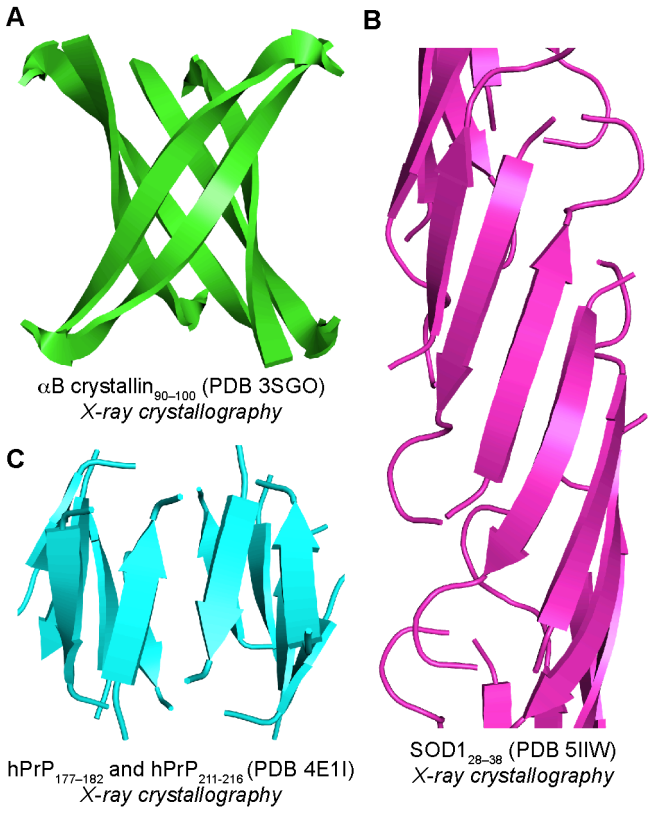

Figure 1.5. Structures of oligomers formed by peptide fragments derived from αB crystallin (A), SOD1 (B), and hPrP (C).

Our laboratory has pioneered elucidation of amyloid oligomer structures through X-ray crystallography of macrocyclic peptides containing fragments from amyloidogenic peptides and proteins. Our general approach involves stabilizing two β-strands in an antiparallel β-sheet conformation by linking the β-strands together at their *N*- and *C*-termini with two delta-linked ornithine turn units ($^{\delta}$Orn) to form a macrocycle. To control aggregation of the peptide we use an unnatural group to block the hydrogen-bonding edge of one of the β-strands. The X-ray

crystallographic structures of these macrocyclic peptides reveal that the peptides assemble hierarchically to form oligomers. The structures of these oligomers provide structural models for oligomers of full-length amyloidogenic peptides and proteins and illustrate their hierarchical assembly from smaller subunits. We then investigate the biophysical and biological properties of the oligomers observed crystallographically. These studies guide the design of new macrocyclic peptides that incorporate additional features from the full-length amyloidogenic peptides and proteins and also provide structural insights into the molecular basis of amyloid disease (Chart 1.1). We envision that these studies will guide the development of probes such as antibodies and fluorophores, and the identification of targets for drug discovery.

Chart 1.1. Our laboratory's approach for gaining insights into the structures of amyloid oligomers.

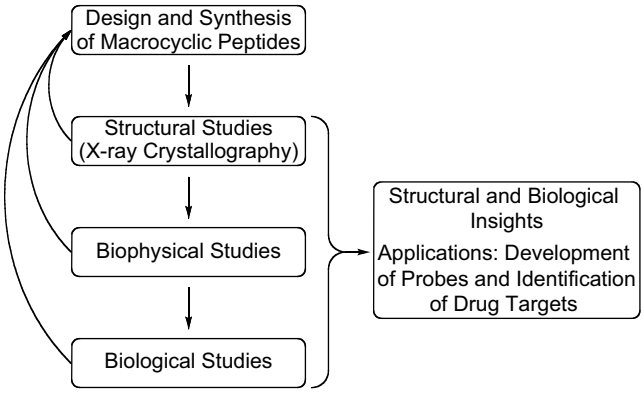

Over the last ten years, our laboratory has designed macrocyclic peptides with the goal of mimicking the β-sheet structure of the amyloidogenic peptide or protein being studied. Early work involved using the tripeptide mimic Hao to template β-sheet formation and block uncontrolled aggregation. These macrocyclic β-sheet peptides contain a natural β-strand from Aβ, tau, B2M, and IAPP and a template strand that contains Hao (Figure 1.6).[44,45,46,47,48] The X-

ray crystallographic structures of these Hao-containing macrocyclic β-sheet peptides revealed the common propensity for these peptides to form flat β-sheets that assemble to form hydrogen-bonded dimers, which sandwich together to form cruciform tetramers (Figure 1.7). Although the Hao-containing macrocyclic β-sheet peptides provided valuable insights into the supramolecular assembly of β-sheets derived amyloidogenic peptides and proteins, the template strand contains the unnatural Hao moiety and is not designed to mimic the natural amyloidogenic peptide or protein.

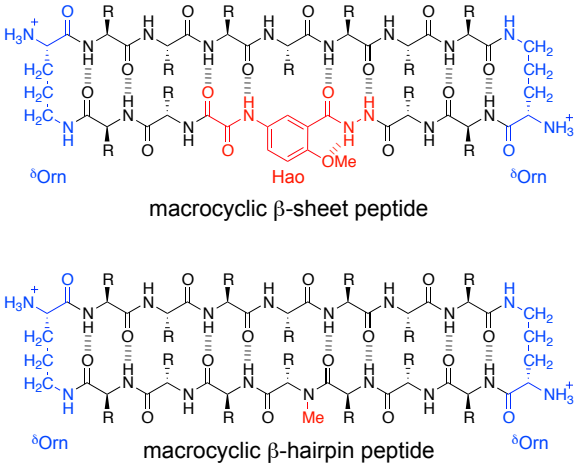

Figure 1.6. Generic chemical structures of a Hao-containing macrocyclic β-sheet peptide and a macrocyclic β-hairpin peptide.

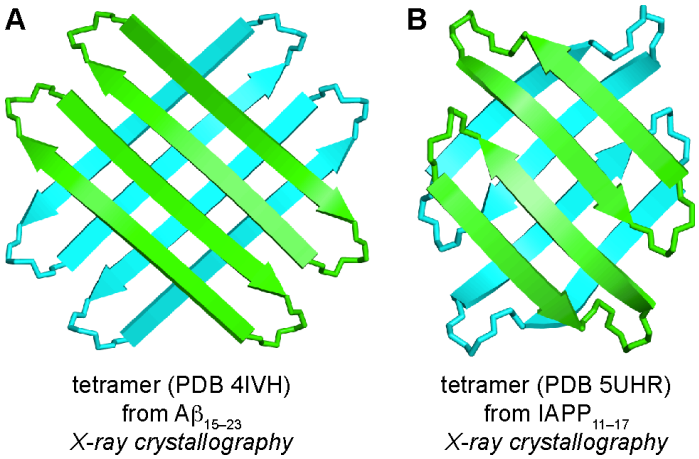

Figure 1.7. X-ray crystallographic structures of cruciform tetramers formed by Hao-containing macrocyclic β-sheet peptides derived from Aβ (A) and IAPP (B).

Inspired by the β-hairpin structures reported by Härd and Hoyer, in 2013 former graduate student Ryan Spencer designed a macrocyclic peptide that better mimics β-hairpins formed by amyloidogenic peptides and proteins. These macrocyclic β-hairpin mimics contain two natural β-strand fragments linked together by two $^{\delta}$Orn turn mimics (Figure 1.6). An *N*-methyl group on the amide backbone of one of the β-strands blocks uncontrolled aggregation by disrupting the ability of the peptide to form a continuous hydrogen-bonded β-sheet network. The design and study of these macrocyclic β-hairpin mimics represented a major breakthrough for our laboratory. The remainder of this dissertation will focus on our studies of these peptides over the past five years. In these studies, X-ray crystallography has proven to be a fountainhead for elucidating the structures of oligomers formed by macrocyclic β-hairpin peptides.[49]

Structures of Oligomers Formed by Macrocyclic β-Hairpin Peptides Derived from Aβ$_{17–36}$.[50] We began our study of amyloid oligomers by designing two macrocyclic β-hairpin peptides that mimics an Aβ$_{17–36}$ β-hairpin. In these macrocyclic β-hairpins, β-strands comprising Aβ$_{17–23}$ and Aβ$_{30–36}$ are linked together by two $^{\delta}$Orn turn mimics to create peptides **1.1** and **1.2** (Figure 1.8). The $^{\delta}$Orn turn mimic that links Asp$_{23}$ and Ala$_{30}$ replaces the Aβ$_{24–29}$ loop. Peptide **1.1**

contains an *N*-methyl group on Gly_{33}, and peptide **1.2** contains an *N*-methyl group on Phe_{20}. To improve the solubility of these peptides, we replaced Met_{35} with the hydrophilic isostere ornithine.

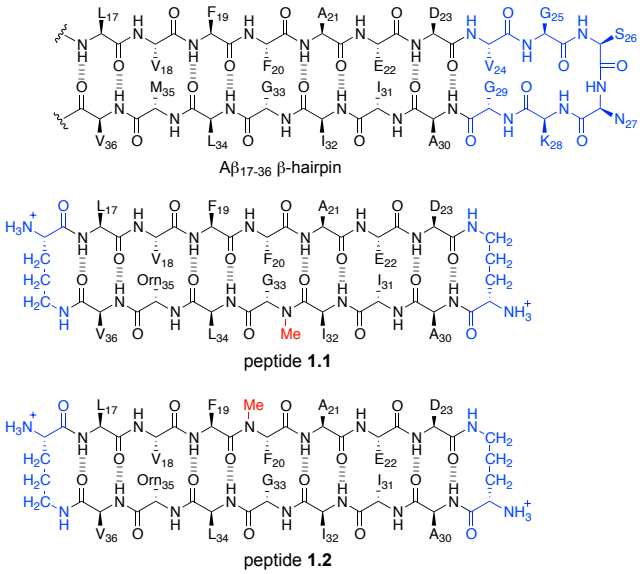

Figure 1.8. Chemical structures of peptides **1.1** and **1.2**, illustrating their relationship to an $A\beta_{17–36}$ β-hairpin.

The X-ray crystallographic structures of peptides **1.1** and **1.2** reveal that both peptides fold to form twisted antiparallel β-sheets that closely mimic the structure of the natural Aβ β-hairpin reported by Härd and Hoyer. The β-hairpin monomers formed by peptides **1.1** and **1.2** each assemble to form triangular trimers (Figure 1.9). The two triangular trimers are virtually identical, indicating that trimer formation is not guided by which β-strand contains the *N*-methyl group. In the triangular trimer formed by peptide **1.1**, three ordered water molecules fill the center hole of the trimer, hydrogen bonding with each other and with the amide backbone of Phe_{20}. In the triangular trimer formed by peptide **1.2**, the three *N*-methyl groups on the Phe_{20} residues fill the center hole of the trimer, replacing the three ordered waters molecules. The

triangular trimers are stabilized by hydrophobic packing between amino acid side chains at the three corners of the trimer and by intermolecular hydrogen bonds between the amide backbones of adjacent monomers. The triangular trimers further assemble to form hexamers, in which two trimers pack face-to-face, and dodecamers, in which four trimers assemble in a tetrahedral fashion.

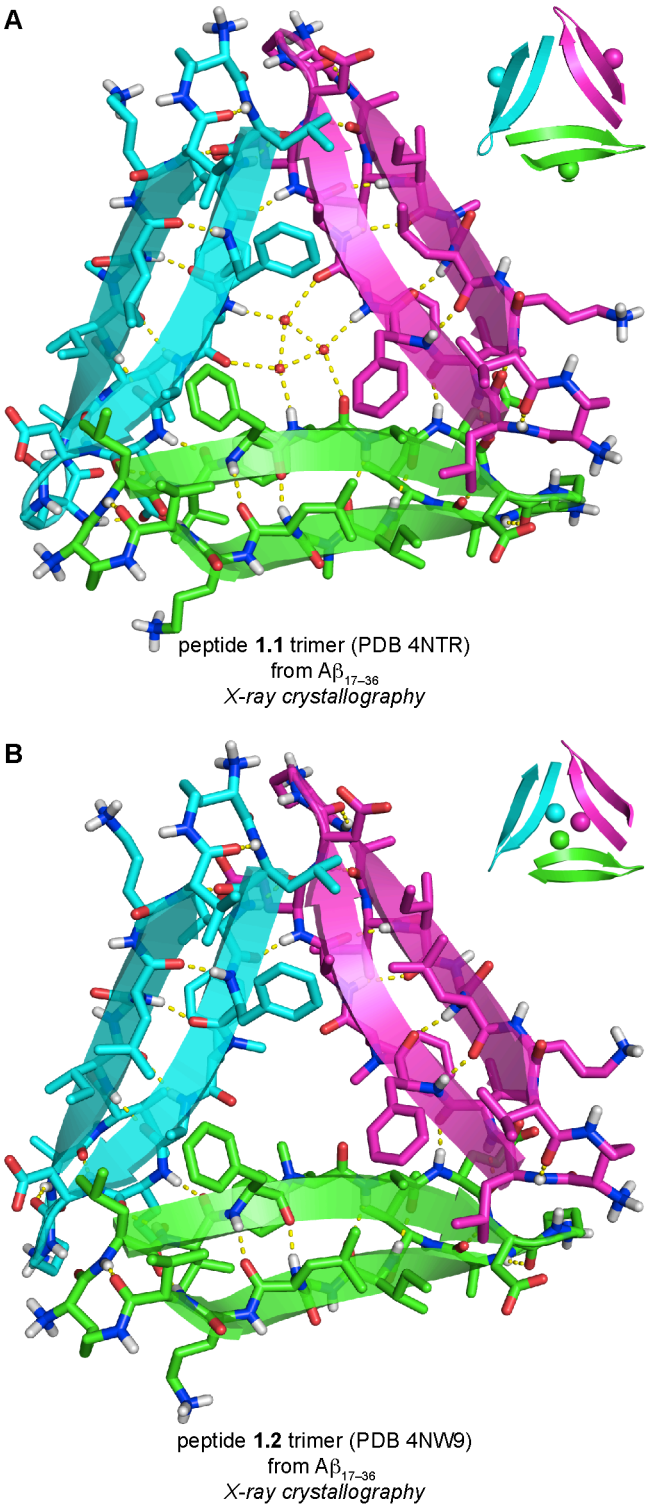

Figure 1.9. X-ray crystallographic structures of the triangular trimers formed by peptide **1.1** (A) and peptide **1.2** (B). In the insets, the *N*-methyl groups on each peptide are shown as spheres.

The X-ray crystallographic structures of the oligomers formed by peptides **1.1** and **1.2** transformed our laboratory's perception about the supramolecular assembly of β-sheets by revealing a richer more complex structural landscape for β-sheet assembly than had been previously observed. The triangular trimers differ from the flat, edge-to-edge-hydrogen-bonded β-sheets observed in the oligomers formed by the Hao-containing macrocyclic β-sheets. The triangular trimer motif appears to be a common mode of assembly of β-hairpins. The foldon domain of bacteriophage T4 fibritin is composed of three β-hairpins that assemble to form a triangular trimer similar to the triangular trimers formed by peptides **1.1** and **1.2**.[51] Triangular trimers have also emerged as a common structural motif formed by other macrocyclic β-hairpin peptides developed by our laboratory. The remainder of this dissertation will focus on my discoveries from the last five years of studying macrocyclic β-hairpins that have built upon these initial studies of peptides **1.1** and **1.2**.

REFERENCES AND NOTES

1 Benilova, I,; Karran, E.; De Strooper, B. The Toxic Aβ Oligomer and Alzheimer's Disease: An Emperor in Need of Clothes. *Nat. Neurosci.* **2012**, *15*, 349–357.

2 Larson, M. E.; Lesné, S. E. *J. Neurochem.* Soluble Aβ Oligomer Production and Toxicity. **2012**, *120*, 125–139.

3 Eanes, E. D.; Glenner, G. G. X-ray Diffraction Studies on Amyloid Filaments. *J. Histochem. Cytochem.* **1968**, *16*, 673–677.

4 Glenner, G. G.; Wong, C. W. Alzheimer's Disease: Initial Report of the Purification and Characterization of a Novel Cerebrovascular Amyloid Protein. *Biochem. Biophys. Res. Commun.* **1984**, *120*, 885–890.

5 Kirschner, D. A.; Abraham, C.; Selkoe, D. J. X-ray Diffraction from Intraneuronal Paired Helical Filaments and Extraneuronal Amyloid Fibers in Alzheimer Disease Indicates Cross-Beta Conformation. *Proc. Natl. Acad. Sci. U.S.A.* **1986**, *83*, 503–507.

6 Masters, C. L.; Simms, G.; Weinman, N. A.; Multhaup, G.; McDonald, B. L.; Beyreuther, K. Amyloid Plaque Core Protein in Alzheimer Disease and Down Syndrome. *Proc. Natl. Acad. Sci. U.S.A.* **1985**, *82*, 4245–4249.

7 Kang, J.; Lemaire, H. G.; Unterbeck, A.; Salbaum, J. M.; Masters, C. L.; Grzeschik, K. H.; Multhaup, G.; Beyreuther, K.; Müller-Hill, B. The Precursor of Alzheimer's Disease Amyloid A4 Protein Resembles a Cell-Surface Receptor. *Nature* **1987**, *325*, 733–736.

8 Blake, C.; Serpell, L. Synchrotron X-ray Studies Suggest that the Core of the Transthyretin Amyloid Fibril is a Continuous β-Sheet Helix. *Structure* **1996**, *4*, 989–998.

9 Malinchik, S. B.; Inouye, H.; Szumowski, K. E.; Kirschner, D. A. Structural Analysis of Alzheimer's β(1-40) Amyloid: Protofilament Assembly of Tubular Fibrils. *Biophys. J.* **1998**, *74*, 537–545.

10 Sunde, M.; Serpell, L. C.; Bartlam, M.; Fraser, P. E.; Pepys, M. B.; Blake, C. C. *J. Mol. Biol.* **1997**, *273*, 729–739.

11 Benzinger, T. L.; Gregory, D. M.; Burkoth, T. S.; Miller-Auer, H.; Lynn, D. G.; Botto, R. E.; Meredith, S. C. Propagating Structure of Alzheimer's β-Amyloid(10-35) is Parallel β-Sheet with Residues in Exact Register. *Proc. Natl. Acad. Sci. U.S.A.* **1998**, *95*, 13407–13412.

12 Gregory, D. M.; Benzinger, T. L.; Burkoth, T. S.; Miller-Auer, H.; Lynn, D. G.; Meredith, S. C.; Botto, R. E. Dipolar Recoupling NMR of Biomolecular Self-Assemblies: Determining Inter- and Intrastrand Distances in Fibrilized Alzheimer's β-Amyloid Peptide. *Solid State Nucl. Magn. Reson.* **1998**, *13*, 149–166.

13 Benzinger, T. L.; Gregory, D. M.; Burkoth, T. S.; Miller-Auer, H.; Lynn, D. G.; Botto, R. E.; Meredith, S. C. Two-Dimensional Structure of β-Amyloid(10-35) Fibrils. *Biochemistry* **2000**, *39*, 3491–3499.

14 Antzutkin, O. N.; Balbach, J. J.; Leapman, R. D.; Rizzo, N. W.; Reed, J.; Tycko, R. Multiple Quantum Solid-State NMR Indicates a Parallel, not Antiparallel, Organization of β-Sheets in Alzheimer's β-Amyloid Fibrils. *Proc. Natl. Acad. Sci. U.S.A.* **2000**, *97*, 13045–13050.

15 Burkoth, T. S.; Benzinger, T. L. S.; Urban V.; Morgan, D. M.; Gregory, D. M.; Thiyagarajan, P.; Botto, R. E.; Meredith, S. C.; Lynn, D. G. Structure of the β-Amyloid(10-35) Fibril *J. Am. Chem. Soc.* **2000**, *122*, 7883–7889.

16 Antzutkin, O. N.; Leapman, R. D.; Balbach, J. J.; Tycko, R. Supramolecular Structural Constraints on Alzheimer's β-Amyloid Fibrils from Electron Microscopy and Solid-State Nuclear Magnetic Resonance. *Biochemistry* **2002**, *41*, 15436–15450.

17 Petkova, A. T.; Ishii, Y.; Balbach, J. J.; Antzutkin, O. N.; Leapman, R. D.; Delaglio, F.; Tycko, R. A Structural Model for Alzheimer's β-Amyloid Fibrils Based on Experimental Constraints from Solid State NMR. *Proc. Natl. Acad. Sci. U.S.A.* **2002**, *99*, 16742–16747.

18 Sikorski, P.; Atkins, E. D.; Serpell, L. C. Structure and Texture of Fibrous Crystals Formed by Alzheimer's Aβ(11-25) Peptide Fragment. *Structure* **2003**, *11*, 915–926.

19 Paravastu, A. K.; Leapman, R. D.; Yau, W. M.; Tycko, R. Molecular Structural Basis for Polymorphism in Alzheimer's β-Amyloid Fibrils. *Proc. Natl. Acad. Sci. U.S.A.* **2008**, *105*, 18349–18354.

20 Petkova, A. T.; Yau, W. M.; Tycko, R. Experimental Constraints on Quaternary Structure in Alzheimer's β-Amyloid Fibrils. *Biochemistry* **2006**, *45*, 498–512.

21 Lu, J. X.; Qiang, W.; Yau, W. M.; Schwieters, C. D.; Meredith, S. C.; Tycko, R. Molecular Structure of β-amyloid Fibrils in Alzheimer's Disease Brain Tissue. *Cell* **2013**, *154*, 1257–1268.

22 Hatami, A.; Monjazeb, S.; Milton, S.; Glabe, C. G. Familial Alzheimer's Disease Mutations within the Amyloid Precursor Protein Alter the Aggregation and Conformation of the Amyloid-β Peptide. *J. Biol. Chem.* **2017**, *292*, 3172–3185.

23 Qiang, W.; Yau, W. M.; Luo, Y.; Mattson, M. P.; Tycko, R. Antiparallel β-sheet Architecture in Iowa-Mutant β-Amyloid Fibrils. *Proc. Natl. Acad. Sci. U.S.A.* **2012**, *109*, 4443–4448.

24 Schütz, A. K.; Vagt, T.; Huber, M.; Ovchinnikova, O. Y.; Cadalbert, R.; Wall, J.; Güntert, P.; Böckmann, A.; Glockshuber, R.; Meier, B. H. Atomic-Resolution Three-Dimensional Structure of Amyloid β Fibrils Bearing the Osaka Mutation *Angew. Chem. Int. Ed. Engl.* **2015**, *54*, 331–335.

25 Wälti, M. A.; Ravotti, F.; Arai, H.; Glabe, C. G.; Wall, J. S.; Böckmann, A.; Güntert, P.; Meier, B. H.; Riek, R. Atomic-Resolution Structure of a Disease-Relevant Aβ(1-42) Amyloid Fibril. *Proc. Natl. Acad. Sci. U.S.A.* **2016**, *113*, 4976–4984.

26 Colvin, M. T.; Silvers, R.; Ni, Q. Z.; Can, T. V.; Sergeyev, I.; Rosay, M.; Donovan, K. J.; Michael, B.; Wall, J.; Linse, S.; Griffin, R. G. Atomic Resolution Structure of Monomorphic Aβ42 Amyloid Fibrils. *J. Am. Chem. Soc.* **2016**, *138*, 9663–9674.

27 Xiao, Y.; Ma, B.; McElheny, D.; Parthasarathy, S.; Long, F.; Hoshi, M.; Nussinov, R.; Ishii, Y. Aβ(1-42) Fibril Structure Illuminates Self-Recognition and Replication of Amyloid in Alzheimer's Disease. *Nat. Struct. Mol. Biol.* **2015**, *22*, 499–505.

28 Gremer, L.; Schölzel, D.; Schenk, C.; Reinartz, E.; Labahn, J.; Ravelli, R. B. G.; Tusche, M.; Lopez-Iglesias, C.; Hoyer, W.; Heise, H.; Willbold, D.; Schröder, G. F. Fibril Structure of Amyloid-β(1-42) by Cryoelectron Microscopy. *Science* **2017**, pii: eaao2825. doi: 10.1126/science.aao2825.

29 Tuttle, M. D.; Comellas, G.; Nieuwkoop, A. J.; Covell, D. J.; Berthold, D. A.; Kloepper, K. D.; Courtney, J. M.; Kim, J. K.; Barclay, A. M.; Kendall, A.; Wan, W.; Stubbs, G.; Schwieters, C. D.; Lee, V. M.; George, J. M.; Rienstra, C. M. Solid-State NMR Structure of a Pathogenic Fibril of Full-Length Human α-Synuclein. *Nat. Struct. Mol. Biol.* **2016**, *23*, 409–415.

30 Fitzpatrick, A. W. P.; Falcon, B.; He, S.; Murzin, A. G.; Murshudov, G.; Garringer, H. J.; Crowther, R. A.; Ghetti, B.; Goedert, M.; Scheres, S. H. W. Cryo-EM Structures of Tau Filaments from Alzheimer's Disease. *Nature* **2017**, *547*, 185–190.

31 Nelson, R.; Sawaya, M. R.; Balbirnie, M.; Madsen, A. Ø.; Riekel, C.; Grothe, R.; Eisenberg, D. Structure of the Cross-β Spine of Amyloid-Like Fibrils. *Nature* **2005**, *435*, 773–778.

32 Sawaya, M. R.; Sambashivan, S.; Nelson, R.; Ivanova, M. I.; Sievers, S. A.; Apostol, M. I.; Thompson, M. J.; Balbirnie, M.; Wiltzius, J. J.; McFarlane, H. T.; Madsen, A. Ø.; Riekel, C.; Eisenberg, D. Atomic Structures of Amyloid Cross-β Spines Reveal Varied Steric Zippers. *Nature* **2007**, *447*, 453–457.

33 Colletier, J. P.; Laganowsky, A.; Landau, M.; Zhao, M.; Soriaga, A. B.; Goldschmidt, L.; Flot, D.; Cascio, D.; Sawaya, M. R.; Eisenberg, D. Molecular Basis for Amyloid-β Polymorphism. *Proc. Natl. Acad. Sci. U.S.A.* **2011**, *108*, 16938–16943.

34 Hoyer, W.; Grönwall, C.; Jonsson, A.; Ståhl, S.; Härd, T. Stabilization of a β-Hairpin in Monomeric Alzheimer's Amyloid-β Peptide Inhibits Amyloid Formation. *Proc. Natl. Acad. Sci. U.S.A.* **2008**, *105*, 5099–5104.

35 Mirecka, E. A.; Shaykhalishahi, H.; Gauhar, A.; Akgül, Ş.; Lecher, J.; Willbold, D.; Stoldt, M.; Hoyer, W. Sequestration of a β-Hairpin for Control of α-Synuclein Aggregation. *Angew. Chem. Int. Ed. Engl.* **2014**, *53*, 4227–4230.

36 Mirecka, E. A.; Feuerstein, S.; Gremer, L.; Schröder, G. F.; Stoldt, M.; Willbold, D.; Hoyer, W. β-Hairpin of Islet Amyloid Polypeptide Bound to an Aggregation Inhibitor. *Sci. Rep.* **2016**, *6*, 33474.

37 Yu, L.; Edalji, R.; Harlan, J. E.; Holzman, T. F.; Lopez, A. P.; Labkovsky, B.; Hillen, H.; Barghorn, S.; Ebert, U.; Richardson, P. L.; Miesbauer, L.; Solomon, L.; Bartley, D.; Walter,

K.; Johnson, R. W.; Hajduk, P. J.; Olejniczak, E. T. Structural Characterization of a Soluble Amyloid β-Peptide Oligomer. *Biochemistry* **2009**, *48*, 1870–1877.

38 Scheidt, H. A.; Morgado, I.; Huster, D. Solid-State NMR Reveals a Close Structural Relationship Between Amyloid-β Protofibrils and Oligomers. *J. Biol. Chem.* **2012**, *287*, 22822–22826.

39 Doi, T.; Masuda, Y.; Irie, K.; Akagi, K.; Monobe, Y.; Imazawa, T.; Takegoshi, K. Solid-state NMR Analysis of the β-Strand Orientation of the Protofibrils of Amyloid β-Protein. *Biochem. Biophys. Res. Commun.* **2012**, *428*, 458–462.

40 Tay, W. M.; Huang, D.; Rosenberry, T. L.; Paravastu, A. K. The Alzheimer's Amyloid-β(1-42) Peptide Forms Off-Pathway Oligomers and Fibrils that are Distinguished Structurally by Intermolecular Organization. *J. Mol. Biol.* **2013**, *425*, 2494–2508.

41 Laganowsky, A.; Liu, C.; Sawaya, M. R.; Whitelegge, J. P.; Park, J.; Zhao, M.; Pensalfini, A.; Soriaga.; A. B.; Landau, M.; Teng, P. K.; Cascio, D.; Glabe, C.; Eisenberg, D. Atomic View of a Toxic Amyloid Small Oligomer. *Science* **2012**, *335*, 1228–1231.

42 Sangwan, S.; Zhao, A.; Adams, K. L.; Jayson, C. K.; Sawaya, M. R.; Guenther, E. L.; Pan, A. C.; Ngo, J.; Moore, D. M.; Soriaga, A. B.; Do, T. D.; Goldschmidt, L.; Nelson, R.; Bowers, M. T.; Koehler, C. M.; Shaw, D. E.; Novitch, B. G.; Eisenberg. D. S. Atomic Structure of a Toxic, Oligomeric Segment of SOD1 Linked to Amyotrophic Lateral Sclerosis (ALS). *Proc. Natl. Acad. Sci. U.S.A.* **2017**, *114*, 8770–8775.

43 Apostol, M. I.; Perry, K.; Surewicz, W. K. Crystal Structure of a Human Prion Protein Fragment Reveals a Motif for Oligomer Formation. *J. Am. Chem. Soc.* **2013**, *135*, 10202–10205.

44 Pham J. D.; Chim, N.; Goulding, C. W.; Nowick, J. S. Structures of Oligomers of a Peptide from β-Amyloid. *J. Am. Chem. Soc.* **2013**, *135*, 12460–12467.

45 Liu, C.; Sawaya, M. R.; Cheng, P. N.; Zheng, J.; Nowick, J. S.; Eisenberg, D. Characteristics of Amyloid-Related Oligomers Revealed by Crystal Structures of Macrocyclic β-Sheet Mimics. *J. Am. Chem. Soc.* **2011**, *133*, 6736–6744.

46 Cheng, P. N.; Liu, C.; Zhao, M.; Eisenberg, D.; Nowick, J. S. Amyloid β-Sheet Mimics that Antagonize Protein Aggregation and Reduce Amyloid Toxicity. *Nat. Chem.* **2012**, *4*, 927–933.

47 Liu, C.; Zhao, M.; Jiang, L.; Cheng, P. N.; Park, J.; Sawaya, M. R.; Pensalfini, A.; Gou, D.; Berk, A. J.; Glabe, C. G.; Nowick, J.; Eisenberg, D. Out-of-Register β-Sheets Suggest a Pathway to Toxic Amyloid Aggregates. *Proc. Natl. Acad. Sci. U.S.A.* **2012**, *109*, 20913–20918.

48 Wang, Y.; Kreutzer, A. G.; Truex, N. L.; Nowick, J. S. A Tetramer Derived from Islet Amyloid Polypeptide. *J. Org. Chem.* **2017**, *82*, 7905–7912.

49 Spencer, R. K.; Nowick, J. S. A Newcomers Guide to Peptide Crystallography. *Israel J. Chem.* **2015**, *55*, 698–710.

50 Spencer, R. K.; Li, H.; Nowick, J. S. X-ray Crystallographic Structures of Trimers and Higher-Order Oligomeric Assemblies of a Peptide Derived from $A\beta_{17–36}$. *J. Am. Chem. Soc.* **2014**, *136*, 5595–5598.

51 Tao, Y.; Strelkov, S. V.; Mesyanzhinov, V. V.; Rossmann, M. G. Structure of Bacteriophage T4 Fibritin: A Segmented Coiled Coil and the Role of the *C*-Terminal Domain. *Structure* **1997**, *5*, 789–798.

Chapter 2

X-ray Crystallographic Structures of a Trimer, Dodecamer, and Annular Pore Formed by an $A\beta_{17–36}$ β-Hairpin

Introduction

High-resolution structures of oligomers formed by the β-amyloid peptide Aβ are desperately needed to understand the molecular basis of Alzheimer's disease and ultimately develop preventions or treatments. In Alzheimer's disease, monomeric Aβ aggregates to form soluble low molecular weight oligomers, such as dimers, trimers, tetramers, hexamers, nonamers, and dodecamers, as well as high molecular weight aggregates, such as annular protofibrils.[1] Over

the last two decades the role of Aβ oligomers in the pathophysiology of Alzheimer's disease has begun to unfold.

Mouse models for Alzheimer's disease have helped shape our current understanding about the Aβ oligomerization that precedes neurodegeneration. Aβ isolated from the brains of young plaque-free Tg2576 mice forms a mixture of low molecular weight oligomers.[2] A 56 kDa soluble oligomer identified by SDS-PAGE was found to be especially important within this mixture. This oligomer was termed Aβ*56 and appears to be a dodecamer of Aβ. Purified Aβ*56 injected intercranially into healthy rats was found to impair memory, providing evidence that this Aβ oligomer may cause memory loss in Alzheimer's disease. Smaller oligomers with molecular weights consistent with trimers, hexamers, and nonamers were also identified within the mixture of low molecular weight oligomers. Treatment of the mixture of low molecular weight oligomers with hexafluoroisopropanol resulted in the dissociation of the putative dodecamers, nonamers, and hexamers into trimers and monomers, suggesting that trimers may be the building block of the dodecamers, nonamers, and hexamers. Recently, Aβ trimers and Aβ*56 were identified in the brains of cognitively normal humans and were found to increase with age.[3]

A type of large oligomers called an annular protofibrils (APFs) have also been observed in the brains of transgenic mice and isolated from the brains of Alzheimer's patients. APFs were first discovered *in vitro* using chemically synthesized Aβ that aggregated into porelike structures that could be observed by atomic force microscopy (AFM) and transmission electron microscopy (TEM).[4,5] The sizes of APFs prepared *in vitro* vary among different studies. Lashuel *et al*. observed APFs with an outer diameter that ranged from 7–10 nm and an inner diameter that ranged from 1.5–2 nm, consistent with molecular weights of 150–250 kDa.[6] Quist *et al*. observed APFs with an outer diameter of 16 nm embedded in a lipid bilayer.[7] Kayed *et al*. observed APFs

with an outer diameter that ranged from 8–25 nm, which were composed of small spherical Aβ oligomers, 3–5 nm in diameter.[8] Although the APFs in these studies differ in size, they share a similar annular morphology and appear to be composed of smaller oligomers.

APFs have also been observed in the brains of APP23 transgenic mice by immunofluorescence with an anti-APF antibody and were found to accumulate in neuronal processes and synapses.[9] In a subsequent study, APFs were isolated from the brains of Alzheimer's patients by immunoprecipitation with an anti-APF antibody. These APFs had an outer diameter that ranged from 11–14 nm and an inner diameter that ranged from 2.5–4 nm.[10]

Dimers of Aβ have also been isolated from the brains of Alzheimer's patients.[11,12,13] Aβ dimers inhibit long-term potentiation in mice and promote hyperphosphorylation of the microtubule-associated protein tau, leading to neuritic damage.[14,15] Aβ dimers have only been isolated from human or transgenic mouse brains that contain the pathognomonic fibrillar Aβ plaques associated with Alzheimer's disease. Furthermore, the endogenous rise of Aβ dimers in the brains of Tg2576 and J20 transgenic mice coincides with the deposition of Aβ plaques. These observations suggest that the Aβ trimers, hexamers, dodecamers, and related assemblies may be associated with presymptomatic neurodegeneration, while Aβ dimers are more closely associated with fibril formation and plaque deposition during symptomatic Alzheimer's disease.[16,17,18,19,20]

The approach of isolating and characterizing Aβ oligomers has not provided any high-resolution structures of Aβ oligomers. Techniques such as SDS-PAGE, TEM, and AFM have only provided information about the molecular weights, sizes, morphologies, and stoichiometry of Aβ oligomers. High-resolution structural studies of Aβ have primarily focused on Aβ fibrils and Aβ monomers. Solid-state NMR spectroscopy studies of Aβ fibrils revealed that Aβ fibrils are generally composed of extended networks of in-register parallel β-sheets.[21,22,23,24,25,26,27] X-ray

crystallographic studies using fragments of Aβ have provided additional information about how Aβ fibrils pack.[28,29] Solution-phase NMR and solid-state NMR have been used to study the structures of the Aβ monomers within oligomeric assemblies.[30,31,32,33,34,35] A major finding from these studies is that oligomeric assemblies of Aβ are primarily composed of antiparallel β-sheets. Many of these studies have reported the monomer subunit as adopting a β-hairpin conformation, in which the hydrophobic central and *C*-terminal regions form an antiparallel β-sheet.

In 2008, Hoyer *et al*. reported the NMR structure of an Aβ monomer bound to an artificial binding protein called an affibody (PDB 2OTK).[36] The structure revealed that monomeric Aβ forms a β-hairpin when bound to the affibody. This Aβ β-hairpin encompasses residues 17–37 and contains two β-strands comprising $A\beta_{17–24}$ and $A\beta_{30–37}$ connected by an $A\beta_{25–29}$ loop. Sequestering Aβ within the affibody prevents its fibrilization and reduces its neurotoxicity, providing evidence that the β-hairpin structure may contribute to the ability of Aβ to form neurotoxic oligomers. In a related study, Sandberg *et al*. constrained Aβ in a β-hairpin conformation by mutating residues A_{21} and A_{30} to cysteine and forming an intramolecular disulfide bond.[37,38] Locking Aβ into a β-hairpin structure resulted in the formation Aβ oligomers, which were observed by size exclusion chromatography (SEC) and SDS-PAGE. The oligomers with a molecular weight of ~100 kDa that were isolated by SEC were toxic toward neuronally derived SH-SY5Y cells. This study provides evidence for the role of β-hairpin structure in Aβ oligomerization and neurotoxicity.

Inspired by these β-hairpin structures, our laboratory developed a macrocyclic β-sheet peptide derived from $A\beta_{17–36}$ designed to mimic an Aβ β-hairpin and reported its X-ray crystallographic structure.[39] This peptide (peptide **2.1**) consists of two β-strands comprising $A\beta_{17–23}$ and $A\beta_{30–36}$ covalently linked by two δ-linked ornithine ($^{\delta}$Orn) β-turn mimics.[40] The $^{\delta}$Orn that

connects residues D_{23} and A_{30} replaces the $A\beta_{24–29}$ loop. The $^{\delta}$Orn that connects residues L_{17} and V_{36} enforces β-hairpin structure. We incorporated an *N*-methyl group at position G_{33} to prevent uncontrolled aggregation and precipitation of the peptide.[41] To improve the solubility of the peptide we replaced M_{35} with the hydrophilic isostere of methionine, ornithine (α-linked) (Figure 2.1B). The X-ray crystallographic structure of peptide **2.1** reveals that it folds to form a β-hairpin that assembles to form trimers, and that the trimers further assemble to form hexamers and dodecamers.

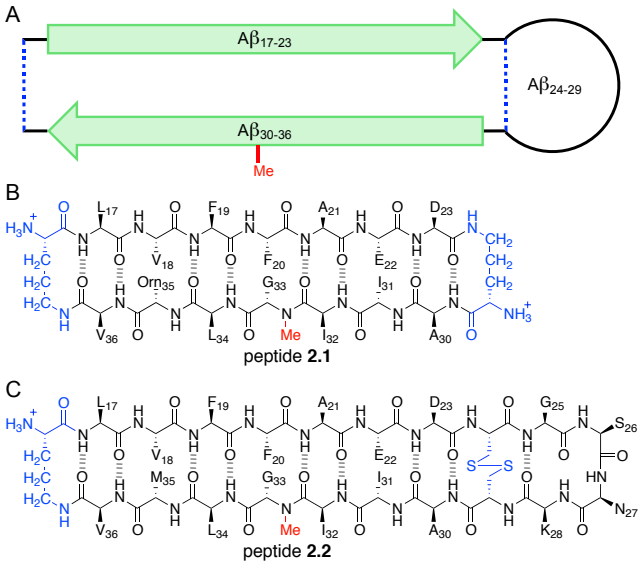

Figure 2.1. (A) Cartoon illustrating the design of peptides **2.1** and **2.2** and their relationship to an $A\beta_{17–36}$ β-hairpin. (B) Chemical structure of peptide **2.1** illustrating $A\beta_{17–23}$ and $A\beta_{30–36}$, M35Orn, the *N*-methyl group, and the δ-linked ornithine turns. (C) Chemical structure of peptide **2.2** illustrating $A\beta_{17–36}$, the *N*-methyl group, the disulfide bond across positions 24 and 29, and the δ-linked ornithine turn.

Our design of peptide **2.1** omitted the $A\beta_{24–29}$ loop. To visualize the $A\beta_{24–29}$ loop, we performed replica-exchange molecular dynamics (REMD) simulations on $A\beta_{17–36}$ using the X-ray crystallographic coordinates of $A\beta_{17–23}$ and $A\beta_{30–36}$ from peptide **2.1**.[39] These studies provided a

working model for a trimer of $A\beta_{17–36}$ β-hairpins and demonstrated that the trimer should be capable of accommodating the $A\beta_{24–29}$ loop.

In the current study, we set out to restore the $A\beta_{24–29}$ loop, reintroduce the methionine residue at position 35, and determine the X-ray crystallographic structures of oligomers that form. We designed peptide **2.2** as a homologue of peptide **2.1** that embodies these ideas. Peptide **2.2** contains a methionine residue at position 35 and an $A\beta_{24–29}$ loop with residues 24 and 29 (Val and Gly) mutated to cysteine and linked by a disulfide bond (Figure 2.1C). Here, we describe the development of peptide **2.2** and report the X-ray crystallographic structures of the trimer, dodecamer, and annular pore observed within the crystal structure.

Results

1. Development of Peptide 2.2. We developed peptide **2.2** from peptide **2.1** by an iterative process, in which we first attempted to restore the $A\beta_{24–29}$ loop without a disulfide linkage. We envisioned peptide **2.3** as a homologue of peptide **2.1** with the $A\beta_{24–29}$ loop in place of the $^{\delta}$Orn that connects D_{23} and A_{30}, and *p*-iodophenylalanine (F^{I}) in place of F_{19}. We routinely use *p*-iodophenylalanine to determine the X-ray crystallographic phases. After determining the X-ray crystallographic structure of the *p*-iodophenylalanine variant we attempt to determine the structure of the native phenylalanine compound by isomorphous replacement.[42] Upon synthesizing peptide **2.3**, we found that it formed an amorphous precipitate in most crystallization conditions screened and failed to afford crystals in any condition.

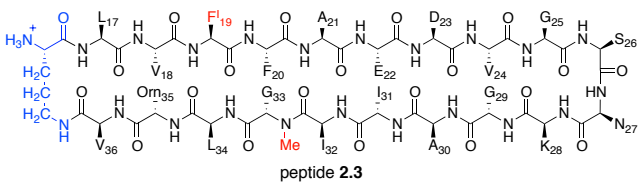

We postulate that the loss of the $^{\delta}$Orn constraint leads to conformational heterogeneity that prevents peptide **2.3** from crystallizing. To address this issue, we next incorporated a disulfide bond between residues 24 and 29 as a conformational constraint that serves as a surrogate for $^{\delta}$Orn. We designed peptide **2.4** to embody this idea, mutating Val_{24} and Gly_{29} to cysteine and forming an interstrand disulfide linkage. We mutated these residues because they occupy the same position as the $^{\delta}$Orn that connects D_{23} and A_{30} in peptide **2.1**. Residues V_{24} and G_{29} form a non-hydrogen-bonded pair, which can readily accommodate disulfide linkages in antiparallel β-sheets. Disulfide bonds across non-hydrogen-bonded pairs stabilize β-hairpins, while disulfide bonds across hydrogen-bonded pairs do not.[43] Although the disulfide bond between positions 24 and 29 helps stabilize the β-hairpin, it does not alter the charge or substantially change the hydrophobicity of the $A\beta_{17–36}$ β-hairpin. We were gratified to find that peptide **2.4** afforded crystals suitable for X-ray crystallography. As the next step in the iterative process, we determined the X-ray crystallographic structure of this peptide (PDB 5HOW).

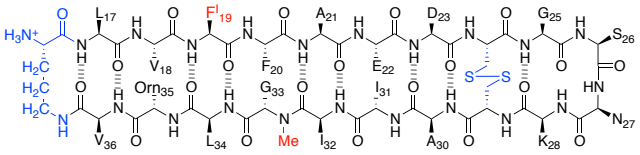

peptide **2.4**

After determining the X-ray crystallographic structure of peptide **2.4** we reintroduced the native phenylalanine at position 19 and the methionine at position 35 to afford peptide **2.2**. We completed the iterative process—from **2.1** to **2.3** to **2.4** to **2.2**—by successfully determining the X-ray crystallographic structure of peptide **2.2** (PDB 5HOX and 5HOY). The following sections describe the synthesis of peptides **2.2**–**2.4** and the X-ray crystallographic structure of peptide **2.2**.

2. Synthesis of Peptides 2.2–2.4. We synthesized peptides **2.2**–**2.4** by similar procedures to those we have developed for other macrocyclic peptides.[39,44,45] Our laboratory routinely prepares macrocyclic peptides by solid-phase synthesis of the corresponding linear peptide on 2-chlorotrityl resin, followed by cleavage of the protected linear peptide from the resin, solution-phase macrolactamization, and deprotection of the resulting macrocyclic peptide. In synthesizing peptides **2.2** and **2.4** we formed the disulfide linkage after macrolactamization and deprotection of the acid-labile side chain protecting groups. We used acid-stable Acm-protected cysteine residues at positions 24 and 29 and removed the Acm groups by oxidation with I_2 in aqueous acetic acid to afford the disulfide linkage. Peptides **2.2**–**2.4** were purified by RP-HPLC.

3. Crystallization, X-ray Crystallographic Data Collection, Data Processing, and Structure Determination of Peptides 2.2 and 2.4. We screened crystallization conditions for peptide **2.4** in a 96-well-plate format using three different Hampton Research crystallization kits (Crystal Screen, Index, and PEG/Ion) with three ratios of peptide and mother liquor per condition (864 experiments). Peptide **2.4** afforded crystals in a single set of conditions containing HEPES buffer and Jeffamine M-600—the same crystallization conditions that afforded crystals of peptide **2.1**. Peptide **2.2** also afforded crystals in these conditions. We further optimized these conditions to rapidly (~72 h) yield crystals suitable for X-ray crystallography. The optimized conditions consist of 0.1 M HEPES at pH 6.4 with 31% Jeffamine M-600 for peptide **2.4**, and 0.1 M HEPES pH 7.1 with 29% Jeffamine M-600 for peptide **2.2**.

Crystal diffraction data for peptides **2.4** and **2.2** were collected in-house with a Rigaku MicroMax 007HF X-ray diffractometer at 1.54 Å wavelength. Crystal diffraction data for peptide **2.2** were also collected at the Advanced Light Source at Lawrence Berkeley National Laboratory with a synchrotron source at 1.00 Å wavelength to achieve higher resolution. Data

from peptides **2.4** and **2.2** suitable for refinement at 2.30 Å were obtained from the diffractometer; data from peptide **2.2** suitable for refinement at 1.90 Å were obtained from the synchrotron.

Data for peptides **2.4** and **2.2** were scaled and merged using XDS.[46] Phases for peptide **2.4** were determined by single-wavelength anomalous diffraction (SAD) phasing by using the coordinates of the iodine anomalous signal from *p*-iodophenylalanine. Phases for peptide **2.2** were determined by isomorphous replacement of peptide **2.4**. The structures of peptides **2.2** and **2.4** were solved and refined in the $P6_122$ space group. Coordinates for hydrogens were generated by phenix.refine during refinement. The asymmetric unit of each peptide consists of six monomers, arranged as two trimers. Peptides **2.2** and **2.4** form morphologically identical structures and assemblies in the crystal lattice.

4. X-ray Crystallographic Structure of Peptide 2.2 and the Oligomers it Forms. The X-ray crystallographic structure of peptide **2.2** reveals that it folds to form a twisted β-hairpin comprising two β-strands connected by a loop (Figure 2.2A). Eight residues make up each surface of the β-hairpin: L_{17}, F_{19}, A_{21}, D_{23}, A_{30}, I_{32}, L_{34}, and V_{36} make up one surface; V_{18}, F_{20}, E_{22}, C_{24}, C_{29}, I_{31}, G_{33}, and M_{35} make up the other surface. The β-strands of the monomers in the asymmetric unit are virtually identical, differing primarily in rotamers of F_{20}, E_{22}, C_{24}, C_{29}, I_{31}, and M_{35} (Figure 2.S1). The disulfide linkages suffered radiation damage under synchrotron radiation.[47,48] We refined three of the β-hairpins with intact disulfide linkages and three with thiols to represent cleaved disulfide linkages in the synchrotron data set (PDB 5HOX). No evidence for cleavage of the disulfides was observed in the refinement of the data set collected on the X-ray diffractometer, and we refined all disulfide linkages as intact (PDB 5HOY).

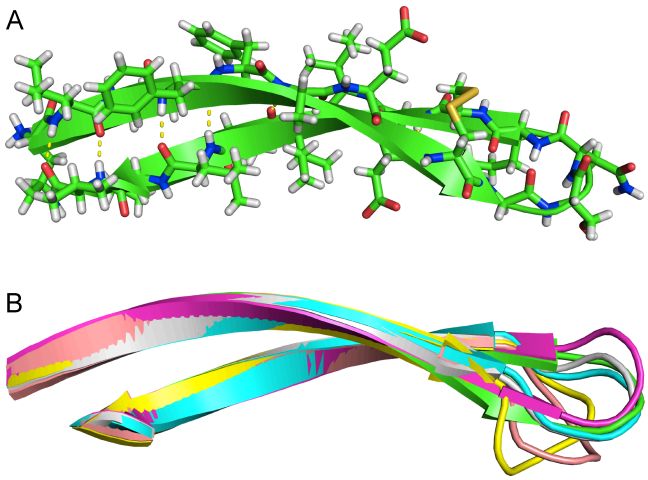

Figure 2.2. X-ray crystallographic structure of peptide **2.2** (PDB 5HOX, synchrotron data set). (A) X-ray crystallographic structure of a representative β-hairpin monomer formed by peptide **2.2**. (B) Overlay of the six β-hairpin monomers in the asymmetric unit. The β-hairpins are shown as cartoons to illustrate the differences in the $A\beta_{25–28}$ loops.

The $A\beta_{25–28}$ loops of the six monomers within the asymmetric unit vary substantially in backbone geometry and side chain rotamers (Figures 2.2B and 3.S1). The electron density for the loops is weak and diffuse compared to the electron density for the β-strands. The B values for the loops are large, indicating that the loops are dynamic and not well ordered. Thus, the differences in backbone geometry and side chain rotamers among the loops are likely of little significance and should be interpreted with caution.

Peptide **2.2** assembles into oligomers similar in morphology to those formed by peptide **2.1**. Like peptide **2.1**, peptide **2.2** forms a triangular trimer, and four trimers assemble to form a dodecamer. In the higher-order assembly of the dodecamers formed by peptide **2.2** a new structure emerges, not seen in peptide **2.1**, an annular pore consisting of five dodecamers.

Trimer. Peptide **2.2** forms a trimer, much like that which we observed previously for peptide **2.1**, in which three β-hairpins assemble to form an equilateral triangle (Figure 2.3A). The trimer maintains all of the same stabilizing contacts as those of peptide **2.1**. Hydrogen bonding and hydrophobic interactions between residues on the β-strands comprising $A\beta_{17–23}$ and $A\beta_{30–36}$

stabilize the core of the trimer. The disulfide bonds between residues 24 and 29 are adjacent to the structural core of the trimer and do not make any substantial intermolecular contacts. Two crystallographically distinct trimers comprise the peptide portion of the asymmetric unit. The two trimers are almost identical in structure, differing slightly among side chain rotamers and loop conformations.

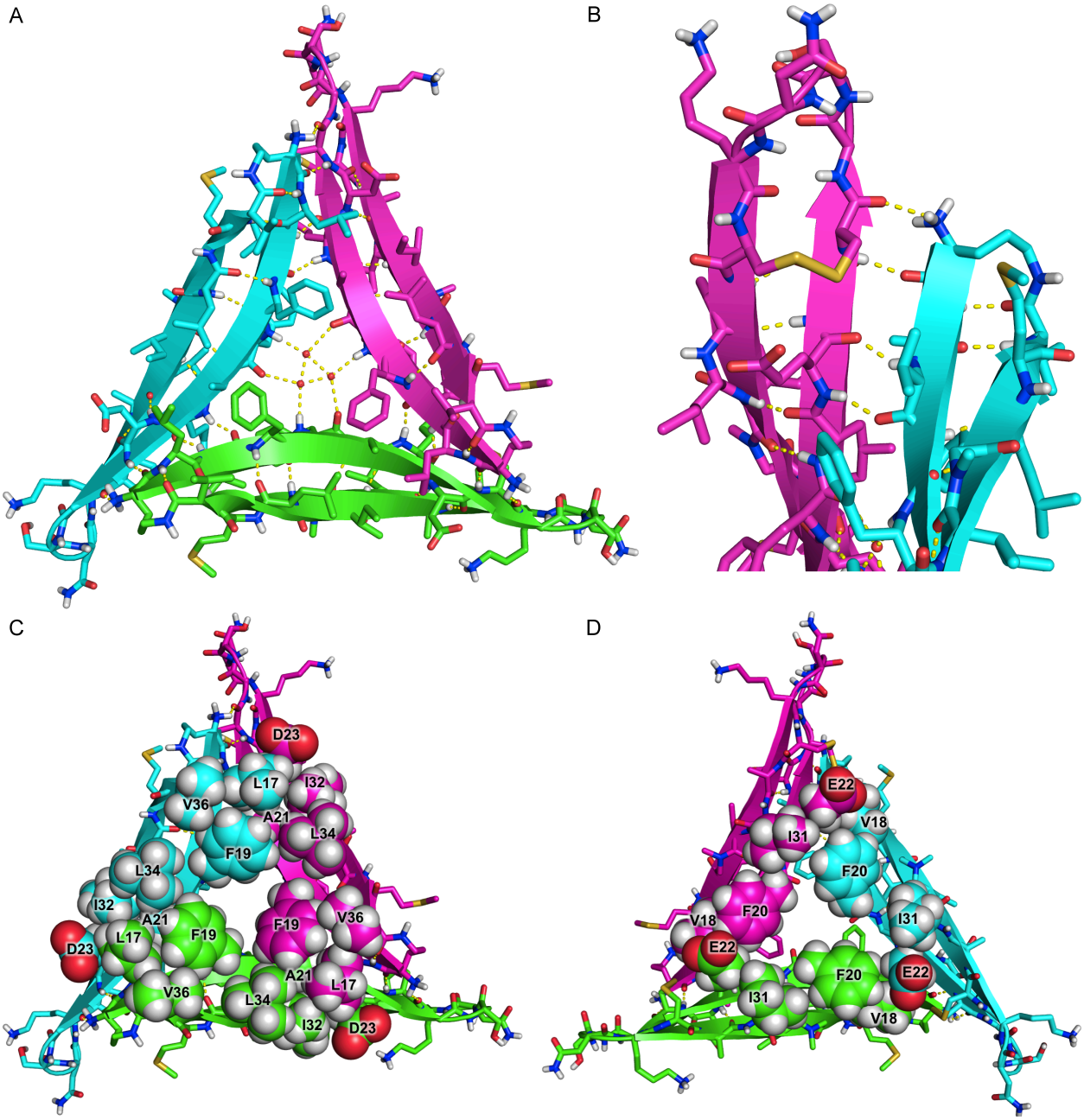

Figure 2.3. X-ray crystallographic structure of the trimer formed by peptide **2.2**. (A) Triangular trimer. The three water molecules in the center hole of the trimer are shown as spheres. (B) Detailed view of the intermolecular hydrogen bonds between the main chains of V_{18} and E_{22}, and $^{\delta}$Orn and C_{24}, at the three corners of the triangular trimer. (C) The F_{19} face of the trimer, with key side chains shown as spheres. (D) The F_{20} face of the trimer, with key side chains as spheres.

A network of 18 intermolecular hydrogen bonds helps stabilize the trimer. At the corners of the trimer, the pairs of β-hairpin monomers form four hydrogen bonds: two between the main

chains of V_{18} and E_{22}, and two between $^{\delta}$Orn and the main chain of C_{24} (Figure 2.3B). Three ordered water molecules fill the hole in the center of the trimer, hydrogen bonding to each other and to the main chain of F_{20} (Figure 2.3A).

Hydrophobic contacts between residues at the three corners of the trimer, where the β-hairpins meet, further stabilize the trimer. At each corner, the side chains of residues L_{17}, F_{19}, and V_{36} of one β-hairpin pack against the side chains of residues A_{21}, I_{32}, L_{34}, and also D_{23} of the adjacent β-hairpin to create a hydrophobic cluster (Figure 2.3C). The three hydrophobic clusters create a large hydrophobic surface on one face of the trimer. The other face of the trimer displays a smaller hydrophobic surface, which includes the side chains of residues V_{18}, F_{20}, and I_{31} of the three β-hairpins (Figure 2.3D). In subsequent discussion, we designate the former surface the "F_{19} face" and the latter surface the "F_{20} face".

Dodecamer. Four trimers assemble to form a dodecamer. The four trimers arrange in a tetrahedral fashion, creating a central cavity inside the dodecamer. Because each trimer is triangular, the resulting arrangement resembles an octahedron. Each of the 12 β-hairpins constitutes an edge of the octahedron, and the triangular trimers occupy four of the eight faces of the octahedron. Figure 2.4A illustrates the octahedral shape of the dodecamer. Figure 2.4B illustrates the tetrahedral arrangement of the four trimers.

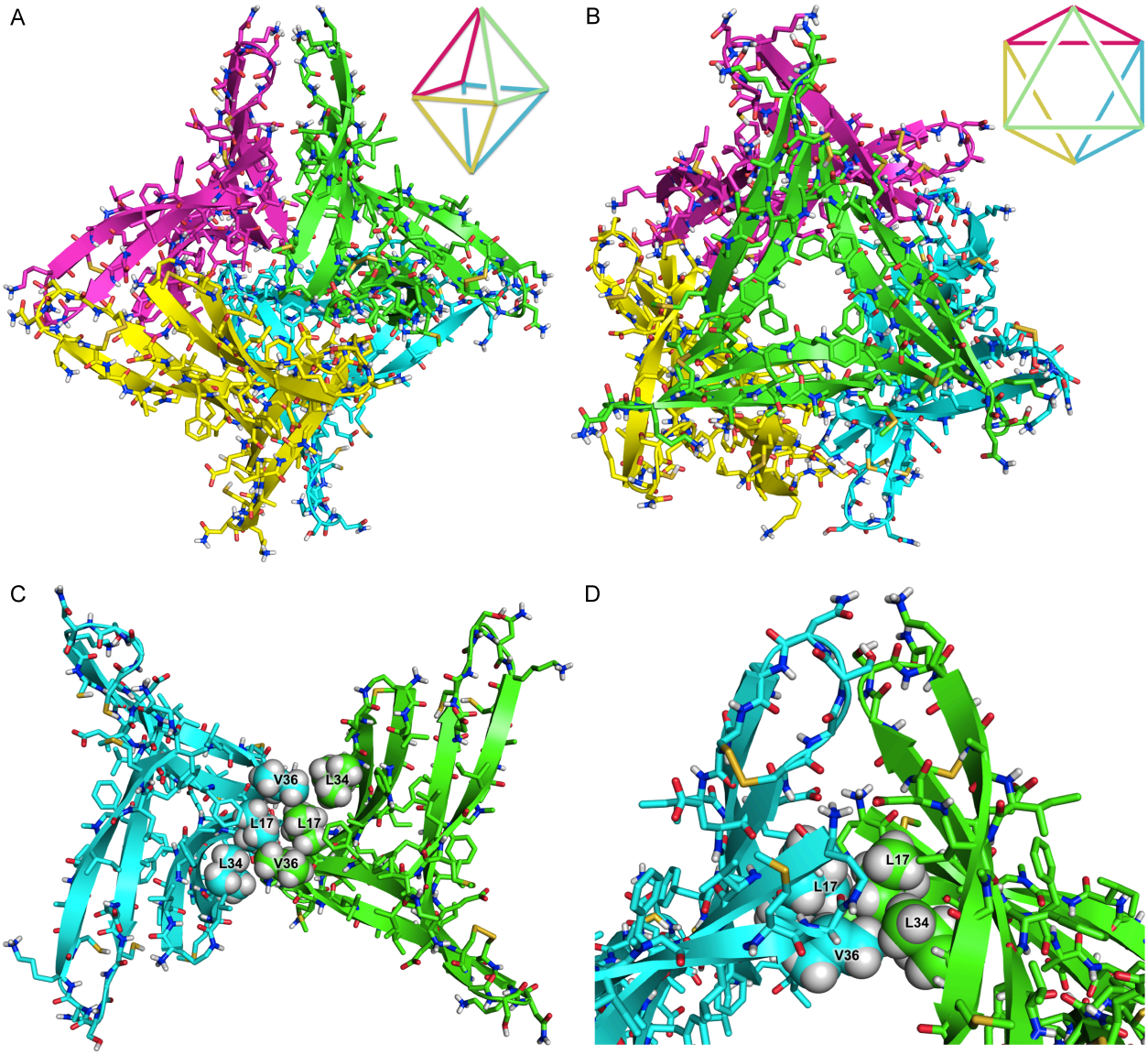

Figure 2.4. X-ray crystallographic structure of the dodecamer formed by peptide **2.2**. (A) View of the dodecamer that illustrates the octahedral shape. (B) View of the dodecamer that illustrates the tetrahedral arrangement of the four trimers that comprise the dodecamer. (C) View of two trimer subunits from inside the cavity of the dodecamer. Residues L_{17}, L_{34}, and V_{36} are shown as spheres, illustrating the hydrophobic packing that occurs at the six vertices of the dodecamer. (D) Detailed view of one of the six vertices of the dodecamer.

The F_{19} faces of the trimers line the interior of the dodecamer. At the six vertices, hydrophobic packing between the side chains of L_{17}, L_{34}, and V_{36} helps stabilize the dodecamer (Figures 2.4C and D). Salt bridges between the side chains of D_{23} and $^{\delta}$Orn at the vertices further

stabilize the dodecamer.[49] Each of the six vertices includes two $A\beta_{25–28}$ loops that extend past the core of the dodecamer without making any substantial intermolecular contacts. The exterior of the dodecamer displays four F_{20} faces (Figure 2.S3). In the crystal lattice, each F_{20} face of one dodecamer packs against an F_{20} face of another dodecamer. Although the asymmetric unit comprises half a dodecamer, the crystal lattice may be thought of as being built of dodecamers.

The electron density map for the X-ray crystallographic structure of peptide **2.2** has long tubes of electron density inside the central cavity of the dodecamer. The shape and length of the electron density is consistent with the structure of Jeffamine M-600, which is an essential component of the crystallization conditions. Jeffamine M-600 is a polypropylene glycol derivative with a 2-methoxyethoxy unit at one end and a 2-aminopropyl unit at the other end. Its average molecular weight is about 600 Da, which corresponds to nine propylene glycol units. Although Jeffamine M-600 is a heterogeneous mixture with varying chain lengths and stereochemistry, we modeled a single stereoisomer with nine propylene glycol units (n = 9) to fit the electron density. The Jeffamine M-600 appears to stabilize the dodecamer by occupying the central cavity and making hydrophobic contacts with residues lining the cavity (Figure 2.S3). In a dodecamer formed by full-length Aβ, the hydrophobic *C*-terminal residues ($A\beta_{37–40}$ or $A\beta_{37–42}$) might play a similar role in filling the dodecamer, and thus create a packed hydrophobic core within the central cavity of the dodecamer.

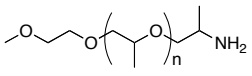

Jeffamine M-600

Annular Pore. Five dodecamers assemble to form an annular porelike structure (Figure 2.5A). Hydrophobic packing between the F_{20} faces of trimers displayed on the outer surface of

each dodecamer stabilizes the porelike assembly. Two morphologically distinct interactions between trimers occur at the interfaces of the five dodecamers: one in which the trimers are eclipsed (Figure 2.5B), and one in which the trimers are staggered (Figure 2.5C). Hydrophobic packing between the side chains of F_{20}, I_{31}, and E_{22} stabilize these interfaces (Figure 2.5D and E). The annular pore contains three eclipsed interfaces and two staggered interfaces. The eclipsed interfaces occur between dodecamers 1 & 2, 1 & 5, and 3 & 4, as shown in Figure 2.5A. The staggered interfaces occur between dodecamers 2 & 3, and 4 & 5. The annular pore is not completely flat, instead, adopting a slightly puckered shape, which accommodates the eclipsed and staggered interfaces. Ten $A\beta_{25–28}$ loops from the vertices of the five dodecamers line the hole in the center of the pore. The hydrophilic side chains of S_{26}, N_{27}, and K_{28} decorate the hole.

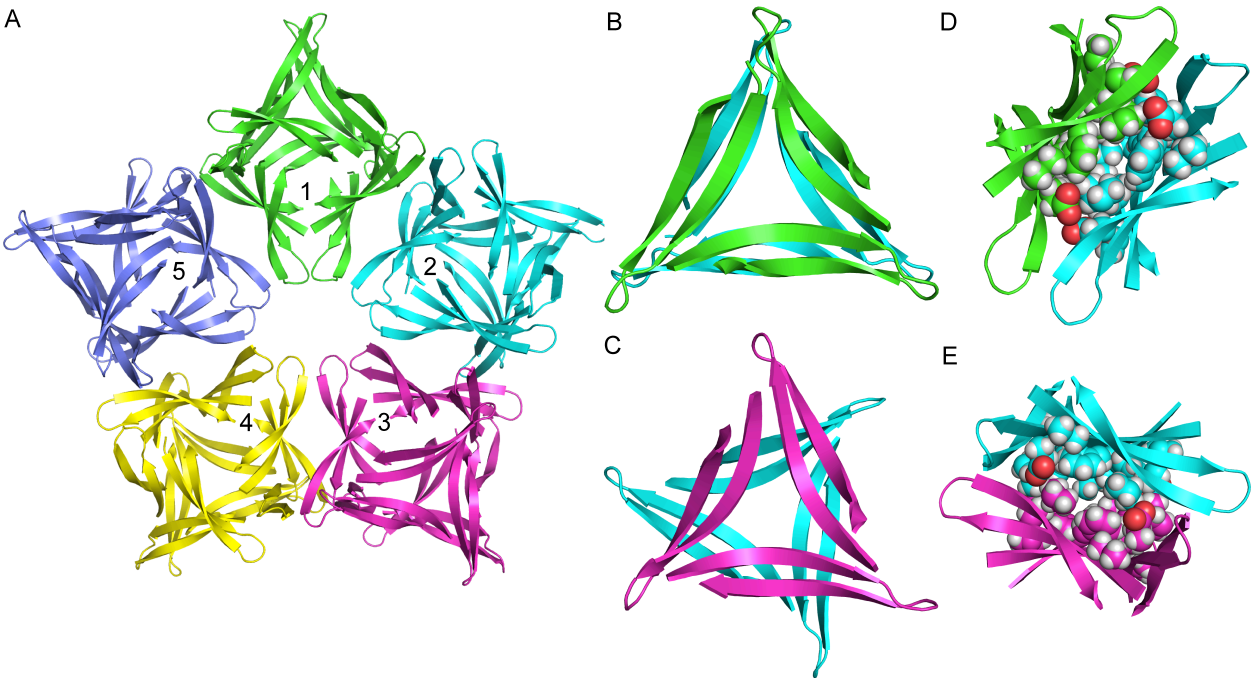

Figure 2.5. X-ray crystallographic structure of the annular pore formed by peptide **2.2**. (A) Annular porelike structure illustrating the relationship of the five dodecamers that form the pore (top view). (B) Eclipsed interface between dodecamers 1 & 2 (side view). The same eclipsed interface also occurs between dodecamers 1 & 5, and 3 & 4. (C) Staggered interface between dodecamers 2 & 3 (side view). The same staggered interface also occurs between dodecamers 4 & 5. (D) Eclipsed interface between dodecamers 1 & 5 (top view). Residues F_{20}, I_{31}, and E_{22} are shown as spheres to detail the hydrophobic packing. (E) Staggered interface between dodecamers 2 & 3 (top view). Residues F_{20}, I_{31}, and E_{22} are shown as spheres to detail the hydrophobic packing.

The annular pore is comparable in size to other large protein assemblies.[50] The outer diameter is ~11–12 nm. The diameter of the hole in the center of the pore is ~2 nm. The thickness of the pore is ~5 nm, which is comparable to that of a lipid bilayer membrane.[51] It is important to note that the annular pore formed by peptide **2.2** is not a discrete unit in the crystal lattice. Rather, the crystal lattice is composed of conjoined annular pores in which all four F_{20} faces on the surface of each dodecamer contact F_{20} faces on other dodecamers (Figure 2.S4). The crystal lattice shows how the dodecamers can further assemble to form larger structures. Each

dodecamer may be thought of as a tetravalent building block with the potential to assemble on all four faces to form higher-order supramolecular assemblies.

Discussion

The X-ray crystallographic study of peptide **2.2** described here provides high-resolution structures of oligomers formed by an $A\beta_{17–36}$ β-hairpin. The crystallographic assembly of peptide **2.2** into a trimer, dodecamer, and annular pore provides a model for the assembly of the full-length Aβ peptide to form oligomers. In this model Aβ folds to form a β-hairpin comprising the hydrophobic central and *C*-terminal regions. Three β-hairpins assemble to form a trimer, and four trimers assemble to form a dodecamer. The dodecamers further assemble to form an annular pore (Figure 2.6).

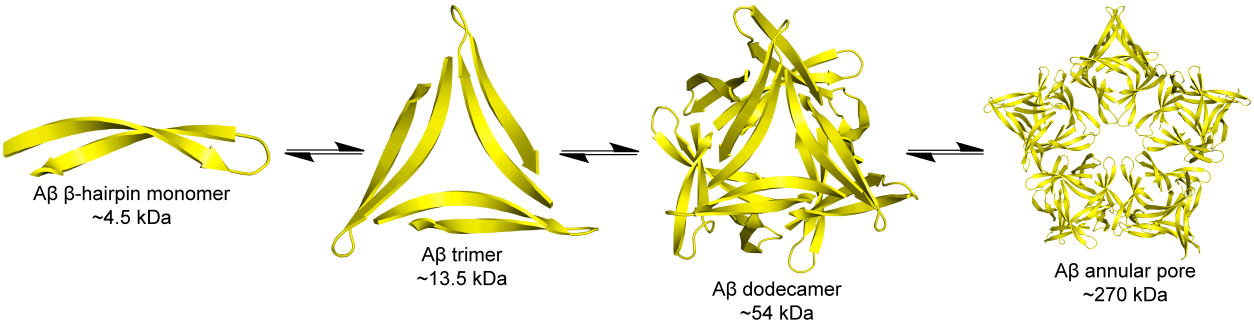

Figure 2.6. Model for the hierarchical assembly of an Aβ β-hairpin into a trimer, dodecamer, and annular pore based on the crystallographic assembly of peptide **2.2**. Monomeric Aβ folds to form a β-hairpin in which the hydrophobic central and *C*-terminal regions form an antiparallel β-sheet. Three β-hairpin monomers assemble to form a triangular trimer. Four triangular trimers assemble to form a dodecamer. Five dodecamers assemble to form an annular pore. The molecular weights shown correspond to an $A\beta_{42}$ monomer (~4.5 kDa), an $A\beta_{42}$ trimer (~13.5 kDa), an $A\beta_{42}$ dodecamer (~54 kDa), and an $A\beta_{42}$ annular pore composed of five dodecamers (~270 kDa).

The model put forth in Figure 2.6 is consistent with the current understanding of endogenous Aβ oligomerization and explains at atomic resolution many key observations about

Aβ oligomers. Two general types of endogenous Aβ oligomers have been observed: Aβ oligomers that occur on a pathway to fibrils, or "fibrillar oligomers", and Aβ oligomers that evade a fibrillar fate, or "non-fibrillar oligomers".[52,53,54] Fibrillar oligomers accumulate in Alzheimer's disease later than non-fibrillar oligomers, and coincide with the deposition of plaques. Non-fibrillar oligomers accumulate early in Alzheimer's disease before plaque deposition.

Fibrillar and non-fibrillar oligomers have structurally distinct characteristics, which are reflected in their reactivity with the fibril-specific OC antibody and the oligomer-specific A11 antibody.[55] Fibrillar oligomers are recognized by the OC antibody, but not the A11 antibody, whereas non-fibrillar oligomers are recognized by the A11 antibody, but not the OC antibody. These criteria have been used to classify the Aβ oligomers that accumulate *in vivo*. Aβ dimers have been classified as fibrillar oligomers, whereas Aβ trimers, Aβ*56, and APFs have been classified as non-fibrillar oligomers.

Larson and Lesné proposed a model for the endogenous production of non-fibrillar oligomers that explains these observations.[53] In this model, folded Aβ monomer assembles into a trimer, the trimer further assembles into hexamers and dodecamers, and the dodecamers further assemble to form annular protofibrils. The hierarchical assembly of peptide **2.2** is consistent with this model; and the trimer, dodecamer and annular pore formed by peptide **2.2** may share similarities to the trimers, Aβ*56, and APFs observed *in vivo*. At this point, we can only speculate whether the trimer and dodecamer formed by peptide **2.2** share structural similarities to Aβ trimers and Aβ*56, as little is known about the structure of Aβ trimers and Aβ*56.

The crystallographically observed annular pore formed by peptide **2.2** is morphologically similar to the APFs formed by full-length Aβ. The annular pore formed by peptide **2.2** is

comparable in size to the APFs prepared *in vitro* or isolated from Alzheimer's brains (Figure 2.7 and Table 2.1). The varying sizes of APFs formed by full-length Aβ might result from differences in the number of oligomer subunits comprising each APF. Although the annular pore formed by peptide **2.2** contains five dodecamer subunits, pores containing fewer or more subunits can easily be envisioned. The dodecamers that comprise the annular pore exhibit two modes of assembly— eclipsed interactions and staggered interactions between the F_{20} faces of trimers within dodecamers. These two modes of assembly might reflect a dynamic interaction between dodecamers, which could permit assemblies of more dodecamers into larger annular pores.

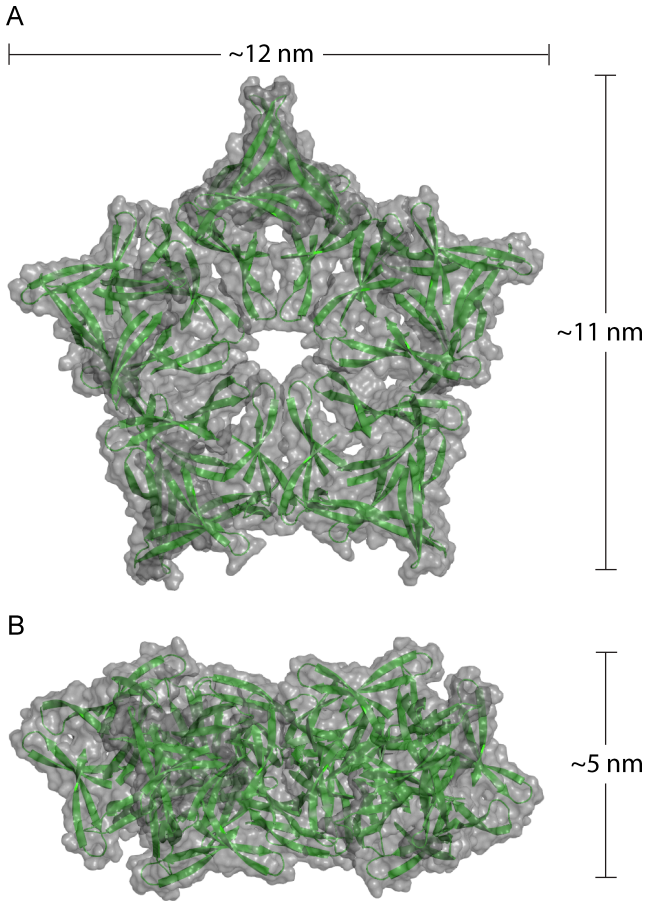

Figure 2.7. Surface views of the annular pore formed by peptide **2.2**. (A) Top view. (B) Side view.

Table 2.1. Annular Pores Formed by Aβ and Peptide 2.2

annular pore source	outer diameter	inner diameter	observation method
peptide **2.2**	~11–12 nm	~2 nm	X-ray crystallography
synthetic Aβ[6]	7–10 nm	1.5–2 nm	TEM
synthetic Aβ[7]	16 nm	not reported	AFM
synthetic Aβ[8]	8–25 nm	not reported	TEM
Alzheimer's brain[10]	11–14 nm	2.5–4 nm	TEM

Dot blot analysis shows that peptide **2.2** is reactive toward the A11 antibody (Figure 2.S5). This reactivity suggests that peptide **2.2** forms oligomers in solution that share structural similarities to the non-fibrillar oligomers formed by full-length Aβ. Further studies are needed to elucidate the species that peptide **2.2** forms in solution and to study their biological properties.

This is an active area of research in our laboratory. Preliminary attempts to study these species by SEC and SDS-PAGE have not provided a clear measure of the structures formed in solution. The difficulty in studying the oligomers formed in solution may reflect the propensity of the dodecamer to assemble on all four F_{20} faces.

The X-ray crystallographic structure and A11 reactivity of peptide **2.2** support the model proposed by Larsen and Lesné and suggest that β-hairpins constitute a fundamental building block for non-fibrillar oligomers.[53] What makes β-hairpins special is that three β-hairpins can nestle together to form trimers, stabilized by a network of hydrogen bonds and hydrophobic interactions. This mode of assembly is not unique to Aβ. The foldon domain of bacteriophage T4 fibritin is composed of three β-hairpins that assemble into a triangular trimer similar to the triangular trimer formed by peptide **2.2**.[56] Additionally, our research group has observed a similar assembly of a β-hairpin peptide derived from β_2-microglobulin.[44]

Conclusion

Although we began these studies with a relatively simple hypothesis—that the trimers and dodecamers formed by peptide **2.1** could accommodate the $A\beta_{24–29}$ loop—an even more exciting finding has emerged—that the dodecamers can assemble to form annular pores. This finding could not have been anticipated from the X-ray crystallographic structure of peptide **2.1** and reveals a new level of hierarchical assembly that recapitulates micrographic observations of annular protofibrils. The crystallographically observed dodecamer, in turn, recapitulates the observation of Aβ*56, which appears to be a dodecamer of Aβ. The crystallographically observed trimer recapitulates the Aβ trimers that are observed even before the onset of symptoms in Alzheimer's disease.

Our approach of constraining $A\beta_{17–36}$ into a β-hairpin conformation and blocking aggregation with an *N*-methyl group has allowed us to crystallize a large fragment of what is generally considered to be an uncrystallizable peptide. We believe this iterative, "bottom up" approach of identifying the minimal modification required to crystallize Aβ peptides will ultimately allow larger fragments of Aβ to be crystallized, thus providing greater insights into the structures of Aβ oligomers.

References and Notes

1 Benilova, I,; Karran, E.; De Strooper, B. *Nat. Neurosci.* **2012**, *15*, 349–357.

2 Lesné, S.; Koh, M. T.; Kotilinek, L.; Kayed, R.; Glabe, C. G.; Yang, A.; Gallagher, M.; Ashe K. H. *Nature* **2006**, *440*, 352–357.

3 Lesné, S. E.; Sherman, M. A.; Grant, M.; Kuskowski, M.; Schneider, J. A.; Bennett D. A.; Ashe, K. H. *Brain* **2013**, *136*, 1383–1398.

4 Hafner, J. H.; Cheung, C. L.; Woolley, A. T.; Lieber, C. M. *Prog. Biophys. Mol. Biol.* **2001**, *77*, 73–110.

5 Lin, H.; Bhatia, R.; Lal, R. *FASEB J.* **2001**, *15*, 2433–2444.

6 Lashuel, H. A.; Hartley, D.; Petre, B. M.; Walz, T.; Lansbury, P. T. Jr. *Nature* **2002**, *418*, 291–292.

7 Quist, A.; Doudevski, I.; Lin, H.; Azimova, R.; Ng, D.; Frangione, B.; Kagan, B.; Ghiso, J.; Lal, R. *Proc. Natl. Acad. Sci. U.S.A.* **2005**, *102*, 10427–10432.

8 Kayed, R.; Pensalfini, A.; Margol, L.; Sokolov, Y.; Sarsoza, F.; Head, E.; Hall, J.; Glabe, C. *J. Biol. Chem.* **2009**, *284*, 4230–4237.

9 Kokubo, H.; Kayed, R.; Glabe, C. G.; Staufenbiel, M.; Saido, T. C.; Iwata, N.; Yamaguchi, H. *Int. J. Alzheimer's Dis.* **2009**, pii: 689285.

10 Lasagna-Reeves, C. A.; Glabe, C. G.; Kayed, R. *J. Biol. Chem.* **2011**, *286*, 22122–22130.

11 Roher, A. E.; Chaney, M. O.; Kuo, Y. M.; Webster, S. D.; Stine, W. B.; Haverkamp, L. J.; Woods, A. S.; Cotter, R. J.; Tuohy, J. M.; Krafft, G. A.; Bonnell, B. S.; Emmerling, M. R. *J. Biol. Chem.* **1996**, *271*, 20631–20635.

12 McLean, C. A.; Cherny, R. A.; Fraser, F. W.; Fuller, S. J.; Smith, M. J.; Beyreuther, K.; Bush, A. I.; Masters, C. L. *Ann. Neurol.* **1999**, *46*, 860–866.

13 McDonald, J. M.; Savva, G. M.; Brayne, C.; Welzel, A. T.; Forster, G.; Shankar, G. M.; Selkoe, D. J.; Ince, P. G.; Walsh, D. M. *Brain* **2010**, *133*, 1328–1341.

14 Shankar, G. M,; Li, S.; Mehta, T. H.; Garcia-Munoz, A.; Shepardson, N. E.; Smith, I,; Brett, F. M.; Farrell, M. A.; Rowan, M. J.; Lemere, C. A.; Regan, C. M.; Walsh, D. M.; Sabatini, B. L.; Selkoe, D. J. *Nat. Med.* **2008**, *14*, 837–842.

15 Jin, M.; Shepardson, N.; Yang, T.; Chen, G.; Walsh, D.; Selkoe, D. J. *Proc Natl Acad Sci U.S.A.* **2011**, *108*, 5819–5824.

16 Mucke, L.; Masliah, E.; Yu, G. Q.; Mallory, M.; Rockenstein, E. M.; Tatsuno, G.; Hu, K.; Kholodenko, D.; Johnson-Wood, K.; McConlogue, L. *J. Neurosci.* **2000**, *20*, 4050–4058.

17 Kawarabayashi, T.; Younkin, L. H.; Saido, T. C.; Shoji, M.; Ashe, K. H.; Younkin, S. G. *J. Neurosci.* **2001**, *21*, 372–381.

18 Kawarabayashi, T.; Shoji, M.; Younkin, L. H.; Wen-Lang, L.; Dickson, D. W.; Murakami, T.; Matsubara, E.; Abe, K.; Ashe, K. H.; Younkin, S. G. *J. Neurosci.* **2004**, *24*, 3801–3809.

19 Meilandt, W. J.; Cisse, M.; Ho, K.; Wu, T.; Esposito, L. A.; Scearce-Levie, K.; Cheng, I. H.; Yu, G. Q.; Mucke, L. *J. Neurosci.* **2009**, *29*, 1977–1986.

20 Shankar, G. M.; Leissring, M. A.; Adame, A.; Sun, X.; Spooner, E.; Masliah, E.; Selkoe, D. J.; Lemere, C. A.; Walsh, D. M. *Neurobiol. Dis.* **2009**, *36*, 293–302.

21 Benzinger, T. L.; Gregory, D. M.; Burkoth, T. S.; Miller-Auer, H.; Lynn, D. G.; Botto, R. E.; Meredith, S. C. *Proc. Natl. Acad. Sci. U.S.A.* **1998**, *95*, 13407–13412.

22 Petkova, A. T, Leapman, R. D.; Guo, Z.; Yau, W. M.; Mattson, M. P.; Tycko, R. *Science* **2005**, *307*, 262–265.

23 Lührs, T.; Ritter, C.; Adrian, M.; Riek-Loher, D.; Bohrmann, B.; Döbeli, H.; Schubert, D.; Riek, R. *Proc. Natl. Acad. Sci. U.S.A.* **2005**, *102*, 17342–17347.

24 Petkova, A. T.; Yau, W. M.; Tycko, R. *Biochemistry* **2006**, *45*, 498–512

25 Paravastu, A. K.; Petkova, A. T.; Tycko, R. *Biophys. J.* **2006**, *90*, 4618–4629.

26 Lu, J. X.; Qiang, W.; Yau, W. M.; Schwieters, C. D.; Meredith, S. C.; Tycko, R. *Cell* **2013**, *154*, 1257–1268.

27 Xiao, Y.; Ma, B.; McElheny, D.; Parthasarathy, S.; Long, F.; Hoshi, M.; Nussinov, R.; Ishii, Y. *Nat. Struct. Mol. Biol.* **2015**, *22*, 499–505.

28 Sawaya, M. R.; Sambashivan, S.; Nelson, R.; Ivanova, M. I.; Sievers, S. A.; Apostol, M. I.; Thompson, M. J.; Balbirnie, M.; Wiltzius, J. J.; McFarlane, H. T.; Madsen, A. Ø.; Riekel, C.; Eisenberg, D. *Nature* **2007**, *447*, 453–457.

29 Colletier, J. P.; Laganowsky, A.; Landau, M.; Zhao, M.; Soriaga, A. B.; Goldschmidt, L.; Flot, D.; Cascio, D.; Sawaya, M. R.; Eisenberg, D. *Proc. Natl. Acad. Sci. U.S.A*. **2011**, *108*, 16938–16943.

30 Yu, L.; Edalji, R.; Harlan, J. E.; Holzman, T. F.; Lopez, A. P.; Labkovsky, B.; Hillen, H.; Barghorn, S.; Ebert, U.; Richardson, P. L.; Miesbauer, L.; Solomon, L.; Bartley, D.; Walter, K.; Johnson, R. W.; Hajduk, P. J.; Olejniczak, E. T. *Biochemistry* **2009**, *48*, 1870–1877.

31 Scheidt, H. A.; Morgado, I.; Huster, D. *J. Biol. Chem.* **2012**, *287*, 22822–22826.

32 Doi, T.; Masuda, Y.; Irie, K.; Akagi, K.; Monobe, Y.; Imazawa, T.; Takegoshi, K. *Biochem. Biophys. Res. Commun.* **2012**, *428*, 458–462.

33 Gu, L.; Liu, C.; Guo, Z. *J. Biol. Chem.* **2013**, *288*, 18673–18683.

34 Tay, W. M.; Huang, D.; Rosenberry, T. L.; Paravastu, A. K. *J. Mol. Biol.* **2013**, *425*, 2494–2508.

35 Potapov, A.; Yau, W.-M.; Ghirlando, R.; Thurber, K. R.; Tycko, R. *J. Am. Chem. Soc*. **2015**, *137*, 8294-8307.

36 Hoyer, W.; Grönwall, C.; Jonsson, A.; Ståhl, S.; Härd, T. *Proc. Natl. Acad. Sci. U.S.A*. **2008**, *105*, 5099–6104.

37 Sandberg, A.; Luheshi, L. M.; Söllvander, S.; Pereira de Barros, T.; Macao, B.; Knowles, T. P.; Biverstål, H.; Lendel, C.; Ekholm-Petterson, F.; Dubnovitsky, A.; Lannfelt, L.; Dobson, C. M.; Härd, T. *Proc. Natl. Acad. Sci. U.S.A*. **2010**, *107*, 15595–15600.

38 Lendel *et al*. recently reported the NMR structure of a hexameric peptide barrel formed by this disulfide constrained Aβ: Lendel, C.; Bjerring, M.; Dubnovitsky, A.; Kelly, R. T.; Filippov, A.; Antzutkin, O. N.; Nielsen, N. C.; Härd, T. *Angew. Chem. Int. Ed. Engl.* **2014**, *53*, 12756–12760.

39 Spencer, R. K.; Li. H.; Nowick, J. S. *J. Am. Chem. Soc.* **2014**, *136*, 5595–5598.

40 Nowick, J. S.; Lam, K. S.; Khasanova, T. V.; Kemnitzer, W. E.; Maitra, S.; Mee, H. T.; Liu, R. *J. Am. Chem. Soc*. **2002**, *124*, 4972-4973.

41 We also created a peptide with an *N*-methyl group at position F20. This peptide forms oligomers with structures similar to those formed by peptide **2.1**.

42 Spencer, R. K.; Nowick, J. S. *Isr. J. Chem.* **2015**, *55*, 698–710.

43 Santiveri, C. M.; León, E.; Rico, M.; Jiménez, M. A. *Chem. Eur. J.* **2008**, *14*, 488–499.

44 Spencer, R. K.; Kreutzer, A. G.; Salveson, P. J.; Li, H.; Nowick, J. S. *J. Am. Chem. Soc.* **2015**, *137*, 6304–6311.

45 Spencer, R.; Chen, K. H.; Manuel, G.; Nowick, J. S. *Eur. J. Org. Chem*. **2013**, *2013*, 3523–3528.

46 Kabsch,W. *Acta. Crystallogr. D, Biol. Crystallogr.* **2010**, *66*, 125–132

47 Weik, M.; Ravelli, R. B.; Kryger, G.; McSweeney, S.; Raves, M. L.; Harel, M.; Gros, P.; Silman, I.; Kroon, J.; Sussman, J. L. *Proc. Natl. Acad. Sci. U.S.A.* **2000**, *97*, 623–628.

48 Leiros, H. K.; McSweeney, S. M.; Smalås, A. O. *Acta. Crystallogr. D, Biol. Crystallogr.* **2001**, *57*, 488–497.

49 The δOrn in peptide **2.2** replaces K16 in Aβ. In a dodecamer of full-length Aβ, the side chain of K16 could form a salt bridge with the side chain of D23.

50 Pieters, B. J.; van Eldijk, M. B.; Nolte, R. J.; Mecinović, J. *Chem. Soc. Rev.* **2015**, *45*, 24–39.

51 Butterfield, S. M.; Lashuel, H. A. *Angew. Chem. Int. Ed. Engl.* **2010**, *49*, 5628–5654.

52 Glabe, C. G. *J. Biol. Chem.* **2008**, *283*, 29639–29643.

53 Larson, M. E.; Lesné, S. E. *J. Neurochem.* **2012**, *120*, 125–139.

54 Liu, P.; Reed, M. N.; Kotilinek, L. A.; Grant, M. K.; Forster, C. L.; Qiang, W.; Shapiro, S. L.; Reichl, J. H.; Chiang, A. C.; Jankowsky, J. L.; Wilmot, C. M.; Cleary, J. P.; Zahs, K. R.; Ashe, K. H. *Cell Rep*. **2015** *11*, 1760–1771.

55 Kayed, R.; Head, E.; Thompson, J. L.; McIntire, T. M.; Milton, S. C.; Cotman, C. W.; Glabe, C. G. *Science* **2003**, *300*, 486–489.

56 Tao, Y.; Strelkov, S. V.; Mesyanzhinov, V. V.; Rossmann, M. G. *Structure* **1997**, *5*, 789–798.

Supporting Information

Table of Contents

Supplemental Figures and Table

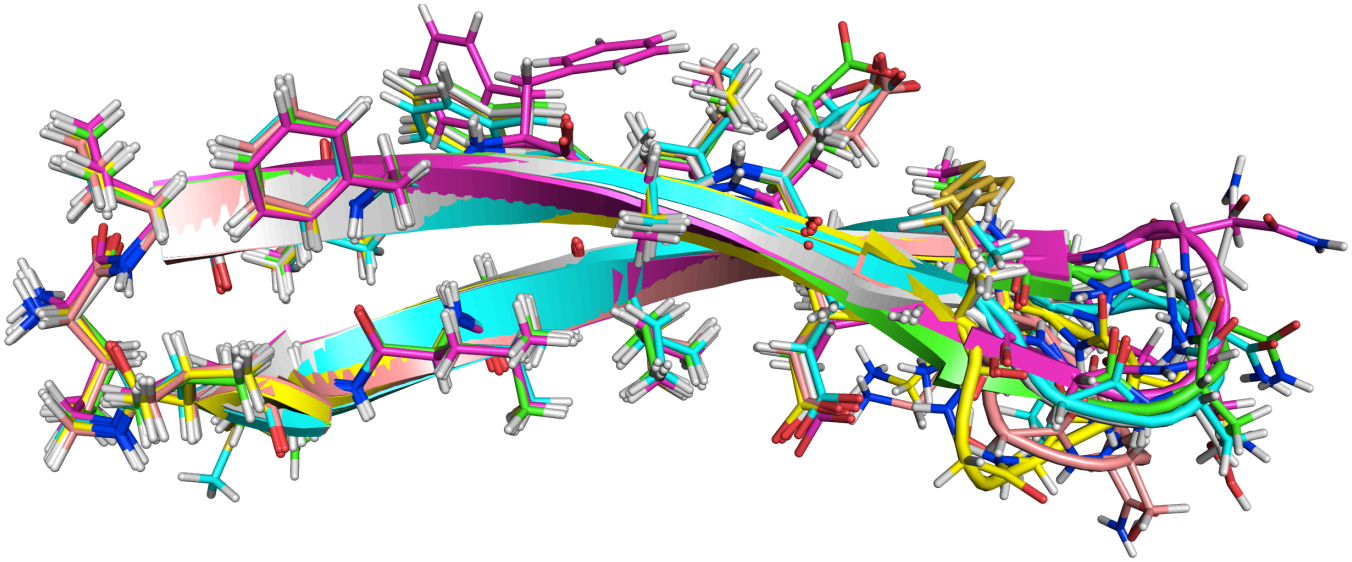

Figure 2.S1. Alignment of the six monomers in the asymmetric unit of peptide **2.2**.

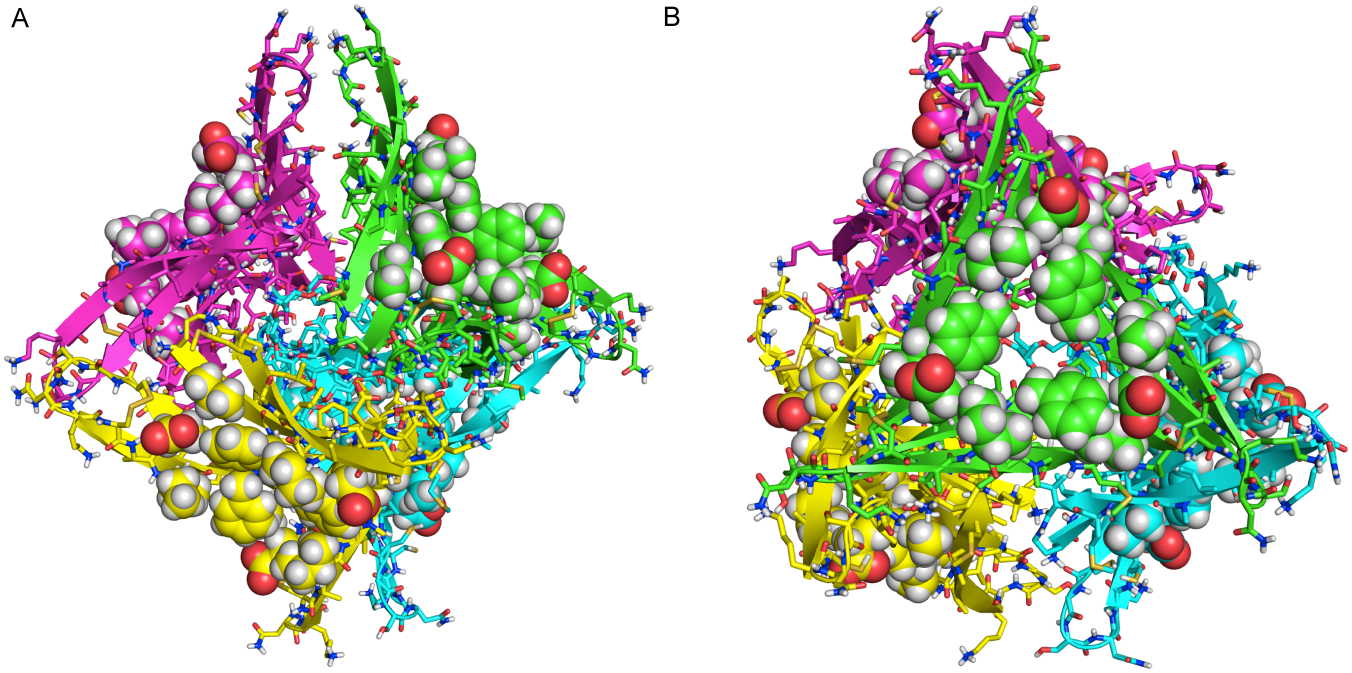

Figure 2.S2. The dodecamer formed by peptide **2.2** displays four F_{20} faces. (A) Octahedral shape of the dodecamer. The residues of the four F_{20} faces of trimers that comprise the dodecamer are shown as spheres. (B) Tetrahedral arrangement of trimers that comprise the dodecamer. The residues of the four F_{20} faces of trimers that comprise the dodecamer are shown as spheres.

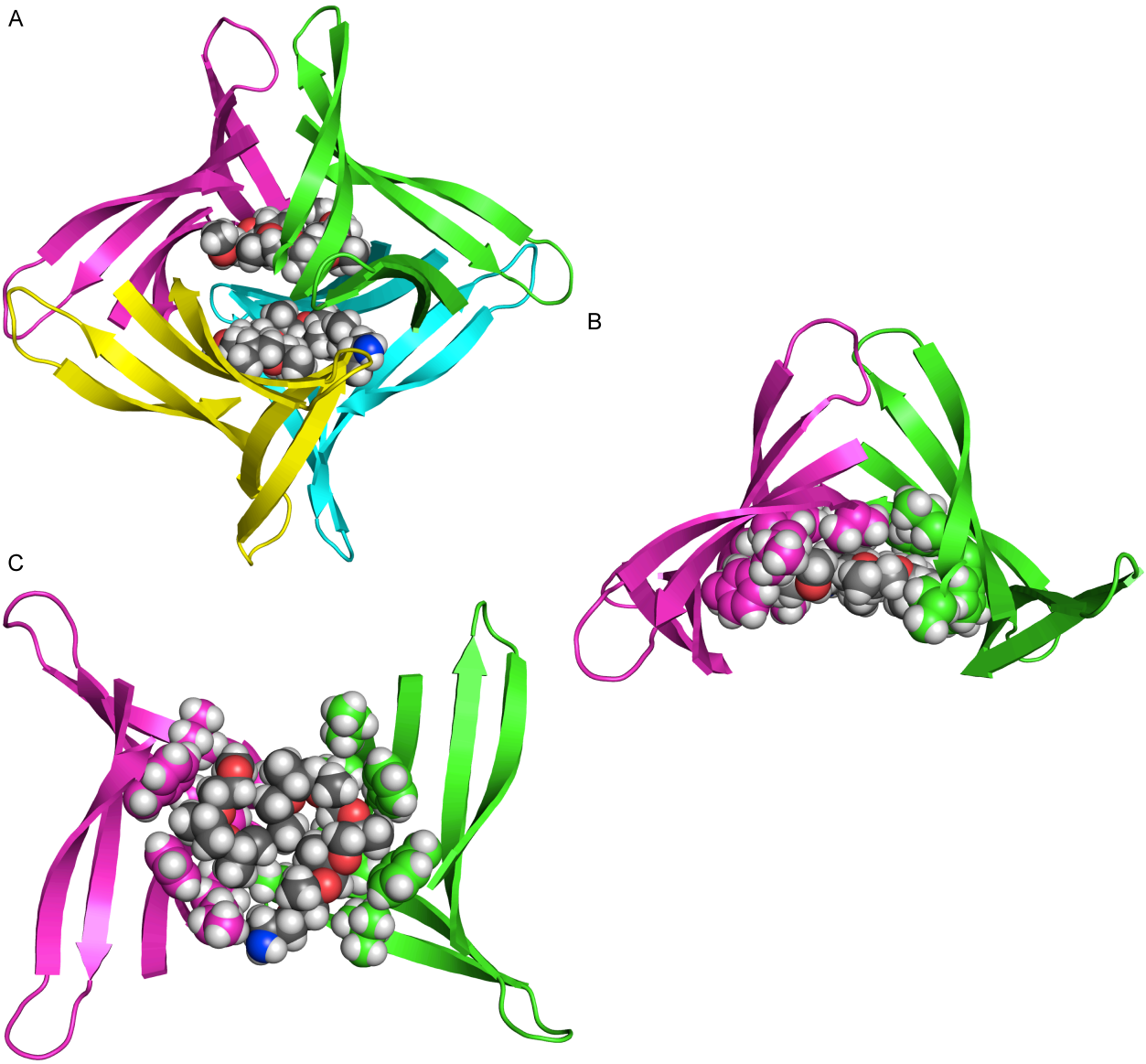

Figure 2.S3. Jeffamine M-600 occupies the central cavity of the dodecamer. (A) The dodecamer formed by peptide **2.2** (cartoons) showing two molecules—one per asymmetric unit—of Jeffamine M-600 (grey) occupying the central cavity of the dodecamer. (B) View of two trimer subunits (magenta and green) from inside the cavity of the dodecamer. In panels B and C Jeffamine M-600 (grey) and key side chains are shown as spheres to illustrate the hydrophobic packing that occurs between Jeffamine M-600 and the side chains that line the central cavity. (C) Side view of two trimer subunits.

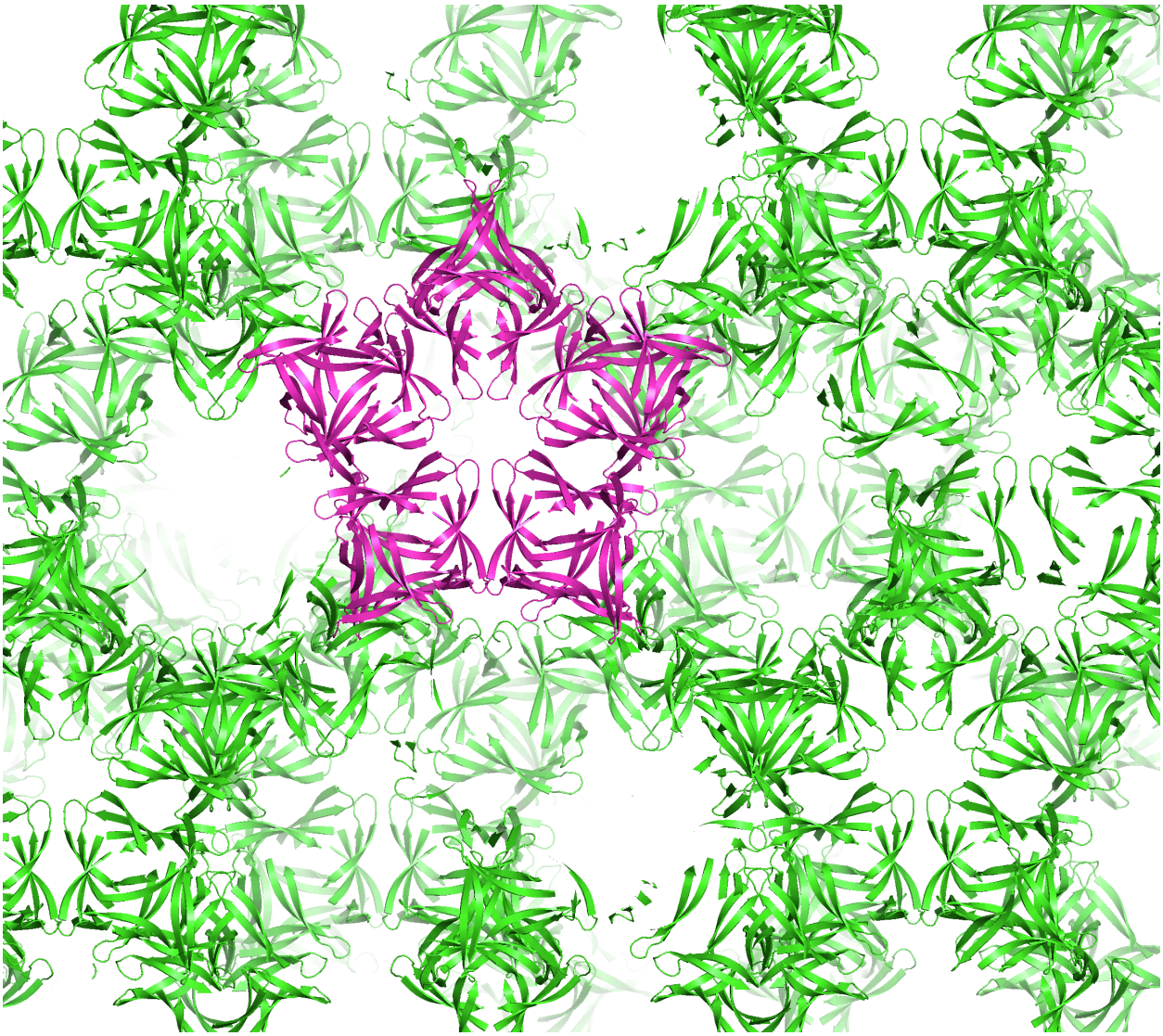

Figure 2.S4. View of the annular pore formed by peptide **2.2** within the crystal lattice.

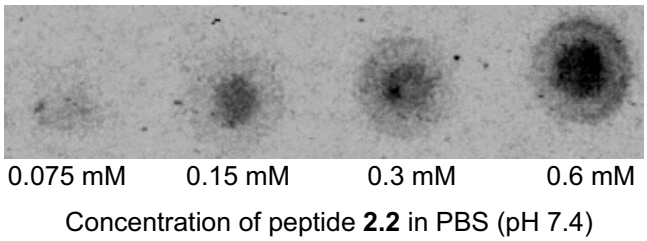

Figure 2.S5. Dot blot showing reactivity of peptide **2.2** with the A11 antibody.

Table 2.S1. Crystallographic properties, crystallization conditions, and data collection and model refinement statistics for peptides **2.2** and **2.4**.

peptide	peptide **2.2** (synchrotron)	peptide **2.2** (X-ray diffractometer)	peptide **2.4** (X-ray diffractometer)
PDB ID	5HOX	5HOY	5HOW
space group	$P6_122$	$P6_122$	$P6_122$
a, *b*, *c* (Å)	97.37, 97.37, 97.59	97.65, 97.65, 97.78	97.31, 97.31, 97.62
α, β, λ (°)	90, 90, 120	90, 90, 120	90, 90, 120
peptide per asymmetric unit	6	6	6
crystallization conditions	0.1 M HEPES, pH 7.1, 29% Jeffamine M-600	0.1 M HEPES, pH 7.1, 29% Jeffamine M-600	0.1 M HEPES, pH 6.4, 31% Jeffamine M-600
		Data collection	
wavelength (Å)	1.00	1.54	1.54
resolution (Å)	30.35–1.9 (1.968–1.900)	28.19–2.295 (2.377–2.295)	28.09–2.295 (2.377–2.295)
total reflections	44136 (4348)	25663 (2527)	25402 (2476)
unique reflections	22069 (2173)	12832 (1264)	12701 (1238)
multiplicity	2.0 (2.0)	2.0 (2.0)	2.0 (2.0)
completeness (%)	99 (100)	100 (100)	100 (99)
mean I/σ	13.82 (0.59)	11.44 (1.01)	15.73 (1.41)
Wilson B factor	46.44	55.58	49.69
R_{merge}	0.01344 (0.9116)	0.03762 (0.6526)	0.05629 (0.4378)
$R_{measure}$	0.019 (1.289)	0.05321 (0.9229)	0.07961 (0.6191)
$CC_{1/2}$	1 (0.597)	0.999 (0.275)	0.994 (0.528)
CC^*	1 (0.865)	1 (0.657)	0.999 (0.831)
		Refinement	
R_{work}	0.2199 (0.4081)	0.2446 (0.3921)	0.2415 (0.3656)
R_{free}	0.2505 (0.4048)	0.2755 (0.4228)	0.2700 (0.4170)
number of non-hydrogen atoms	1020	1011	973
RMS_{bonds}	0.027	0.021	0.025
RMS_{angles}	1.67	0.91	1.24
Ramachandran favored (%)	93	90	88
outliers (%)	0.97	0	0
clashscore	2.53	1.52	0.00
average B-factor	76.90	72.49	70.28
Number of TLS groups	15	13	17

Materials and Methods

Scheme 2.S1. Synthesis of peptide **2.2**.

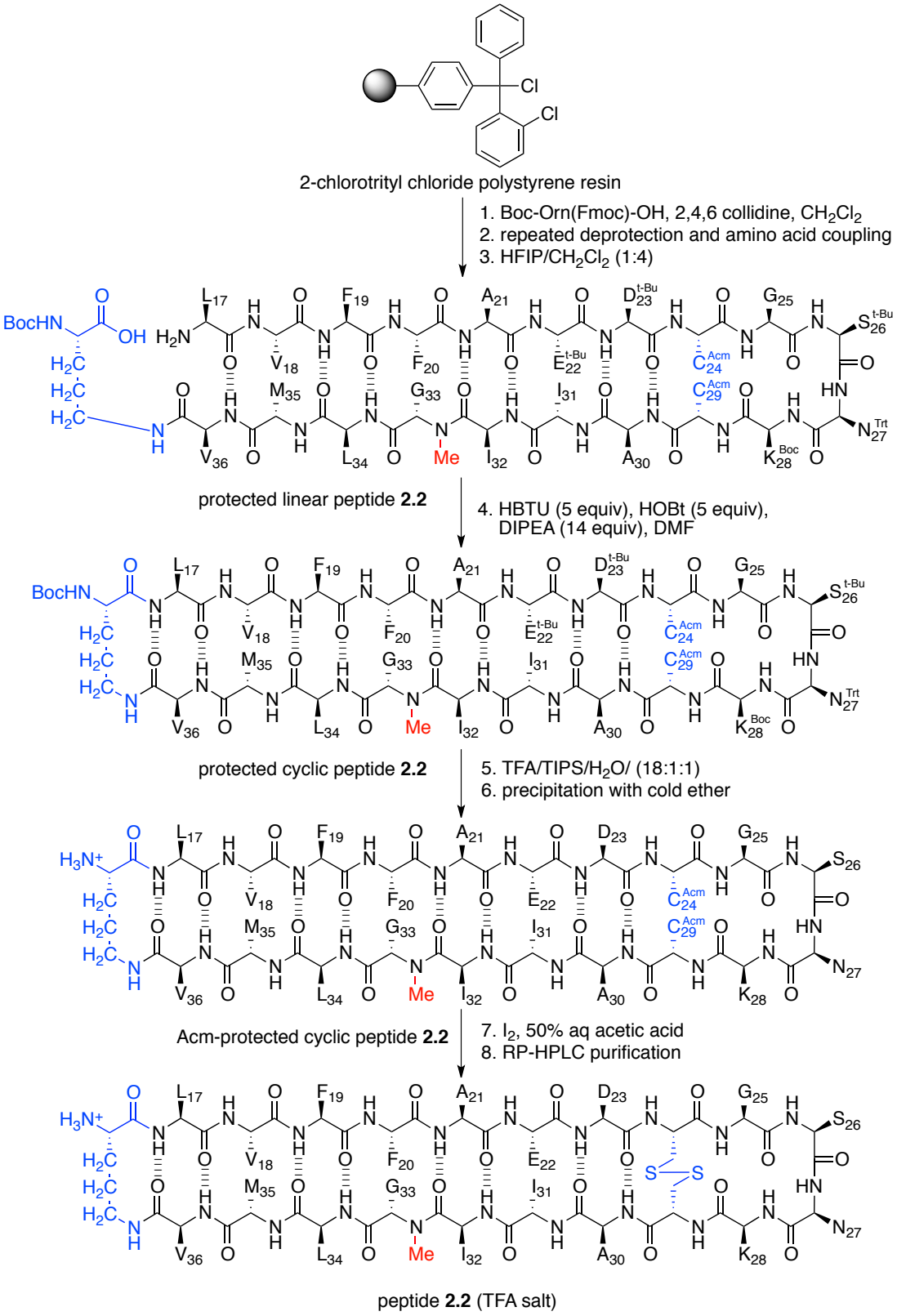

General information

All chemicals were used as received unless otherwise noted. Methylene chloride (CH_2Cl_2) was passed through alumina under nitrogen prior to use. Anhydrous, amine free dimethylformamide (DMF) was purchased from Alfa Aesar. Analytical reverse-phase HPLC was performed on an Agilent 1200 equipped with an Aeris PEPTIDE 2.6u XB-C18 column (Phenomonex). Semi-preparative reverse-phase HPLC was performed on a Beckman Gold Series P equipped with a Zorbax SB-C18 column (Agilent). HPLC grade acetonitrile and 18 MΩ H_2O, each containing 0.1% trifluoroacetic acid (TFA), were used for analytical and semi-preparative reverse-phase HPLC. All peptides were prepared and used as the trifluoroacetate salts, and were assumed to have one trifluoroacetic acid per ammonium group on each peptide.

*Synthesis of peptides **2.2**–**2.4***[1]

a. *Loading of the resin.* 2-Chlorotrityl chloride resin (300 mg, 1.2 mmol/g) was added to a Bio-Rad Poly-Prep chromatography column (10 mL, 0.8×4.0 cm). The resin was suspended in dry CH_2Cl_2 (10 mL) and allowed to swell for 30 min. The solution was drained from the resin and a solution of Boc-Orn(Fmoc)-OH (0.50 equiv, 82 mg, 0.18 mmol) in 6% (v/v) 2,4,6-collidine in dry CH_2Cl_2 (8 mL) was added immediately and the mixture was gently agitated for 12 h. The solution was then drained and a mixture of CH_2Cl_2/MeOH/*N*,*N*-diisopropylethylamine (DIPEA) (17:2:1, 10 mL) was added immediately. The mixture was gently agitated for 1 h to cap the unreacted 2-chlorotrityl chloride resin sites. The resin was then washed with dry CH_2Cl_2 (2x) and dried by passing nitrogen through the vessel. This procedure typically yields 0.12–0.15 mmol of loaded resin (0.4–0.5 mmol/g loading).

b. *Peptide coupling.* The 2-chlorotrityl-Orn(Fmoc)-Boc generated from the previous step was transferred to a microwave-assisted solid-phase peptide synthesizer reaction vessel and

submitted to cycles of automated peptide coupling with Fmoc-protected amino acid building blocks using a CEM Liberty 1 Automated Microwave Peptide Synthesizer. The linear peptide was synthesized from *C*-terminus to the *N*-terminus. Each coupling cycle consisted of i. Fmoc-deprotection with 20% (v/v) piperidine in DMF for 2 min. at 50 °C (2x), ii. washing with DMF (3x), iii. coupling of the amino acid (0.75 mmol, 5 equiv) in the presence of HCTU (0.675 mmol, 4.5 equiv) and 20% *N*-methylmorpholine (NMM) in DMF for 10 min. at 50 °C, iv. washing with DMF (3x). After coupling of the last amino acid, the terminal Fmoc group was removed with 20% (v/v) piperidine in DMF (10 min. 50 °C). The resin was transferred from the reaction vessel of the peptide synthesizer to a Bio-Rad Poly-Prep chromatography column.

c. *Cleavage of the peptide from the resin.* The linear peptide was cleaved from the resin by agitating the resin for 1 h with a solution of 1,1,1,3,3,3-hexafluoroisopropanol (HFIP) in CH_2Cl_2. (1:4, 7 mL).[2] The suspension was filtered and the filtrate was collected in a 250 mL round-bottomed flask. The resin was washed with additional HFIP in CH_2Cl_2 (1:4, 7 mL) and then with CH_2Cl_2 (2×10 mL). The combined filtrates were concentrated by rotary evaporation to give a white solid. The white solid was further dried by vacuum pump to afford the crude protected linear peptide, which was macrolactamized without further purification.

d. *Macrolactamization of the linear peptide.* The crude protected linear peptide was dissolved in dry DMF (150 mL). HOBt (114 mg, 0.75 mmol, 5 equiv) and HBTU (317 mg, 0.75 mmol, 5 equiv) were added to the solution. DIPEA (0.33 mL, 1.8 mmol, 12 equiv) was added to the solution and the mixture was stirred under nitrogen for 24 h. The mixture was concentrated under reduced pressure to afford the crude protected cyclic peptide.

e. *Global deprotection of the acid-labile protecting groups.* The protected cyclic peptide was dissolved in TFA/triisopropylsilane (TIPS)/H_2O (18:1:1, 20 mL) in a 250 mL round-

bottomed flask equipped with a nitrogen-inlet adaptor. The solution was stirred for 1.5 h. The reaction mixture was then concentrated by rotary evaporation under reduced pressure to afford the crude cyclic peptide (peptide **2.3**), or the crude Acm-protected cyclic peptide (peptide **2.2** or peptide **2.4**) as a thin yellow film on the side of the round-bottomed flask. Peptide **2.3** was immediately subjected to purification by reverse-phase HPLC (RP-HPLC), as described below. Peptides **2.2** and **2.4** were precipitated with ice-cold ether and the Acm groups were removed to afford a disulfide linked cyclic peptide.

f. *Ether precipitation of peptides **2.2** and **2.4**.* The yellow film was dissolved in trifluoroacetic acid (TFA) (3 mL) and transferred in 0.5 mL aliquots to six different 15 mL polypropylene conical tubes. Ice-cold ether (14 mL) was added to each conical tube to precipitate the peptide. The peptide was pelleted by centrifugation and the supernatant was discarded [CAUTION: the conical tubes must be sealed tightly during centrifugation]. The peptide pellets were dissolved in acetonitrile (~10 mL per pellet), transferred to a 1 L round-bottomed flask, and the solution was concentrated by rotary evaporation under reduced pressure to afford a white solid. The white solid was further dried by vacuum pump to afford the crude Acm-protected cyclic peptide. The Acm groups were removed and the disulfide linkage was formed without further purification.

g. *Acm deprotection and disulfide linkage formation.* The 1 L flask containing the Acm-protected peptide was charged with 250 mL of 50% (v/v) aq acetic acid and swirled to dissolve the peptide. A 25 mL portion of 1.0 M HCl and a 5 mL portion of a solution of 0.10 M I_2 in glacial acetic acid was added, and the flask was fitted with a nitrogen-inlet adaptor. The solution was stirred magnetically for 2 h. The progress of the reaction was monitored by RP-HPLC and electrospray ionization mass spectrometry (ESI-MS). The reaction mixture was then

concentrated by rotary evaporation under reduced pressure to afford the crude disulfide-linked peptide as a brown solid. The brown solid was dissolved in TFA, and precipitated with ice-cold ether as described in the preceding section to afford the crude disulfide-linked peptide as an off-white solid.

h. *Reversed-phase HPLC purification of peptides **2.2**–**2.4***. The peptide was dissolved in H_2O and acetonitrile (7:3, 10 mL), and the solution was filtered through a 0.2 μm syringe filter and purified by RP-HPLC (gradient elution with 20-50% CH_3CN over 50 min). The pure fractions were lyophilized to afford 15 mg of peptide **2.3**, 9 mg of peptide **2.4**, and 10 mg of peptide **2.2**.

*Crystallization procedure for peptides **2.2**–**2.4***[1]

Initial crystallization conditions were determined using the hanging-drop vapor-diffusion method. Crystallization conditions were screened for peptides **2.3** and **2.4** using three crystallization kits in a 96-well plate format (Hampton Index, PEG/Ion, and Crystal Screen). Three 150 nL hanging drops that differed in the ratio of peptide to well solution were made per condition in each 96-well plate for a total of 864 experiments. Hanging drops were made by combining an appropriate volume of peptide **2.3** (10 mg/mL in 18 MΩ water) or peptide **2.4** (10 mg/mL in 18 MΩ water) with an appropriate volume of well solution to create three 150 nL hanging drops with 1:1, 1:2, and 2:1 peptide:well solution. The hanging drops were made using a TTP LabTech Mosquito nanodisperse instrument. Peptide **2.3** did not grow crystals in any of the 864 conditions screened. Crystals of peptide **2.4** grew rapidly (~72 h) in a solution of 0.1 M HEPES buffer at pH 7.0 and Jeffamine M-600 at pH 7.0 (30% v/v).

We did not screen crystallization conditions for peptide **2.2**, as it afforded crystals suitable for X-ray diffraction in the same conditions, and with the same peptide concentration (10 mg/mL 18 MΩ water) as peptide **2.4**. Peptide **2.2** forms a cloudy suspension when a 10 mg/mL solution in 18 MΩ water is prepared. To better solvate peptide **2.2** for crystallographic experiments we sonicated the 10 mg/mL solution for ~2 h until it was less cloudy.

We optimized crystallization conditions for peptides **2.2** and **2.4** using a 4x6 matrix Hampton VDX 24-well plate. We varied the HEPES buffer pH in each row in increments of 0.5 pH units (6.5, 7.0, 7.5, and 8.0) and the pH 7.0 Jeffamine M-600 concentration in each column in increments of 2% (24%, 26%, 28%, 30%, 32%, and 34% v/v). For the first well in the 4x6 matrix we combined 100 μL of 1 M HEPES at pH 6.5, 480 μL of a 50% (v/v) solution of pH 7.0 Jeffamine M-600, and 420 μL of 18 MΩ water. [The 50% pH 7.0 Jeffamine M-600 solution was prepared by combining 200 mL of Jeffamine M-600 (pH 10) and 200 mL of 18 MΩ water, titrating with hydrochloric acid to pH 7.0, and filtering through a 0.2 μm syringe filter]. The other wells were prepared in analogous fashion, by combining 100 μL of HEPES buffer of varying pH, pH 7.0 Jeffamine M-600 in varying amounts, and 18 MΩ water for a total volume of 1 mL in each well.

Three hanging-drops were prepared per borosilicate glass slide by combining a solution of peptides **2.2** or **2.4** (1 μL, 10 mg/mL) and the well solution (1 μL) in a ratio of 1:1, 2:1, and 1:2. Slides were inverted and pressed firmly against the silicone grease surrounding each well. Crystals of peptides **2.2** and **2.4** grew in ~72 h. Crystallization conditions were further optimized using smaller variations in HEPES buffer pH (in increments of 0.25 pH units) and Jeffamine M-600 concentrations (in increments of 1%). Crystals were harvested with a nylon loop attached to

a copper or steel pin and flash frozen in liquid nitrogen prior to data collection. The optimized crystallization conditions for peptides **2.2** and **2.4** are summarized in Table 2.S1.

*X-ray crystallographic data collection, data processing, and structure determination for peptides **2.2** and **2.4.***

Diffraction data for peptides **2.2** and **2.4** were collected on a Rigaku Micromax-007HF X-ray diffractometer with a rotating copper anode at 1.54 Å wavelength with 0.5° oscillation. Diffraction data were collected using CrystalClear. Diffraction data were scaled and merged using XDS.[4] Coordinates for the anomalous signals were determined by HySS in the Phenix software suite 1.10.1.[4] Electron density maps were generated using anomalous coordinates determined by HySS as initial positions in Autosol. Molecular manipulations of the models were performed with Coot. Coordinates were refined with phenix.refine.

Diffraction data for peptide **2.2** were also collected at Lawrence Berkeley National Laboratory (Berkeley, California) on synchrotron beamline 8.2.1 at 1.00 Å wavelength with 0.5° oscillation and a detector distance of 220 mm.[3] Diffraction data were scaled and merged using XDS.[4] Electron density maps were generated by isomorphous replacement of coordinates from peptide **2.4** using Phaser in software suite Phenix 1.10.1.[5] Molecular manipulations of the models were performed with Coot.[6] Coordinates were refined with phenix.refine.

*Dot blot analysis of peptide **2.2**.*

A 10 mg/mL (3.85 mM) stock solution of peptide **2.2** was prepared gravimetrically by dissolving 1.27 mg of peptide in 127 μL of 18 MΩ water. The stock solution was sonicated for at

least 2 h to further solvate the peptide. An aliquot of the stock solution was diluted with 18 MΩ water to make a 1.2 mM solution, which was serially diluted with 18 MΩ water to create 0.6 mM, 0.3mM, and 0.15 mM solutions of peptide **2.2**. A 5 μL aliquot of each solution from the serial dilution was combined with 5 μL a 2X solution of phosphate buffered saline (PBS) at pH 7.4 to create 0.6 mM, 0.3 mM, 0.15 mM, and 0.075 mM buffered solutions of peptide **2.2**. A 1 μL aliquot of each buffered solution of peptide **2.2** was spotted onto nitrocellulose membrane, and allowed to air dry (~5 min). The weight of peptide spotted onto the membrane from the 0.6 mM, 0.3 mM, 0.15 mM, and 0.075 mM solutions corresponds to 1.5 μg, 0.75 μg, 0.38 μg, and 0.19 μg, respectively. Non-reactive sites were blocked with 10% non-fat milk in low-Tween tris-buffered saline (TBS-lT: 20 mM Tris, 137 mM NaCl, 0.01% Tween 20, pH 7.6) for 1 h at room temperature with rocking. The membrane was washed with TBS-lT for 5 min (3X). The membrane was then incubated while rocking overnight at 4 °C in primary A11 antibody (200 μg/mL) in 5% milk in TBS-lT. The next day, the membrane was washed with TBS-lT for 5 min (3X). The membrane was then incubated while rocking with horseradish peroxidase conjugated goat anti-rabbit antibody (100 μg/mL) (Jackson ImmunoResearch catalog# 111-035-003) in 5% milk in TBS-lT for 1 h at room temperature. The membrane was then washed with TBS-lT for 5 min (3X). A 10 mL portion of chemiluminescence substrate (Thermo Scientific SuperSignal West Femto Maximum Sensitivity Substrate, product# 34095) was prepared according to manufacture's protocol and poured onto the membrane. The membrane was allowed to incubate in the chemiluminescence substrate for ~10 min before imaging. The blot was imaged using a standard SLR camera.[7]

References and Notes

1 These procedures follow closely those that our laboratory has previously published, with the exception that we used a CEM Liberty 1 automated microwave peptide synthesizer instead of a Protein Technologies PS3 peptide synthesizer and that we used Acm-protected Cys to introduce disulfide linkages. The procedures in this section are adapted from and in some cases taken verbatim from Spencer, R. K.; Kreutzer, A. G.; Salveson, P. J.; Li, H.; Nowick, J. S. *J. Am. Chem. Soc.* **2015**, *137*, 6304–6311.

2 Bollhagen, R.; Schmiedberger, M.; Barlosb, K.; Grell, E. *J. Chem. Soc., Chem. Commun.*, **1994**, 2559–2560.

3 The Berkeley Center for Structural Biology is supported in part by the National Institutes of Health, National Institute of General Medical Sciences, and the Howard Hughes Medical Institute. The Advanced Light Source is supported by the Director, Office of Science, Office of Basic Energy Sciences, of the U.S. Department of Energy under Contract No. DE-AC02-05CH11231.

4 Kabsch, W. *Acta Cryst.*, **2010**, *D66*, 125–132.

5 Adams, P. D.; Afonine, P. V.; Bunkóczi, G.; Chen, V. B.; Davis, I. W.; Echols, N.; Headd, J. J.; Hung, L.-W.; Kapral, G. J.; Grosse-Kunstleve, R. W.; McCoy, A. J.; Moriarty, N. W.; Oeffner, R.; Read, R. J.; Richardson, D. C.; Richardson, J. S.; Terwilliger, T. C.; Zwart., P. H. *Acta Cryst.*, **2010**, *D66*, 213–221.

6 Emsley, P.; Lohkamp, B.; Scott, W. G.; Cowtan, K. *Acta. Cryst.*, **2010**, *D66*, 486–501.

7 Khoury, M. K.; Parker, I.; Aswad, D.W. *Anal. Biochem.* **2010**, *397*, 129–131

Characterization Data

*Characterization of peptide **2.2***

Analytical HPLC trace of peptide **2.2**.

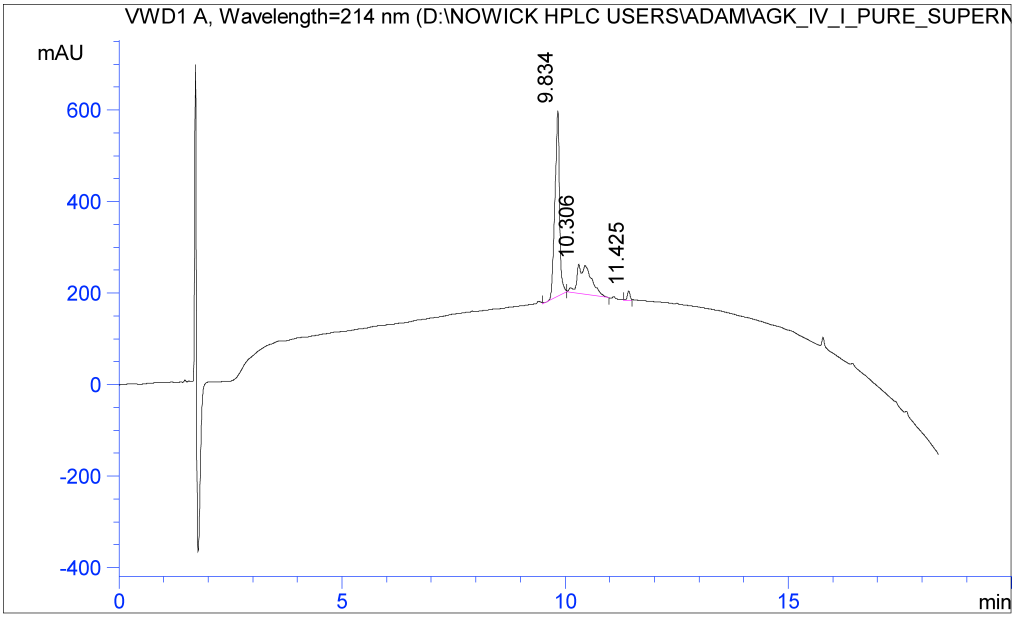

Peak #	RT [min]	Type	Width [min]	Area mAU*s	Height [mAU]	Area %
1	9.834	MM	0.118	2879.515	82.701	65.992
2	10.306	MM	0.362	1386.542	12.913	31.776
3	11.425	MM	0.075	97.364	4.386	2.231

Mass spectra of peptide **2.2.**

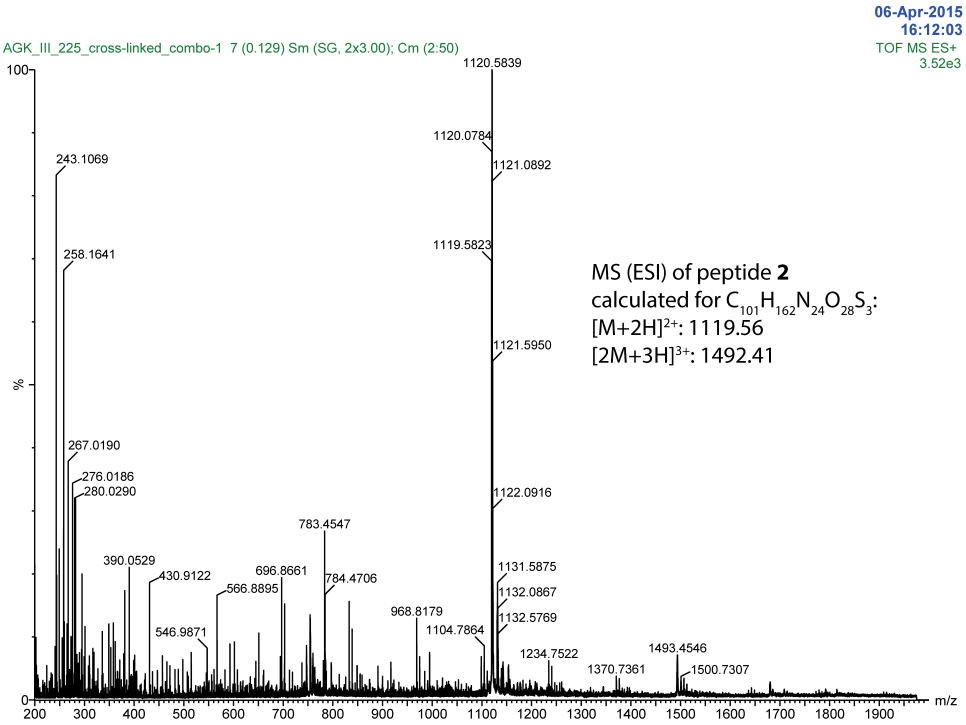

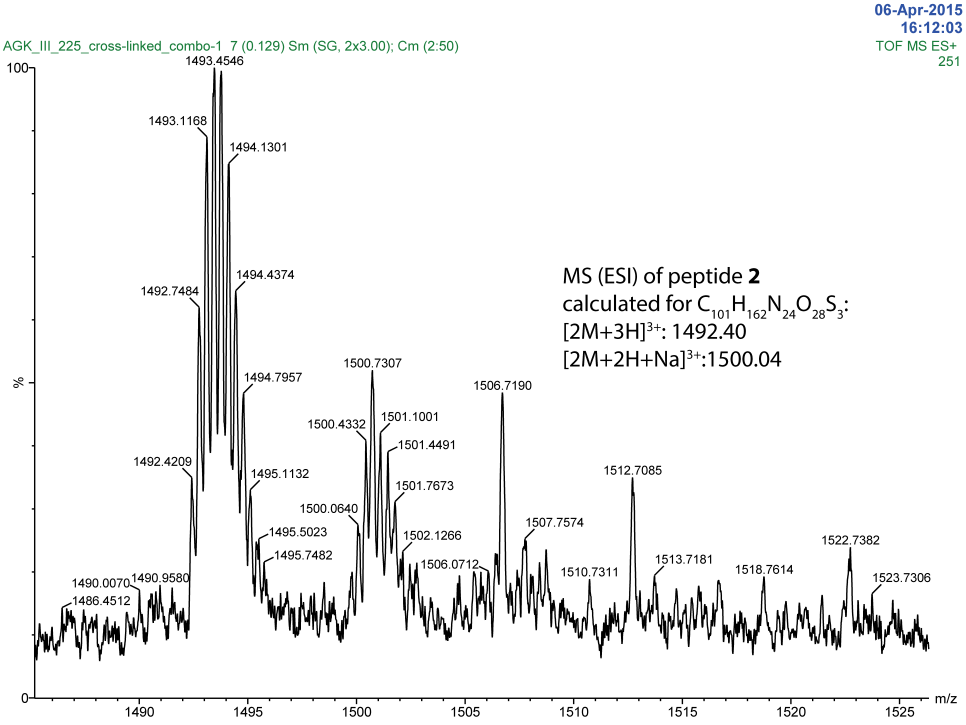

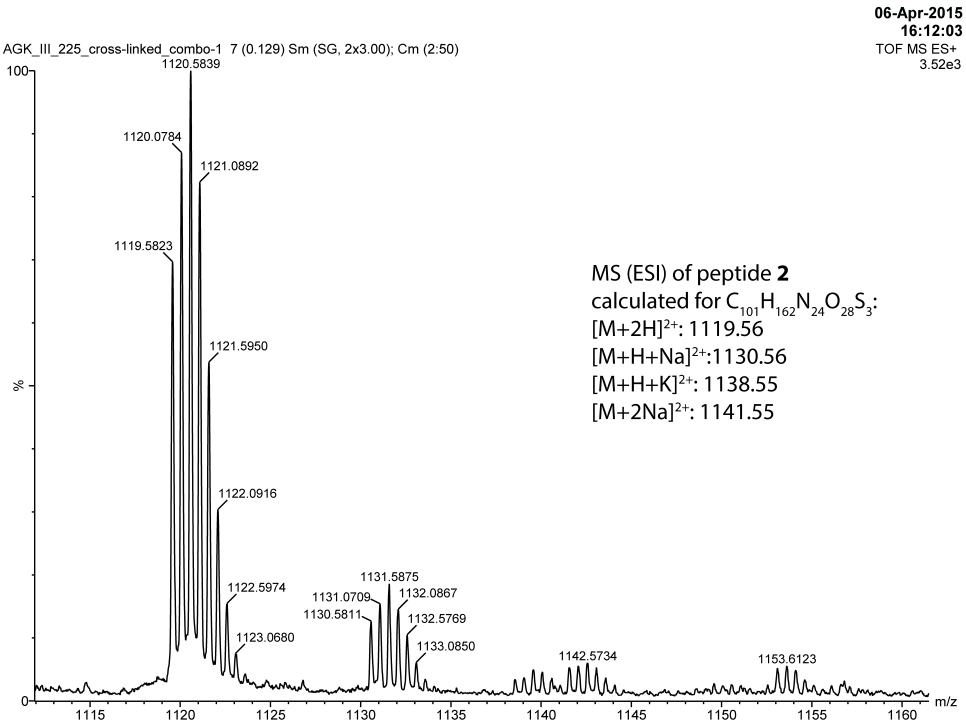
06-Apr-2015
16:12:03
AGK_III_225_cross-linked_combo-1 7 (0.129) Sm (SG, 2x3.00); Cm (2:50)
TOF MS ES+
3.52e3
1120.5839
1120.0784
1121.0892
1119.5823
1121.5950
1122.0916
1122.5974
1123.0680
1131.5875
1131.0709
1132.0867
1130.5811
1132.5769
1133.0850
1142.5734
1153.6123
%
m/z
MS (ESI) of peptide 2
calculated for C101H162N24O28S3:
[M+2H]2+: 1119.56
[M+H+Na]2+:1130.56
[M+H+K]2+: 1138.55
[M+2Na]2+: 1141.55

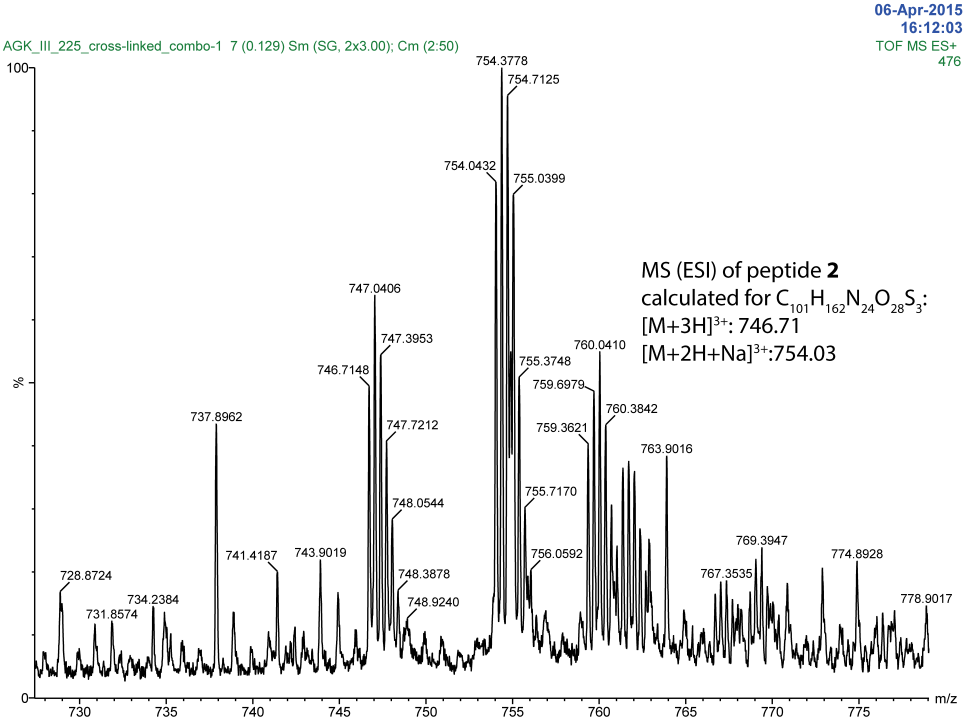
06-Apr-2015
16:12:03
AGK_III_225_cross-linked_combo-1 7 (0.129) Sm (SG, 2x3.00); Cm (2:50)
TOF MS ES+
476
754.3778
754.7125
754.0432
755.0399
747.0406
747.3953
746.7148
760.0410
755.3748
759.6979
737.8962
747.7212
760.3842
759.3621
763.9016
748.0544
755.7170
741.4187
743.9019
756.0592
769.3947
774.8928
728.8724
748.3878
767.3535
734.2384
748.9240
778.9017
731.8574
%
m/z
MS (ESI) of peptide 2
calculated for C101H162N24O28S3:
[M+3H]3+: 746.71
[M+2H+Na]3+:754.03

*Characterization of peptide **2.3***

Analytical HPLC trace of peptide **2.3**.

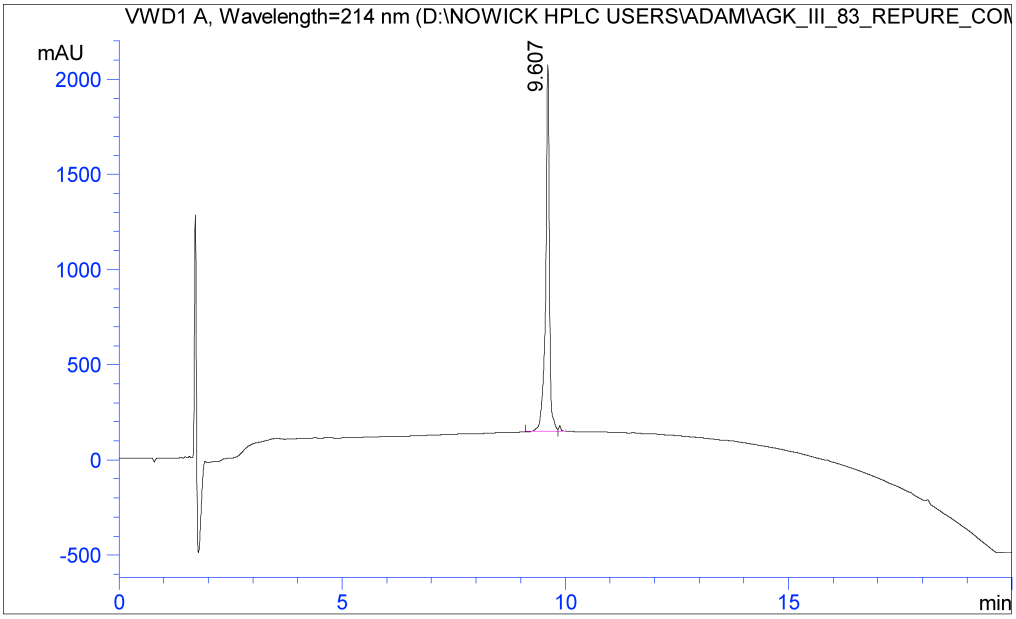

Peak #	RT [min]	Type	Width [min]	Area mAU*s	Height [mAU]	Area %
1	9.607	VV	0.194	38855.883	100.000	100.000

Mass spectra of peptide **2.3.**

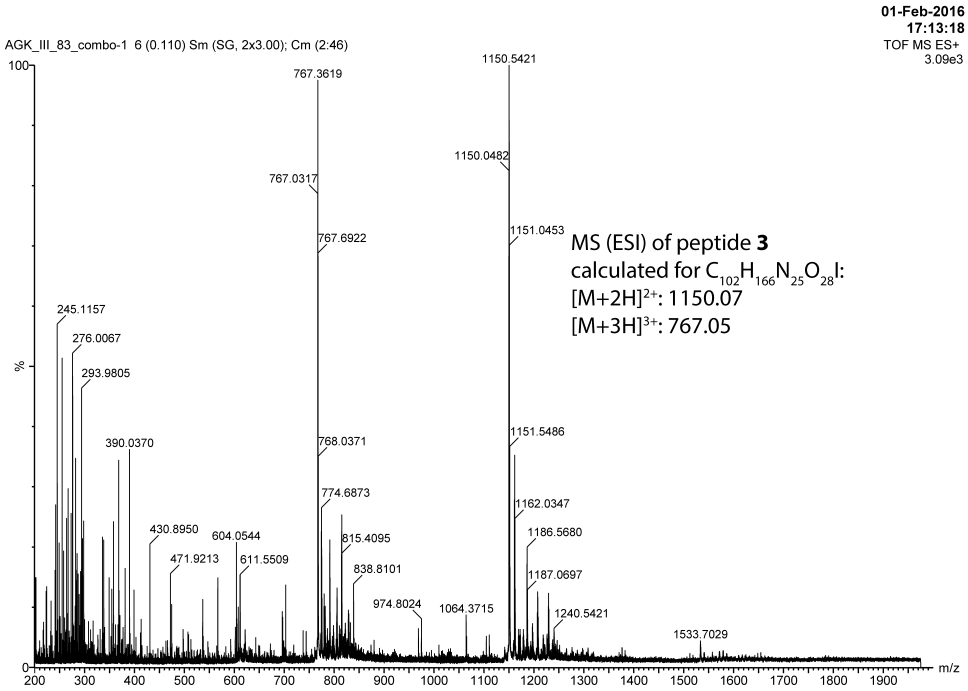

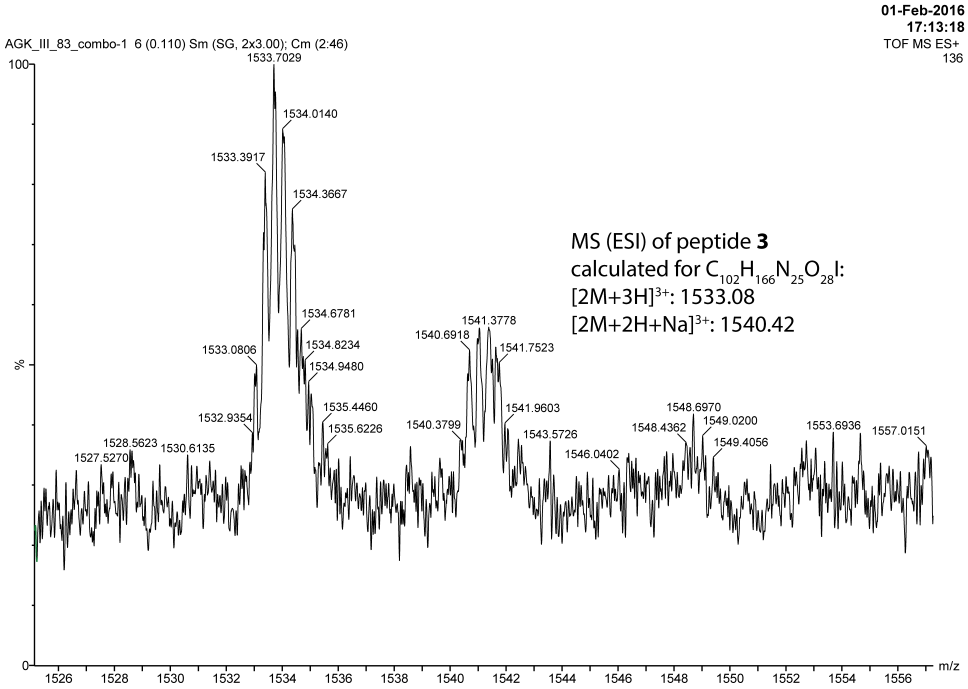

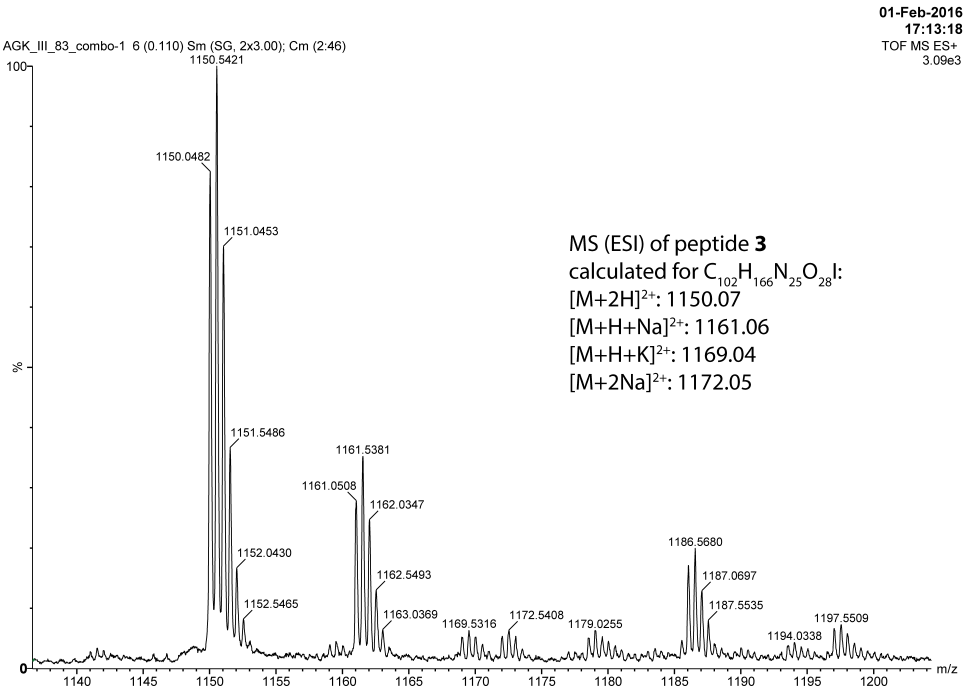
01-Feb-2016
17:13:18
TOF MS ES+
3.09e3
AGK_III_83_combo-1 6 (0.110) Sm (SG, 2x3.00); Cm (2:46)
1150.5421
1150.0482
1151.0453
1151.5486
1161.5381
1161.0508
1162.0347
1152.0430
1162.5493
1152.5465
1163.0369
1169.5316
1172.5408
1179.0255
1186.5680
1187.0697
1187.5535
1194.0338
1197.5509
MS (ESI) of peptide 3
calculated for C102H166N25O28I:
[M+2H]2+: 1150.07
[M+H+Na]2+: 1161.06
[M+H+K]2+: 1169.04
[M+2Na]2+: 1172.05
%
m/z

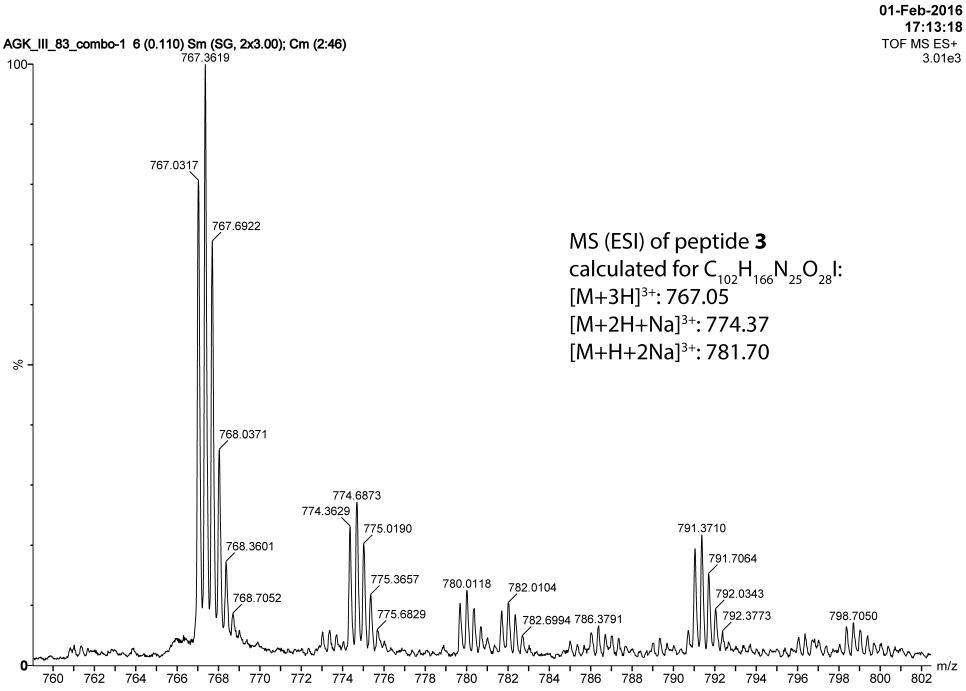
01-Feb-2016
17:13:18
TOF MS ES+
3.01e3
AGK_III_83_combo-1 6 (0.110) Sm (SG, 2x3.00); Cm (2:46)
767.3619
767.0317
767.6922
768.0371
774.6873
774.3629
775.0190
768.3601
775.3657
780.0118
782.0104
768.7052
775.6829
782.6994
786.3791
791.3710
791.7064
792.0343
792.3773
798.7050
MS (ESI) of peptide 3
calculated for C102H166N25O28I:
[M+3H]3+: 767.05
[M+2H+Na]3+: 774.37
[M+H+2Na]3+: 781.70
%
m/z

*Characterization of peptide **2.4***

Analytical HPLC trace of peptide **2.4**.

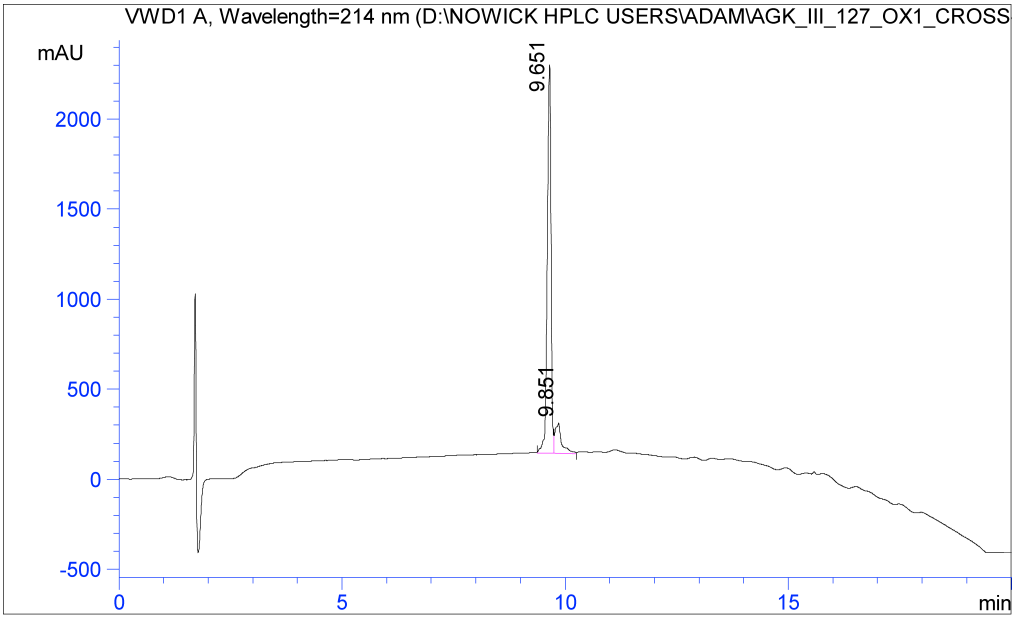

Signal 1:VWD1 A, Wavelength=214 nm

Peak #	RT [min]	Type	Width [min]	Area mAU*s	Height [mAU]	Area %
1	9.651	BV	0.094	12783.123	92.780	87.948
2	9.851	VV	0.136	1751.695	7.220	12.052

Mass spectra of peptide **2.4.**

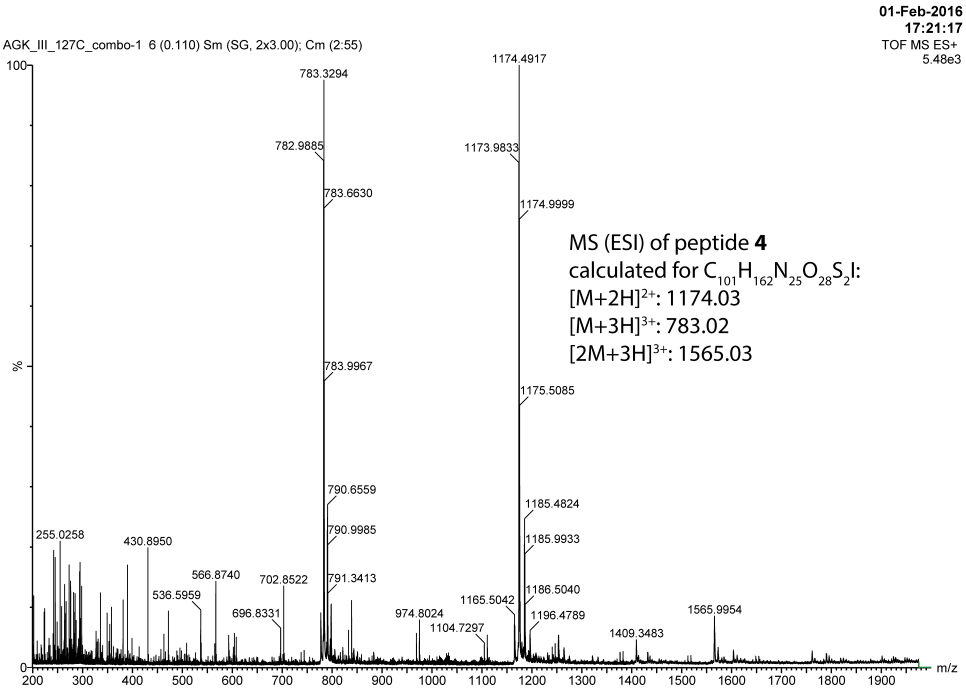

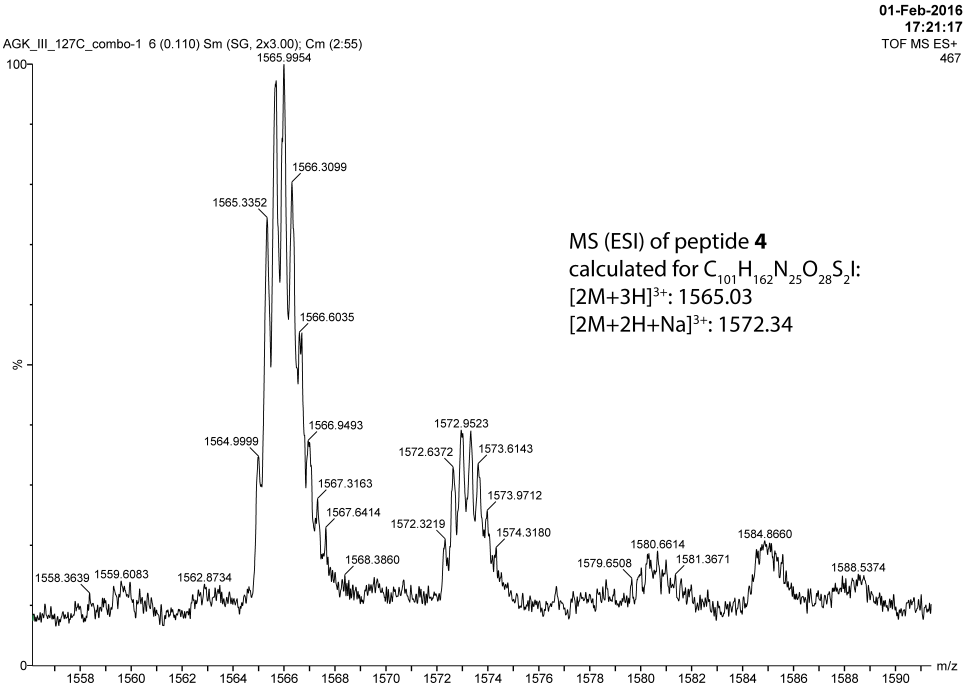

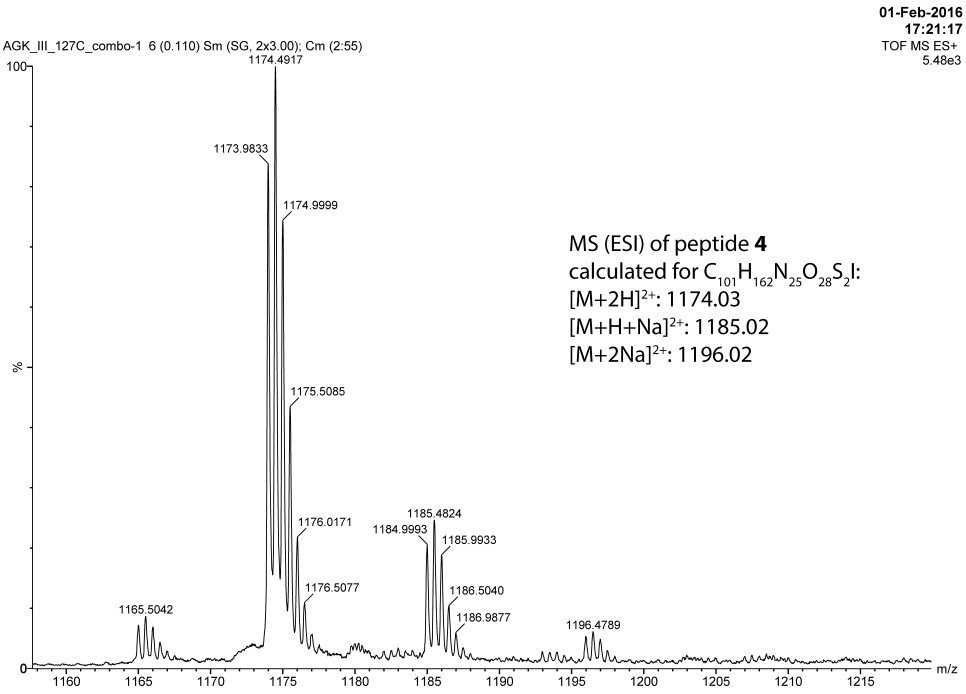

MS (ESI) of peptide **4**
calculated for $C_{101}H_{162}N_{25}O_{28}S_2I$:
$[M+2H]^{2+}$: 1174.03
$[M+H+Na]^{2+}$: 1185.02
$[M+2Na]^{2+}$: 1196.02

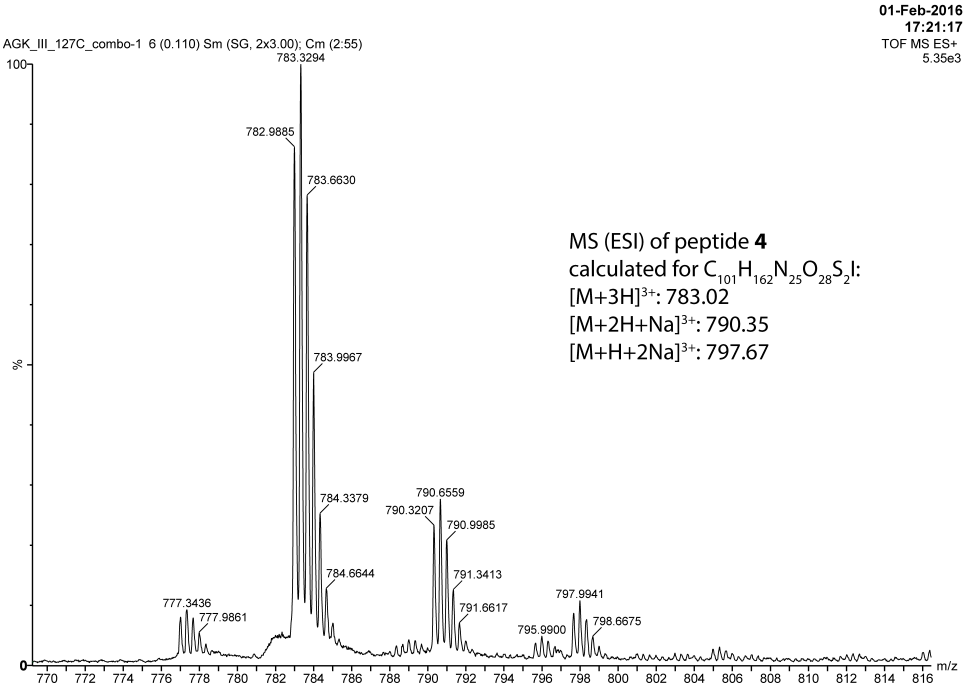

MS (ESI) of peptide **4**
calculated for $C_{101}H_{162}N_{25}O_{28}S_2I$:
$[M+3H]^{3+}$: 783.02
$[M+2H+Na]^{3+}$: 790.35
$[M+H+2Na]^{3+}$: 797.67

Chapter 3

Stabilization, Assembly, and Toxicity of Trimers Derived from Aβ

Introduction

In Alzheimer's disease, the β-amyloid peptide Aβ assembles to form a multitude of soluble oligomers as well as insoluble fibrils.[1,2] The Aβ oligomers have emerged as neurotoxic agents that lead to neurodegeneration in Alzheimer's disease. The heterogeneity and metastability of the Aβ oligomers presents a tremendous challenge in understanding the molecular basis of Alzheimer's disease. Specifically, the lack of homogeneous oligomers precludes detailed correlation of the biological properties of Aβ oligomers with their structural and biophysical properties.

To reduce the heterogeneity among assemblies of the Aβ peptide, researchers have prepared and studied Aβ oligomers that consist of Aβ monomers linked by chemical crosslinks.[3,4,5,6,7,8,9] These studies have helped determine the importance of different residues in Aβ oligomerization and have demonstrated that $A\beta_{40}$ and $A\beta_{42}$ form different types of oligomers. Crosslinked oligomers have been found to be toxic toward rat pheochromocytoma (PC12) cells and to inhibit long-term potentiation in rats, providing evidence for the role of Aβ oligomers in neurodegeneration in Alzheimer's disease. Although crosslinking Aβ decreases the heterogeneity of Aβ oligomers, crosslinking has not yet produced structurally homogeneous oligomers. The high-resolution structures of the crosslinked oligomers that have been generated thus far, through either a single disulfide bond or through photo-induced crosslinking of unmodified proteins (PICUP), remain unknown.

In the past couple of years, our laboratory has identified and elucidated hitherto undiscovered modes of supramolecular assembly of macrocyclic β-sheet peptides derived from amyloidogenic peptides and proteins.[10,11,12,13] We previously reported the X-ray crystallographic structures of two homologous trimers formed by two macrocyclic β-sheet peptides derived from $A\beta_{17-36}$.[10,14] These peptides contain $A\beta_{17-23}$ and $A\beta_{30-36}$ β-strands covalently linked by two δ-linked ornithine ($^{\delta}$Orn) turn mimics and are designed to mimic an $A\beta_{17-36}$ β-hairpin.[15] Figure 3.1 illustrates these peptides, **3.1** and **3.2**, and shows their relationship to an $A\beta_{17-36}$ β-hairpin. The $^{\delta}$Orn that connects residues D_{23} and A_{30} replaces the $A\beta_{24-29}$ loop; the $^{\delta}$Orn that connects residues L_{17} and V_{36} reinforces β-sheet structure.[16] We incorporated ornithine (α-linked) as a hydrophilic isostere of methionine at position 35 to improve the solubility of the peptides.[14] Peptides **3.1** and **3.2** both contain an *N*-methyl group to block uncontrolled aggregation: peptide **3.1** contains an *N*-methyl group on G_{33}; peptide **3.2** contains an *N*-methyl group on F_{20}.

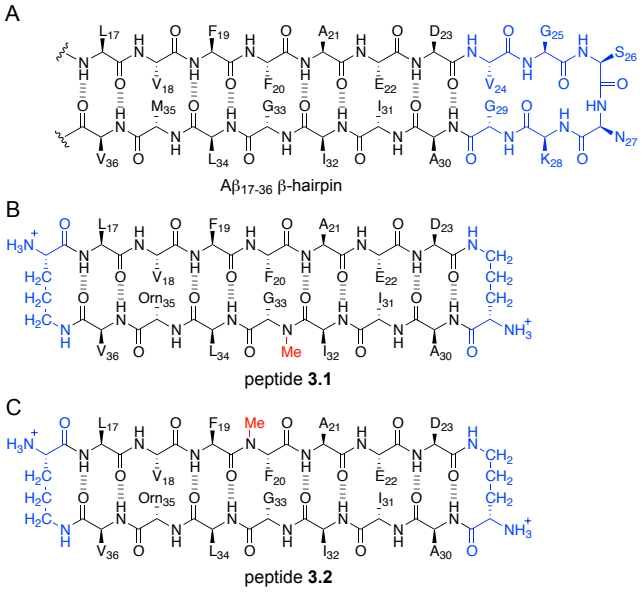

Figure 3.1. Chemical structures of an $A\beta_{17–36}$ β-hairpin and peptides **3.1** and **3.2**. The $A\beta_{24–29}$ loop region of the $A\beta_{17–36}$ β-hairpin is shown in blue to illustrate its relationship to the $^{\delta}$Orn that connects D_{23} and A_{30} in peptides **3.1** and **3.2**.

X-ray crystallography revealed that peptides **3.1** and **3.2** fold to form β-hairpins that assemble to form oligomers. In the X-ray crystallographic structures of peptides **3.1** and **3.2**, three β-hairpins assemble in a triangular fashion to form trimers, which are stabilized by hydrogen bonding and hydrophobic interactions between monomers (Figure 3.2). At the three corners of each trimer, the main chain of residue V_{18} on one macrocyclic β-sheet hydrogen bonds with the main chain of residue E_{22} on the adjacent macrocyclic β-sheet. Clustering between hydrophobic residues at the corners of each trimer provides additional stability. In the crystal lattice, the trimers further assemble to form hexamers and dodecamers. The trimers, hexamers, and dodecamers formed by peptide **3.1** are morphologically identical to the trimers, hexamers, and dodecamers formed by peptide **3.2**.

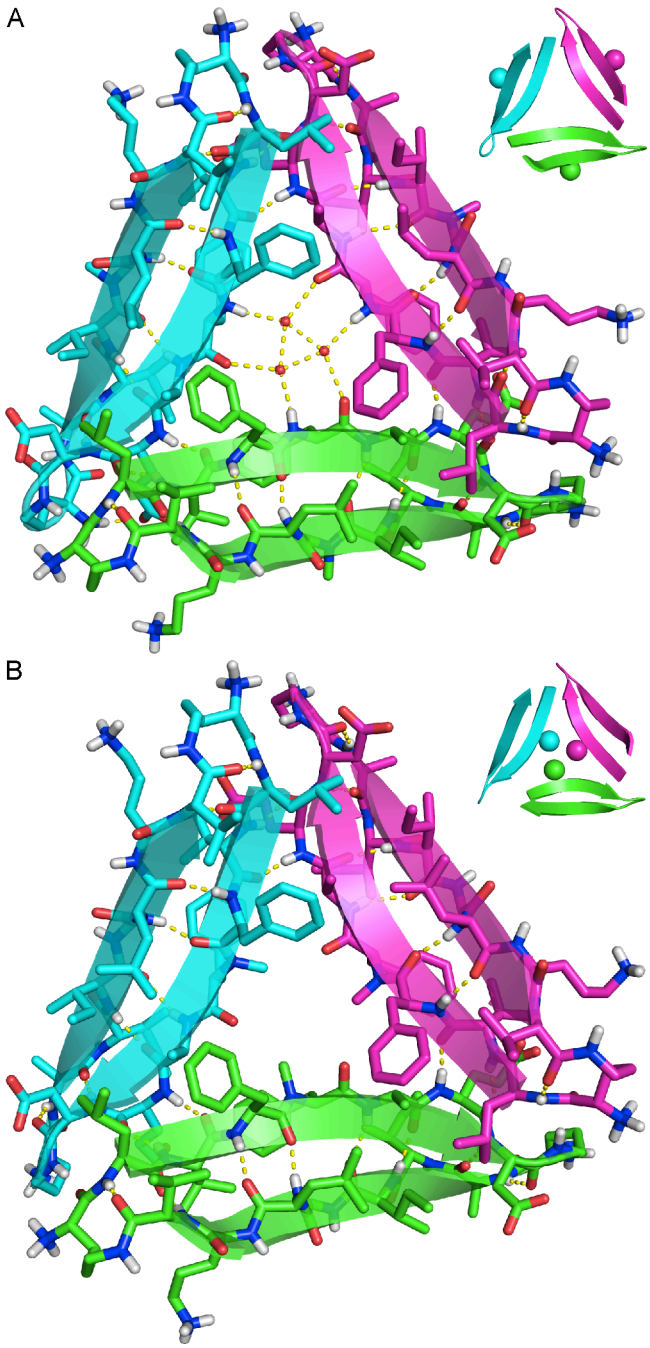

Figure 3.2. (A) X-ray crystallographic structure of the triangular trimer formed by peptide **3.1** (PDB 4NTR). The three ordered water molecules in the center of the trimer that form hydrogen bonds with the main chain of F_{20} are shown as small red spheres. In the inset, the *N*-methyl groups on G_{33} are shown as spheres. (B) X-ray crystallographic structure of the triangular trimer formed by peptide **3.2** (PDB 4NW9). In the inset, the *N*-methyl groups on F_{20} are shown as spheres.

The oligomers formed by peptides **3.1** and **3.2** are labile and dynamic in aqueous solution, making it difficult to correlate their biological and biophysical properties with their X-ray crystallographic structures. In the current study, we aimed to covalently stabilize the trimers formed by peptides **3.1** and **3.2** through chemical crosslinking, with the goal of investigating the biological significance of this triangular assembly (Chart 3.1). This paper describes the design, synthesis, and study of crosslinked trimers **3.5** and **3.6** (Figure 3.3). Peptides **3.3** and **3.4** are generated as cysteine-containing homologues of peptides **3.1** and **3.2** and are crosslinked to form trimers **3.5** and **3.6**. The X-ray crystallographic structures of trimers **3.5** and **3.6** are determined and the higher-order assemblies that they form are elucidated at high resolution. Trimers **3.5** and **3.6** are also shown to form higher-order oligomers in aqueous solution that are toxic toward the human neuroblastoma cell line SH-SY5Y.

Chart 3.1. Design of trimers **3.5** and **3.6**.

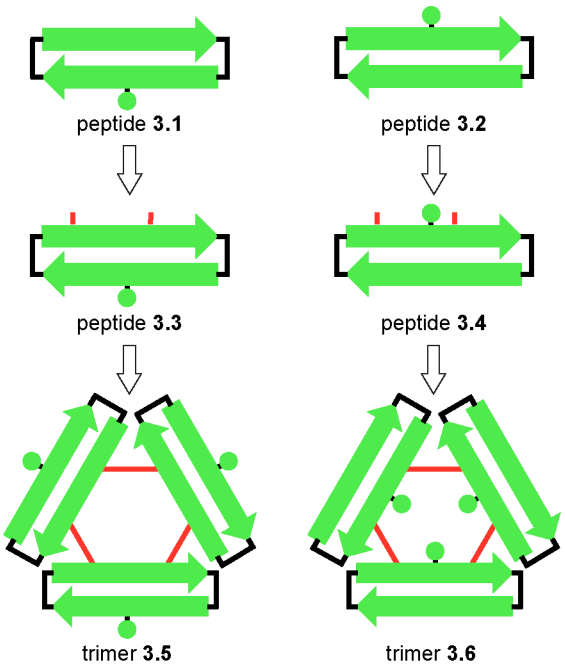

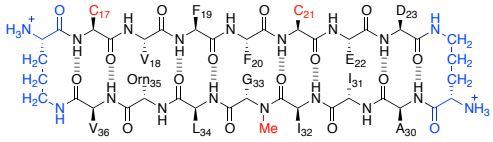

peptide **3.3**

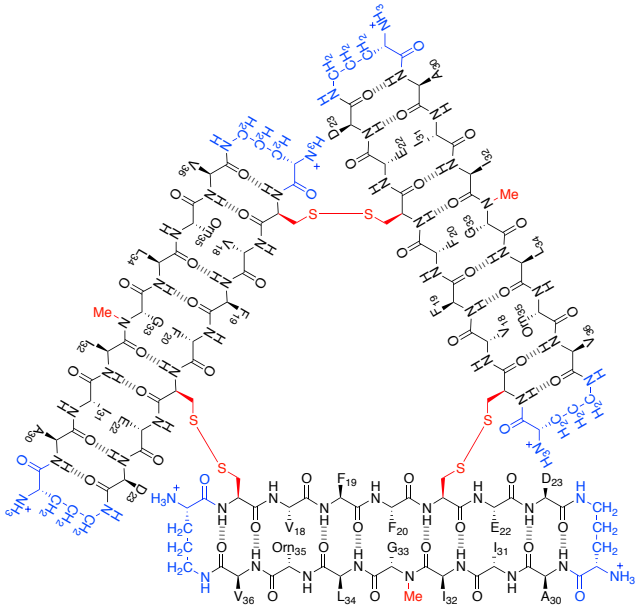

trimer **3.5**

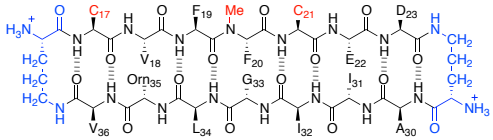

peptide **3.4**

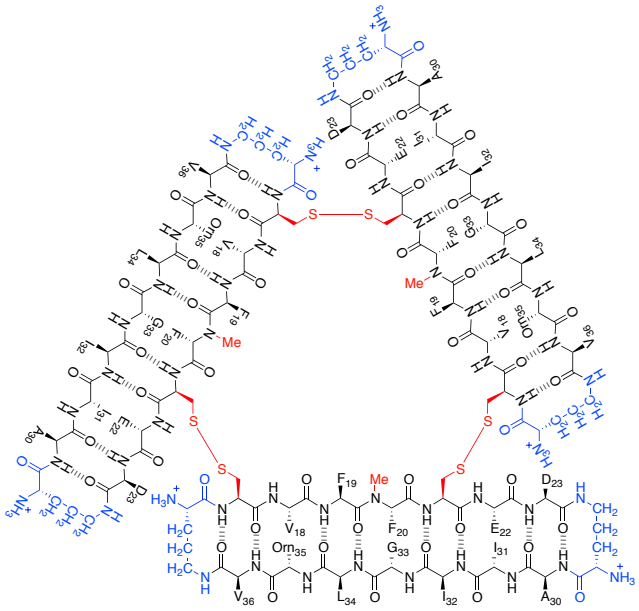

trimer **3.6**

Figure 3.3. Chemical structures of peptides **3.3** and **3.4** and trimers **3.5** and **3.6**.

Results

Design and Synthesis of Peptides 3.3 and 3.4 and Trimers 3.5 and 3.6. The X-ray crystallographic structures of the trimers formed by peptides **3.1** and **3.2** revealed a strategy for crosslinking these peptides into stable trimers. At the three corners of the triangular trimers, the side chain of residue L_{17} of one monomer subunit packs against the side chain of residue A_{21} of another monomer subunit. We hypothesized that mutating both L_{17} and A_{21} to cysteine would allow crosslinking the peptides to form covalent trimers containing three disulfide linkages. The resulting C_{17}–C_{21} crosslinks would be almost isosteric with L_{17} and A_{21}, maintaining a similar level of hydrophobicity and not altering the charge of the trimer.

We synthesized peptides **3.3** and **3.4** by similar procedures to those we have developed for other macrocyclic β-sheet peptides: synthesis of the corresponding linear peptide on 2-chlorotrityl resin, followed by cleavage of the protected linear peptide from the resin, solution-phase macrocyclization, and global deprotection of the resulting macrocyclic peptide.[10,11,12,13,17] We purified peptides **3.3** and **3.4** by reverse-phase HPLC (RP-HPLC) followed by lyophilization of pure fractions. Typical syntheses on a 0.1 mmol scale afforded ~55 mg of peptides **3.3** and **3.4** in ≥95% purity. We rigorously purified peptides **3.3** and **3.4** to minimize off-target products in the subsequent oxidation reactions.

We anticipated that oxidation of peptides **3.3** and **3.4** to form trimers would be challenging. The peptides have the potential to form complex mixtures of monomeric, dimeric, trimeric, and higher oligomeric oxidation products. Five different oxidation products of trimer size or smaller are possible in the oxidation reactions of peptides **3.3** and **3.4**: (1) a monomer that contains an intramolecular disulfide bond between C_{17} and C_{21}, (2) an antiparallel *bis*-disulfide crosslinked dimer, (3) a parallel *bis*-disulfide crosslinked dimer, (4) an asymmetric *tris*-disulfide

crosslinked trimer, and (5) a symmetric *tris*-disulfide crosslinked trimer (Figure 3.4). The desired trimers **3.5** and **3.6** are symmetric *tris*-disulfide crosslinked trimers.

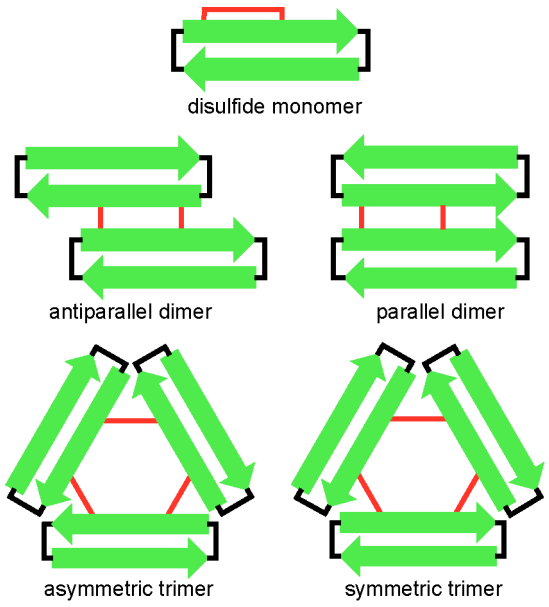

Figure 3.4. Cartoon illustrating the anticipated products of trimer size or smaller in the oxidation reactions of peptides **3.3** and **3.4**.

We developed a two-step procedure for preparing trimers **3.5** and **3.6** from peptides **3.3** and **3.4**. In the first step, we allow peptides **3.3** and **3.4** to oxidize at relatively high concentration of peptide (6 mM) in 20% (v/v) aqueous DMSO for 48 h.[18,19] In the second step, we dilute the reaction mixture with water to a low concentration (~250 μM) and allow the oxidized peptides to equilibrate over 48 h. Through this procedure, peptides **3.3** and **3.4** crosslink to form substantial amounts of the desired symmetric crosslinked trimers **3.5** and **3.6**. In the oxidation reaction of peptide **3.3**, we observe three major products—trimer **3.5**, a crosslinked dimer, and the disulfide monomer (Figure 3.5A).[20] In the oxidation reaction of peptide **3.4**, we observe two major products—trimer **3.6** and the disulfide monomer; we do not observe appreciable amounts of either possible crosslinked dimer (Figure 3.5B). We purified trimers **3.5** and **3.6** by RP-HPLC

followed by lyophilization of pure fractions to yield ~15 mg of trimer **3.5** and ~20 mg of trimer **3.6**—each with ≥95% purity—from a 0.1 mmol scale synthesis of peptides **3.3** and **3.4**.

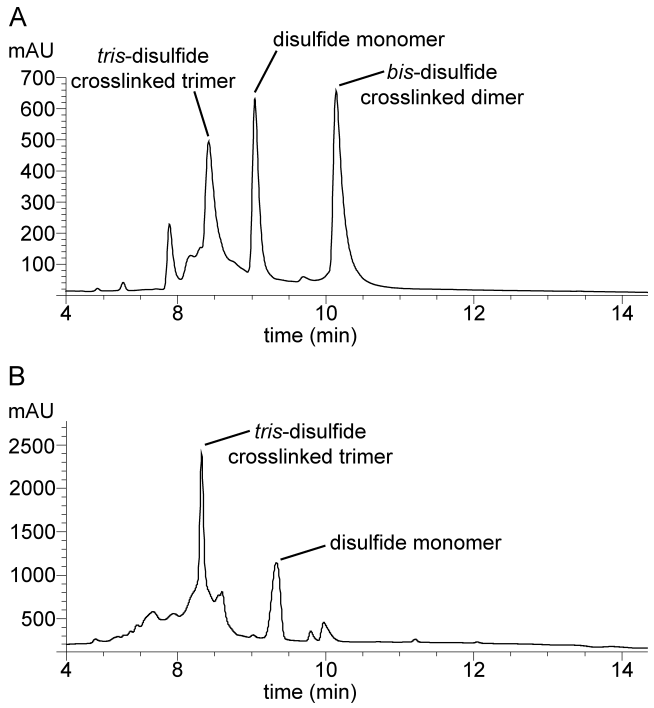

Figure 3.5. Analytical RP-HPLC traces of the mixture of products formed upon oxidation of peptide **3.3** (A) and peptide **3.4** (B). Analytical RP-HPLC was performed on a C18 column with an elution gradient of 5–95% CH_3CN over 20 minutes.

X-ray Crystallographic Structure Determination of Trimers 3.5 and 3.6. We elucidated the structures of trimers **3.5** and **3.6** by X-ray crystallography. One of the challenges in X-ray crystallography is determining the X-ray crystallographic phases. Doing so often requires incorporation of a heavy atom—such as selenium, bromine, or iodine—through covalent modification.[21] In previously solving the X-ray crystallographic structures of peptides **3.1** and **3.2**, we prepared homologues containing *p*-iodophenylalanine. In solving the X-ray crystallographic structures of trimers **3.5** and **3.6**, we employed two techniques for X-ray crystallographic phase determination that have not been widely used for peptides: sulfur single-

wavelength anomalous diffraction (S-SAD) and post-crystallization incorporation of iodide ions into the crystal lattice.

We used S-SAD to determine the X-ray crystallographic structure of trimer **3.6**. The intrinsic anomalous scattering of the sulfur atoms in the asymmetric unit provided sufficient data to determine the X-ray crystallographic phases. We collected five data sets from a single crystal of trimer **3.6** using an X-ray diffractometer equipped with a rotating copper anode, and we merged the data sets to increase the strength of the anomalous signal from sulfur.[22,23] We then used the X-ray crystallographic structure generated by S-SAD (PDB 5SUS) as a search model for molecular replacement to solve the X-ray crystallographic phases of a higher resolution data set collected using a synchrotron radiation source (PDB 5SUR).

We used iodide ion incorporation and conventional SAD phasing to determine the X-ray crystallographic structure of trimer **3.5**. To incorporate the iodide ions into the crystal lattice we soaked a crystal of trimer **3.5** in a mixture of crystallization buffer and aqueous potassium iodide (KI).[24] The X-ray crystallographic structure of the KI-soaked trimer **3.5** (PDB 5SUU) was used as a search model for molecular replacement to determine the X-ray crystallographic phases of a higher resolution data set of unsoaked trimer **3.5** collected using a synchrotron radiation source (PDB 5SUT).

X-ray Crystallographic Structure and Supramolecular Assembly of Trimer 3.5. The X-ray crystallographic structure of trimer **3.5** reveals the hypothesized trimer, with three disulfide linkages between the monomeric subunits (Figure 3.6).[25] As we envisioned, replacement of L_{17} and A_{21} with cysteine does not perturb the triangular trimer structure. Trimer **3.5** is composed of three folded macrocyclic β-sheets and is virtually identical to the trimers formed by peptides **3.1** and **3.2**. Trimer **3.5** maintains the intersheet hydrogen bonds and

hydrophobic clustering of amino acid side chains previously described for the trimers formed by peptides **3.1** and **3.2**.[10] At each corner of trimer **3.5**, the main chain of residue V_{18} on one monomeric subunit hydrogen bonds with the main chain of residue E_{22} on the adjacent monomeric subunit (Figure 3.9A).

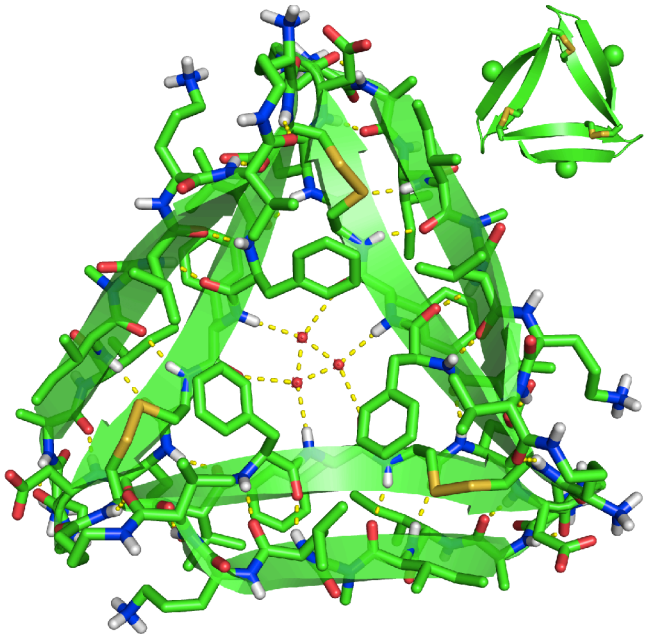

Figure 3.6. X-ray crystallographic structure of trimer **3.5** (PDB 5SUT). In the inset, the *N*-methyl groups on G_{33} are shown as spheres.

The *N*-methyl groups in trimer **3.5** are located on the outer hydrogen-bonding edges of the trimer. These *N*-methyl groups block the outer hydrogen-bonding edges of the trimer from hydrogen bonding with other trimers in the crystal lattice. Three ordered water molecules fill the hole in the center of trimer **3.5**, hydrogen bonding with each other and with the main chain of residue F_{20}.

Clusters of hydrophobic residues in trimer **3.5** create two hydrophobic surfaces (Figure 3.S1). The front surface displays the side chains of residues F_{19}, I_{32}, L_{34}, and V_{36}, as well as the

C_{17}–C_{21} disulfide linkages. We term this surface the "F_{19} face". The back surface displays the side chains of residues V_{18}, F_{20}, and I_{31}. We term this face the "F_{20} face". Trimer **3.5** packs on both the F_{19} face and the F_{20} face to form higher-order assemblies in the crystal lattice.

In the X-ray crystallographic structure of trimer **3.5**, two trimers pack to form a sandwich-like hexamer (Figure 3.7). In the hexamer, the F_{20} face of one trimer packs against the F_{20} face of another trimer (Figure 3.7B). The hexamers further assemble to form columns by stacking on their F_{19} faces (Figure 3.7C). The columns are arranged in a hexagonal fashion in the crystal lattice (Figure 3.S2). The hexamer formed by trimer **3.5** is morphologically identical to the hexamers formed by peptides **3.1** and **3.2**.

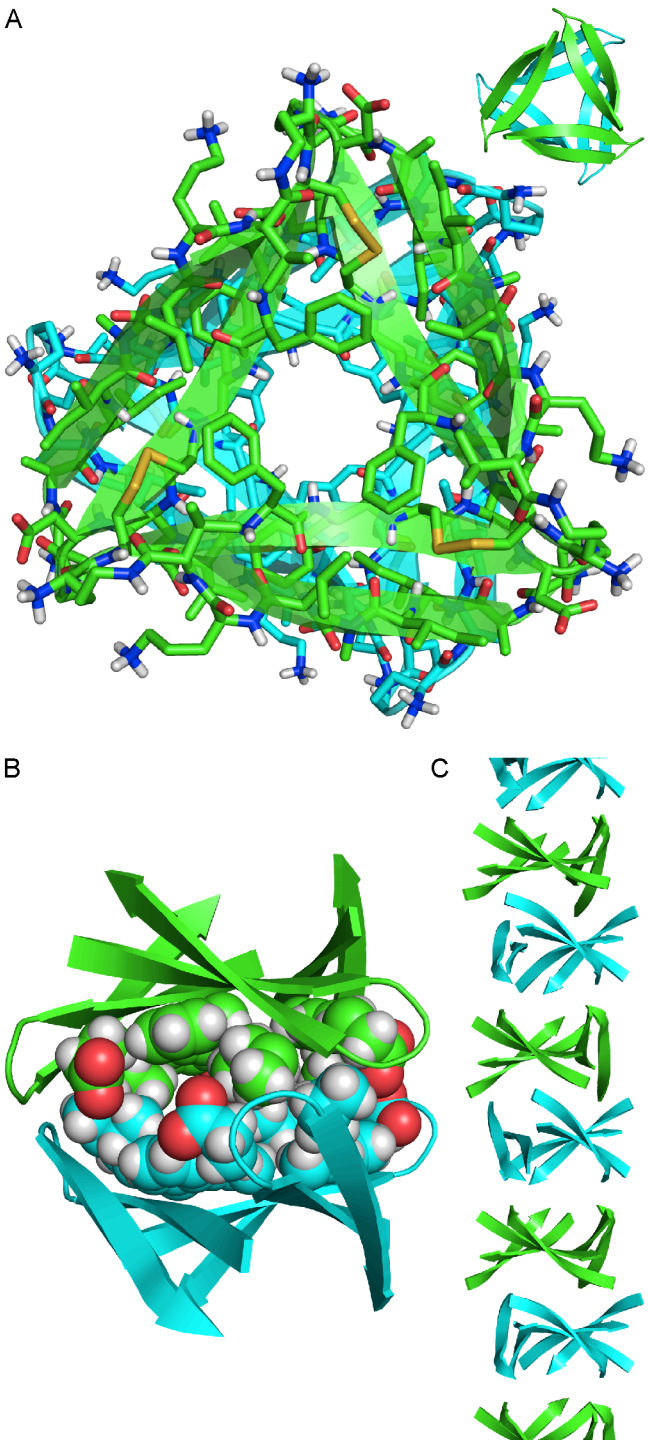

Figure 3.7. X-ray crystallographic structure of the sandwich-like hexamer formed by trimer **3.5**. (A) Top view. (B) Side view. The side chains of residues F_{20}, I_{31}, and E_{22} are shown as spheres to illustrate the hydrophobic packing that occurs at the interface between the two trimers. (C) Column of stacked hexamers in the crystal lattice.

This mode of assembly, in which the hydrophobic faces displayed on triangular trimers pack together to form hexamers, appears to be characteristic of triangular trimers formed by amyloid-derived macrocyclic β-sheets and β-hairpins. Our laboratory has also observed this mode of assembly by a larger peptide derived from $A\beta_{17–36}$ and by a macrocyclic β-sheet peptide derived from β_2-microglobulin.[11,16]

X-ray Crystallographic Structure and Supramolecular Assembly of Trimer 3.6. The X-ray crystallographic structure of trimer **3.6** reveals a symmetric trimer that is crosslinked through disulfide linkages between C_{17} of one monomeric subunit and C_{21} of the adjacent monomeric subunit (Figure 3.8).[26] Although trimer **3.6** is composed of three folded macrocyclic β-sheets, it differs in conformation from the trimers formed by peptides **3.1** and **3.2**, and also differs in conformation from trimer **3.5**. In the three other trimers, the main chains of residues V_{18} and E_{22} are hydrogen bonded at the corners of the trimer. In trimer **3.6** residues V_{18} and E_{22} shift out of alignment by two residues, such that residue V_{18} is across from residue F_{20} and residue E_{22} is across from $^{\delta}$Orn (Figure 3.9B). In further contrast to trimer **3.5**, the *N*-methyl groups in trimer **3.6** are sequestered in the center hole of the trimer, exposing the outer hydrogen-bonding edges and allowing trimer **3.6** to hydrogen bond with other trimers in the crystal lattice.

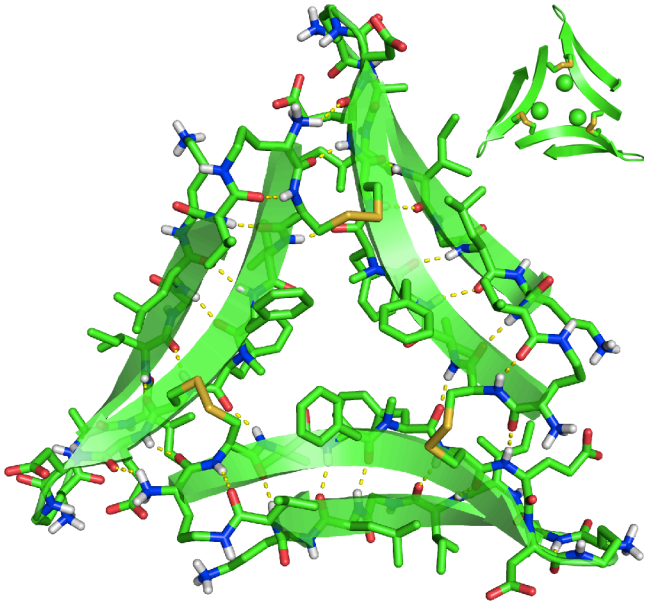

Figure 3.8. X-ray crystallographic structure of trimer **3.6** (PDB 5SUR). In the inset, the *N*-methyl groups on F_{20} are shown as spheres.

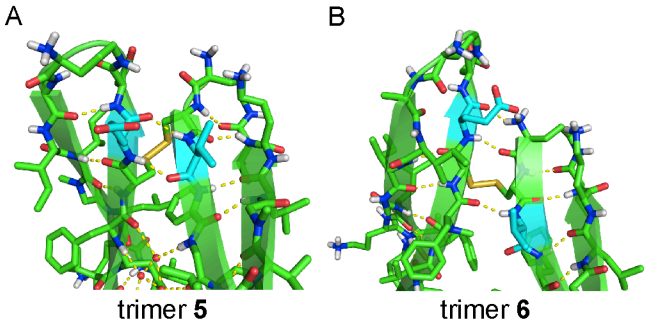

Figure 3.9. Contacts between the monomer subunits in trimer **3.5** and trimer **3.6**. (A) Trimer **3.5**. Residues V_{18} and E_{22} (highlighted in cyan) are aligned. (B) Trimer **3.6**. Residues V_{18} and E_{22} (highlighted in cyan) are shifted out of alignment by two residues. The side chain of one F_{20} residue on trimer **3.5** is omitted for clarity.

Clusters of hydrophobic residues in trimer **3.6** create two hydrophobic surfaces, which we term the "F_{19} face" and the "F_{20} face" (Figure 3.S1). The F_{19} face displays the hydrophobic side chains of residues F_{19}, I_{32}, L_{34}, and V_{36}, as well as the C_{17}–C_{21} disulfide linkages. The F_{20} face displays the hydrophobic side chains of residues V_{18}, F_{20}, and I_{31}.

In the X-ray crystallographic structure of trimer **3.6**, four trimers assemble in a tetrahedral fashion to form a ball-shaped dodecamer (Figure 3.10). The dodecamer is stabilized by a network of hydrogen bonds among the outer edges of the four trimers: the main chains of residues G_{33} and Orn_{35} on one trimer hydrogen bond with the main chains of residues I_{31} and $^{\delta}Orn$ on the adjacent trimers. The hydrophobic residues on the F_{20} faces of the four trimers line the inside of the dodecamer, creating a hydrophobic cavity approximately 2 nm in diameter.[27]

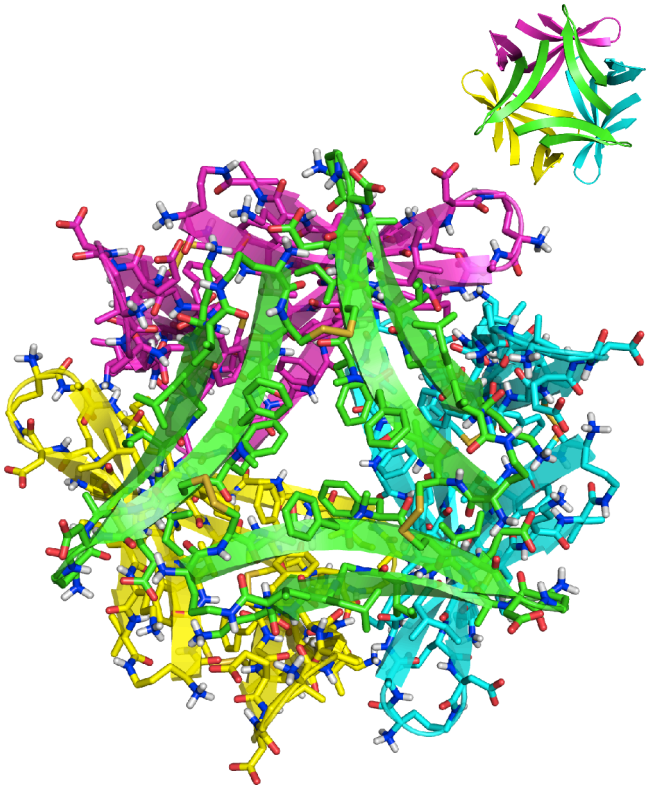

Figure 3.10. X-ray crystallographic structure of the ball-shaped dodecamer formed by trimer **3.6**.

The ball-shaped dodecamers pack to form the crystal lattice. Within the crystal lattice, six dodecamers assemble to form annular porelike structures (Figure 3.11A). Hydrophobic packing between the F_{19} faces displayed on the exterior of each dodecamer stabilizes these annular porelike structures. At the interfaces between the dodecamers in the annular pore, the trimers

pack to form sandwich-like hexamers (Figures 11B and C). The interfaces are stabilized by hydrophobic packing between the side chains of residues on the F_{19} faces of each trimer.

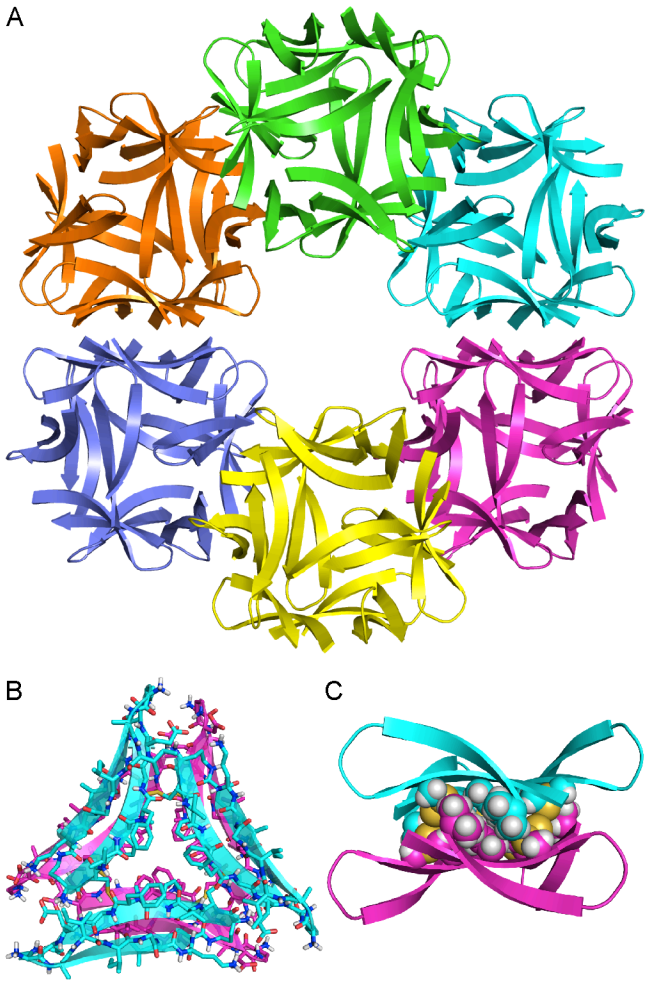

Figure 3.11. (A) X-ray crystallographic structure of an annular pore formed by trimer **3.6**. (B) A sandwich-like hexamer formed by the trimers at the interface between two dodecamers in the annular pore (top view). (C) Side view of a sandwich-like hexamer. The side chains of residues on the F_{19} faces of the trimers are shown as spheres to illustrate the hydrophobic packing at the interface.

As illustrated above, trimer **3.5** and trimer **3.6** form different higher-order assemblies within the crystal lattice. Trimer **3.5** packs to form sandwich-like hexamers; trimer **3.6** assembles to form ball-shaped dodecamers that pack to form annular pores. The difference in the position

of the *N*-methyl groups on the two trimers may explain the differences in the assemblies that form. In trimer **3.6**, the *N*-methyl group on residue F_{20} is sequestered in the center hole of the trimer, exposing the outer hydrogen-bonding edges and allowing trimer **3.6** to hydrogen bond with the three other trimer **3.6** subunits that comprise the ball-shaped dodecamer. In trimer **3.5**, the *N*-methyl group on residue G_{33} inhibits dodecamer formation by blocking hydrogen bonding with other trimers. Instead, trimer **3.5** forms a sandwich-like hexamer that is primarily stabilized by packing between the hydrophobic surfaces of the two trimers.

Biological Studies of Trimers 3.5 and 3.6. Trimers **3.5** and **3.6** provide tools to investigate the biological significance of the triangular assembly. We compared trimers **3.5** and **3.6** and peptides **3.1** and **3.2** in a series of biological and biophysical experiments to evaluate the effect of covalent stabilization of the trimers and to correlate differences in biological and solution-phase behavior with differences in structure.

Aβ is known to be toxic toward neurons and neuronally derived cells.[1,28] To corroborate the toxicity of Aβ, we prepared oligomers of $Aβ_{42}$ and studied their toxicity toward the human neuroblastoma cell line SH-SY5Y. Aβ oligomers were prepared according to the procedure developed by Teplow and coworkers using recombinantly expressed $Aβ_{42}$ pretreated with NH_4OH (purchased from rPeptide).[29,30] Under the conditions of the oligomer preparation, $Aβ_{42}$ appears as a mixture of oligomers as assessed by SDS-PAGE (Figure 3.12A). We treated SH-SY5Y cells with varying concentrations of the mixture of $Aβ_{42}$ oligomers and evaluated toxicity using a lactate dehydrogenase (LDH) release assay. The $Aβ_{42}$ increased LDH release in a dose-dependent manner at concentrations as low as 2.5 μM, corroborating the toxicity of $Aβ_{42}$ observed by other laboratories (Figure 3.12B).

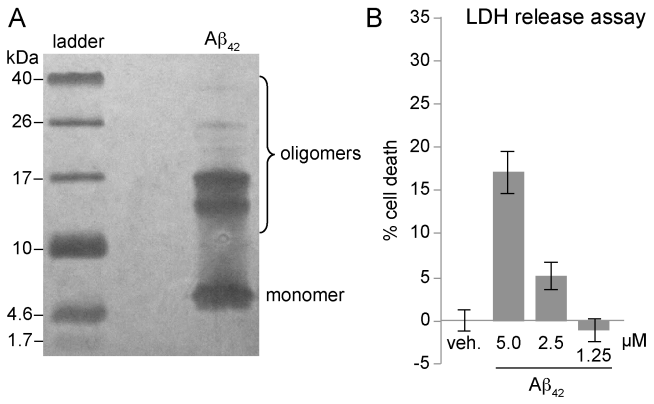

Figure 3.12. $A\beta_{42}$ forms a mixture of oligomers and is toxic toward SH-SY5Y cells. (A) Silver-stained SDS-PAGE gel. $A\beta_{42}$ was run at 250 μM. (B) Lactate dehydrogenase (LDH) release assay. Data represent the mean of five replicate wells +/− s.d. Deionized water (vehicle, veh.) was used as a negative control.

LDH release assay. To test whether trimers **3.5** and **3.6** elicit toxicity similar to $A\beta_{42}$, we evaluated the toxicity of the trimers toward SH-SY5Y cells using an LDH release assay. Deionized water (vehicle) and peptides **3.1** and **3.2** were used as controls. Trimer **3.6** increased LDH release in a dose-dependent manner at concentrations as low as 1.5 μM, indicating toxicity toward SH-SY5Y cells (Figure 3.13A). LDH release was observed as early as 48 h after addition to the cells and reached a maximum after 72 h (Figure 3.S3). The toxicity of trimer **3.6** does not arise from *in situ* reduction to peptide **3.4**, as peptide **3.4** showed no toxicity in LDH release assays (Figure 3.S4). At equivalent concentrations, trimer **3.5** exhibited less toxicity than trimer **3.6**, eliciting LDH release at concentrations as low as 3 μM. In contrast, monomeric peptides **3.1** and **3.2** showed little or no LDH release.

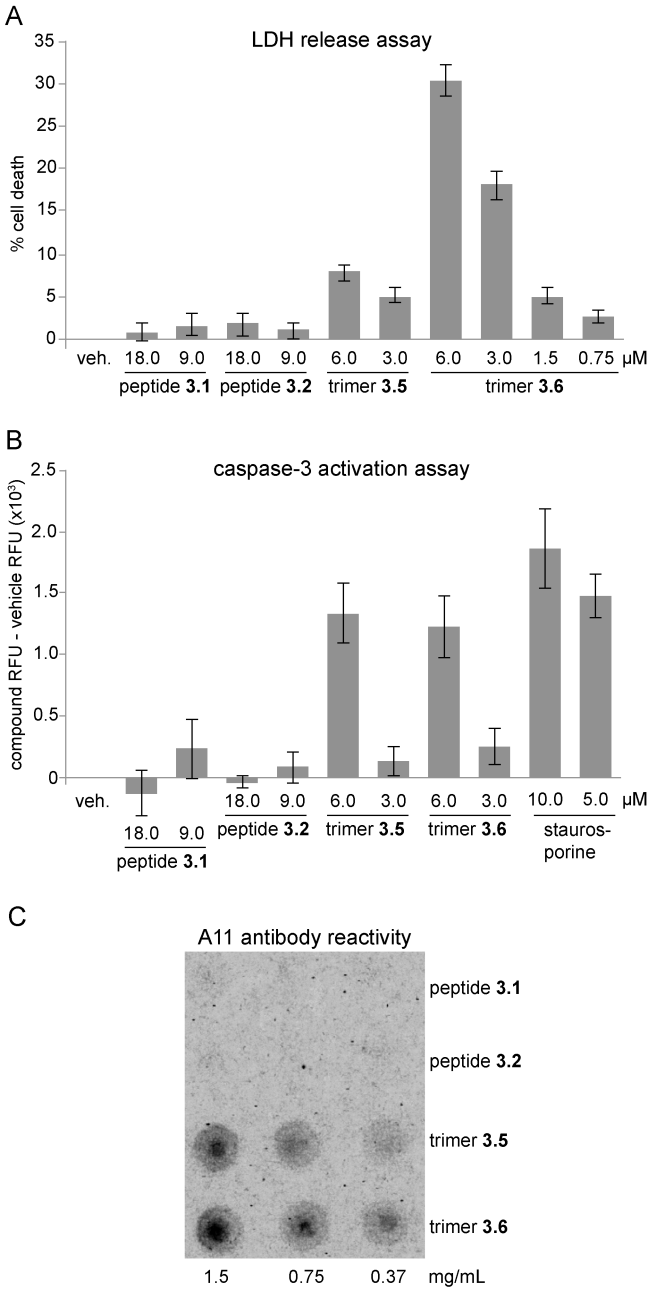

Figure 3.13. Biological studies of trimers **3.5** and **3.6** and peptides **3.1** and **3.2**. (A) LDH release assay. Data represent the mean of five replicate wells +/− s.d. Deionized water (vehicle, veh.) was used as a negative control. (B) Caspase-3 activation assay. Data represent the mean of five replicate wells +/− s.d. Staurosporine was used as a positive control. (C) Dot blot analysis of A11 antibody reactivity of trimers **3.5** and **3.6** and peptides **3.1** and **3.2**.

Caspase-3 activation assay. One way in which Aβ oligomers elicit toxicity is by inducing caspase-3 mediated apoptosis.[31,32] We used a rhodamine-based caspase-3 activity assay to

evaluate whether trimers **3.5** and **3.6** also induce caspase-3 mediated apoptosis. At 6 μM, both trimer **3.5** and trimer **3.6** induced apoptosis within 72 h after addition to SH-SY5Y cells, whereas peptides **3.1** and **3.2** showed little or no effect (Figure 3.13B). Caspase-3 activity levels after treatment with trimer **3.5** or trimer **3.6** were comparable to that of the known caspase-3 activator staurosporine. These results suggest that trimers **3.5** and **3.6** may elicit toxicity by activating apoptosis.

A11 antibody reactivity. The LDH release and caspase-3 activation studies indicate that trimers **3.5** and **3.6** behave like oligomers of full-length Aβ and provide evidence for the biological significance of the triangular assembly. To further evaluate how the biological properties of trimers **3.5** and **3.6** compare to those of full-length Aβ, we examined the reactivity of the trimers with the oligomer-specific antibody A11 by dot blot analysis. Trimers **3.5** and **3.6** react with the A11 antibody, but peptides **3.1** and **3.2** do not (Figure 3.13C).

Reactivity with the A11 antibody is a hallmark of certain types of Aβ oligomers.[33,34] The A11 antibody specifically recognizes oligomeric assemblies of Aβ, but does not recognize Aβ monomers or fibrils. The structures of the Aβ oligomers recognized by the A11 antibody are not known. The results from the dot blot experiment show that the A11 antibody recognizes trimers **3.5** and **3.6** as Aβ oligomers and suggest that oligomers of full-length Aβ may also contain triangular trimers.

Solution-Phase Biophysical Studies of Trimers 3.5 and 3.6. The differences in LDH release, caspase-3 activation, and A11 antibody reactivity between trimers **3.5** and **3.6** and peptides **3.1** and **3.2**, suggest that covalent stabilization of the triangular trimer is necessary for these small peptides to mimic the oligomers of full-length Aβ at micromolar concentrations. Although peptides **3.1** and **3.2** assemble to form triangular trimers at the millimolar

concentrations of crystallography experiments, they may be too small to assemble at the micromolar concentrations of biological and biophysical experiments. We turned to SDS-PAGE, size exclusion chromatography (SEC), and circular dichroism (CD) spectroscopy to probe the solution-phase behavior of trimers **3.5** and **3.6** and peptides **3.1** and **3.2**, and thus explore these hypotheses.

SDS-PAGE. Tricine SDS-PAGE followed by silver staining reveals that trimers **3.5** and **3.6** assemble to form SDS-stable oligomers (Figure 3.14A).[35,36] Trimer **3.5** migrates as a single band at a molecular weight consistent with a hexamer. Trimer **3.6** migrates as two bands: one consistent with the molecular weight of a dodecamer, the other consistent with the molecular weight of a trimer. The dodecamer band shows pronounced streaking, suggesting equilibria with lower molecular weight oligomers, such as nonamers and hexamers. Peptides **3.1** and **3.2** migrate as broad bands at molecular weights consistent with monomer or dimer.

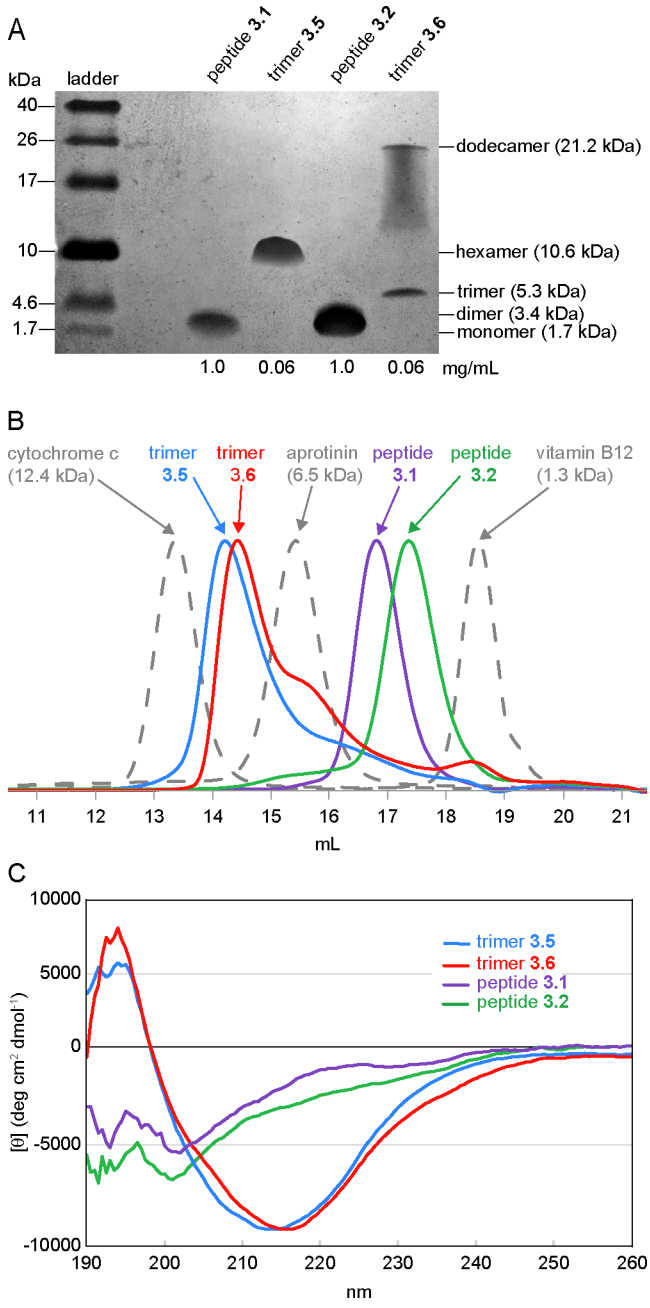

Figure 3.14. Solution-phase biophysical studies of trimers **3.5** and **3.6** and peptides **3.1** and **3.2**. (A) Silver stained SDS-PAGE gel. SDS-PAGE was performed in Tris buffer at pH 6.8 with 2% (w/v) SDS. Molecular weights calculated for the monomer, dimer, trimer, hexamer, and dodecamer are listed in parentheses. (B) Size exclusion chromatography chromatograms. SEC was performed on 1.0-mg/mL solutions of trimers **3.5** and **3.6** and peptides **3.1** and **3.2** in 50 mM sodium acetate/50 mM acetic acid (pH 4.7) with a Superdex 75 10/300 column.[37] (C) Circular dichroism spectra. Spectra were acquired at 0.3 mg/mL (50 μM trimers **3.5** and **3.6**; 150 μM peptides **3.1** and **3.2**) in 10 mM potassium phosphate buffer at pH 7.4.

Size exclusion chromatography. SEC reveals that trimers **3.5** and **3.6** also assemble to form higher-order oligomers in acetate buffer (Figure 3.14B).[37] The elution profiles of trimers **3.5** and **3.6** were compared to those of size standards and peptides **3.1** and **3.2**. The size standards vitamin B12 (1.3 kDa), aprotinin (6.5 kDa), and cytochrome c (12.4 kDa) eluted at 18.6 mL, 15.4 mL, and 13.4 mL, respectively. Trimer **3.5** elutes at 14.3 mL; trimer **3.6** elutes at 14.5 mL. These elution volumes fall between the elution volumes of the 6.5 kDa and 12.4 kDa standards and are thus consistent with the molecular weight of a hexamer (10.6 kDa). The peaks for trimers **3.5** and **3.6** tail slightly, which may reflect a trimer-hexamer equilibrium in which the hexamer predominates. The tail of trimer **3.6** shows a distinct hump at 15.6 mL, suggesting a slow equilibrium between the trimer and the hexamer.

Under the conditions of the SEC experiments, peptides **3.1** and **3.2** do not assemble to form trimers. Peptide **3.1** elutes at 16.8 mL; peptide **3.2** elutes at 17.3 mL. These volumes are lower than would be expected for a 1.7 kDa monomer and higher than would be expected for a 5.3 kDa trimer, suggesting that peptides **3.1** and **3.2** may form dimers in solution.

Circular dichroism. Circular dichroism spectra reflect the cooperative folding and assembly of macrocyclic β-sheet peptides (Figure 3.14C). The CD spectra of trimers **3.5** and **3.6** exhibit typical β-hairpin character as evidenced by negative bands at ~215 nm and positive bands at ~195 nm.[38,39,40] In contrast, the CD spectra of peptides **3.1** and **3.2** show little β-hairpin structure. These results indicate that covalent stabilization not only locks in conformation, but also promotes folding of the monomeric subunits into β-hairpins. Table 3.1 summarizes the results of the structural and biological studies described above.

Table 3.1. Structures, stoichiometries, and biological activities of trimers 3.5 and 3.6 and peptides 3.1 and 3.2.

compound	PDB ID	oligomer size by			A11 reactivity	LDH release	caspase-3 activation
		crystallography	SEC	SDS-PAGE			
trimer **3.5**	5SUT	6	6	6	yes	some	yes
trimer **3.6**	5SUR	6 and 12*	6	3 and 12	yes	yes	yes
peptide **3.1**[10]	4NTR	3, 6, and 12	1-2	1-2	no	no	no
peptide **3.2**[10]	4NW9	3, 6, and 12	1-2	1-2	no	no	no

*In the X-ray crystallographic structure of trimer **3.6**, the dodecamers further assemble to form annular porelike structures.

Discussion

X-ray crystallography provides a facile means to probe the structures of oligomers formed by β-hairpin peptides derived from amyloidogenic peptides and proteins. The solution-phase studies of trimers **3.5** and **3.6** provide evidence that their crystallographically observed assemblies are meaningful, and are not simply artifacts of the trimers packing to form a lattice. The hexamer formed by trimer **3.5** in the SDS-PAGE and SEC studies likely resembles the sandwich-like hexamer observed crystallographically, in which two trimers pack on their hydrophobic surfaces. The dodecamer formed by trimer **3.6** in the SDS-PAGE study likely resembles the ball-shaped dodecamer observed crystallographically, in which four trimers assemble in a tetrahedral fashion. Furthermore, the hexamer formed by trimer **3.6** in the SEC study may resemble the hexamer formed at the interface of the dodecamers in the annular pore.

The differences in solution-phase assembly between trimer **3.5** and trimer **3.6** may explain the greater toxicity of trimer **3.6** in the LDH release assay. The increased LDH release from cells treated with trimer **3.6** may reflect the propensity of trimer **3.6** to form dodecamers in a lipophilic environment, such as SDS micelles or cell membranes. In cell membranes, the

dodecamers may further assemble to form annular pores and induce LDH leakage. The greater LDH release induced by trimer **3.6**, in spite of comparable caspase-3 activation, suggests that LDH release and apoptosis might occur through different mechanisms.

β-Hairpins are thought to be the building blocks of some Aβ oligomers.[41,42,43,44] The crystallographic and solution-phase assembly of trimers **3.5** and **3.6** support a model in which full-length Aβ folds into β-hairpins that come together to form triangular trimers that further assemble to form ball-shaped dodecamers.[10,16] Dodecamers that are composed of triangular trimers arranged in a tetrahedral fashion are special because they display four hydrophobic faces that can pack with the hydrophobic faces of other dodecamers to form larger assemblies. The hierarchical assembly of triangular trimers into dodecamers that further assemble to form annular porelike structures is an emergent property of the triangular trimers observed by our laboratory. This mode of assembly may explain some of the large oligomeric assemblies observed for Aβ and other amyloidogenic peptides and proteins.

One type of large oligomeric assembly formed by Aβ has been termed annular protofibrils (APFs).[45,46,47] APFs share a common donut-shaped morphology and appear to be composed of smaller spherical oligomers. APFs have also been observed for other amyloidogenic peptides and proteins, such as α-synuclein, islet amyloid polypeptide, and tau.[48,49] The annular porelike assembly formed by trimer **3.6** could serve as a structural model for an APF formed by Aβ. Furthermore, the hierarchical assembly of trimers into dodecamers, which further assemble to form annular porelike structures, might be a common mode of hierarchical assembly for other amyloidogenic peptides and proteins.

Trimers are especially important among the various oligomers formed by full-length Aβ. Concentrations of Aβ trimers are elevated in cognitively normal adults who are at risk for

Alzheimer's disease.[2,50,51] Trimers also appear to be the building blocks of the putative dodecamer of Aβ, termed Aβ*56, which was isolated from the brains of Tg2576 transgenic mice and shown to impair memory in healthy rats.[52] Furthermore, Aβ trimers, but not monomers or dimers, have been shown to promote aggregation of the microtubule associated protein tau, which is also involved in the progression Alzheimer's disease.[53] Although the significance of triangular assemblies of Aβ β-hairpins in Alzheimer's disease remains to be determined, the results described in this paper further support a model in which trimers are a central feature of Aβ oligomers.

Conclusion

The studies described in this paper embody our laboratory's strategy for studying well-defined oligomers derived from Aβ. Stabilizing fragments of the Aβ peptide in a macrocyclic β-sheet peptide and blocking uncontrolled aggregation with an *N*-methyl group permits crystallization and elucidation of higher-order assemblies the peptide can form. The X-ray crystallographic structures of the higher-order assemblies can be used to develop strategies to crosslink the peptide and thus stabilize oligomers. The crosslinked oligomers provide a tool to investigate the biological significance of the crystallographically observed oligomers.

Trimers **3.5** and **3.6** constitute the first crosslinked oligomers of an Aβ-derived peptide in which the X-ray crystallographic structures are known. The results presented in this paper support the triangular trimer, as well as sandwich-like hexamers and ball-shaped dodecamers as biologically significant assemblies of the Aβ peptide. Trimers **3.5** and **3.6** assemble to form stable oligomers in solution and recapitulate the toxicity and A11 antibody reactivity of Aβ oligomers.

Trimers **3.5** and **3.6** offer the promise of relating Aβ oligomer structure with biological activity. The X-ray crystallographic structures of trimers **3.5** and **3.6** and the trimers formed by peptides **3.1** and **3.2** can serve as starting points for rationally designing small molecules that bind Aβ oligomers. The X-ray crystallographic structure of the trimer formed by peptide **3.1** has already been used in docking studies to explain the fluorescence of probes that bind Aβ oligomers.[54,55] Trimers **3.5** and **3.6** provide stable targets that can be used to further evaluate binding of probes such as these. Trimers **3.5** and **3.6** may also serve as a starting point for discovering small molecules that inhibit the toxicity of Aβ oligomers. In addition, trimers **3.5** and **3.6** may serve as antigens for generating antibodies as probes for amyloid oligomers or as therapies for Alzheimer's disease. We are currently investigating these applications and will report our findings in due course.

References and Notes

1 Benilova, I,; Karran, E.; De Strooper, B. *Nat. Neurosci.* **2012**, *15*, 349–357.

2 Larson, M. E.; Lesné, S. E. *J. Neurochem.* **2012**, *120*, 125–139.

3 Bitan, G.; Lomakin, A.; Teplow, D. B. *J. Biol. Chem.* **2001**, *276*, 35176–35184.

4 Bitan, G.; Kirkitadze, M. D.; Lomakin, A.; Vollers, S. S.; Benedek, G. B.; Teplow, D. B. *Proc. Natl. Acad. Sci. U S A.* **2003**, *100*, 330–335.

5 Bitan, G.; Vollers, S. S.; Teplow, D. B. *J. Biol. Chem.* **2003**, *278*, 34882–34889.

6 Ono, K.; Condron, M. M.; Teplow, D. B. *Proc. Natl. Acad. Sci. U S A.* **2009**, *106*, 14745–1 4750.

7 Shankar, G. M.; Li, S.; Mehta, T. H.; Garcia-Munoz, A.; Shepardson, N. E.; Smith, I.; Brett, F. M.; Farrell, M. A.; Rowan, M. J.; Lemere, C. A.; Regan, C. M.; Walsh, D. M.; Sabatini, B. L.; Selkoe, D. J. *Nat. Med.* **2008**, *14*, 837–842.

8 O'Nuallain, B.; Freir, D. B.; Nicoll, A. J.; Risse, E.; Ferguson, N.; Herron, C. E.; Collinge, J.; Walsh, D. M. *J. Neurosci.* **2010**, *30*, 14411–14419.

9 O'Malley, T. T.; Oktaviani, N. A.; Zhang, D.; Lomakin, A.; O'Nuallain, B.; Linse, S.; Benedek, G. B.; Rowan, M. J.; Mulder, F. A.; Walsh, D. M. *Biochem. J.* **2014**, *461*, 413–426.

10 Spencer, R. K.; Li. H.; Nowick, J. S. *J. Am. Chem. Soc.* **2014**, *136*, 5595–5598.

11 Spencer, R. K.; Kreutzer, A. G.; Salveson, P. J.; Li, H.; Nowick, J. S. *J. Am. Chem. Soc.* **2015**, *137*, 6304–6311.

12 Salveson, P. J.; Spencer, R. K.; Nowick J. S. *J. Am. Chem. Soc.* **2016**, *138*, 4458–4467.

13 Yoo, S.; Kreutzer, A. G.; Truex, N. L.; Nowick, J. S. *Chem. Sci.* **2016**, *7*, 6946–6951.

14 We have subsequently solved the X-ray crystallographic structure of a homologue of peptide **3.1** with methionine at position 35 and have observed an identical triangular trimer (unpublished results).

15 Nowick, J. S.; Brower, J. O. *J. Am. Chem. Soc.* **2003**, *125*, 876–877.

16 We recently published the X-ray crystallographic structure of an $A\beta_{17–36}$ β-hairpin containing the $A\beta_{24–29}$ loop. This peptide forms the same type of triangular trimer as peptides **3.1** and **3.2**. Kreutzer, A. G.; Hamza, I. H.; Spencer, R. K.; Nowick J. S. *J. Am. Chem. Soc.* **2016**, *138*, 4634–4642.

17 Spencer, R.; Chen, K. H.; Manuel, G.; Nowick, J. S. *Eur. J. Org. Chem*. **2013**, *2013*, 3523–3528.

18 Tam, J. P.; Wu, C. R.; Liu, W.; Zhang, J. W. *J. Am. Chem. Soc.* **1991**, *113*, 6657–6662.

19 Khakshoor, O.; Nowick, J. S. *Org. Lett.* **2009**, *11*, 3000-3003.

20 We confirmed the identity of each product in the oxidation reactions of peptides **3.3** and **3.4** using electrospray ionization mass spectrometry (ESI-MS). Although the monomers, dimers, and trimers share common mass-to-charge ratios that depend on their ionization states, each product has a unique isotope pattern, allowing us to easily identify monomer, dimer, and trimer.

21 Spencer, R. K.; Nowick, J. S. *Isr. J. Chem.* **2015**, *55*, 698–710.

22 Liu, Q.; Dahmane, T.; Zhang, Z.; Assur, Z.; Brasch, J.; Shapiro, L.; Mancia, F.; Hendrickson, W. A. *Science* **2012**, *336*, 1033–1037.

23 Sarma, G. N.; Karplus, P. A. *Acta. Crystallogr. D Biol. Crystallogr.* **2006**, *62*, 707–716.

24 Dauter, Z.; Dauter, M.; Rajashankar, K. R. *Acta. Crystallogr. D Biol. Crystallogr.* **2000**, *56*, 232–237.

25 Trimer **3.5** does not appear as a discrete entity in the asymmetric unit of the X-ray crystallographic structure. Instead, the asymmetric unit contains two monomeric macrocyclic β-sheet subunits, which form two crystallographically distinct trimers through symmetry operations. The two crystallographically distinct trimers are virtually identical, differing primarily in rotamers of I_{31}, I_{32}, and Orn_{35}.

26 Trimer **3.6** does not appear as a discrete entity in the asymmetric unit of the X-ray crystallographic structure. Instead, the asymmetric unit contains four monomeric macrocyclic β-sheet subunits, which form two crystallographically distinct trimers. The two crystallographically distinct trimers are virtually identical, differing primarily in rotamers of E_{22}, D_{23}, and I_{32}.

27 We modeled four molecules of the crystallization co-solvent 1,6-hexanediol in the asymmetric unit of trimer **3.6**. All four molecules reside within the hydrophobic cavity of the ball-shaped dodecamer, making contacts with the F_{20} faces of the trimer subunits and further stabilizing the dodecamer.

28 Li, Y. P.; Bushnell, A. F.; Lee, C. M.; Perlmutter, L. S.; Wong, S. K. *Brain Res.* **1996**, *738*, 196–204.

29 Teplow, D. B. *Methods Enzymol.* **2006**, *413*, 20–33.

30 Fezoui, Y.; Hartley, D. M.; Harper, J. D.; Khurana, R.; Walsh, D. M.; Condron, M. M.; Selkoe, D. J.; Lansbury, P. T. Jr.; Fink, A. L.; Teplow, D. B. *Amyloid* **2000**, *7*, 166–178.

31 Harada, J.; Sugimoto, M. *Brain Res.* **1999**, *842*, 311–323.

32 Jo, J.; Whitcomb, D. J.; Olsen, K. M.; Kerrigan, T. L.; Lo, S. C.; Bru-Mercier, G.; Dickinson, B.; Scullion, S.; Sheng, M.; Collingridge, G.; Cho, K. *Nat. Neurosci.* **2011**, *14*, 545–547.

33 Kayed, R.; Head, E.; Thompson, J. L.; McIntire, T. M.; Milton, S. C.; Cotman, C. W.; Glabe, C. G. *Science* **2003**, *300*, 486–489.

34 Glabe, C. G. *J. Biol. Chem.* **2008**, *283*, 29639–29643.

35 Schägger, H. *Nat. Protoc.* **2006**, *1*, 16–22.

36 Simpson, R. J. *CSH Protoc.* **2007**, doi: 10.1101/pdb.prot4727.

37 A buffer of 50 mM sodium acetate and 50 mM acetic acid (pH 4.7) was used in the SEC studies. We initially attempted to perform the SEC studies in 0.1 M potassium phosphate buffer at pH 7.4 and in 50 mM Tris buffer at pH 6.8 with 150 mM NaCl. We observed prolonged retention under both conditions suggesting non-specific interaction with the column matrix.

38 Ramírez-Alvarado; M.; Blanco; F. J.; Serrano, L. *Nat. Struct. Biol.* **1996**, *3*, 604–612.

39 Maynard, A. J.; Sharman, G. J.; Searle, M. S. *J. Am. Chem. Soc.* **1998**, *120*, 1996–2007.

40 Anderson, J. M.; Jurban, B.; Huggins, K. N.; Shcherbakov, A. A.; Shu, I.; Kier, B.; Andersen, N. H. *Biochemistry* **2016**, *55*, 5537–5553.

41 Yu, L.; Edalji, R.; Harlan, J. E.; Holzman, T. F.; Lopez, A. P.; Labkovsky, B.; Hillen, H.; Barghorn, S.; Ebert, U.; Richardson, P. L.; Miesbauer, L.; Solomon, L.; Bartley, D.; Walter, K.; Johnson, R. W.; Hajduk, P. J.; Olejniczak, E. T. *Biochemistry* **2009**, *48*, 1870–1877.

42 Scheidt, H. A.; Morgado, I.; Huster, D. *J. Biol. Chem.* **2012**, *287*, 22822–22826.

43 Doi, T.; Masuda, Y.; Irie, K.; Akagi, K.; Monobe, Y.; Imazawa, T.; Takegoshi, K. *Biochem. Biophys. Res. Commun.* **2012**, *428*, 458–462.

44 Tay, W. M.; Huang, D.; Rosenberry, T. L.; Paravastu, A. K. *J. Mol. Biol.* **2013**, *425*, 2494–2508.

45 Hafner, J. H.; Cheung, C. L.; Woolley, A. T.; Lieber, C. M. *Prog. Biophys. Mol. Biol.* **2001**, *77*, 73–110.

46 Lin, H.; Bhatia, R.; Lal, R. *FASEB J.* **2001**, *15*, 2433–2444.

47 Lashuel, H. A.; Hartley, D.; Petre, B. M.; Walz, T.; Lansbury, P. T. Jr. *Nature* **2002**, *418*, 291–292.

48 Quist, A.; Doudevski, I.; Lin, H.; Azimova, R.; Ng, D.; Frangione, B.; Kagan, B.; Ghiso, J.; Lal, R. *Proc. Natl. Acad. Sci. U.S.A.* **2005**, *102*, 10427–10432.

49 Kayed, R.; Pensalfini, A.; Margol, L.; Sokolov, Y.; Sarsoza, F.; Head, E.; Hall, J.; Glabe, C. *J. Biol. Chem.* **2009**, *284*, 4230–4237.

50 Lesné, S. E.; Sherman, M. A.; Grant, M.; Kuskowski, M.; Schneider, J. A.; Bennett D. A.; Ashe, K. H. *Brain* **2013**, *136*, 1383–1398.

51 Handoko, M.; Grant, M.; Kuskowski, M.; Zahs, K. R.; Wallin, A.; Blennow, K.; Ashe, K. H. *JAMA Neurol.* **2013**, *70*, 594–599.

52 Lesné, S.; Koh, M. T.; Kotilinek, L.; Kayed, R.; Glabe, C. G.; Yang, A.; Gallagher, M.; Ashe K. H. *Nature* **2006**, *440*, 352–357.

53 Sherman, M. A.; LaCroix, M.; Amar, F.; Larson, M. E.; Forster, C.; Aguzzi, A.; Bennett, D. A.; Ramsden, M.; Lesné, S. E. *J. Neurosci.* **2016**, *36*, 9647–9658.

54 Teoh, C. L.; Su, D.; Sahu, S.; Yun, S. W.; Drummond, E.; Prelli, F.; Lim, S.; Cho, S.; Ham, S.; Wisniewski, T.; Chang, Y. T. *J. Am. Chem. Soc.* **2015**, *137*, 13503-13509.

55 Lv, G.; Sun, A.; Wei, P.; Zhang, N.; Lan, H.; Yi, T. *Chem. Commun. (Cambridge U. K.).* **2016**, *52*, 8865–8868.

Supporting Information

Table of Contents

Supporting Figures and Tables

Materials and Methods

Supporting Figures and Tables

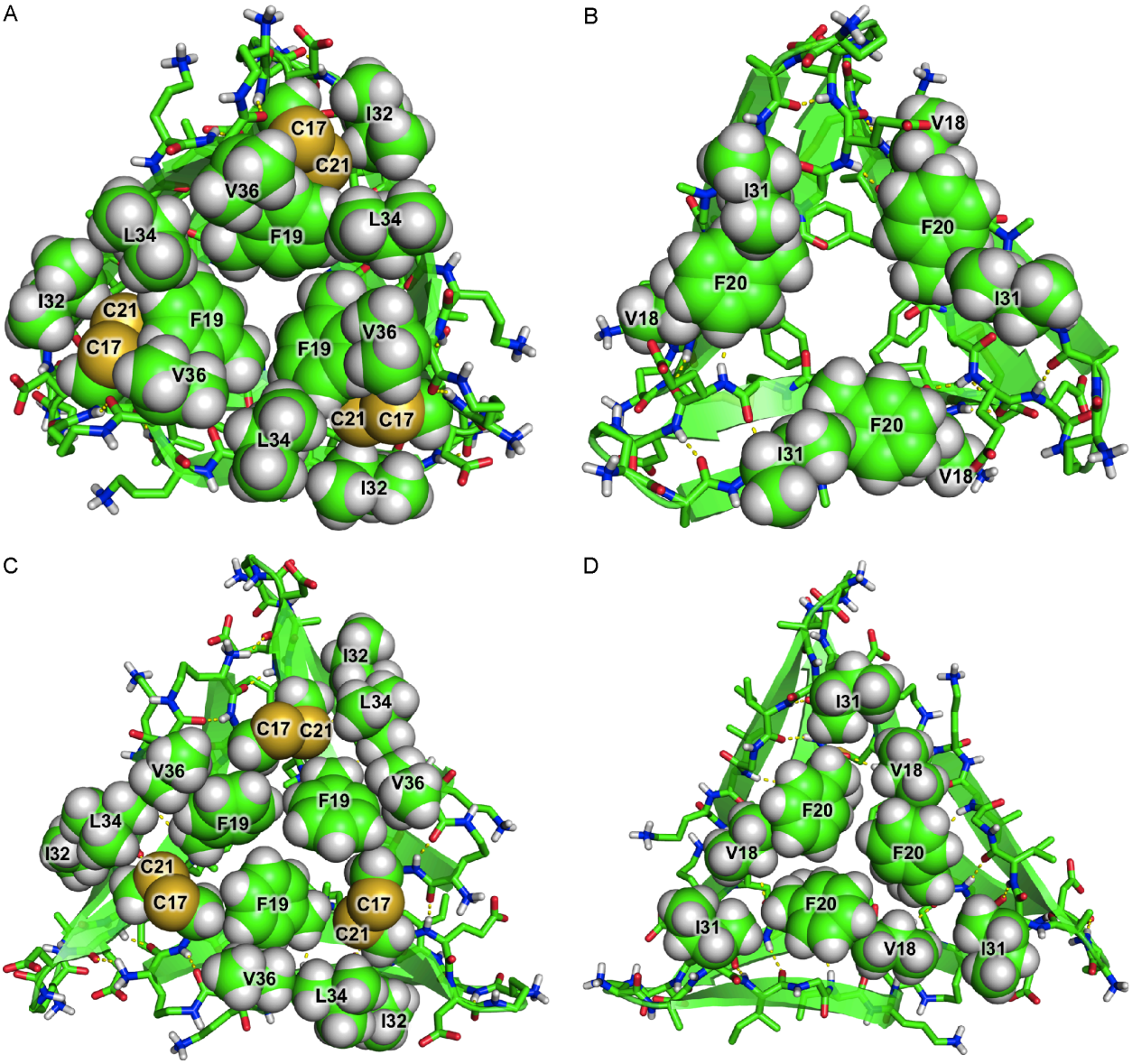

Figure 3.S1. Hydrophobic surfaces of trimers **3.5** and **3.6** (PDB 5SUT and 5SUR). (A) The F_{19} face of trimer **3.5**. (B) The F_{20} face of trimer **3.5**. (C) The F_{19} face of trimer **3.6**. (D) The F_{20} face of trimer **3.6**.

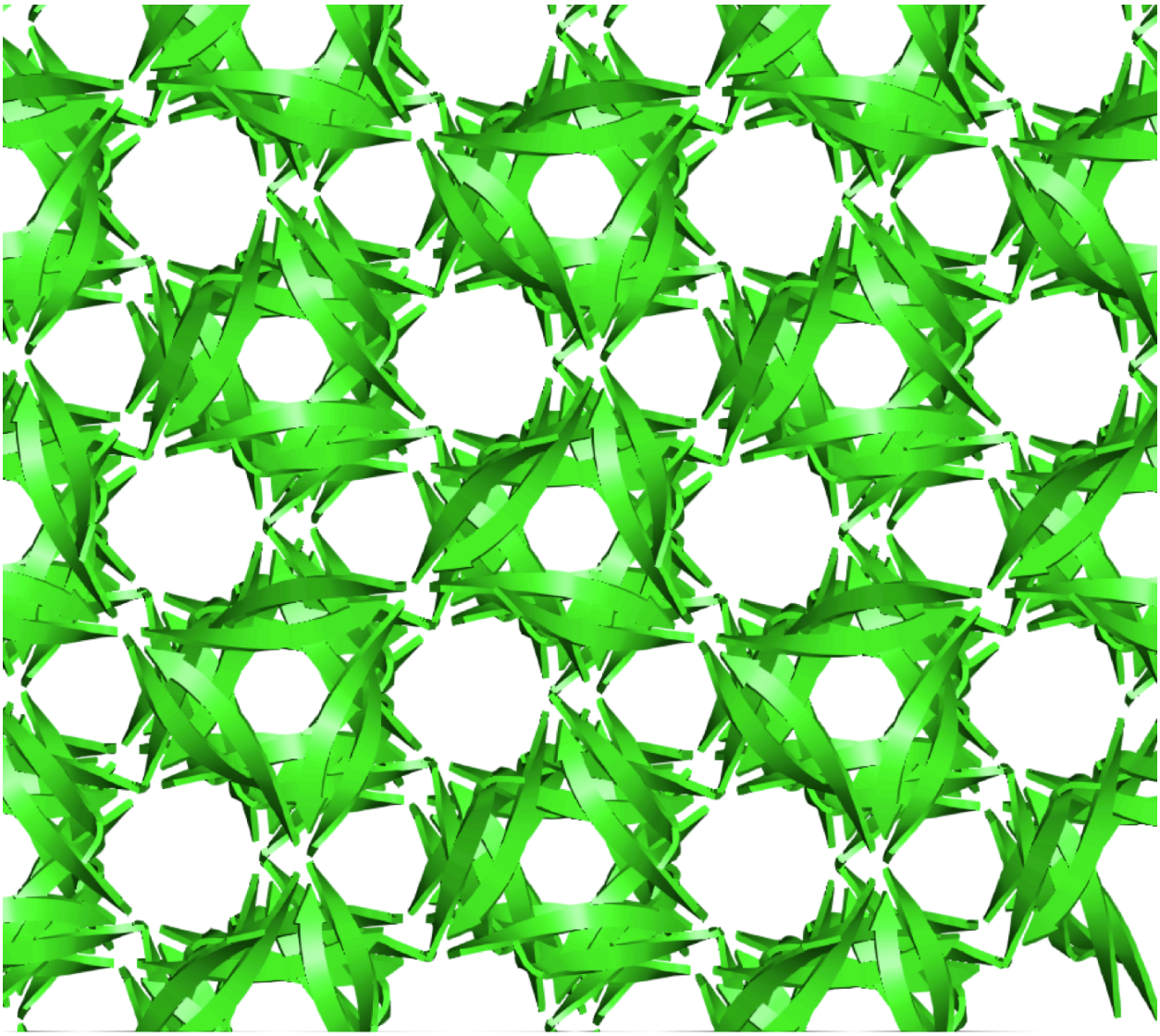

Figure 3.S2. Hexagonal arrangement of the columns of hexamers formed by trimer **3.5** in the crystal lattice (PDB 5SUT).

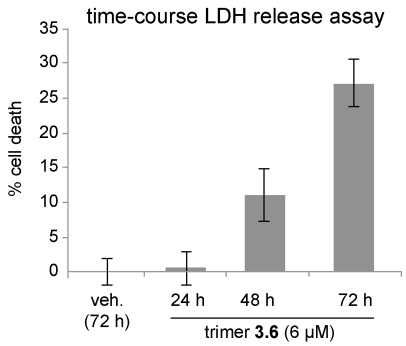

Figure 3.S3. Time-course LDH release assay of trimer **3.6**. Data represent the mean of five replicate wells +/− s.d. Deionized water (vehicle, veh.) was used as a negative control.

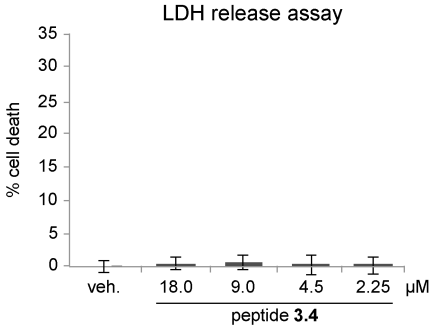

Figure 3.S4. LDH release assay of peptide **3.4**. Data represent the mean of five replicate wells +/− s.d. Deionized water (vehicle, veh.) was used as a negative control.

Table 3.S1. Crystallographic properties, crystallization conditions, and data collection and model refinement statistics for trimer **3.5**.

peptide	trimer **3.5** (synchrotron)	trimer **3.5** (X-ray diffractometer)
PDB ID	5SUT	5SUU
space group	*R*32	*R*32
a, *b*, *c* (Å)	49.59, 49.59, 64.18	50.23, 50.23, 64.80
α, β, λ (°)	90, 90, 120	90, 90, 120
peptides per asymmetric unit	2	2
crystallization conditions	0.1 M HEPES buffer at pH 7.3, 34% Jeffamine M-600 at pH 7.0	0.1 M HEPES buffer at pH 6.5, 32% Jeffamine M-600 at pH 7.0
wavelength (Å)	1.00	1.54
resolution (Å)	25.71–1.90 (1.97–1.902)	25.12–2.032 (2.104–2.032)
total reflections	5003 (502)	14674 (785)
unique reflections	2511 (255)	2115 (199)
multiplicity	2.0 (2.0)	6.9 (3.9)
completeness (%)	100 (100)	98.01 (90.87)
mean I/σ	32.71 (13.78)	33.18 (12.05)
Wilson B factor	21.97	19.35
R_{merge}	0.009174 (0.0249)	0.05975 (0.1306)
$R_{measure}$	0.01297 (0.03521)	0.06427
$CC_{1/2}$	1.000 (0.997)	0.999 (0.97)
CC^{*}	1.000 (0.999)	1.000 (0.992)
R_{work}	0.2053 (0.2177)	0.2163 (0.2512)
R_{free}	0.2160 (0.2297)	0.2398 (0.3544)
number of non-hydrogen atoms	260	262
RMS_{bonds}	0.027	0.007
RMS_{angles}	1.49	1.24
Ramachandran favored (%)	100	100
outliers (%)	0	0
clashscore	0	4.30
average B-factor	27.17	29.50
number of TLS groups	0	0
ligands/ions	Cl (1)	I (1), Cl (4)
water molecules	13	10

Table 3.S2. Crystallographic properties, crystallization conditions, and data collection and model refinement statistics for trimer **3.6**.

peptide	trimer **3.6** (synchrotron)	trimer **3.6** (X-ray diffractometer)
PDB ID	5SUR	5SUS
space group	$P6_322$	$P6_322$
a, *b*, *c* (Å)	57.40, 57.40, 94.14	57.08, 57.08, 93.68
α, β, λ (°)	90, 90, 120	90, 90, 120
peptides per asymmetric unit	4	4
crystallization conditions	0.1 M Tris buffer at pH 7.83, 0.2 M $MgCl_2$, 3.32 M 1,6-hexanediol	0.1 M Tris buffer at pH 7.70, 0.2 M $MgCl_2$, 3.45 M 1,6-hexanediol
wavelength (Å)	0.97	1.54
resolution (Å)	30.35–1.80 (1.866–1.801)	26.4–2.349 (2.433–2.349)
total reflections	17658 (1680)	8286 (792)
unique reflections	8947 (854)	4143 (395)
multiplicity	2.0 (2.0)	98.6 (77.9)
completeness (%)	99 (100)	100 (100)
mean I/σ	23.12 (1.13)	57.82 (13.40)
Wilson B factor	40.24	38.15
R_{merge}	0.01053 (0.6542)	0.089 (0.546)
$R_{measure}$	0.0149 (0.9252)	0.01254 (0.05735)
$CC_{1/2}$	0.972 (0.581)	0.945 (0.812)
CC^*	0.946 (0.692)	0.900 (0.279)
R_{work}	0.2114 (0.3543)	0.2241 (0.2355)
R_{free}	0.2523 (0.3648)	0.2823 (0.3445)
number of non-hydrogen atoms	564	521
RMS_{bonds}	0.011	0.011
RMS_{angles}	1.06	0.98
Ramachandran favored (%)	100	100
outliers (%)	0	0
clashscore	2.72	5.62
average B-factor	58.89	52.12
number of TLS groups	4	4
ligands/ions	Na (2), Cl (2), 1,6-hexanediol (4)	Na (1), Cl (1)
water molecules	35	27

Materials and Methods[1]

General information

All chemicals were used as received unless otherwise noted. Methylene chloride (CH_2Cl_2) was passed through alumina under nitrogen prior to use. Anhydrous, amine-free *N,N*-dimethylformamide (DMF) was purchased from Alfa Aesar. Deionized water (18 MΩ) was obtained from a Barnstead NANOpure Diamond water purification system. Analytical reverse-phase HPLC was performed on an Agilent 1200 instrument equipped with a Phenomonex Aeris PEPTIDE 2.6u XB-C18 column. Preparative reverse-phase HPLC was performed on a Beckman Gold Series P instrument equipped with an Agilent Zorbax SB-C18 column. HPLC grade acetonitrile and deionized water, each containing 0.1% trifluoroacetic acid (TFA), were used for analytical and preparative reverse-phase HPLC. All peptides were prepared and used as the trifluoroacetate salts and were assumed to have one trifluoroacetic acid molecule per amine group on each peptide.

*Synthesis of peptides **3.1**–**3.4**.*

a. *Loading of the resin.* 2-Chlorotrityl chloride resin (300 mg, 1.2 mmol/g) was added to a Bio-Rad Poly-Prep chromatography column (10 mL). The resin was suspended in dry CH_2Cl_2 (10 mL) and allowed to swell for 30 min. The solution was drained from the resin and a solution of Boc-Orn(Fmoc)-OH (0.50 equiv, 82 mg, 0.18 mmol) in 6% (v/v) 2,4,6-collidine in dry CH_2Cl_2 (8 mL) was added immediately and the suspension was gently agitated for 12 h. The solution was then drained and a mixture of CH_2Cl_2/MeOH/*N*,*N*-diisopropylethylamine (DIPEA) (17:2:1, 10 mL) was added immediately. The mixture was gently agitated for 1 h to cap the

unreacted 2-chlorotrityl chloride resin sites. The resin was then washed with dry CH_2Cl_2 (2x) and dried by passing nitrogen through the vessel. This procedure typically yields 0.12–0.15 mmol of loaded resin (0.4–0.5 mmol/g loading).

b. *Peptide coupling.* The Boc-Orn(Fmoc)-2-chlorotrityl resin generated from the previous step was transferred to a microwave-assisted solid-phase peptide synthesizer reaction vessel and submitted to cycles of automated peptide coupling with Fmoc-protected amino acid building blocks using a CEM Liberty 1 Automated Microwave Peptide Synthesizer. The linear peptide was synthesized from the *C*-terminus to the *N*-terminus. Each coupling cycle consisted of i. Fmoc-deprotection with 20% (v/v) piperidine in DMF for 2 min. at 50 °C (2x), ii. washing with DMF (3x), iii. coupling of the amino acid (0.75 mmol, 5 equiv) in the presence of HCTU (0.675 mmol, 4.5 equiv) and 20% (v/v) *N*-methylmorpholine (NMM) in DMF for 10 min. at 50 °C, iv. washing with DMF (3x). Special coupling conditions were used for the phenylalanine that followed the *N*-methylphenylalanine in peptides **3.2** and **3.4**: The phenylalanine was double coupled (0.75 mmol, 5 equiv.) and allowed to react at ambient temperature for 1 h per coupling with HATU (5 equiv) and HOAt (5 equiv) in 20% (v/v) NMM in DMF. After coupling of the last amino acid, the terminal Fmoc group was removed with 20% (v/v) piperidine in DMF (10 min. 50 °C). The resin was transferred from the reaction vessel of the peptide synthesizer to a Bio-Rad Poly-Prep chromatography column.

c. *Cleavage of the peptide from the resin.* The linear peptide was cleaved from the resin by agitating the resin for 1 h with a solution of 1,1,1,3,3,3-hexafluoroisopropanol (HFIP) in CH_2Cl_2. (1:4, 7 mL).[2] The suspension was filtered and the filtrate was collected in a 250 mL round-bottomed flask. The resin was washed with additional HFIP in CH_2Cl_2 (1:4, 7 mL) and then with CH_2Cl_2 (2×10 mL). The combined filtrates were concentrated by rotary evaporation to

give a white solid. The white solid was further dried by vacuum pump to afford the crude protected linear peptide, which was cyclized without further purification.

d. *Cyclization of the linear peptide.* The crude protected linear peptide was dissolved in dry DMF (150 mL). HOBt (114 mg, 0.75 mmol, 5 equiv) and HBTU (317 mg, 0.75 mmol, 5 equiv) were added to the solution. DIPEA (0.33 mL, 1.8 mmol, 12 equiv) was added to the solution and the mixture was stirred under nitrogen for 24 h. The mixture was concentrated under reduced pressure to afford the crude protected cyclic peptide.

e. *Global deprotection of the cyclic peptide.* The protected cyclic peptide was dissolved in TFA/triisopropylsilane (TIPS)/H_2O (18:1:1, 20 mL) in a 250 mL round-bottomed flask equipped with a nitrogen-inlet adaptor. The solution was stirred for 1.5 h. The reaction mixture was then concentrated by rotary evaporation under reduced pressure to afford the crude cyclic peptide as a thin yellow film on the side of the round-bottomed flask. The crude cyclic peptide was immediately subjected to purification by reverse-phase HPLC (RP-HPLC), as described below.

f. *Reverse-phase HPLC purification.* The peptide was dissolved in H_2O and acetonitrile (7:3, 10 mL), and the solution was filtered through a 0.2 μm syringe filter and purified by RP-HPLC (gradient elution with 20–50% CH_3CN over 50 min). Pure fractions were concentrated by rotary evaporation and lyophilized. Typical syntheses yielded ~55 mg of the peptide as the TFA salt.

*Synthesis of trimers **3.5** and **3.6**.*

Trimers **3.5** and **3.6** were synthesized by oxidizing peptides **3.3** and **3.4** in 20% aqueous DMSO.[3,4] A 6 mM solution of either lyophilized peptide **3.3** or **3.4** was prepared gravimetrically

by dissolving the peptide in an appropriate amount of 20% (v/v) aqueous DMSO prepared with deionized water. The reaction was carried out in a capped 25-mL glass scintillation vial with rocking at room temperature for 48–72 h. Next, the reaction mixture was diluted to a concentration of 300-μM peptide and transferred to a 500-mL round-bottomed flask. The solution was stirred with a magnetic stir bar for an additional 48 h. After 48 h, the reaction mixture was concentrated to ≤ 5 mL by rotary evaporation and immediately subjected to RP-HPLC purification (gradient elution with 20-50% CH_3CN over 60 min). Pure fractions were concentrated by rotary evaporation and lyophilized. Typical syntheses yielded ~15 mg trimer **3.5** and ~20 mg of trimer **3.6** from a 0.1 mmol scale synthesis of peptides **3.3** and **3.4**.

*Crystallization procedure for trimer **3.5***.

Trimer **3.5** afforded crystals in the same conditions that afforded crystals of peptides **3.1** and **3.2**: 0.1 M HEPES buffer and Jeffamine M-600. We further optimized these conditions according to the procedures detailed in the supporting information of Spencer *et al*. to yield crystals of trimer **3.5** suitable for X-ray crystallography. The optimized conditions consist of 0.1 M HEPES at pH 7.3 with 34% Jeffamine M-600.

Crystallization conditions for trimer **3.5** were optimized using a 4x6 matrix Hampton VDX 24-well plate. The HEPES buffer pH was varied in each row in increments of 0.5 pH units (6.5, 7.0, 7.5, and 8.0) and the Jeffamine M-600 concentration in each column in increments of 2% (26%, 28%, 30%, 32%, 34%, 36%). The first well in the 4x6 matrix was prepared by combined 100 μL of 1 M HEPES buffer at pH 6.5, 520 μL of 50% (v/v) aqueous Jeffamine M-600, and 380 μL of deionized water. The other wells were prepared in analogous fashion, by

combining 100 μL of HEPES buffer of varying pH and 50% (v/v) aqueous Jeffamine M-600 in varying amounts, and deionized water for a total volume of 1 mL in each well.

Three hanging-drops were prepared per borosilicate glass slide by combining a solution of trimer **3.5** (10 mg/mL in deionized water) and the well solution in the following amounts: 1 μL:1 μL, 2 μL:1 μL, and 1 μL:2 μL. Slides were inverted and pressed firmly against the silicone grease surrounding each well. Crystals of trimer **3.5** suitable for X-ray diffraction grew in ~2 days. Crystallization conditions were further optimized using smaller variations in HEPES buffer pH (in increments of 0.25 pH units) and Jeffamine M-600 concentrations (in increments of 1%). Crystals were harvested with a nylon loop attached to a copper or steel pin and flash frozen in liquid nitrogen prior to data collection. The optimized crystallization conditions for trimer **3.5** are summarized in Table S1.

*Crystallization procedure for trimer **3.6***.

Initial crystallization conditions for trimer **3.6** were determined using the hanging-drop vapor-diffusion method. Crystallization conditions were screened using three crystallization kits in a 96-well plate format (Hampton Index, PEG/Ion, and Crystal Screen). Three 150 nL hanging drops that differed in the ratio of peptide to well solution were made per condition in each 96-well plate for a total of 864 experiments. Hanging drops were made by combining an appropriate volume of trimer **3.6** (10 mg/mL in deionized water) with an appropriate volume of well solution to create three 150-nL hanging drops with 1:1, 1:2, and 2:1 peptide:well solution. The hanging drops were made using a TTP LabTech Mosquito nanodisperse instrument. Crystals of trimer **3.6** grew in ~48 h in a solution of 0.1 M Tris buffer at pH 7.0 with 0.2 M $MgCl_2$ and 3.5 M 1,6-hexanediol.

Crystallization conditions for trimer **3.6** were optimized using a 4x6 matrix Hampton VDX 24-well plate. The Tris buffer pH was varied in each row in increments of 0.5 pH units (6.5, 7.0, 7.5, and 8.0) and the 1,6-hexanediol concentration in each column in increments of 0.2 M (3.0 M, 3.2 M, 3.4 M, 3.6 M, 3.8 M, 4.0 M). The first well in the 4x6 matrix was prepared by combined 100 μL of 1 M Tris buffer at pH 6.5, 100 μL of 2 M $MgCl_2$, 600 μL of 5 M 1,6-hexanediol, and 200 μL of deionized water. The other wells were prepared in analogous fashion, by combining 100 μL of Tris buffer of varying pH, 100 μL of 2 M $MgCl_2$, 5 M 1,6-hexanediol in varying amounts, and deionized water for a total volume of 1 mL in each well.

Three hanging-drops were prepared per borosilicate glass slide by combining a solution of trimer **3.6** (10 mg/mL in deionized water) and the well solution in the following amounts: 1 μL:1 μL, 2 μL:1 μL, and 1 μL:2 μL. Slides were inverted and pressed firmly against the silicone grease surrounding each well. Crystals of trimer **3.6** suitable for X-ray diffraction grew in ~5 days. Crystallization conditions were further optimized using smaller variations in Tris buffer pH (in increments of 0.25 pH units) and 1,6-hexanediol concentrations (in increments of 0.1 M). Crystals were harvested with a nylon loop attached to a copper or steel pin and flash frozen in liquid nitrogen prior to data collection. The optimized crystallization conditions for trimer **3.6** are summarized in Table S2.

*X-ray crystallographic data collection, data processing, and structure determination for trimers **3.5** and **3.6**.*

Diffraction data for trimers **3.5** and **3.6** were collected on a Rigaku Micromax-007HF X-ray diffractometer with a rotating copper anode at 1.54 Å wavelength with 0.5° oscillation. Diffraction data were collected using CrystalClear. Diffraction data were scaled and merged

using XDS.[6] Coordinates for the anomalous signals were determined by HySS in the Phenix software suite 1.10.1.[7] Electron density maps were generated using anomalous coordinates determined by HySS as initial positions in Autosol. Molecular manipulation of the model was performed with Coot.[5] Coordinates were refined with phenix.refine.

Diffraction data for trimer **3.5** were also collected at the Advanced Light Source at Lawrence Berkeley National Laboratory with a synchrotron source at 1.00-Å wavelength to achieve higher resolution. Data for trimer **3.5** suitable for refinement at 2.03 Å were obtained from the diffractometer; data for trimer **3.5** suitable for refinement at 1.90 Å were obtained from the synchrotron. Diffraction data were scaled and merged using XDS.[6] The electron density map was generated by molecular replacement using the coordinates from the structure of trimer **3.5** generated by soaking in KI using Phaser in the Phenix software suite 1.10.1.[7] Molecular manipulation of the model was performed with Coot. Coordinates were refined with phenix.refine.

Diffraction data for trimer **3.6** were also collected at the Stanford Synchrotron Radiation Lightsource (SSRL) with a synchrotron source at 0.97-Å wavelength.[8] Diffraction data were scaled and merged using XDS.[6] The electron density map was generated by molecular replacement using the coordinates from the structure of trimer **3.6** generated by S-SAD using Phaser in the Phenix software suite 1.10.1.[7] Molecular manipulation of the model was performed with Coot. Coordinates were refined with phenix.refine.

Preparation of $A\beta_{42}$ oligomers

Recombinantly expressed $A\beta_{42}$ was purchased as the NH_4OH treated salt from rPeptide (catalog# A-1167-2). $A\beta_{42}$ oligomers were prepared according to the procedure developed by Teplow and coworkers.[9,10] A 1.0-mg aliquot of $A\beta_{42}$ received from rPeptide was dissolved in 1.0 mL of 2 mM NaOH, and sonicated in an ultrasonic water bath for 1 min. The pH of the $A\beta_{42}$ solution after NaOH addition was ~10.5. Next, the $A\beta_{42}$ solution was aliquotted into 0.0055-μmol aliquots in 0.5-mL microcentrifuge tubes. A hole in the top of each microcentrifuge tube was created by pushing a 22-gauge needle through the top of the tube. The samples were then frozen at -80 °C for ~5 hours, and lyophilized overnight. After lyophilization, the $A\beta_{42}$ aliquots were stored in a desiccator at -20 °C until use.

For LDH and caspase-3 activation assays a 0.0055-μmol aliquot of $A\beta_{42}$ was dissolved in 11 μL of 20 mM HEPES buffer at pH 7.4, and then immediately diluted with 99 μL of phenol red free, serum free DMEM:F12 (1:1) media to create a 50 μM $A\beta_{42}$ working solution. The 50 μM $A\beta_{42}$ working solution was serially diluted with DMEM:F12 (1:1) media to create 25- and 12.5-μM working solutions.

For SDS-PAGE a 0.0055-μmol aliquot of $A\beta_{42}$ was dissolved in 11 μL of 20 mM HEPES buffer at pH 7.4, and then immediately diluted with 11 μL of 2X SDS-PAGE loading buffer (100 mM Tris buffer at pH 6.8, 20% (v/v) glycerol, and 4% w/v SDS).

LDH release and caspase-3 activation assays.

The toxicity of peptides **3.1** and **3.2** and trimers **3.5** and **3.6** toward SH-SY5Y cells was assessed by LDH release and caspase-3 activation assays. Cells were incubated in the presence or absence of equivalent concentrations of peptides **3.1** and **3.2** or trimers **3.5** and **3.6** for 72 h in

96-well plates. The LDH release assay was performed using the Pierce LDH Cytotoxicity Assay Kit from Thermo Scientific. The caspase-3 assay was performed using the Roche APO-One Homogeneous Caspase-3/7 Assay. Experiments were performed in replicates of five, and an additional 10 wells were used for controls. Cells were cultured in the inner 60 wells (rows B–G, columns 2–11) of the 96-well plate. DMEM:F12 media (100 μL) was added to the outer wells (rows A and H and columns 1 and 12), in order to ensure the greatest reproducibility of data generated from the inner wells.

a. *Preparation of stock solutions of peptides **3.1** and **3.2** and trimers **3.5** and **3.6**.* 10-mg/mL stock solutions of peptides **3.1** and **3.2** and trimers **3.5** and **3.6** were prepared gravimetrically by dissolving 1.0 mg of each compound in 100 μL of deionized water that was either filtered through a 0.2 μm syringe filter or autoclaved. The stock solution was used to create 180-μM working solutions of peptides **3.1** and **3.2** or 60-μM working solutions of trimers **3.5** and **3.6**. [These solutions contain equivalent concentrations of peptide.] The 180-μM working solutions of peptides **3.1** and **3.2** were serially diluted with deionized water to create 90-μM working solutions of peptides **3.1** and **3.2**. The 60-μM working solutions of trimers **3.5** and **3.6** were serially diluted with deionized water to create 30-, 15-, and 7.5-μM working solutions of trimers **3.5** and **3.6**.

b. *Preparation of SH-SY5Y cells for LDH release and caspase-3 activation assays.* SH-SY5Y cells were plated in a 96-well plate at 30,000 cells per well. Cells were incubated in 100 μL of a 1:1 mixture of DMEM:F12 media supplemented with 10% fetal bovine serum, 100 U/mL penicillin, and 100 μg/mL streptomycin at 37 °C in a 5% CO_2 atmosphere and allowed to adhere to the bottom of the plate for 24 hours.

c. *Treatment of SH-SY5Y cells with peptides **3.1** and **3.2** and trimers **3.5** and **3.6**.* After 24 hours, the culture media was removed and replaced with 90 μL of serum-free DMEM:F12 media. A 10-μL aliquot of the working solution of peptide **3.1** or **3.2** or trimer **3.5** or **3.6** was added to each well, for well concentrations of 18 μM and 9 μM for peptides **3.1** and **3.2**, 6 μM and 3 μM for trimer **3.5**, and 6 μM, 3 μM, 1.5 μM, and 0.75 μM for trimer **3.6**. Experiments were run in replicates of five. Five wells were used as controls and received 10-μL aliquots of deionized water (vehicle). Another five wells were left untreated, to be subsequently used as controls with lysis buffer for the LDH release assay, or staurosporine for the caspase-3 activation assay. Cells were incubated at 37 °C in a 5% CO_2 atmosphere for 72 hours.

d. *LDH release assay.* After 72 hours, 10 μL of 10x lysis buffer—included with the assay kit—was added to the five untreated wells, and the cells were incubated for an additional 45 minutes. After 45 min, a 50-μL aliquot of the supernatant media from each well was transferred to a new 96-well plate and 50 μL of LDH substrate solution, prepared according to manufacturer's protocol, was added to each well. The treated plates were stored in the dark for 30 min, then 100 μL of stop solution was added to each well. The absorbance of each well was measured at 490 and 680 nm (A_{490} and A_{680}). Data were processed by calculating the differential absorbance for each well ($A_{490}-A_{680}$) and comparing those values to those of the lysis buffer controls and the untreated controls:

$$\%\ \text{cell death} = [(A_{490}-A_{680})_{\text{compound}} - (A_{490}-A_{680})_{\text{vehicle}}] / [(A_{490}-A_{680})_{\text{lysis}} - (A_{490}-A_{680})_{\text{vehicle}}]$$

e. *Caspase-3 activation assay.* After 67 hours, 10 μL of 150 μM or 50 μM staurosporine was added to the remaining five wells, and the cells were incubated for an additional 5 h. Next, the compound-containing media was removed and replaced with 25 μL of fresh serum-free DMEM/F12 media. A 25-μL aliquot of caspase-3 substrate, prepared according to

manufacturer's protocol, was then added to each well. The plate was sealed with a clear adhesive plate sealer, and fluorescence was monitored over 18 h while shaking at 250 rpm using a Gemini XPS fluorescence plate reader (excitation at 499 nm, emission at 521 nm). Data from the 18 h time point were processed by subtracting the relative fluorescence unit (RFU) values of the vehicle control wells from the RFU values of wells treated with peptides **3.1** and **3.2** and trimers **3.5** and **3.6**.

*Dot blot analysis of peptides **3.1** and **3.2** and trimers **3.5** and **3.6**.*

10-mg/mL stock solutions of peptides **3.1** and **3.2** and trimers **3.5** and **3.6** were prepared gravimetrically by dissolving 1.0 mg of each compound in 100 μL of deionized water that was filtered through a 0.2 μm syringe filter. An aliquot of each stock solution was diluted with deionized water to make 3.0-mg/mL solutions. The 3.0-mg/mL solutions were then serially diluted with deionized water to create 1.5-, 0.75-, and 0.37-mg/mL solutions. A 5 μL aliquot of each solution from the serial dilution was combined with 5 μL of a 2X solution of phosphate buffered saline (PBS) at pH 7.4 to generate 1.5-, 0.75-, 0.37-, and 0.18-mg/mL buffered solutions of peptides **3.1** and **3.2** and trimers **3.5** and **3.6**. A 1.0-μL aliquot of each buffered solution was spotted onto a nitrocellulose membrane and allowed to air dry (~5 min). Non-reactive sites were blocked with 10% (w/v) non-fat powdered milk in low-Tween Tris-buffered saline (TBS-lT: 20 mM Tris, 137 mM NaCl, 0.01% Tween 20, pH 7.6) for 1 h at room temperature with rocking. The membrane was then incubated while rocking overnight at 4 °C in primary A11 antibody (200 μg/mL) in 5% (w/v) non-fat powdered milk in TBS-lT. The next day, the membrane was washed with TBS-lT for 5 min (3X). The membrane was then incubated while rocking with horseradish peroxidase conjugated goat anti-rabbit antibody (100 μg/mL) (Jackson

ImmunoResearch catalog# 111-035-003) in 5% (w/v) non-fat powdered milk in TBS-lT for 1 h at room temperature. The membrane was then washed with TBS-lT for 5 min (3X). A 10-mL portion of chemiluminescence substrate (Thermo Scientific SuperSignal West Femto Maximum Sensitivity Substrate, product# 34095) was prepared according to manufacture's protocol and poured onto the membrane. The membrane was allowed to incubate in the chemiluminescence substrate for ~10 min before imaging. The blot was imaged using a standard digital SLR camera.[11]

Size exclusion chromatography.

The oligomerization of peptides **3.1** and **3.2** and trimers **3.5** and **3.6** was studied by size-exclusion chromatography (SEC) at 4 °C in 50 mM sodium acetate/50 mM acetic acid buffer (sodium acetate buffer, pH 4.7) as follows: Each peptide or trimer was dissolved in deionized water to a concentration of 10 mg/mL. The peptide or trimer solutions were then diluted to 1 mg/mL by adding 80 μL of the 10-mg/mL solutions to 720 μL of sodium acetate buffer. The peptide or trimer solutions were loaded onto a GE Superdex 75 10/300 GL column at 0.5 mL/min over 1 min. After loading, the samples were run with sodium acetate buffer at 1 mL/min. Chromatograms were recorded at 214 nm and normalized to the highest absorbance value. Standards (cytochrome C, aprotinin, and vitamin B12) were run in the same fashion.

SDS-PAGE and silver staining.

The oligomerization of peptides **3.1** and **3.2** and trimers **3.5** and **3.6** was studied by Tricine SDS-PAGE. Reagents and gels for Tricine SDS-PAGE were prepared according to

recipes and procedures detailed in Schägger, H. *Nat. Protoc.* **2006**, *1*, 16–22.[12]

Sample preparation. Each peptide or trimer was dissolved in deionized water to a concentration of 10 mg/mL. Aliquots of the 10-mg/mL solutions were diluted with deionized water to create 2.0-mg/mL solutions of peptides **3.1** and **3.2** and 0.12-mg/mL solutions of trimers **3.5** and **3.6**. The 1.0-mg/mL solutions of peptides **3.1** and **3.2** and the 0.12-mg/mL solutions of trimers **3.5** and **3.6** were further diluted with 2X SDS-PAGE loading buffer (100 mM Tris buffer at pH 6.8, 20% (v/v) glycerol, and 4% SDS) to create 1.0-mg/mL working solutions of peptides **3.1** and **3.2** and 0.06-mg/mL working solutions of trimers **3.5** and **3.6**. A 5.0-μL aliquot of each working solution was run on a 16% polyacrylamide gel with a 4% stacking polyacrylamide gel. The gels were run at a constant 60 volts at 4 °C.

Staining with silver nitrate was used to visualize peptides **3.1** and **3.2** and trimers **3.5** and **3.6** in the SDS-PAGE gel. Reagents for silver staining were prepared according to procedures detailed in Simpson, R. J. *CSH Protoc.* **2007**.[13] Briefly, the gel was removed from the casting glass and rocked in fixing solution (50% (v/v) methanol and 5% (v/v) acetic acid in deionized water) for 20 min. Next, the fixing solution was discarded and the gel was rocked in 50% (v/v) aqueous methanol for 10 min. Next, the 50% methanol was discarded and the gel was rocked in deionized water for 10 min. Next, the water was discarded and the gel was rocked in 0.02% (w/v) sodium thiosulfate in deionized water for 1 min. The sodium thiosulfate was discarded and the gel was rinsed with deionized water for 1 min (2X). After the last rinse, the gel was submerged in chilled 0.1% (w/v) silver nitrate in deionized water and rocked at 4 °C for 20 min. Next, the silver nitrate solution was discarded and the gel was rinsed with deionized water for 1 min (2X). To develop the gel, the gel was incubated in developing solution (2% (w/v) sodium carbonate, 0.04% (w/v) formaldehyde until the desired intensity of staining was reached

(~1–3 min). When the desired intensity of staining was reached, the development was stopped by discarding the developing solution and submerging the gel in 5% aqueous acetic acid.

Circular dichroism spectroscopy.

A 0.30 mg/mL solution of either trimer **3.5** or **3.6** or peptide **3.1** or **3.2** was prepared by adding 15 μL of 10 mg/mL stock solutions in deionized water to 385 μL of 10 mM potassium phosphate buffer at pH 7.4. Each solution was transferred to a 1 mm quartz cuvette for data acquisition. CD spectra were acquired on a Jasco J-810 circular dichroism spectropolarimeter at room temperature. Data were collected using 0.2 nm intervals from 260 nm to 190 nm and averaged over five accumulations with smoothing.

References and Notes

1 These procedures follow closely those that our laboratory has previously published. The procedures in this section are adapted from and in some cases taken verbatim from Kreutzer, A. G.; Hamza, I. L.; Spencer, R. K.; Nowick J. S. *J. Am. Chem. Soc.* **2016**, *138*, 4634–4642, Spencer, R. K.; Kreutzer, A. G.; Salveson, P. J.; Li, H.; Nowick, J. S. *J. Am. Chem. Soc. 137*, **2015**, 6304–6311, and Spencer, R. K.; Li. H.; Nowick, J. S. *J. Am. Chem. Soc.* **2014**, *136*, 5595–5598.

2 Bollhagen, R.; Schmiedberger, M.; Barlosb, K.; Grell, E. *J. Chem. Soc., Chem. Commun.* **1994**, 2559–2560.

3 Tam, J. P.; Wu, C. R.; Liu, W.; Zhang, J. W. *J. Am. Chem. Soc.* **1991**, *113*, 6657–6662.

4 Khakshoor, O.; Nowick, J. S. *Org. Lett.* **2009**, *11*, 3000-3003.

5 Emsley, P.; Lohkamp, B.; Scott, W. G.; Cowtan, K. *Acta. Cryst.* **2010**, *D66*, 486–501.

6 Kabsch, W. *Acta Cryst.* **2010**, *D66*, 125–132.

7 Adams, P. D.; Afonine, P. V.; Bunkóczi, G.; Chen, V. B.; Davis, I. W.; Echols, N.; Headd, J. J.; Hung, L.-W.; Kapral, G. J.; Grosse-Kunstleve, R. W.; McCoy, A. J.; Moriarty, N. W.; Oeffner, R.; Read, R. J.; Richardson, D. C.; Richardson, J. S.; Terwilliger, T. C.; Zwart., P. H. *Acta Cryst.* **2010**, *D66*, 213–221.

8 The Berkeley Center for Structural Biology is supported in part by the National Institutes of Health, National Institute of General Medical Sciences, and the Howard Hughes Medical Institute. The Advanced Light Source is supported by the Director, Office of Science, Office

of Basic Energy Sciences, of the U.S. Department of Energy under Contract No. DE-AC02-05CH11231.

9 Teplow, D. B. *Methods Enzymol.* **2006**, *413*, 20–33.

10 Fezoui, Y.; Hartley, D. M.; Harper, J. D.; Khurana, R.; Walsh, D. M.; Condron, M. M.; Selkoe, D. J.; Lansbury, P. T. Jr.; Fink, A. L.; Teplow, D. B. *Amyloid*. **2000**, *7*, 166–178.

11 Khoury, M. K.; Parker, I.; Aswad, D.W. *Anal. Biochem.* **2010**, *397*, 129–131.

12 Schägger, H. *Nat. Protoc.* **2006**, *1*, 16–22.

13 Simpson, R. J. *CSH Protoc.* **2007**, doi: 10.1101/pdb.prot4727.

Characterization Data

*Characterization of peptide **3.1***

Analytical HPLC trace of peptide **3.1**.

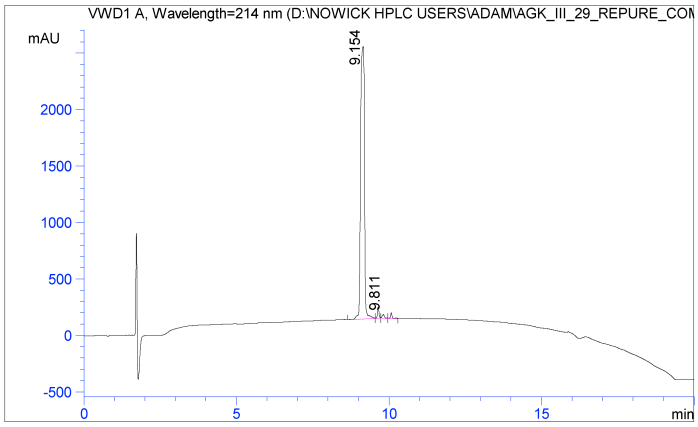

Signal 1:VWD1 A, Wavelength=214 nm

Peak #	RT [min]	Type	Width [min]	Area mAU*s	Height [mAU]	Area %
1	9.154	MM	0.144	20963.105	92.861	96.669
2	9.649	MM	0.056	340.649	3.898	1.571
3	9.811	MM	0.088	165.284	1.202	0.762
4	10.078	MM	0.068	216.490	2.039	0.998

Mass spectrum and expansions of peptide **3.1**.

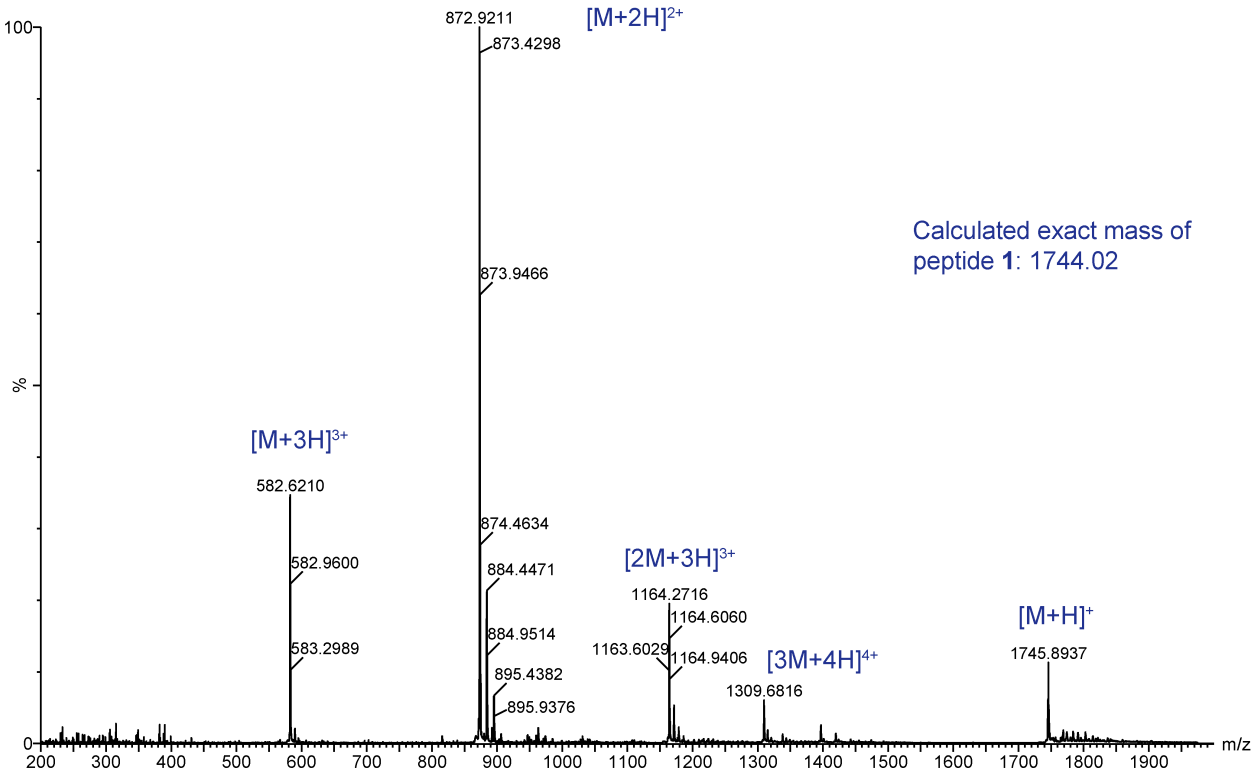

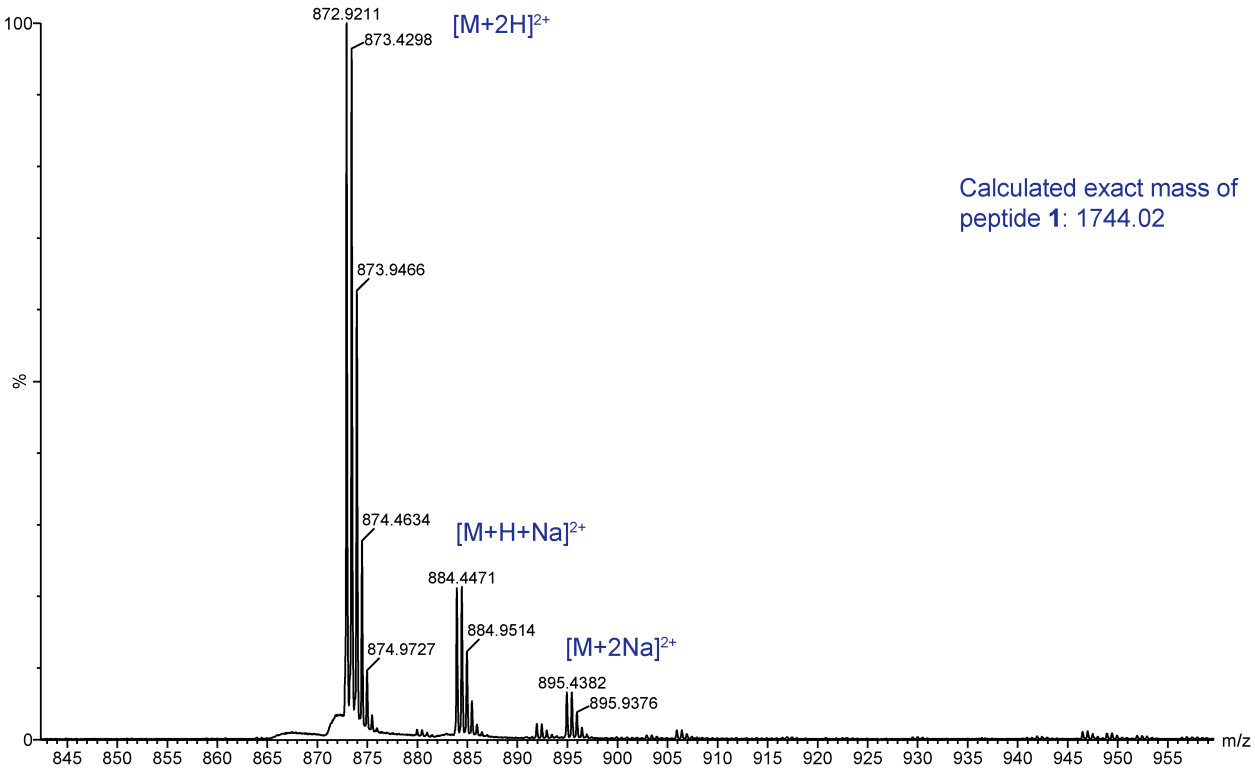

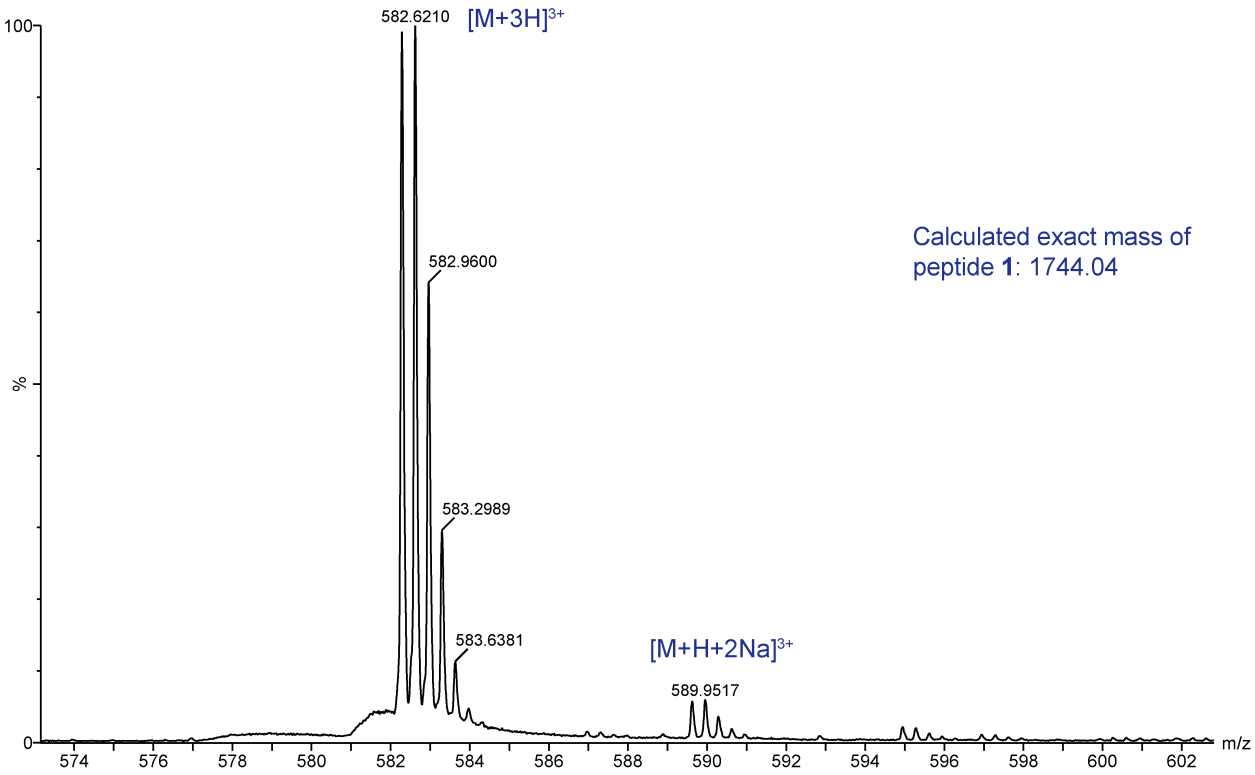
582.6210
[M+3H]3+
582.9600
583.2989
583.6381
[M+H+2Na]3+
589.9517
Calculated exact mass of peptide 1: 1744.04
100
%
0
574
576
578
580
582
584
586
588
590
592
594
596
598
600
602
m/z

*Characterization of peptide **3.2***

Analytical HPLC trace of peptide **3.2**.

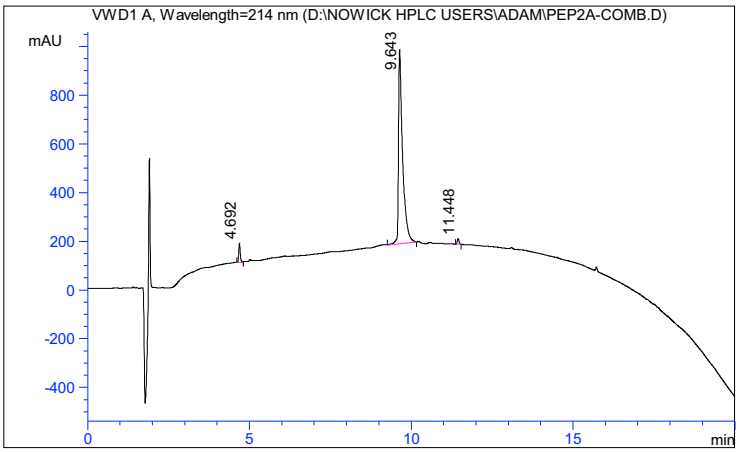

Signal 1:VWD1 A, Wavelength=214 nm

Peak #	RT [min]	Type	Width [min]	Area mAU*s	Height [mAU]	Area %
1	4.692	MM	0.058	278.627	8.806	3.732
2	9.643	MM	0.148	7104.079	88.643	95.157
3	11.448	MM	0.060	82.934	2.551	1.111

Mass spectrum and expansions of peptide **3.2**.

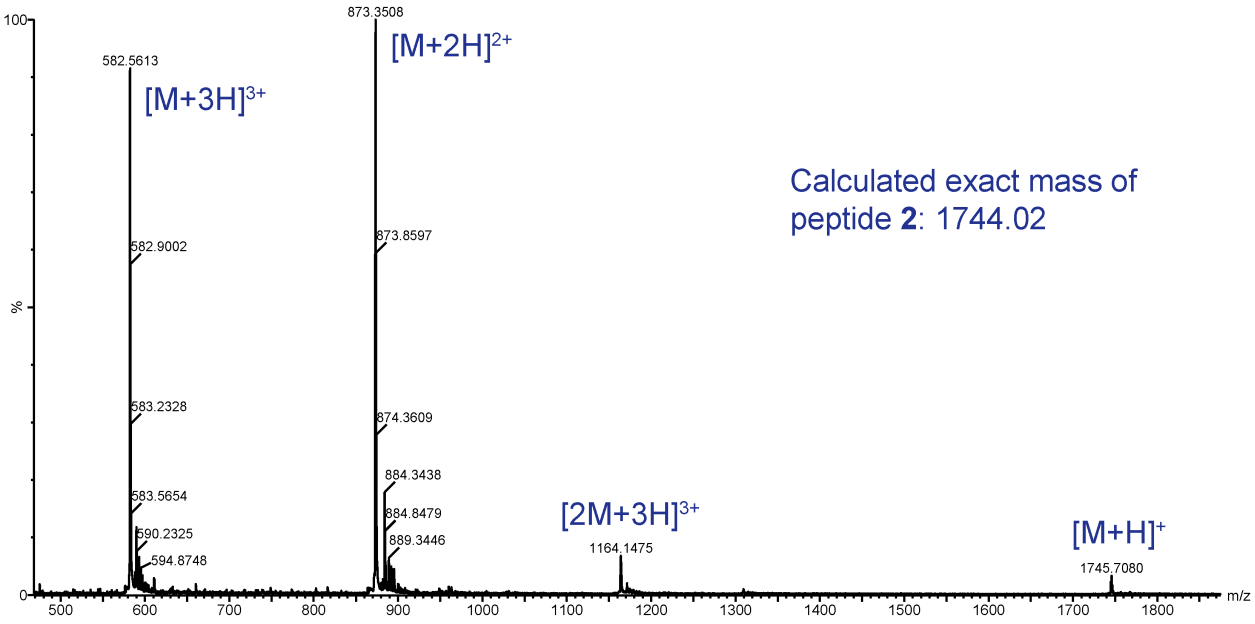

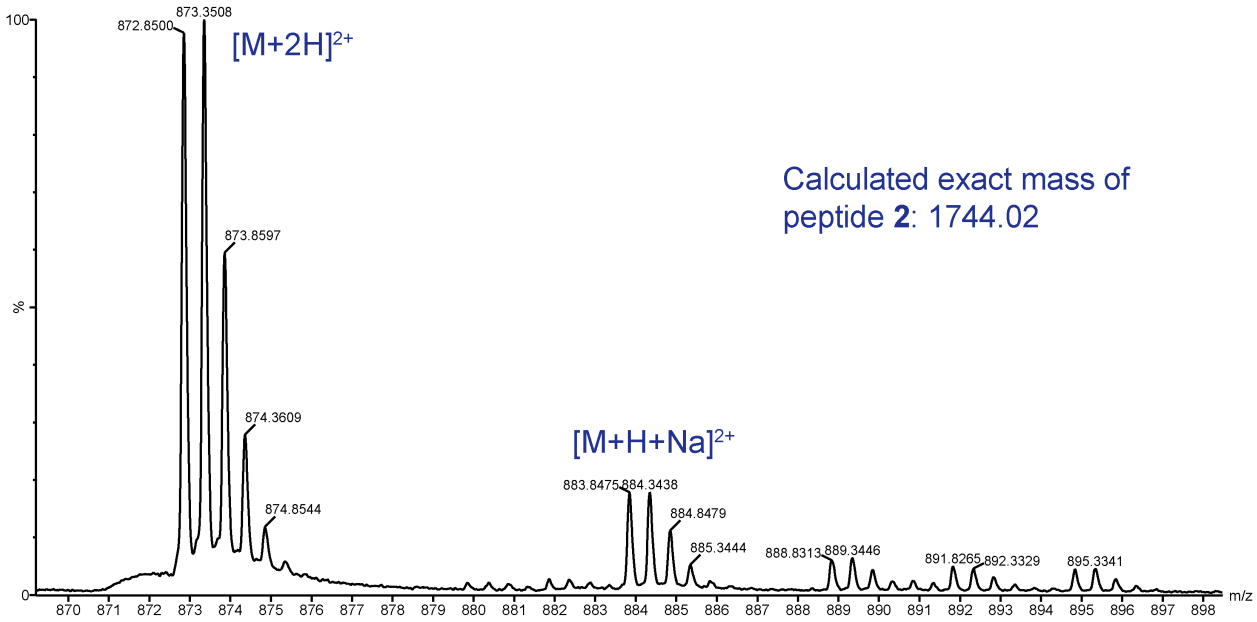

Calculated exact mass of peptide **2**: 1744.02

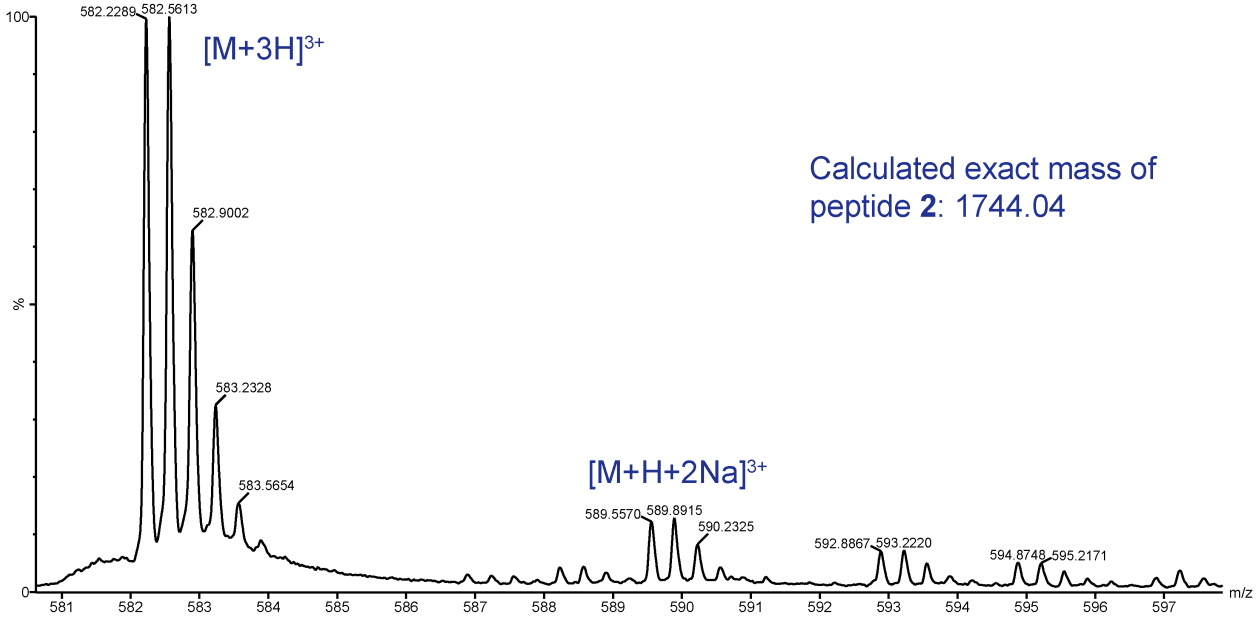

Calculated exact mass of peptide **2**: 1744.04

*Characterization of peptide **3.3***

Analytical HPLC trace of peptide **3.3**.

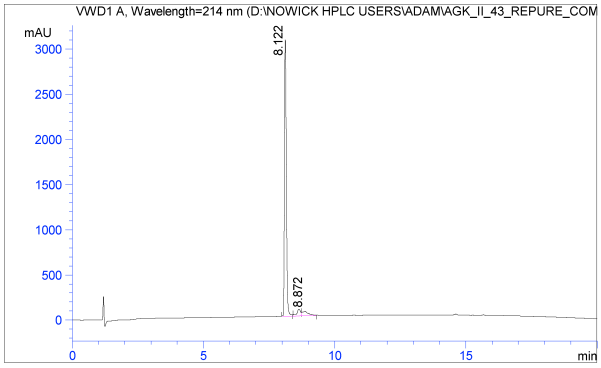

Signal 1:VWD1 A, Wavelength=214 nm

Peak #	RT [min]	Type	Width [min]	Area mAU*s	Height [mAU]	Area %
1	8.122	BB	0.081	15238.801	96.038	90.206
2	8.641	BV	0.149	763.724	2.318	4.521
3	8.872	VB	0.218	890.721	1.645	5.273

Mass spectrum and expansions of peptide **3.3**.

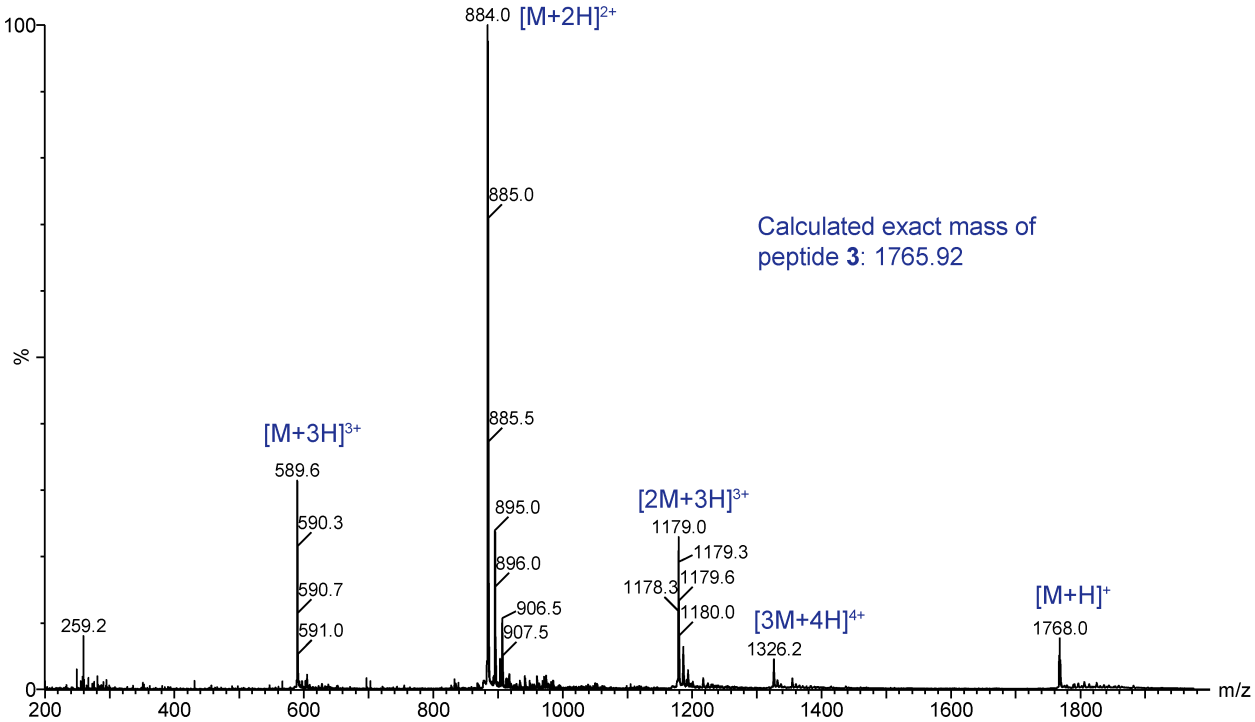

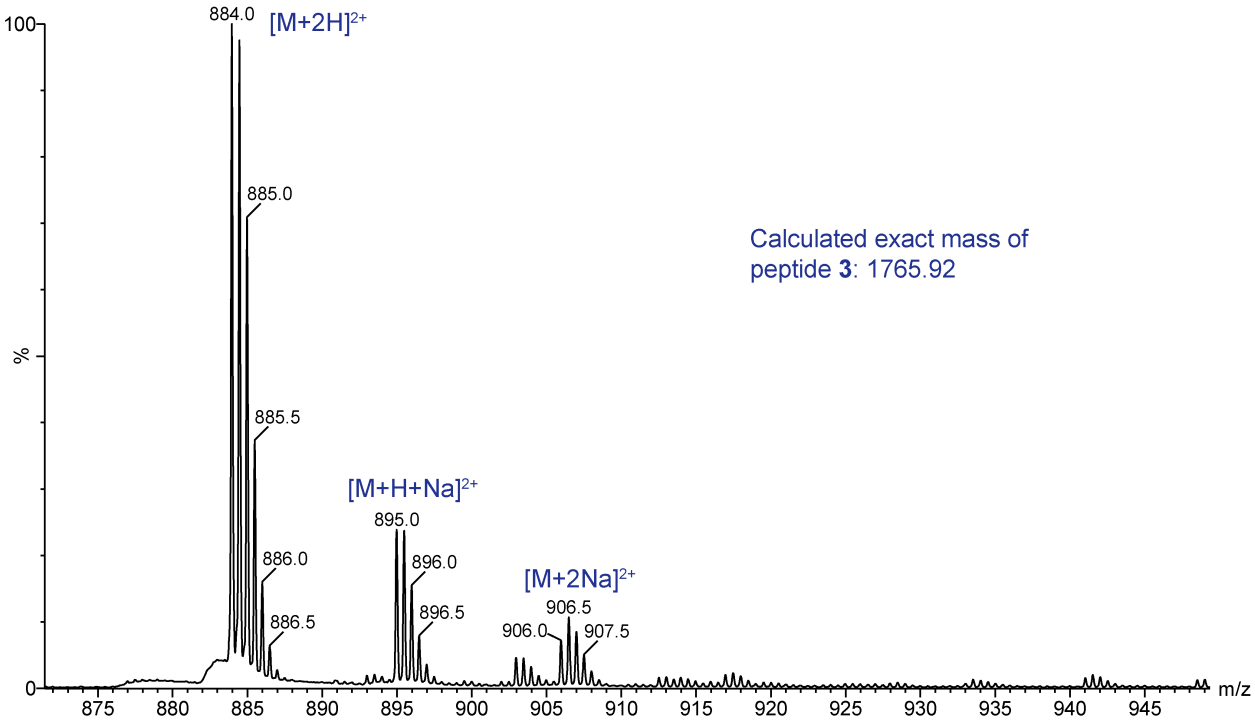
100
%
0
884.0
[M+2H]2+
885.0
885.5
886.0
886.5
[M+H+Na]2+
895.0
896.0
896.5
[M+2Na]2+
906.0
906.5
907.5
Calculated exact mass of
peptide 3: 1765.92
875
880
885
890
895
900
905
910
915
920
925
930
935
940
945
m/z

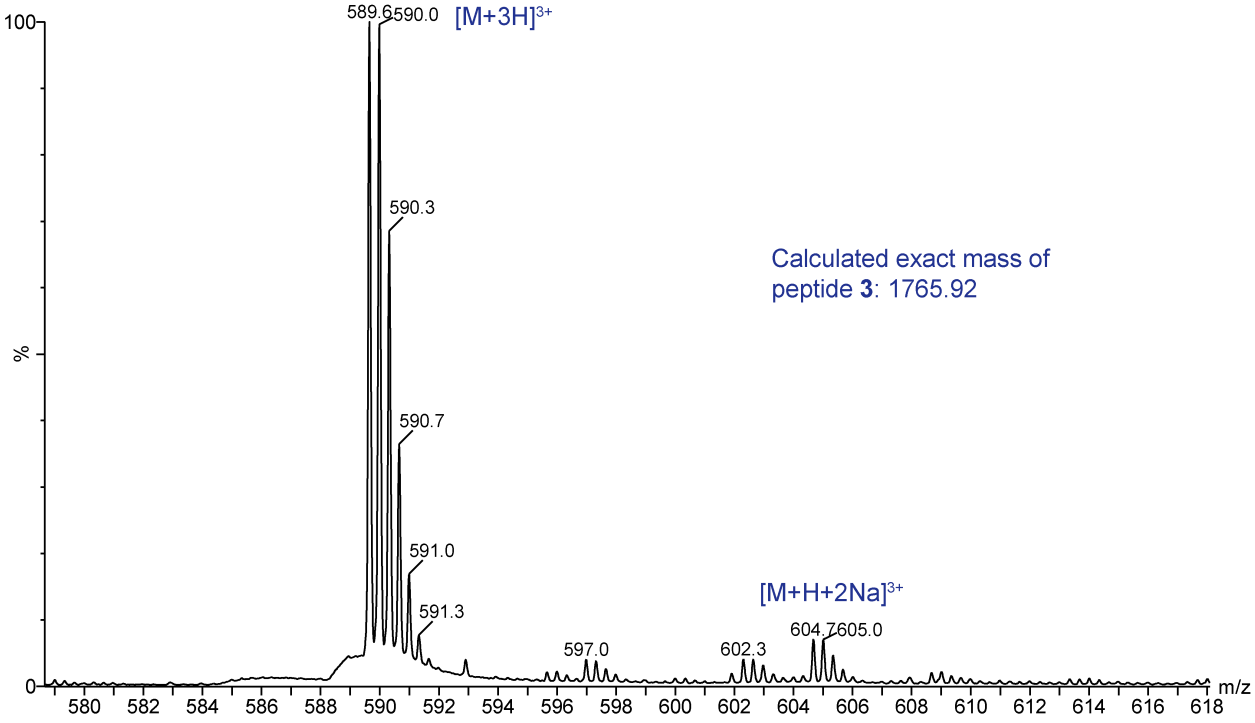
100
%
0
589.6
590.0
[M+3H]3+
590.3
590.7
591.0
591.3
597.0
602.3
604.7
605.0
[M+H+2Na]3+
Calculated exact mass of
peptide 3: 1765.92
580
582
584
586
588
590
592
594
596
598
600
602
604
606
608
610
612
614
616
618
m/z

*Characterization of peptide **3.4***

Analytical HPLC trace of peptide **3.4**.

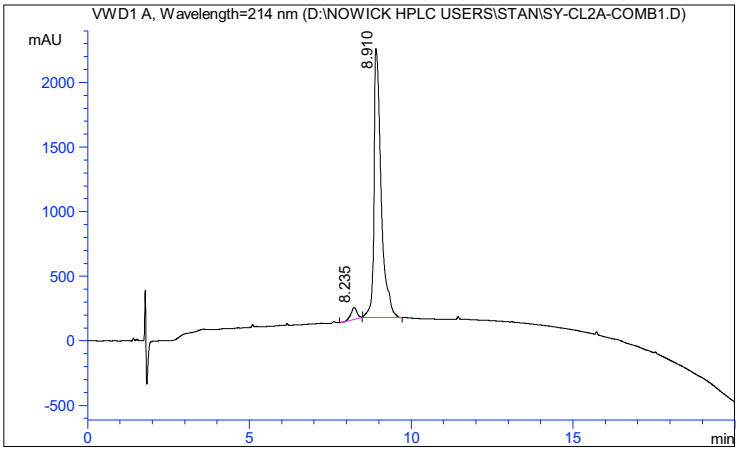

Signal 1:VWD1 A, Wavelength=214 nm

Peak #	RT [min]	Type	Width [min]	Area mAU*s	Height [mAU]	Area %
1	8.235	MM	0.225	1285.120	4.362	3.856
2	8.910	MM	0.256	32039.193	95.638	96.144

Mass spectrum and expansions of peptide **3.4**.

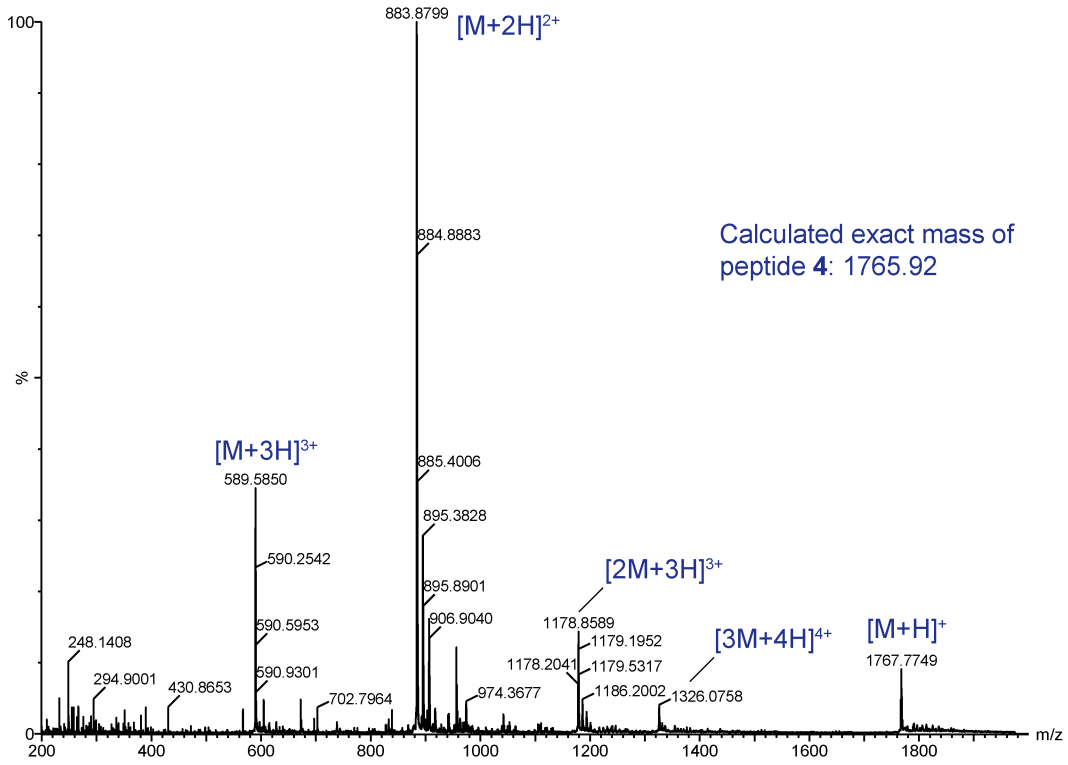

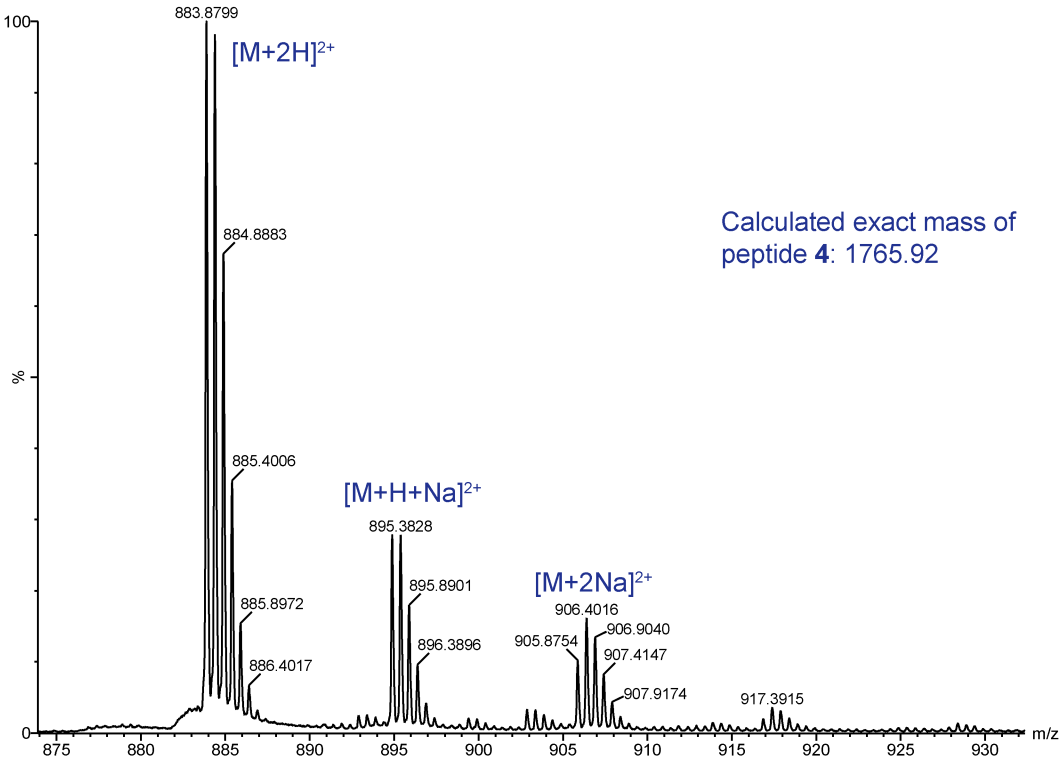

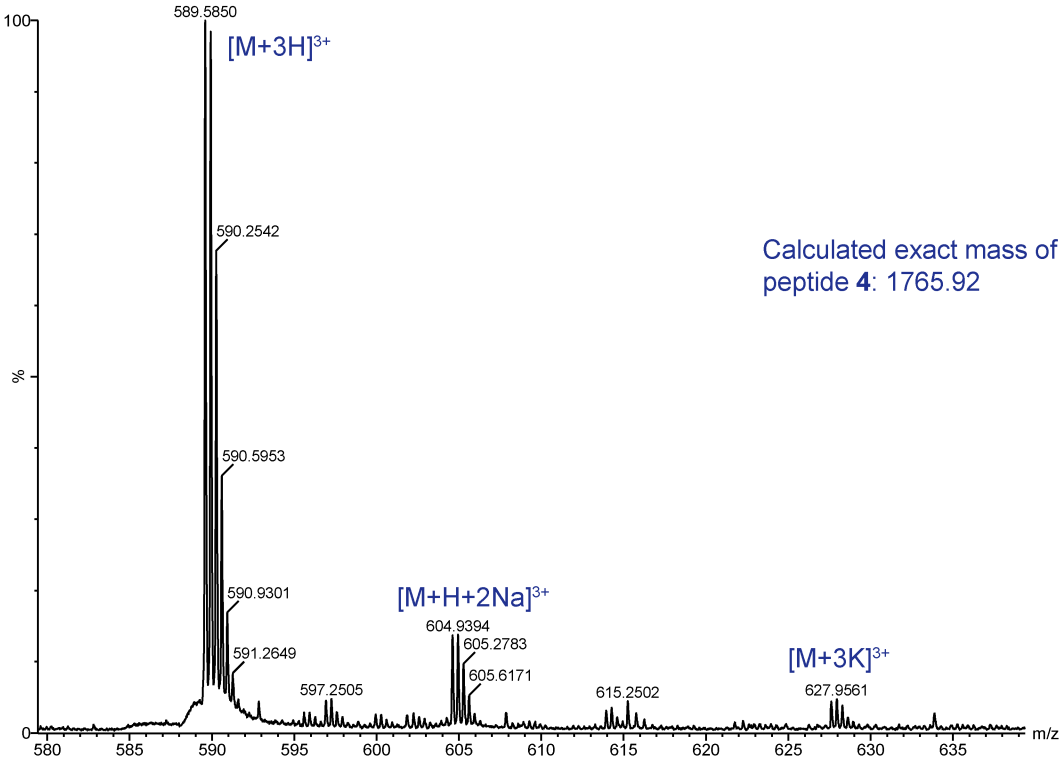
589.5850
[M+3H]3+
590.2542
590.5953
590.9301
591.2649
597.2505
[M+H+2Na]3+
604.9394
605.2783
605.6171
615.2502
[M+3K]3+
627.9561
100
%
0
580
585
590
595
600
605
610
615
620
625
630
635
m/z
Calculated exact mass of peptide 4: 1765.92

*Characterization of trimer **3.5***

Analytical HPLC trace of trimer **3.5**.

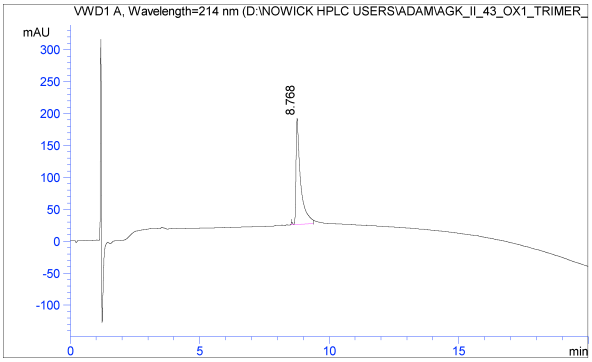

Signal 1:VWD1 A, Wavelength=214 nm

Peak #	RT [min]	Type	Width [min]	Area mAU*s	Height [mAU]	Area %
1	8.768	BB	0.174	2057.338	100.000	100.000

Mass spectrum and expansions of trimer **3.5**.

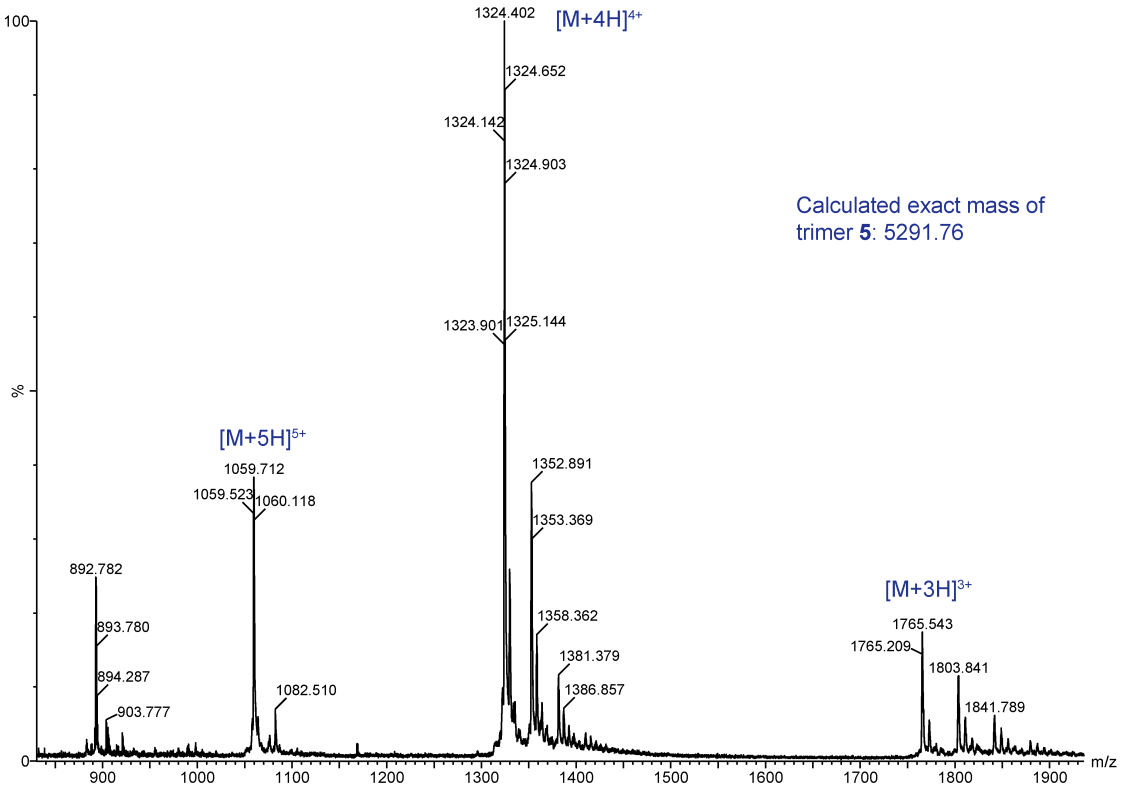

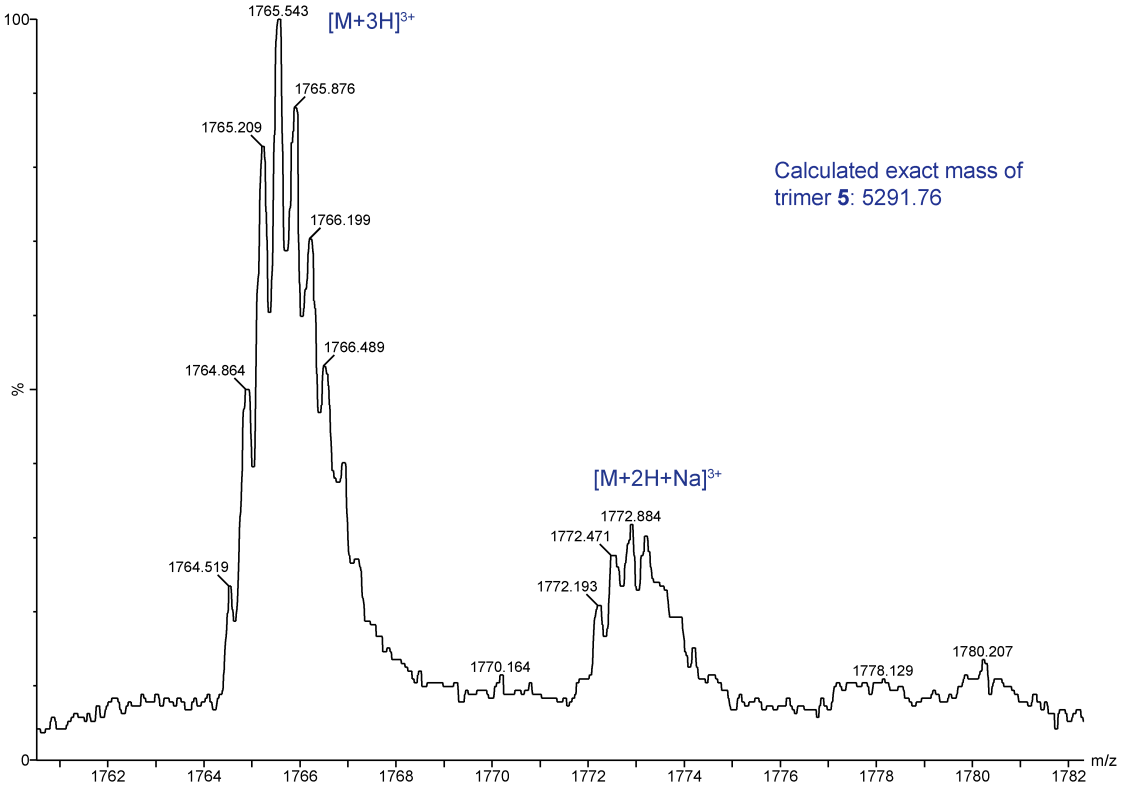

Calculated exact mass of trimer **5**: 5291.76

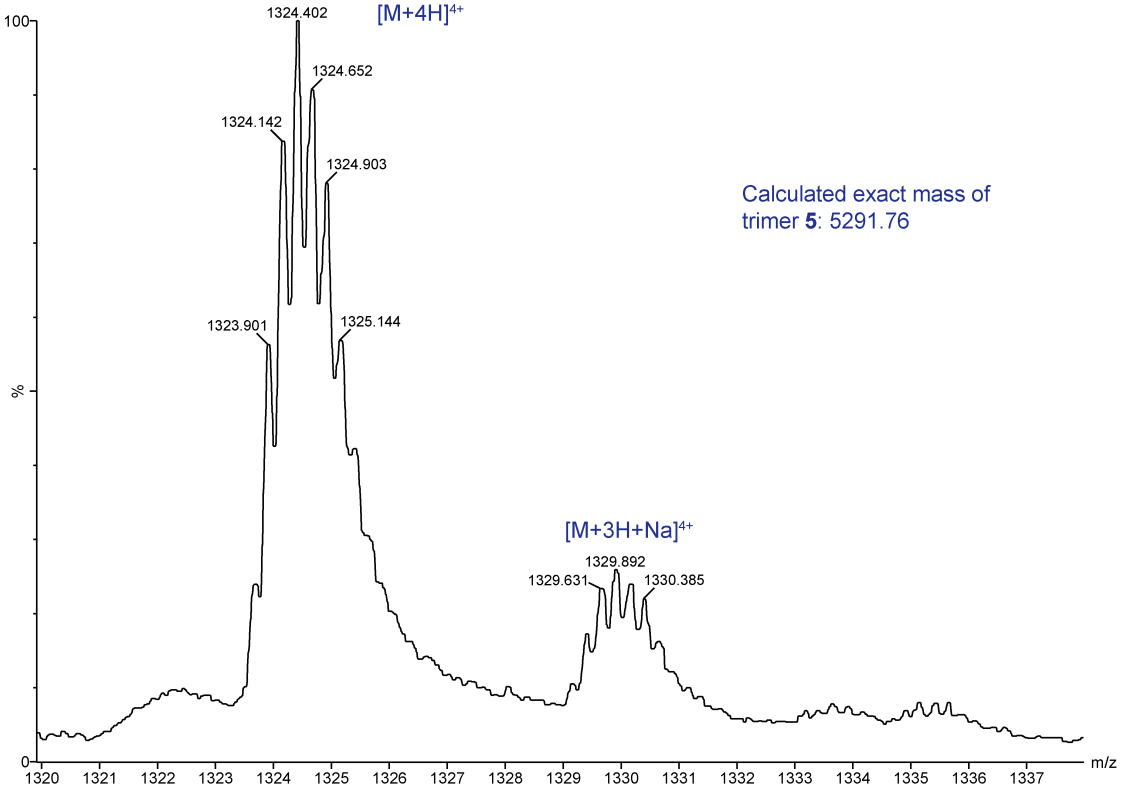

Calculated exact mass of trimer **5**: 5291.76

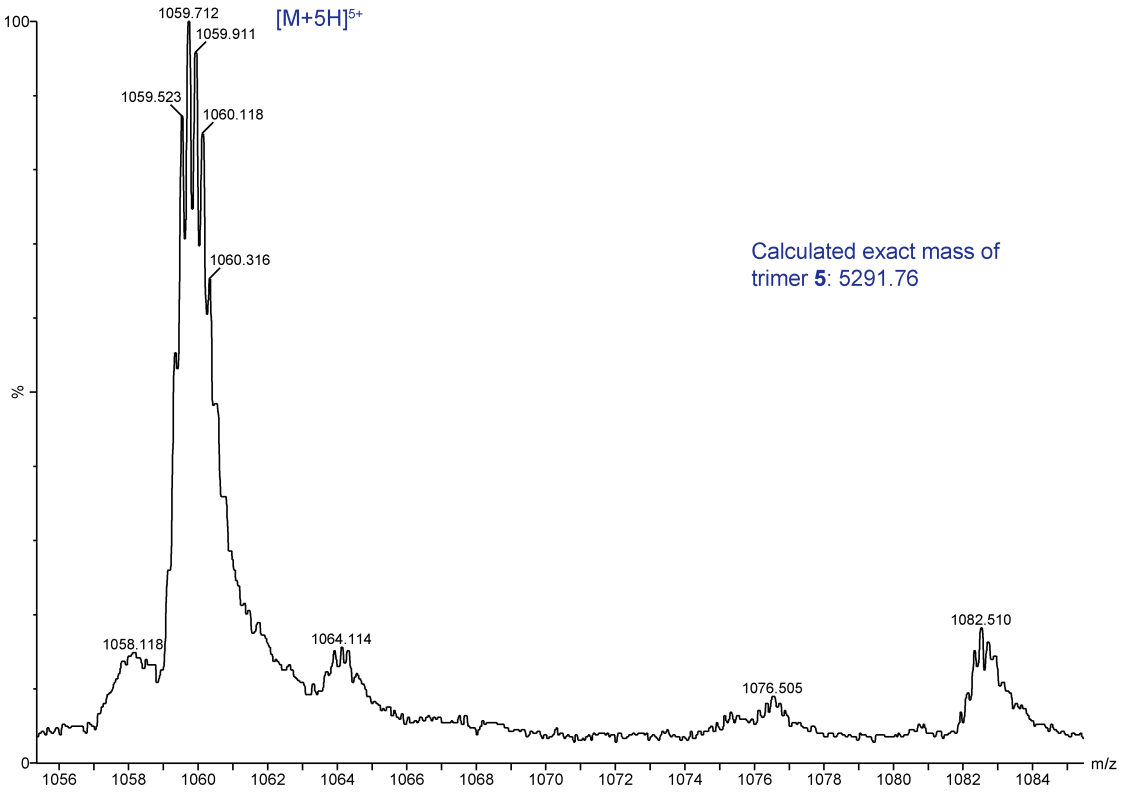
[M+5H]5+
1059.712
1059.911
1059.523
1060.118
1060.316
1058.118
1064.114
1076.505
1082.510
100
%
0
m/z
1056
1058
1060
1062
1064
1066
1068
1070
1072
1074
1076
1078
1080
1082
1084
Calculated exact mass of
trimer 5: 5291.76

*Characterization of trimer **3.6***

Analytical HPLC trace of trimer **3.6**.

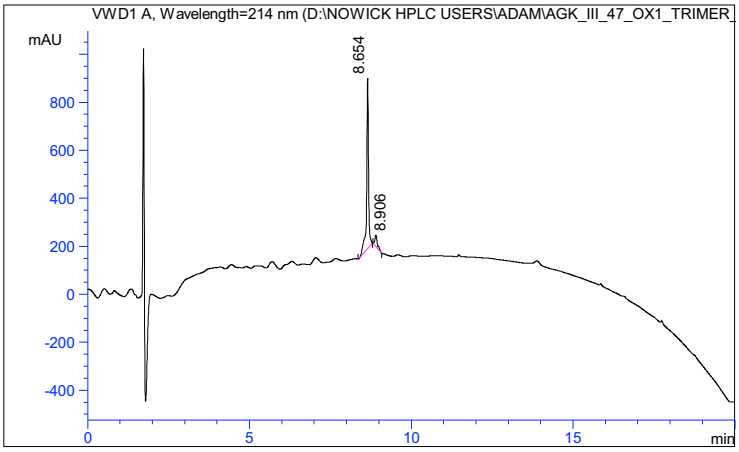

Signal 1:VWD1 A, Wavelength=214 nm

Peak #	RT [min]	Type	Width [min]	Area mAU*s	Height [mAU]	Area %
1	8.654	MM	0.068	2907.973	93.730	91.555
2	8.906	MM	0.094	268.220	6.270	8.445

Mass spectra expansions of trimer **3.6**.

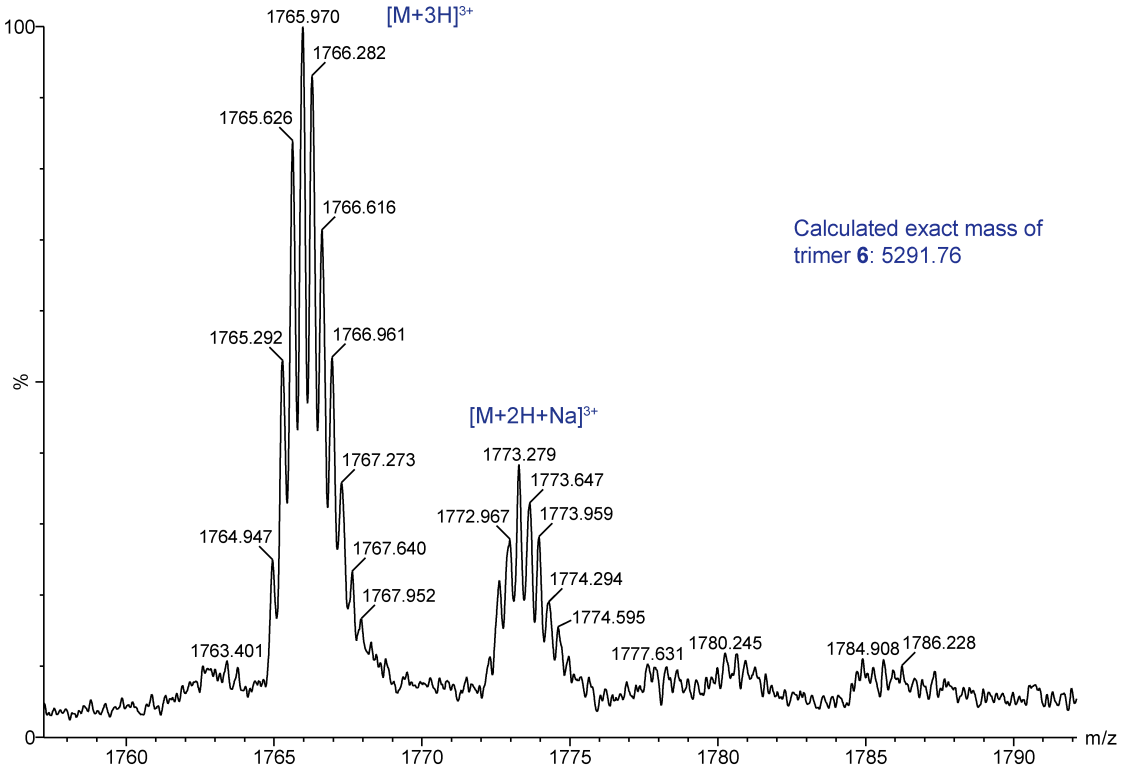

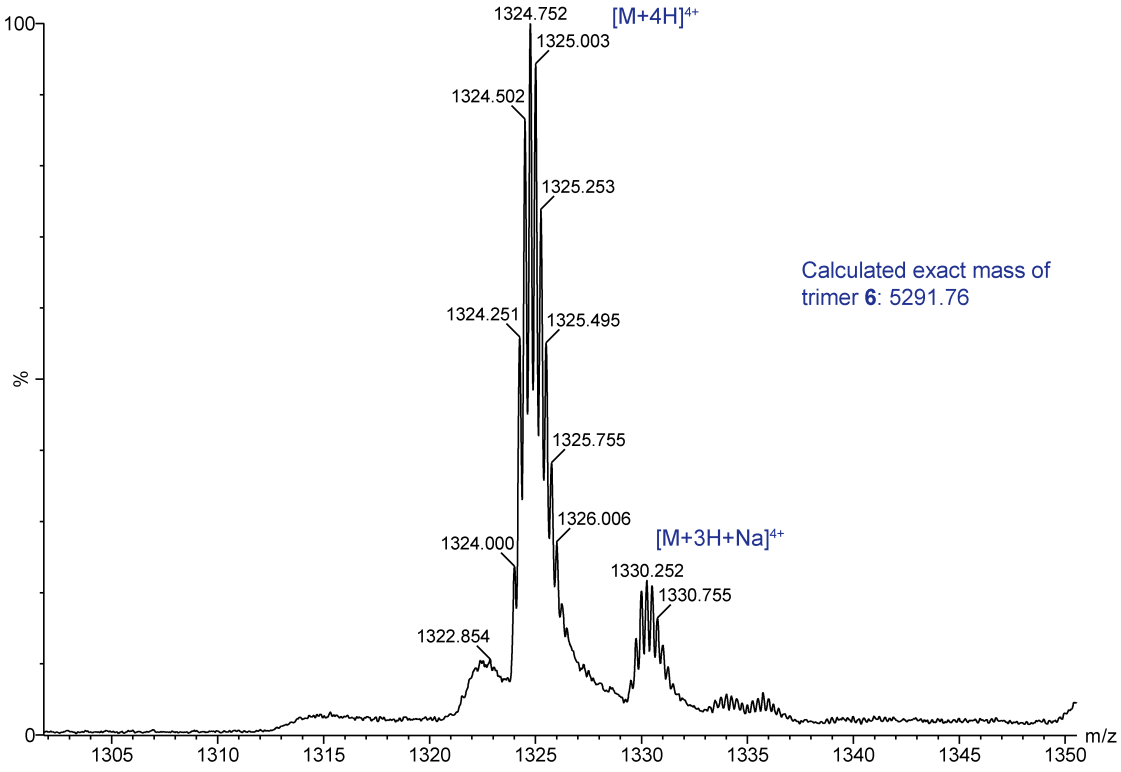

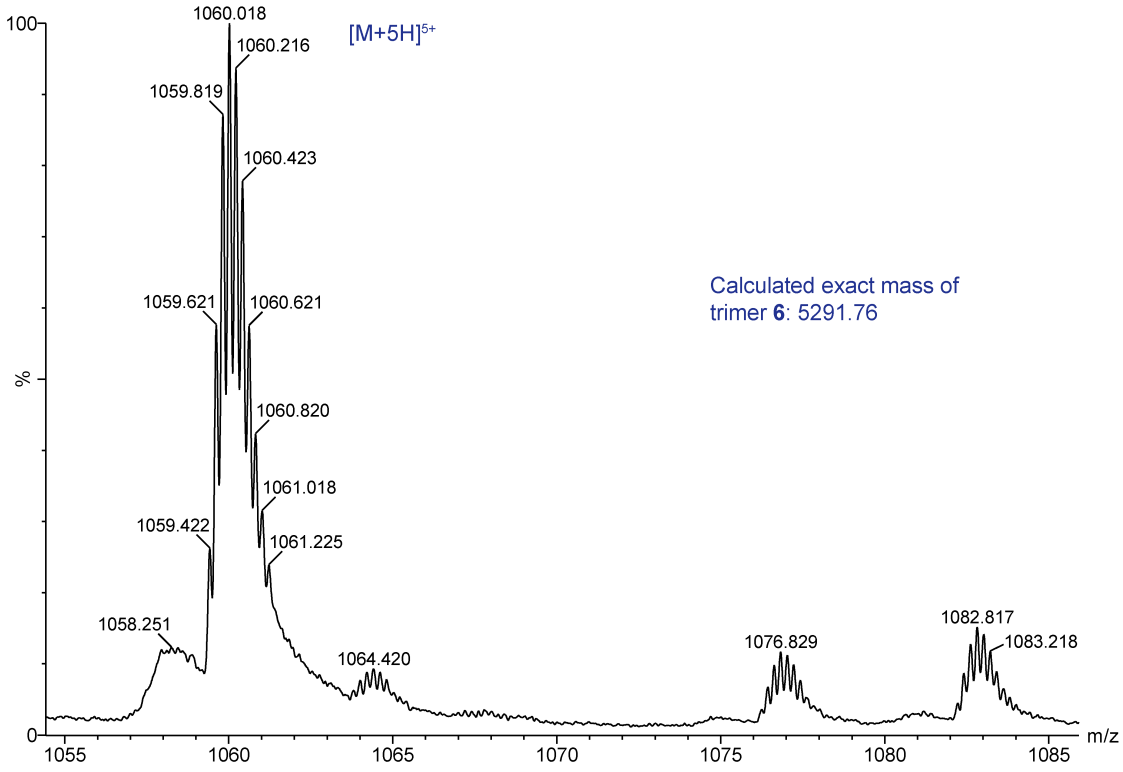
100
%
0
1060.018
1060.216
1059.819
1060.423
1059.621
1060.621
1060.820
1061.018
1059.422
1061.225
1058.251
1064.420
1076.829
1082.817
1083.218
[M+5H]5+
Calculated exact mass of
trimer 6: 5291.76
1055
1060
1065
1070
1075
1080
1085
m/z

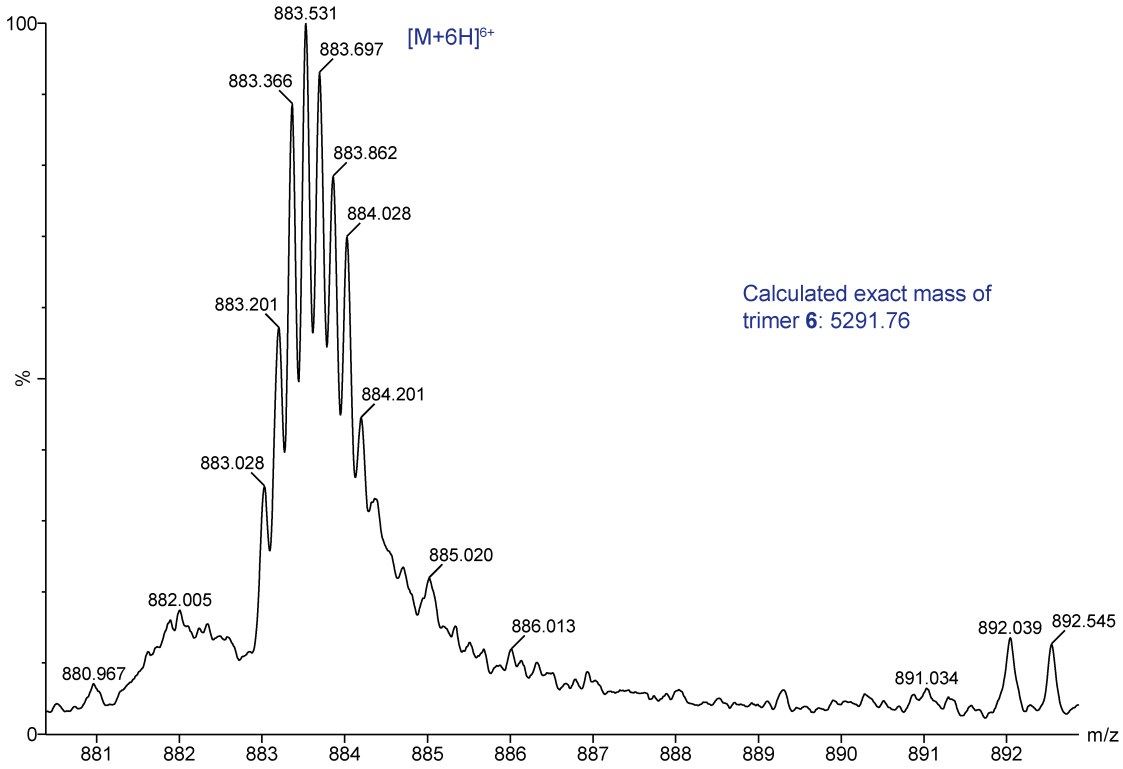
100
%
0
883.531
883.697
883.366
883.862
884.028
883.201
884.201
883.028
885.020
882.005
886.013
880.967
891.034
892.039
892.545
[M+6H]6+
Calculated exact mass of
trimer 6: 5291.76
881
882
883
884
885
886
887
888
889
890
891
892
m/z

Chapter 4

A Hexamer of a Peptide Derived from $A\beta_{16–36}$

Introduction

Elucidating the structures of oligomers formed by amyloidogenic peptides and proteins represents a frontier in structural biology and constitutes a major challenge in understanding the molecular basis of amyloid diseases. The heterogeneity and metastability of amyloid oligomers hinders the isolation of homogeneous amyloid oligomers suitable for structural elucidation by NMR spectroscopy and X-ray crystallography. More than thirty different amyloidogenic peptides and proteins have been identified, yet only a few high-resolution structures have shed light on amyloid oligomers thus far.

X-ray crystallographic studies of fragments of amyloidogenic peptides and proteins have provided insights into the structures of amyloid oligomers.[1,2,3,4] Eisenberg and coworkers

determined the X-ray crystallographic structure of a β-barrel-like oligomer, termed a *cylindrin*, formed by an 11-residue peptide fragment from αB crystallin.[1] The cylindrin oligomer is composed of six β-strands that form a twisted antiparallel β-sheet that closes back on itself to form a cylinder. Surewicz and coworkers determined the X-ray crystallographic structure of a hexameric oligomer formed by a disulfide-stabilized β-sheet fragment from human prion protein (hPrP).[2] The hPrP oligomer is composed of three four-stranded antiparallel β-sheets that pack to form a hydrophobic core. Our laboratory determined the X-ray crystallographic structure of a tetramer formed by a macrocyclic peptide containing a nine-residue fragment from the β-amyloid peptide Aβ.[4] Although the peptide fragments in these three different studies vary in sequence, the three structures share common features of being discrete oligomers composed of antiparallel β-sheets that form packed hydrophobic cores.

Biological and solution-phase studies have revealed that oligomers formed by different amyloidogenic peptides and proteins share common biological and structural properties.[5,6] Amyloid oligomers are typically toxic toward cells, an important characteristic that is thought to play a role in the pathogenesis of amyloid diseases.[1,7,8] Amyloid oligomers are typically stable to sodium dodecyl sulfate (SDS), migrating as discrete assemblies in SDS-PAGE experiments.[9,10] Amyloid oligomers appear to be composed of antiparallel β-sheets, while amyloid fibrils are generally composed of parallel β-sheets.[11,12,13,14,15,16] Furthermore, the monomer building blocks of many amyloid oligomers are thought to adopt the simplest arrangement of an antiparallel β-sheet—a β-hairpin.[17,18,19,20,21,22,23,24,25]

Our laboratory has determined the X-ray crystallographic structures of oligomers formed by macrocyclic β-sheet peptides designed to mimic β-hairpins from amyloidogenic peptides and proteins.[26,27,28,29,30] These β-hairpin peptides contain two heptapeptide β-strand fragments locked

in an antiparallel β-sheet by two δ-linked ornithine ($^{\delta}$Orn) turn mimics, and also contain an *N*-methyl group that blocks uncontrolled aggregation.[31,32,33] These design features permit crystallization of the β-hairpin peptides and structural elucidation of the higher-order oligomers they can form. The β-hairpin peptides have two surfaces: a major surface that displays eight of the fourteen side chains, and a minor surface that displays the remaining six side chains. Figure 4.1 shows a generic structure of these β-hairpin peptides and highlights the major and minor surfaces in red and blue.

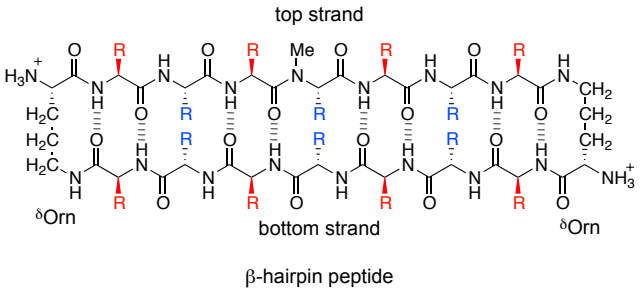

Figure 4.1. Generic chemical structure of a β-hairpin peptide. Two heptapeptide β-strands—a top strand and a bottom strand—are connected by two $^{\delta}$Orn turns. The β-hairpin peptide has a major surface that displays eight residues (red) and a minor surface that displays six residues (blue).

To date, our laboratory has elucidated the X-ray crystallographic structures of oligomers formed by β-hairpin peptides derived from Aβ,[26,27,28,34] alpha-synuclein,[29] and β_2-microglobulin.[30] These structures revealed the propensity for β-hairpin peptides to form oligomers in the crystal state, including dimers, trimers, hexamers, octamers, nonamers, and dodecamers. The different oligomers identified in these studies demonstrate the diversity and polymorphism of the structures that different amyloid-derived β-hairpin peptides can form.

Previously, we reported the X-ray crystallographic structures of oligomers formed by β-hairpin peptide **4.1** (Figure 4.2A), which is derived from an $A\beta_{17–36}$ β-hairpin (Figure 4.2B).[26,35]

Peptide **4.1** contains $A\beta_{17–23}$ and $A\beta_{30–36}$ β-strands linked by two $^{\delta}$Orn turn units; the $^{\delta}$Orn turn that links Asp_{23} and Ala_{30} replaces the $A\beta_{24–29}$ loop of the $A\beta_{17–36}$ β-hairpin. Peptide **4.1** also contains an *N*-methyl group on Phe_{20} and α-linked ornithine at position 35 as a hydrophilic isostere of methionine. The X-ray crystallographic structure reveals that peptide **4.1** assembles hierarchically to form a triangular trimer that further assembles with a second triangular trimer to form a sandwich-like hexamer (Figure 4.3).[36]

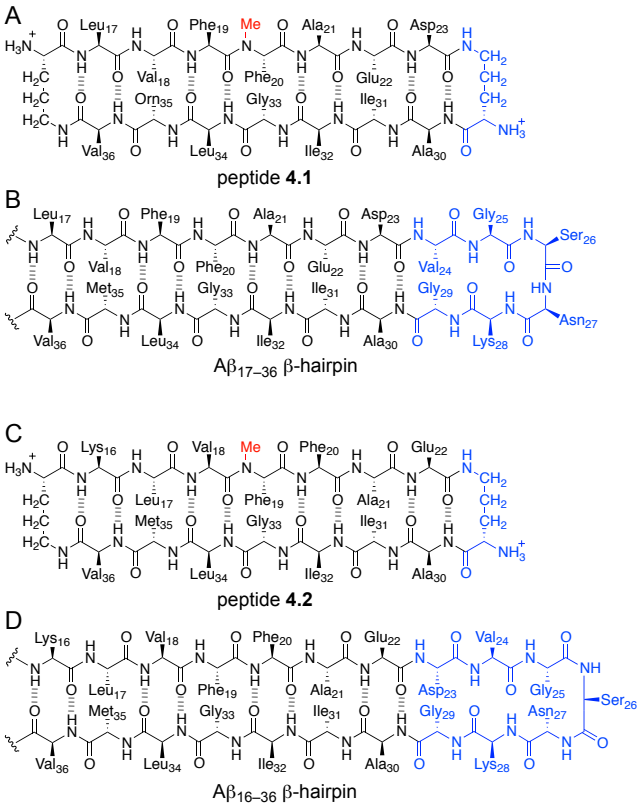

Figure 4.2. Macrocyclic β-sheet peptides designed to mimic two different β-hairpin registrations of Aβ. (A) Chemical structure of peptide **4.1**. The $^{\delta}$Orn turn that connects Asp_{23} and Ala_{30} (blue) replaces $A\beta_{24–29}$. (B) Chemical structure of an $A\beta_{17–36}$ β-hairpin. (C) Chemical structure of peptide **4.2**. The $^{\delta}$Orn turn that connects Glu_{22} and Ala_{30} (blue) replaces $A\beta_{23–29}$. (D) Chemical structure of an $A\beta_{16–36}$ β-hairpin.

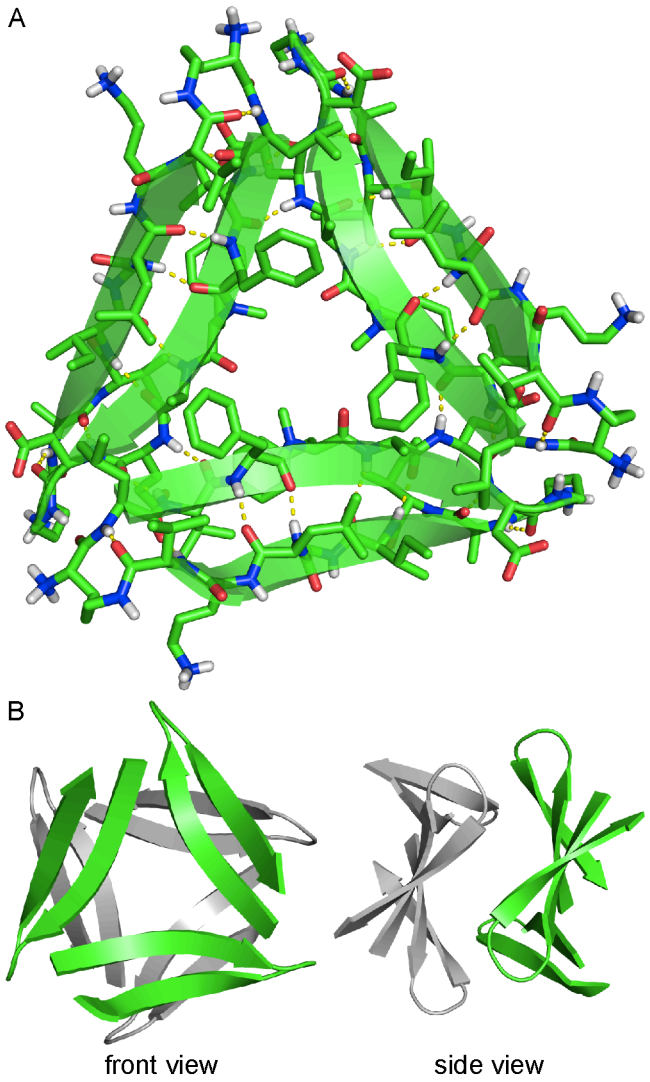

Figure 4.3. (A) X-ray crystallographic structure of the trimer formed by peptide **4.1** (PDB 4NW9). (B) Front view and side view of the X-ray crystallographic structure of the hexamer formed by two trimers of peptide **4.1**.

In the current study, we set out to explore how shifting registration by one amino acid toward the *N*-terminus affects the structural and biological properties of a β-hairpin peptide. Shifting β-hairpin registration is significant, because it changes both the pairings of the residues within the β-hairpin and the surfaces upon which the side chains are displayed. In the $A\beta_{17–36}$ β-hairpin, from which peptide **4.1** is derived, Ile_{31} pairs with Glu_{22}; in the shifted $A\beta_{16–36}$ β-hairpin, Ile_{31} pairs with Ala_{21}. In the $A\beta_{17–36}$ β-hairpin, the side chain of Glu_{22} shares the same surface as

the side chain of Ile_{31}; in the $A\beta_{16–36}$ β-hairpin, the side chain of Glu_{22} is on the opposite surface. We find that the resulting shifted β-hairpin peptide not only assembles in the crystal state to form oligomers, but also exhibits both solution-phase assembly and toxicity reminiscent of amyloid oligomers.

Here we describe the X-ray crystallographic, solution-phase, and biological studies of peptide **4.2** (Figure 4.2C), which is designed to mimic the $A\beta_{16–36}$ β-hairpin (Figure 4.2D). Peptide **4.2** contains $A\beta_{16–22}$ and $A\beta_{30–36}$ β-strands linked by two $^{\delta}$Orn turn units, an *N*-methyl group on Phe_{19}, and the native methionine residue at position 35. Peptide **4.2** runs as a hexamer in SDS-PAGE and appears to form dimers and trimers in size exclusion chromatography (SEC). The oligomers formed by peptide **4.2** are toxic toward the human neuroblastoma cell line SH-SY5Y. X-ray crystallography reveals that peptide **4.2** also assembles to form a hexamer in the crystal state. The hexamer may be thought of as being composed of either dimers or trimers. The hexamer formed by peptide **4.2** is significant because it shares key characteristics with the oligomers formed by full-length amyloidogenic peptides and proteins and provides a structural model for an oligomer of Aβ.

Results and Discussion

Oligomerization of Peptide 4.2. Peptide **4.2** assembles to form a hexamer in SDS-PAGE. Tricine SDS-PAGE followed by silver staining shows that the 1.8 kDa peptide **4.2** migrates just above the 10 kDa band of the ladder (Figure 4.4A).[37] The band from peptide **4.2** is comet-shaped and streaks downward, suggesting that the hexamer is in equilibrium with lower molecular weight species. To further confirm the oligomerization state of peptide **4.2**, we compared it to covalent trimer peptides **4.5** and **4.6** (Figures 4.S1 and 4.S2, PDB 5SUT and

5SUR), which we had previously determined to migrate respectively as 10.6 kDa hexamers and 21.2 kDa dodecamers in equilibrium with the 5.3 kDa trimers.[28] Peptide **4.2** migrates at the same molecular weight as the hexamer band of peptide **4.5**, providing further evidence that peptide **4.2** assembles to form a hexamer in SDS-PAGE. In contrast, peptide **4.1** does not assemble to form a hexamer in SDS-PAGE. Peptide **4.1** migrates well below the trimer band of peptide **4.6**, and slightly below the 4.6 kDa band of the ladder, suggesting that peptide **4.1** migrates as a monomer or dimer.

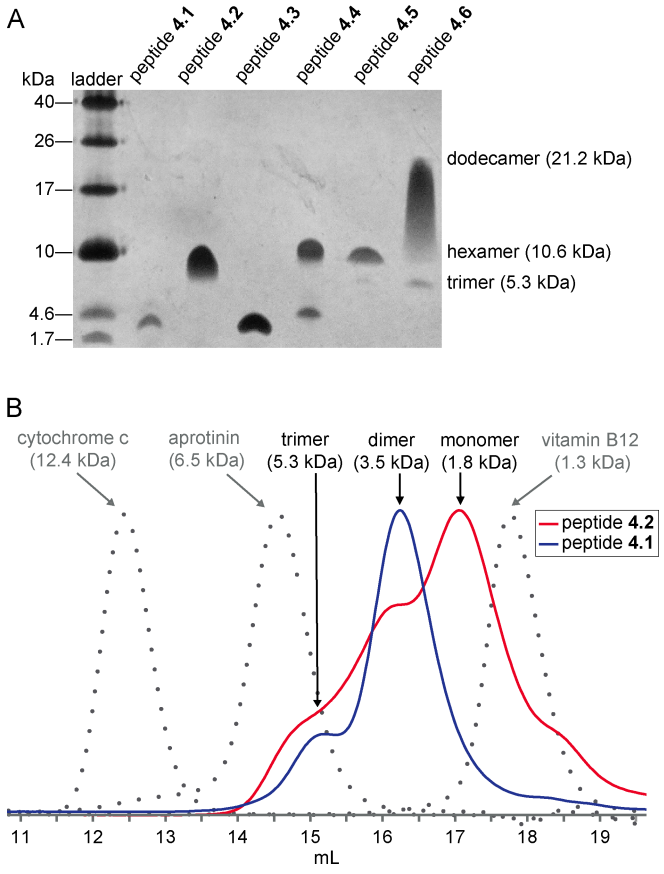

Figure 4.4. Peptide **4.2** assembles in solution to form oligomers. (A) Silver-stained SDS-PAGE gel. SDS-PAGE was performed on 0.15 mg/mL samples of peptides **4.1**–**4.4** and 0.05 mg/mL samples of peptides **4.5** and **4.6** in Tris buffer at pH 6.8 with 2% (w/v) SDS. Molecular weights calculated for the trimer, hexamer, and dodecamer are listed in parentheses. (B) Size exclusion chromatography chromatograms. SEC was performed on a 1.0-mg/mL solution of peptide in 50 mM Tris buffer at pH 7.4 with 150 mM NaCl on a Superdex 75 10/300 column.

Table 4.1. Size exclusion chromatography data for peptides **4.1**–**4.4**.

compound	molecular weight	elution volume (mL)	oligomer size
peptide **4.1**	1.74 kDa	16.2, 15.1	dimer, trimer
peptide **4.2**	1.77 kDa	17.0, 16.1, 14.8	monomer, dimer, trimer
peptide **4.3**	1.79 kDa	17.6	monomer
peptide **4.4**	1.72 kDa	17.0	monomer
vitamin B12	1.3 kDa	17.8	
aprotinin	6.5 kDa	14.6	
cytochrome c	12.4 kDa	12.4	

Size exclusion chromatography reveals that peptide **4.2** also assembles to form oligomers in the absence of SDS. The elution profile of peptide **4.2** was compared to the size standards vitamin B12, aprotinin, and cytochrome c, as well as peptide **4.1**. Peptide **4.2** elutes as a broad peak with three distinct humps (Figure 4.4B). The elution volumes of the humps are consistent with the molecular weights of a monomer, dimer, and trimer, respectively. The broadness of the humps suggests moderately slow exchange between the trimer, dimer, and monomer. Peptide **4.1** elutes as two distinct peaks: a larger peak with an elution volume consistent with the molecular weight of a dimer, and a smaller peak with an elution volume consistent with the molecular weight of a trimer (Figure 4.4B). Table 4.1 summarizes the SEC data for peptides **4.1** and **4.2**.

These solution-phase studies show that peptide **4.2** assembles to form oligomers in solution. In SDS-PAGE, peptide **4.2** assembles to form a hexamer. In SEC in Tris buffer, peptide **4.2** assembles to form dimers and trimers. These results suggest the intriguing hypothesis that the hexamer in SDS-PAGE may be composed of dimers or trimers that further assemble to form a hexamer in the lipophilic environment of SDS micelles. We turned to X-ray crystallography to gain insights into the structures of these oligomers, and thus further explore this hypothesis.

X-ray Crystallographic Structure of Peptide 4.2. Peptide **4.2** afforded crystals suitable for X-ray diffraction from aqueous HEPES buffer with sodium citrate and isopropanol. To determine the X-ray crystallographic phases of peptide **4.2**, we soaked a crystal of the peptide in potassium iodide to incorporate iodide ions into the crystal lattice and performed conventional single-wavelength anomalous diffraction (SAD) phasing.[28,38,39] The X-ray crystallographic structure of the KI-soaked peptide **4.2** (PDB 5W4I) was then used as a search model for molecular replacement to determine the X-ray crystallographic phases of a higher resolution data set of unsoaked peptide **4.2**, which was collected using a synchrotron radiation source (PDB 5W4H).

The X-ray crystallographic structure of peptide **4.2** reveals that the peptide folds to form a twisted β-hairpin. The side chains displayed on the major and minor surfaces of peptide **4.2** differ from those displayed on the major and minor surfaces of peptide **4.1**. The major surface of the peptide **4.2** β-hairpin displays the side chains of Lys_{16}, Val_{18}, Phe_{20}, Glu_{22}, Ala_{30}, Ile_{32}, Leu_{34}, and Val_{36}, while the major surface of the peptide **4.1** β-hairpin displays the side chains of Leu_{17}, Phe_{19}, Ala_{21}, Asp_{23}, Ala_{30}, Ile_{32}, Leu_{34}, and Val_{36} (Figure 4.5A). The minor surface of the peptide **4.2** β-hairpin displays the side chains of Leu_{17}, Phe_{19}, Ala_{21}, Ile_{31}, Gly_{33}, and Met_{35}, while the minor surface of the peptide **4.1** β-hairpin displays the side chains of Val_{18}, Phe_{20}, Glu_{22}, Ile_{31}, Gly_{33}, and Orn_{35} (Figure 4.5B). Thus, the minor surface of peptide **4.2** is wholly hydrophobic, while the minor surface of peptide **4.1** is not.

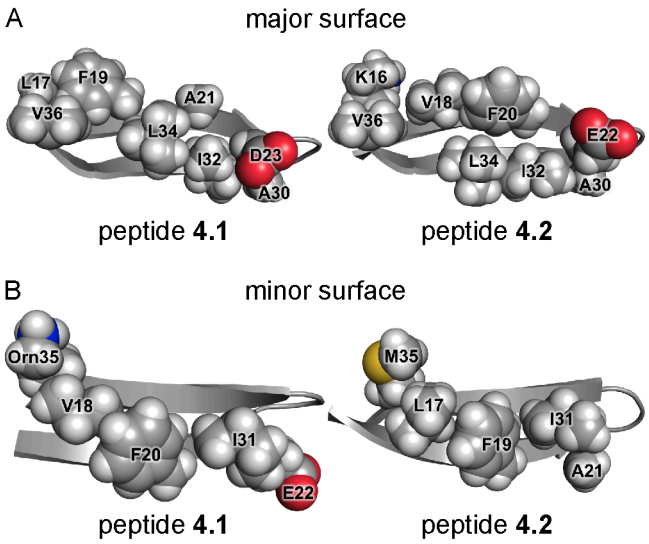

Figure 4.5. X-ray crystallographic structures of peptide **4.1** (PDB 4NW9) and peptide **4.2** (PDB 5W4H). (A) Major surfaces of peptides **4.1** and **4.2**. (B) Minor surfaces of peptides **4.1** and **4.2**.

In the X-ray crystallographic structure of peptide **4.2**, six β-hairpin monomers assemble to form a hexamer. The hexamer is composed of smaller oligomers and can be interpreted either as a trimer of dimers or as a dimer of trimers. Figure 4.6 shows the structure of the hexamer and illustrates these two interpretations. In Figure 4.6B, one dimer subunit is colored green; in Figure 4.6C, one trimer subunit is colored cyan. The following subsections detail the structure of the hexamer as well as the structures of the component dimers or trimers.

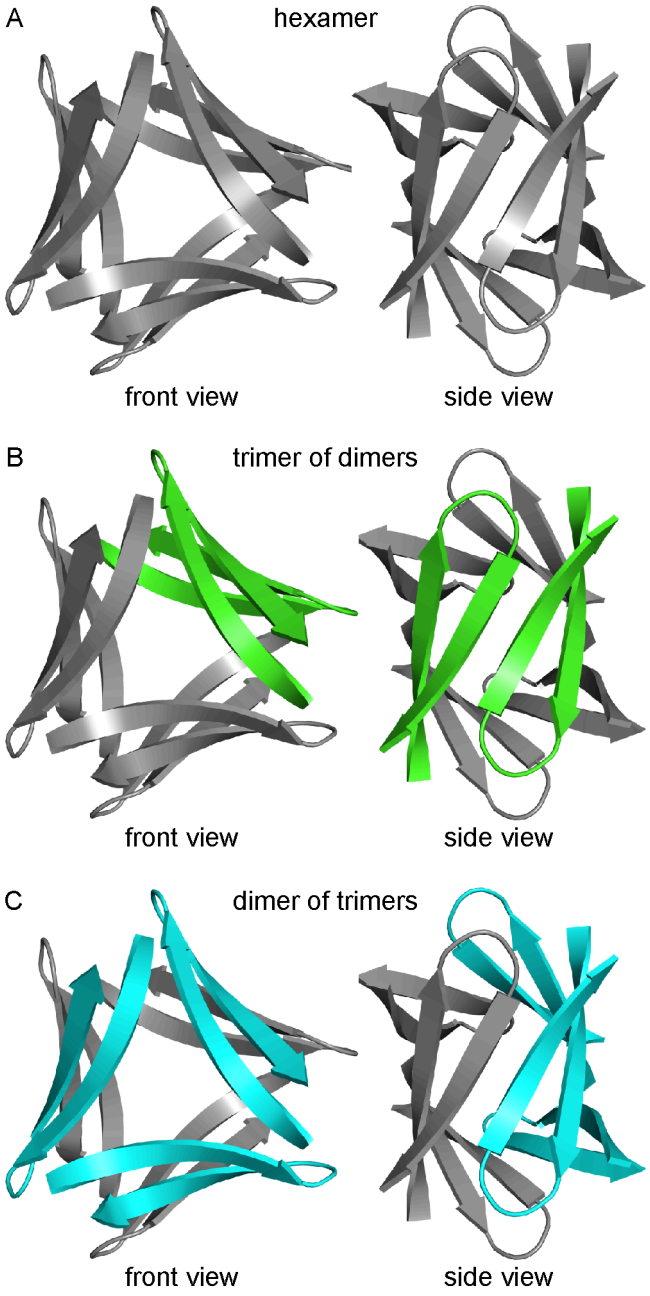

Figure 4.6. The hexamer formed by peptide **4.2** can be interpreted either as a trimer of dimers or as a dimer of trimers. (A) X-ray crystallographic structure of the hexamer formed by peptide **4.2**. (B) Interpretation of the hexamer as a trimer of dimers. One dimer subunit is colored green. (C) Interpretation of the hexamer as a dimer of trimers. One trimer subunit is colored cyan.

Hexamer. The hexamer formed by peptide **4.2** resembles a barrel with three openings (Figure 4.7). The interior of the barrel is filled with the side chains of residues on the minor

surface of peptide **4.2**—Leu_{17}, Phe_{19}, Ala_{21}, Ile_{31}, Gly_{33}, and Met_{35}—creating a packed hydrophobic core that stabilizes the hexamer (Figure 4.7C). A network of hydrogen bonds between the main chains of the monomer subunits further stabilizes the hexamer. The outer surface of the hexamer displays the side chains of residues on the major surface of peptide **4.2**—Lys_{16}, Val_{18}, Phe_{20}, Glu_{22}, Ala_{30}, Ile_{32}, Leu_{34}, and Val_{36}.

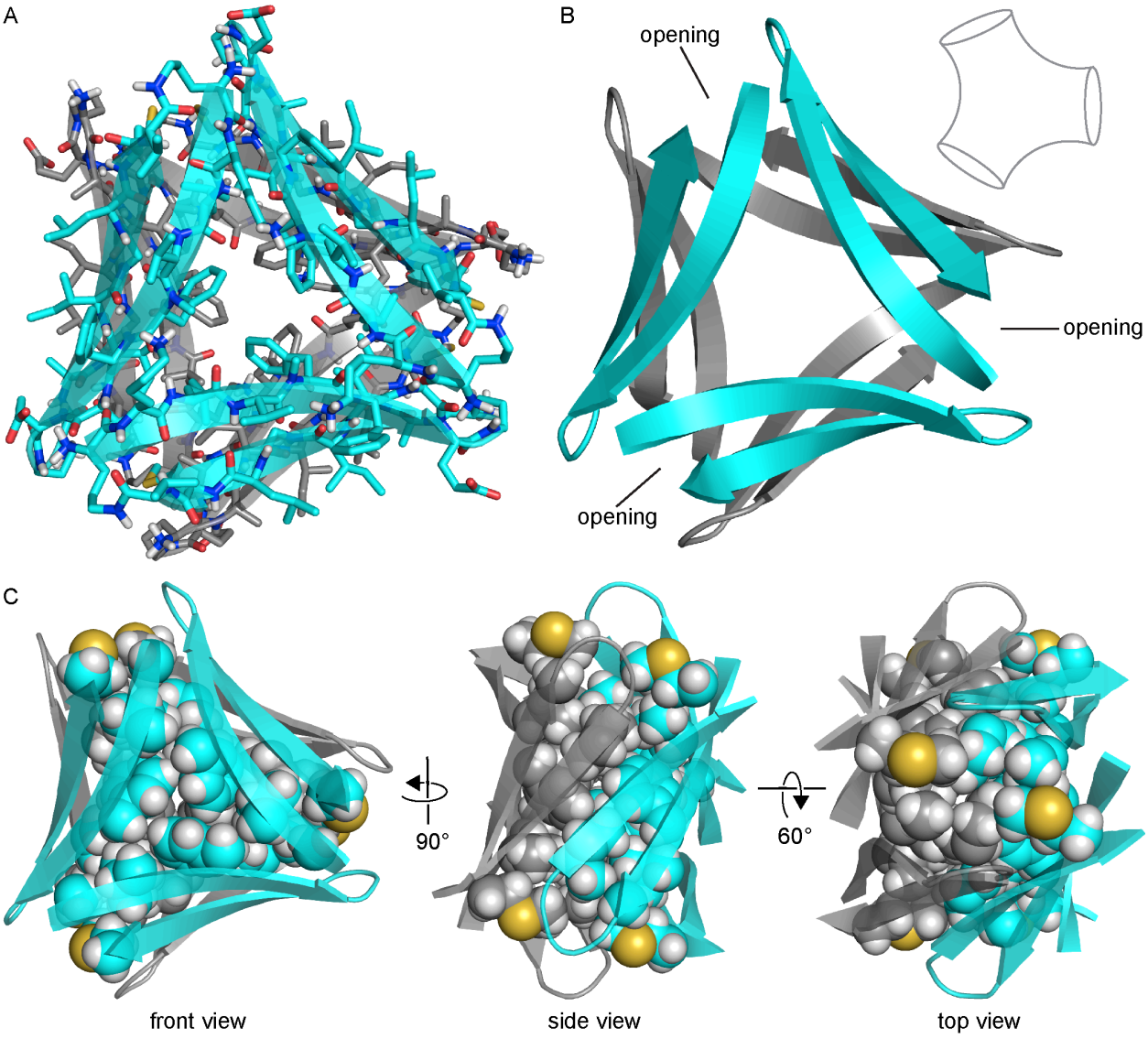

Figure 4.7. X-ray crystallographic structure of the hexamer formed by peptide **4.2** (PDB 5W4H). (A) Cartoon and stick model. (B) Cartoon model illustrating the three barrel-like openings. The inset shows a schematic representation of the general shape of the hexamer. (C) Three different views of the hexamer. Side chains of residues that pack in the hydrophobic core of the hexamer are shown as spheres. The top view looks inside one of the three barrel-like openings.

The hexamer formed by peptide **4.2** is more hydrogen bonded and better packed than the hexamer formed by peptide **4.1** (Figure 4.S3). The hexamer formed by peptide **4.2** forms a continuous hydrogen-bonding network containing 30 intermolecular hydrogen bonds, whereas the hexamer formed by peptide **4.1** does not form a continuous hydrogen-bonding network and

contains only 18 intermolecular hydrogen bonds. In the hexamer formed by peptide **4.1**, each β-hairpin monomer is only hydrogen bonded to the two adjacent β-hairpin monomers within the triangular trimer; in the hexamer formed by peptide **4.2**, each β-hairpin monomer is hydrogen bonded not only to the two adjacent monomers within the triangular trimer, but also to the adjacent monomer within the β-sheet dimer. For these reasons, the hexamer formed by peptide **4.2** can either be interpreted as a trimer of β-sheet dimers or as a dimer of triangular trimers, whereas the hexamer formed by peptide **4.1** is unambiguously a dimer of triangular trimers.

Six sets of side chains from Leu_{17}, Phe_{19}, Ala_{21}, Ile_{31}, and Met_{35} pack together to form a hydrophobic core that stabilizes the hexamer formed by peptide **4.2**. While the minor surface of peptide **4.2** displays five hydrophobic side chains, that of peptide **4.1** displays only three—Val_{18}, Phe_{20}, and Ile_{31}. The hexamer formed by peptide **4.1** lacks the massive hydrophobic core and is only loosely packed at the interface between trimers. The buried surface area of the hexamer formed by peptide **4.2** is 5102 $Å^2$, whereas the buried surface area of the hexamer formed by peptide **4.1** is only 3514 $Å^2$.

Dimer. Two peptide **4.2** β-hairpin monomers assemble edge-to-edge to form a hydrogen-bonded dimer, creating a four-stranded antiparallel β-sheet (Figure 4.8A). (Three such dimers make up the hexamer.) The β-hairpin monomers are shifted out of registration by two residues toward the *N*-termini, such that Ala_{30} on one monomer is across from Leu_{34} on the adjacent monomer (Figure 4.8B). Four intermolecular hydrogen bonds between Ile_{31} and Gly_{33} of one monomer and Gly_{33} and Ile_{31} of the adjacent monomer help stabilize the dimer.

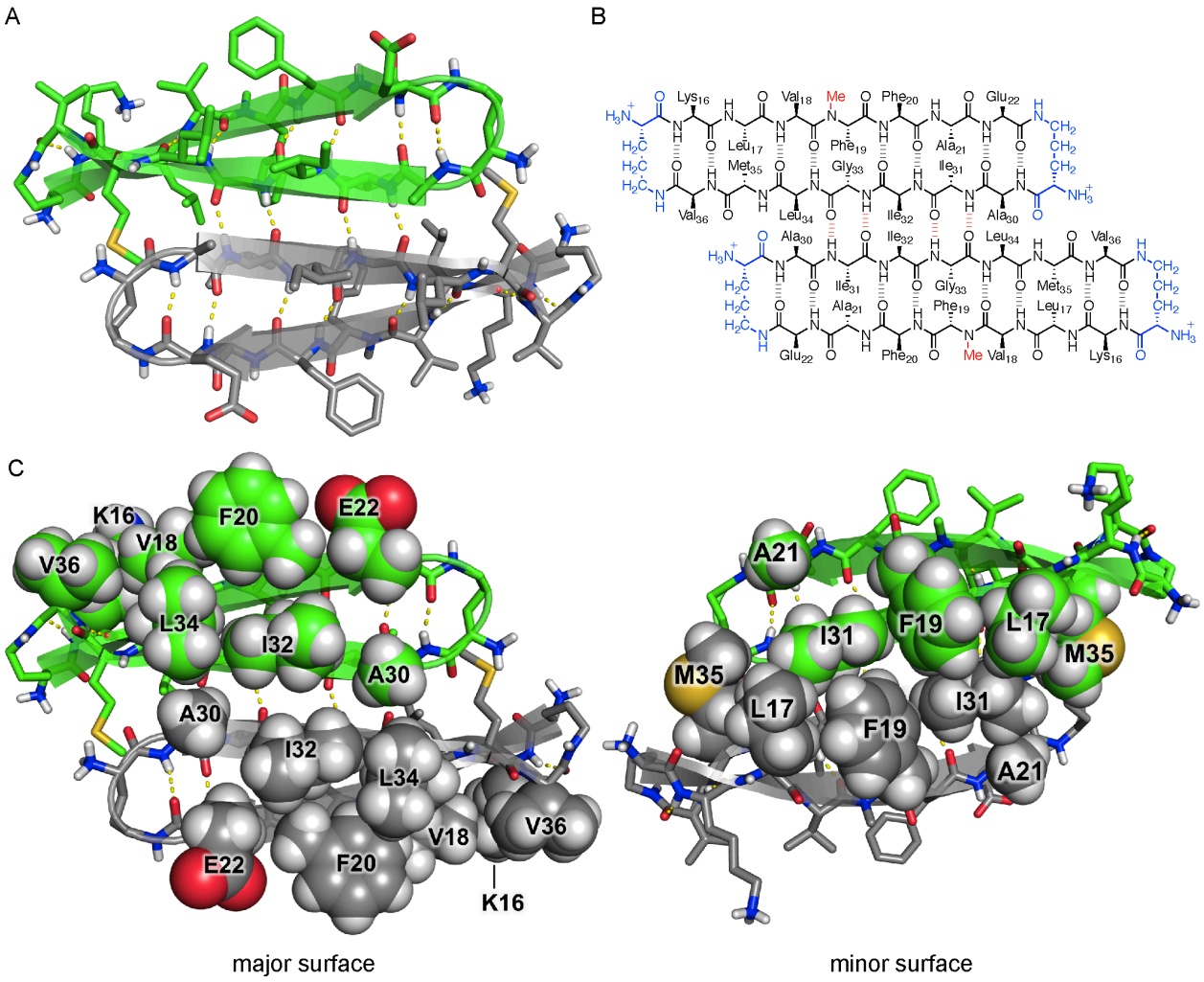

Figure 4.8. The β-sheet dimer formed by peptide **4.2**. (A) X-ray crystallographic structure (PDB 5W4H). (B) Chemical structure. The intermolecular hydrogen bonds between Ile_{31} and Gly_{33} are shown in red. (C) View of the dimer illustrating the major and minor surfaces.

The β-sheet dimer has two surfaces: one surface displays the side chains of residues on the major surface of peptide **4.2**; the other surface displays the side chains of residues on the minor surface of peptide **4.2** (Figure 4.8C). Hydrophobic packing between the side chains of residues on the minor surface further stabilizes the dimer: Leu_{17}, Phe_{19}, and Ile_{31} on one monomer pack against Ile_{31}, Phe_{19}, and Leu_{17} on the adjacent monomer. There are no substantial intermolecular contacts between the side chains of residues on the major surface of the dimer.

Trimer. Three peptide **4.2** β-hairpin monomers assemble to form a triangular trimer (Figure 4.9A). (Two such trimers make up the hexamer.) The trimer is stabilized by intermolecular edge-to-edge hydrogen bonds between monomers, which create four-stranded β-sheets at each corner of the trimer. At each corner, the main chain of $^{\delta}$Orn of one monomer hydrogen bonds with the main chain of Ala_{21} of the adjacent monomer, and the carbonyl of Phe_{19} of one monomer hydrogen bonds with the NH of Leu_{17} of the adjacent monomer (Figure 4.9B).

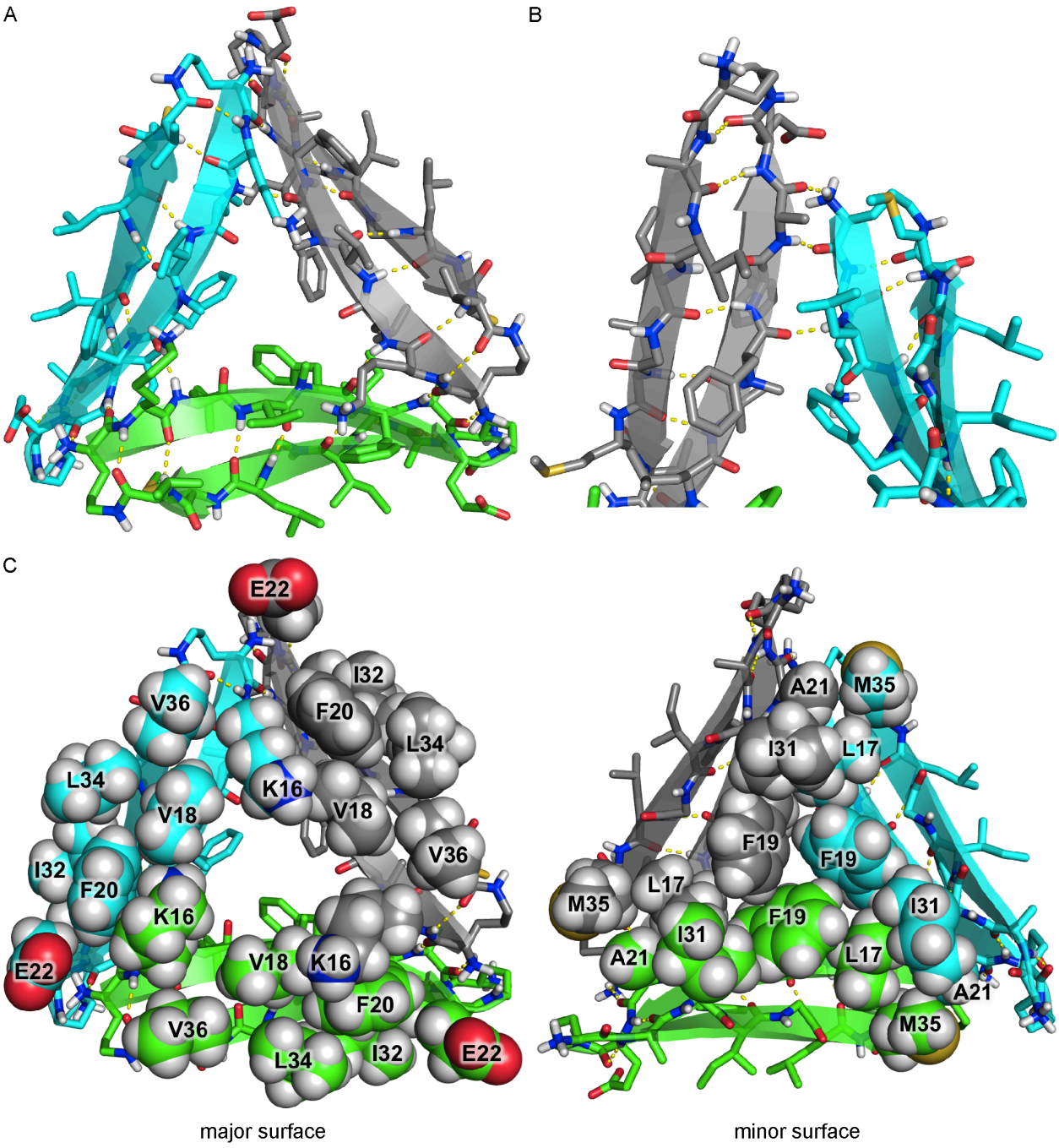

Figure 4.9. X-ray crystallographic structure of the trimer formed by peptide **4.2** (PDB 5W4H). (A) Cartoon and stick model. (B) Detail view of a corner of the triangular trimer showing the intermolecular hydrogen bonding between monomers, which creates a four-stranded β-sheet. (C) View of the trimer illustrating the major and minor surfaces.

The triangular trimer has two surfaces that display the amino acid side chains of the major surfaces and the minor surfaces of the component β-hairpin monomers (Figure 4.9C).

Hydrophobic packing between the side chains of residues on the minor surface further stabilizes the trimer: Met_{35}, Leu_{17}, and Phe_{19} on one monomer pack against Ala_{21}, Ile_{31}, and Phe_{19} on the adjacent monomer. There are no substantial intermolecular contacts between side chains of residues on the major surface of the trimer.

The hexamer, trimer, and dimer observed in the X-ray crystallographic structure of peptide **4.2** recapitulate the oligomers observed in SDS-PAGE and SEC. The assembly of the hexamer from either dimers or trimers may explain how the peptide **4.2** dimers and trimers observed in SEC come together to form the hexamer in SDS-PAGE. The structure of the hexamer shows key stabilizing contacts, such as edge-to-edge hydrogen bonding and hydrophobic packing. To better understand the importance of these contacts in the solution-phase oligomerization of peptide **4.2**, we designed peptides **4.3** and **4.4**. The following sections describe studies of these peptides and also provide insights into why $A\beta_{16–36}$-derived peptide **4.2** forms a hexamer in SDS-PAGE, but $A\beta_{17–36}$-derived peptide **4.1** does not.

***N*-Methylation of Peptide 4.2 Disrupts Oligomerization.** To test whether the hexamer observed in SDS-PAGE is similar in structure to the hexamer observed crystallographically, we prepared a homologue containing an additional *N*-methyl group designed to disrupt hexamer formation. Peptide **4.3** is a homologue of peptide **4.2** bearing an additional *N*-methyl group on Gly_{33} (Figure 4.10A). In the X-ray crystallographic structure of the hexamer formed by peptide **4.2**, the backbone of Gly_{33} on one monomer hydrogen bonds with the backbone of Ile_{31} on an adjacent monomer (Figure 4.8B). Introduction of an *N*-methyl group on Gly_{33} should prevent hydrogen bonding and thus disrupt the hexamer. In SDS-PAGE, peptide **4.3** does not migrate as a hexamer (Figure 4.4A). Instead, peptide **4.3** migrates similarly to peptide **4.1**, and thus appears to run as a monomer or dimer. This result supports a model in which the hexamer formed by

peptide **4.2** in SDS-PAGE is similar in structure to the hexamer observed crystallographically. In SEC, peptide **4.3** elutes at a volume consistent with the molecular weight of a monomer (Table 4.1), further demonstrating that *N*-methylation on Gly_{33} disrupts oligomer formation.

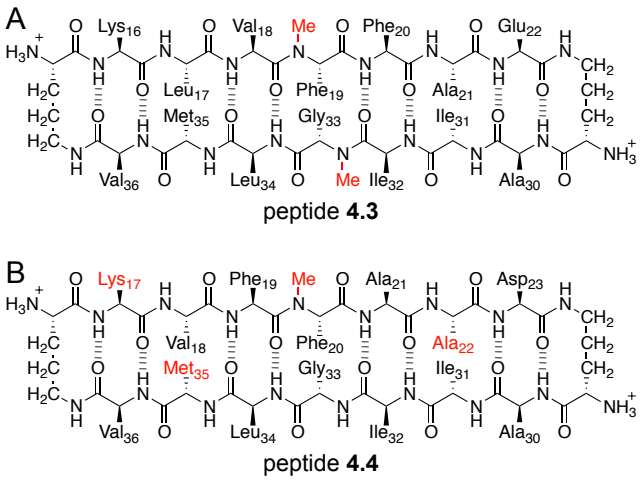

Figure 4.10. (A) Chemical structure of peptide **4.3**, a homologue of peptide **4.2** bearing an additional *N*-methyl group. (B) Chemical structure of peptide **4.4**, a triple mutant of peptide **4.1**. The mutated residues are shown in red.

Mutation of Peptide 4.1 Induces Oligomerization. The SDS-PAGE and X-ray crystallographic studies of peptides **4.1** and **4.2** demonstrate that shifting the registration of a β-hairpin peptide affects its oligomerization. In the X-ray crystallographic structures, the hexamer formed by peptide **4.2** is better packed and has more hydrogen bonds than the hexamer formed by peptide **4.1**. In SDS-PAGE, peptide **4.2** assembles to form a hexamer, whereas peptide **4.1** does not. The difference in the hydrophobicity and charge of the minor surfaces of peptides **4.1** and **4.2** may explain this difference in oligomerization. The minor surface of peptide **4.1** displays two charged hydrophilic side chains and three hydrophobic side chains, whereas the minor surface of peptide **4.2** displays five hydrophobic side chains (Figure 4.11).

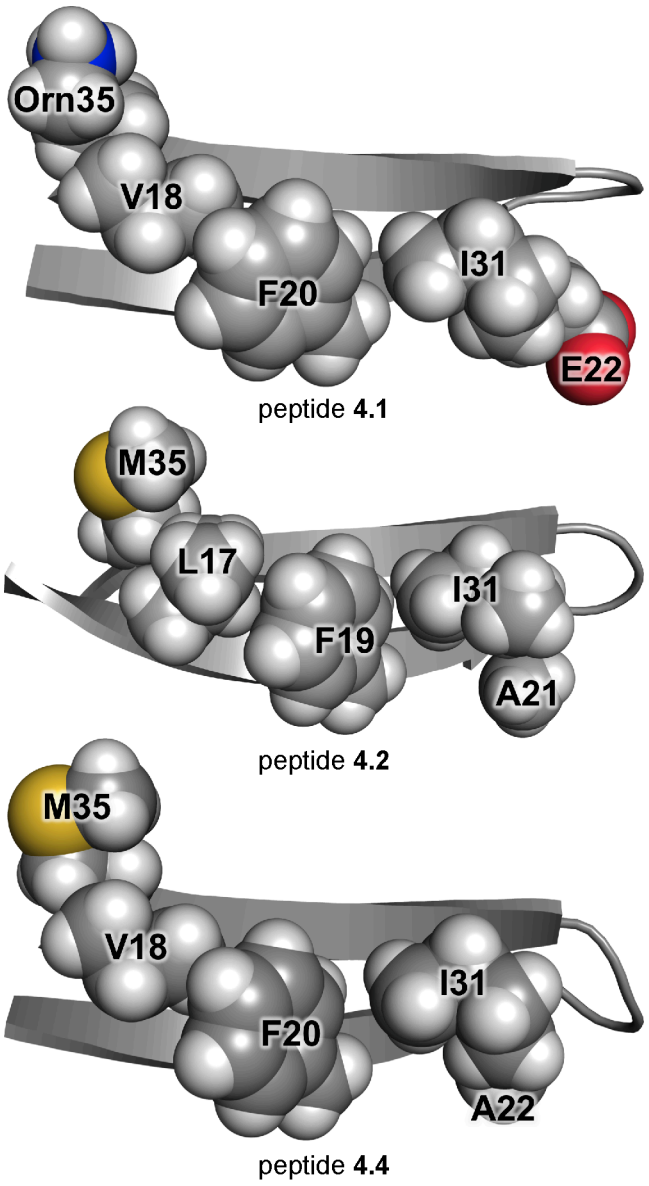

Figure 4.11. X-ray crystallographic structures of peptides **4.1**, **4.2**, and **4.4**, highlighting the minor surfaces of the peptides (PDB 4NW9, 5W4H, and 5W4J).

To explore the importance of charge and hydrophobicity in oligomerization, we prepared peptide **4.4** (Figure 4.10B). Peptide **4.4** is a triple mutant of peptide **4.1**, with L17K, E22A, and Orn35M mutations. Peptide **4.4** may be thought of as a chimera in which three residues of peptide **4.2** are grafted onto peptide **4.1** to eliminate charge on the minor surface. In peptide **4.4**, Ala_{22} and Met_{35} occupy the same sites on the minor surface as Ala_{21} and Met_{35} in peptide **4.2**.

The Lys_{17} residue in peptide **4.4** sits on the major surface, occupying the same site as Lys_{16} in peptide **4.2** and providing charge to enhance solubility. The remaining 11 residues of peptide **4.4** are identical to those of peptide **4.1**.

SDS-PAGE reveals that peptide **4.4** assembles to form an oligomer that migrates at a slightly higher molecular weight than the hexamer formed by peptide **4.2** (Figure 4.4A). Replacement of the charged residues with hydrophobic residues on the minor surface of peptide **4.1** converts a peptide that does not form oligomers in aqueous SDS to a peptide that oligomerizes. This experiment confirms the importance of an uncharged, hydrophobic surface in the oligomerization of β-hairpin peptides. In SEC, peptide **4.4** elutes at a volume consistent with the molecular weight of a monomer (Table 4.1), suggesting that SDS promotes oligomerization of peptide **4.4** in the SDS-PAGE experiment.

The slightly higher position of the peptide **4.4** oligomer band in SDS-PAGE suggests that the oligomer formed by peptide **4.4** may differ in structure from the hexamer formed by peptide **4.2**. To gain insights into the structure of the oligomer formed by peptide **4.4**, we turned to X-ray crystallography. Peptide **4.4** afforded crystals suitable for X-ray diffraction in aqueous HEPES buffer with potassium chloride and pentaerythritol propoxylate. We determined the X-ray crystallographic phases of peptide **4.4** by sulfur single-wavelength anomalous diffraction (S-SAD) using the anomalous signal from the sulfur in methionine.[40,41]

X-ray crystallography reveals that peptide **4.4** folds to form β-hairpins similar to those formed by peptides **4.1** and **4.2** (Figure 4.11). The minor surface of peptide **4.4** is nearly identical to that of peptide **4.2**, except that Val_{18} takes the place of Leu_{17}. Peptide **4.4** assembles differently than peptides **4.1** and **4.2**, forming packed columns in the crystal lattice rather than discrete oligomers (Figure 4.12B). The columns are composed of antiparallel β-sheet dimers that are

laminated on both faces through hydrophobic interactions. Each dimer consists of an antiparallel β-sheet formed by two peptide **4.4** β-hairpins (Figure 4.12A). The dimer is shifted out of registration by two residues toward the *C*-termini, such that Met_{35} pairs with Gly_{33}. The oligomer formed by peptide **4.4** in SDS-PAGE might be composed of three or four of these dimers packing through hydrophobic interactions.

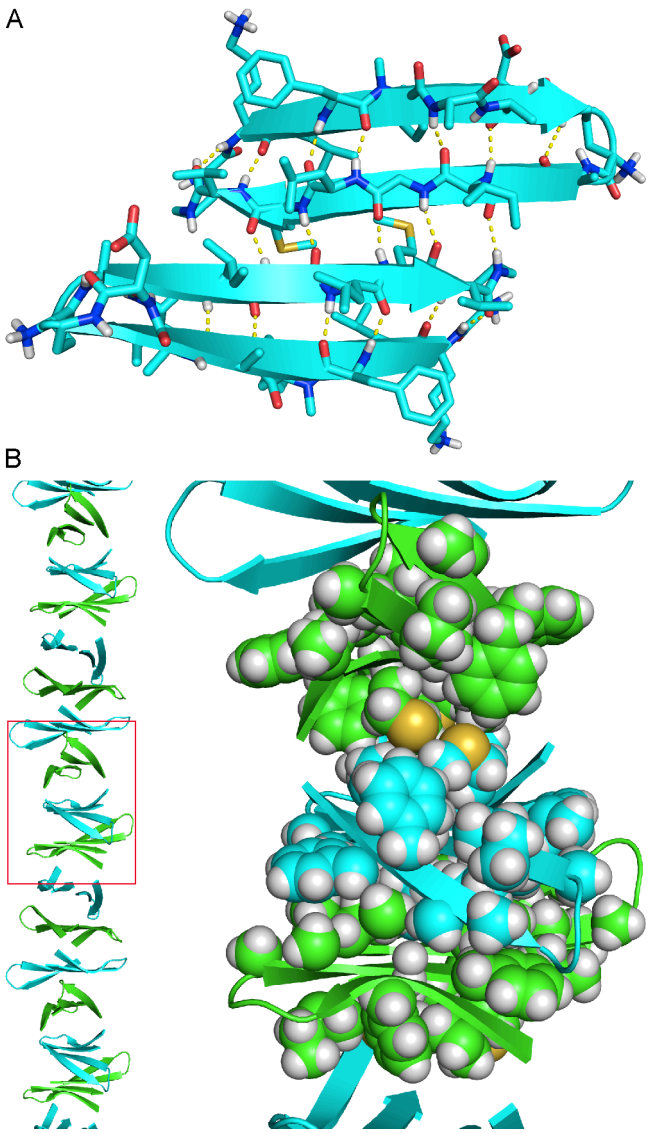

Figure 4.12. X-ray crystallographic structure of peptide **4.4** (PDB 5W4J). (A) Structure of the antiparallel β-sheet dimer formed by peptide **4.4**. (B) Column of laminated antiparallel β-sheet dimers. The right panel shows a detail view of the hydrophobic packing that occurs at the interfaces of the dimers.

Biological Studies of Peptides 4.1–4.4. Many oligomers formed by full-length Aβ are toxic toward cells.[7,8] To test whether the oligomers formed by peptide **4.2** are also toxic, we evaluated the toxicity of peptide **4.2** toward neuronally derived SH-SY5Y cells using a lactate dehydrogenase (LDH) release assay. We compared peptide **4.2** to peptide **4.3** to investigate how the hexamer-forming $A\beta_{16–36}$-derived peptide compares to a non-oligomerizing homologue. We

also evaluated the toxicity of peptides **4.1** and **4.4** to better understand the relationship between oligomerization and toxicity.

Peptide **4.2** shows an increase in LDH release at concentrations as low as 50 μM, indicating toxicity toward SH-SY5Y cells (Figure 4.13). Peptide **4.3**, the non-oligomerizing homologue of peptide **4.2**, is not toxic toward SH-SH5Y cells at concentrations as high as 200 μM, suggesting that oligomerization of peptide **4.2** to form a hexamer is important for toxicity. No dose dependence is observed in the LDH release induced by peptide **4.2** at concentrations of 50, 100, and 200 μM, suggesting that oligomerization is cooperative and toxicity occurs above a critical concentration. Peptide **4.1** is toxic toward SH-SY5Y cells at concentrations as low as 100 μM, and peptide **4.4** is toxic toward SH-SY5Y cells at concentrations as low as 50 μM.

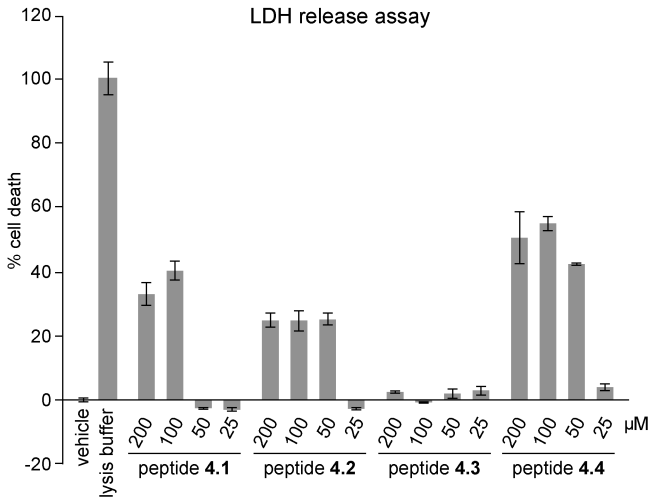

Figure 4.13. LDH release assay of peptides **4.1**–**4.4**. Data represent the mean of five replicate wells +/− s.d. Deionized water (vehicle) was used as a negative control.

We envision that the onset of toxicity of peptides **4.1**, **4.2**, and **4.4** between 25 μM and 100 μM reflects the propensity of the hydrophobic peptides to form oligomers in the presence of the lipophilic cell membranes. In this model, none of the peptides are oligomeric in cell

membranes at 25 μM. As the concentration is increased, oligomerization occurs, the oligomers disrupt the integrity of the cell membranes, and cell damage or death occurs.

Crystallographically Based Model of an $A\beta_{12–40}$ Hexamer. We envision that the full-length Aβ peptide can assemble in the same fashion as peptide **4.2** to form a barrel-like hexamer composed of β-sheet dimers or triangular trimers. To better understand what a hexamer containing the $A\beta_{23–29}$ loop and additional *N*- and *C*-terminal residues might look like, we modeled $A\beta_{12–40}$ into the crystallographic coordinates of the hexamer. We built residues 23–29 (DVGSNKG), 12–15 (VHHQ), and 37–40 (GGVV) into the crystallographic coordinates of the six peptide **4.2** monomers that comprise the hexamer, and we performed replica-exchange molecular dynamics (REMD) to generate realistic conformations of the loops and the *N*- and *C*-terminal regions of the β-hairpins (Figure 4.14).[42,43]

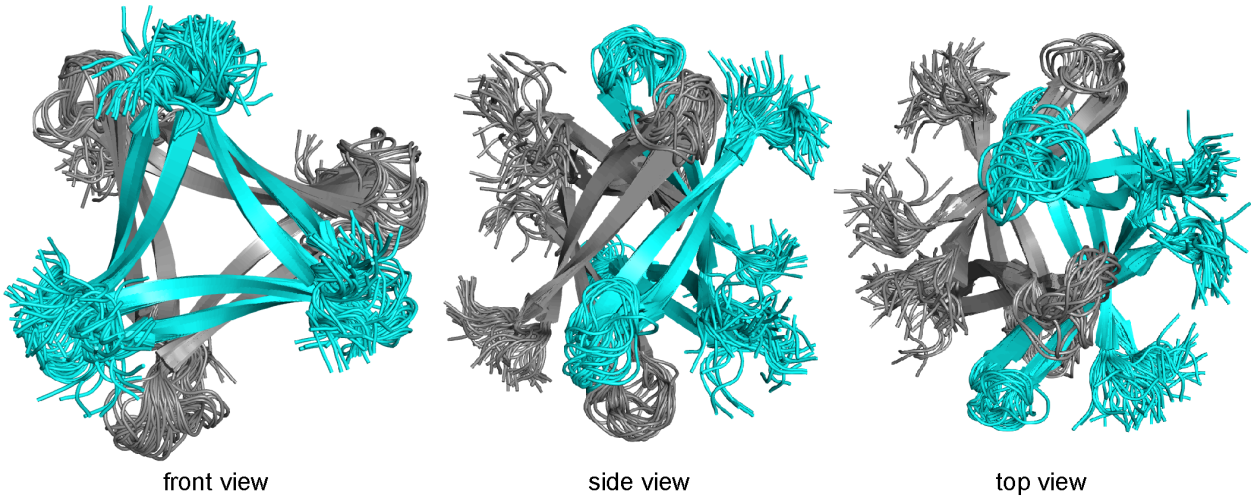

Figure 4.14. Crystallographically based model of an $A\beta_{12–40}$ barrel-like hexamer. Superposition of 31 structures generated by replica-exchange molecular dynamics.

The REMD simulation shows that full-length Aβ could form a barrel-like hexamer. The hexamer can accommodate the $A\beta_{23–29}$ loop and the remaining *N*- and *C*-terminal residues

without steric clashes. In a hexamer formed by full-length Aβ, the loops from two monomers and the *N*- and *C*-termini from another two monomers would extend past the barrel-like openings. The loops might fold over the barrel-like openings and shield the hydrophobic core of the hexamer, which would otherwise be exposed to solvent.

Summary and Conclusion

These X-ray crystallographic, biophysical, and biological studies of β-hairpins derived from Aβ provide insights into amyloid oligomers. X-ray crystallography revealed that β-hairpin peptide **4.2** assembles to form a hexamer composed of dimers and trimers. SDS-PAGE and SEC revealed that peptide **4.2** assembles to form oligomers in solution that recapitulate the oligomers observed crystallographically. In the SDS-PAGE experiment, peptide **4.2** assembles to form a hexamer, which recapitulates the barrel-like hexamer observed crystallographically. In the SEC experiment, peptide **4.2** assembles to form a dimer and trimer, which recapitulate the β-sheet dimer and triangular trimer observed crystallographically. The difference between the assemblies observed in the SEC and SDS-PAGE experiments may be explained by the membrane-like environment of SDS micelles, which appears to promote the assembly of the dimers and trimers into the hexamer.

The differing propensities of peptides **4.1** and **4.2** to oligomerize in SDS-PAGE may result from differences in hydrophobicity and charge on the minor surfaces of each peptide. The oligomerization of the chimera peptide **4.4** in SDS-PAGE supports the importance of a hydrophobic minor surface in solution-phase assembly. We recently demonstrated that stabilizing the trimer formed by peptide **4.1** through covalent crosslinking allows solution-phase assembly to form higher-order oligomers, such as hexamers and dodecamers.[28] The current study

demonstrates that hydrophobic interactions between monomers that are not covalently crosslinked can stabilize higher-order oligomers in the same fashion. This finding is significant, because it shows that suitably folded β-hairpin peptides containing amyloidogenic sequences can form stable oligomers.

The X-ray crystallographic structure of the hexamer formed by peptide **4.2** shares structural features with the αB crystallin cylindrin oligomer reported by Eisenberg et al. and the hPrP oligomer reported by Surewicz et al.[1,2] Like these oligomers, the hexamer formed by peptide **4.2** is a discrete oligomer composed of antiparallel β-sheets that form a continuous hydrogen-bonding network and a hydrophobic core. These features have emerged as common structural motifs among oligomers formed by amyloidogenic peptides and proteins. We have also seen this motif in a barrel-like hexamer formed by a β-hairpin peptide derived from β_2-microglobulin that assembles in a similar fashion to the hexamer formed by peptide **4.2**.[30]

Hexamers of Aβ have been isolated from the brains of Tg2576 transgenic mice as well as from human brains and are thought to play a role in the early stages of Alzheimer's disease.[9,44] The barrel-like hexamer formed by peptide **4.2** exhibits many of the biological and solution-phase characteristics of oligomers formed by full-length Aβ. Like Aβ oligomers, the hexamer assembles in the presence of SDS and is toxic toward cells. Despite these similarities, the significance of the barrel-like hexamer in Alzheimer's disease remains to be determined and is a current area of investigation in our laboratory.

REFERENCES AND NOTES

1 Laganowsky, A. Liu, C., Sawaya, M. R., Whitelegge, J. P., Park, J., Zhao, M., Pensalfini, A., Soriaga, A. B., Landau, M., Teng, P. K., Cascio, D., Glabe, C., Eisenberg, D. (2012) Atomic view of a toxic amyloid small oligomer. *Science 335*, 1228–1231.

2 Apostol, M. I., Perry, K., Surewicz, W. K. (2013) Crystal structure of a human prion protein fragment reveals a motif for oligomer formation. *J. Am. Chem. Soc. 135*, 10202–10205.

3 Liu, C., Sawaya, M. R., Cheng, P. N., Zheng, J., Nowick, J. S., Eisenberg, D. (2011) Out-of-register β-sheets suggest a pathway to toxic amyloid aggregates. *J. Am. Chem. Soc. 133*, 6736–6744.

4 Pham, J. D., Chim, N., Goulding, C. W., Nowick, J. S. (2013) Structures of oligomers of a peptide from β-amyloid. *J. Am. Chem. Soc. 135*, 12460–12467.

5 Kayed, R., Head, E., Thompson, J. L., McIntire, T. M., Milton, S. C., Cotman, C. W., Glabe, C. G. (2003) Common structure of soluble amyloid oligomers implies common mechanism of pathogenesis. *Science 300*, 486–489.

6 Glabe, C. G. (2008) Structural classification of toxic amyloid oligomers. *J. Biol. Chem. 283*, 29639–29643.

7 Benilova, I,, Karran, E., De Strooper, B. (2012) The toxic Aβ oligomer and Alzheimer's disease: an emperor in need of clothes. *Nat. Neurosci. 15*, 349–357.

8 Larson, M. E., Lesné, S. E. (2012) Soluble Aβ oligomer production and toxicity. *J. Neurochem. 120*, 125–139.

9 Lesné, S., Koh, M. T., Kotilinek, L., Kayed, R., Glabe, C. G., Yang, A., Gallagher, M., Ashe K. H. (2006) A specific amyloid-beta protein assembly in the brain impairs memory. *Nature 440*, 352–357.

10 Shankar, G. M,, Li, S., Mehta, T. H., Garcia-Munoz, A., Shepardson, N. E., Smith, I,, Brett, F. M., Farrell, M. A., Rowan, M. J., Lemere, C. A., Regan, C. M., Walsh, D. M., Sabatini, B. L., Selkoe, D. J. (2008) Amyloid-beta protein dimers isolated directly from Alzheimer's brains impair synaptic plasticity and memory. *Nat. Med. 14*, 837–842.

11 Wälti, M. A., Ravotti, F., Arai, H., Glabe, C. G., Wall, J. S., Böckmann, A., Güntert, P., Meier, B. H., Riek, R. (2016) Atomic-resolution structure of a disease-relevant Aβ(1-42) amyloid fibril. *Proc. Natl. Acad. Sci. U.S.A. 113*, 4976–4984.

12 Colvin, M. T., Silvers, R., Ni, Q. Z., Can, T. V., Sergeyev, I., Rosay, M., Donovan, K. J., Michael, B., Wall, J., Linse, S., Griffin, R. G. (2016) Atomic Resolution Structure of Monomorphic Aβ42 Amyloid Fibrils. *J. Am. Chem. Soc. 138*, 9663–9674.

13 Lu, J. X., Qiang, W., Yau, W. M., Schwieters, C. D., Meredith, S. C., Tycko, R. (2013) Molecular structure of β-amyloid fibrils in Alzheimer's disease brain tissue. *Cell 154*, 1257–1268.

14 Tuttle, M. D., Comellas, G., Nieuwkoop, A. J., Covell, D. J., Berthold, D. A., Kloepper, K. D., Courtney, J. M., Kim, J. K., Barclay, A. M., Kendall, A., Wan, W., Stubbs, G., Schwieters, C. D., Lee, V. M., George, J. M., Rienstra, C. M. (2016) Solid-state NMR structure of a pathogenic fibril of full-length human α-synuclein. *Nat. Struct. Mol. Biol. 23*, 409–415.

15 Gu, L., Liu, C., Guo, Z. (2013) Structural insights into Aβ42 oligomers using site-directed spin labeling. *J. Biol. Chem. 288*, 18673–18683.

16 Potapov, A., Yau, W.-M., Ghirlando, R., Thurber, K. R., Tycko, R. (2015) Successive Stages of Amyloid-β Self-Assembly Characterized by Solid-State Nuclear Magnetic Resonance with Dynamic Nuclear Polarization. *J. Am. Chem. Soc*. *137*, 8294–8307.

17 Hoyer, W., Grönwall, C., Jonsson, A., Ståhl, S., Härd, T. (2008) Stabilization of a beta-hairpin in monomeric Alzheimer's amyloid-beta peptide inhibits amyloid formation. *Proc. Natl. Acad. Sci. U.S.A. 105*, 5099–6104.

18 Sandberg, A., Luheshi, L. M., Söllvander, S., Pereira de Barros, T., Macao, B., Knowles, T. P., Biverstål, H., Lendel, C., Ekholm-Petterson, F., Dubnovitsky, A., Lannfelt, L., Dobson, C. M., Härd, T. (2010) Stabilization of neurotoxic Alzheimer amyloid-beta oligomers by protein engineering. *Proc. Natl. Acad. Sci. U.S.A. 107*, 15595–15600.

19 Lendel, C., Bjerring, M., Dubnovitsky, A., Kelly, R. T., Filippov, A., Antzutkin, O. N., Nielsen, N. C., Härd, T. (2014) A hexameric peptide barrel as building block of amyloid-β protofibrils. *Angew. Chem. Int. Ed. Engl. 53*, 12756–12760.

20 Mirecka, E. A., Shaykhalishahi, H., Gauhar, A., Akgül, Ş., Lecher, J., Willbold, D., Stoldt, M., Hoyer, W. (2014) Sequestration of a β-hairpin for control of α-synuclein aggregation. *Angew. Chem. Int. Ed. Engl. 53*, 4227–4230.

21 Mirecka, E. A., Feuerstein, S., Gremer, L., Schröder, G. F., Stoldt, M., Willbold, D., Hoyer, W. (2016) β-Hairpin of Islet Amyloid Polypeptide Bound to an Aggregation Inhibitor. *Sci. Rep. 6*, 33474.

22 Yu, L., Edalji, R., Harlan, J. E., Holzman, T. F., Lopez, A. P., Labkovsky, B., Hillen, H., Barghorn, S., Ebert, U., Richardson, P. L., Miesbauer, L., Solomon, L., Bartley, D., Walter, K., Johnson, R. W., Hajduk, P. J., Olejniczak, E. T. (2009) Structural characterization of a soluble amyloid beta-peptide oligomer. *Biochemistry 48*, 1870–1877.

23 Scheidt, H. A., Morgado, I., Huster, D. (2012) Solid-state NMR reveals a close structural relationship between amyloid-β protofibrils and oligomers. *J. Biol. Chem. 287*, 22822–22826.

24 Doi, T., Masuda, Y., Irie, K., Akagi, K., Monobe, Y., Imazawa, T., Takegoshi, K. (2012) Solid-state NMR analysis of the β-strand orientation of the protofibrils of amyloid β-protein. *Biochem. Biophys. Res. Commun. 428*, 458–462.

25 Tay, W. M., Huang, D., Rosenberry, T. L., Paravastu, A. K. (2013) The Alzheimer's amyloid-β(1-42) peptide forms off-pathway oligomers and fibrils that are distinguished structurally by intermolecular organization. *J. Mol. Biol. 425*, 2494–2508.

26 Spencer, R. K., Li. H., Nowick, J. S. (2014) X-ray crystallographic structures of trimers and higher-order oligomeric assemblies of a peptide derived from Aβ(17–36). *J. Am. Chem. Soc. 136*, 5595–5598.

27 Kreutzer, A. G., Hamza, I. H., Spencer, R. K., Nowick J. S. (2016) X-ray Crystallographic Structures of a Trimer, Dodecamer, and Annular Pore Formed by an Aβ17–36 β-Hairpin. *J. Am. Chem. Soc. 138*, 4634–4642.

28 Kreutzer, A. G., Yoo, S., Spencer, R. K., Nowick, J. S. (2017) Stabilization, Assembly, and Toxicity of Trimers Derived from Aβ. *J. Am. Chem, Soc. 139*, 966–975.

29 Salveson, P. J., Spencer, R. K., Nowick J. S. (2016) X-ray Crystallographic Structure of Oligomers Formed by a Toxic β-Hairpin Derived from α-Synuclein: Trimers and Higher-Order Oligomers. *J. Am. Chem. Soc. 138*, 4458–4467.

30 Spencer, R. K., Kreutzer, A. G., Salveson, P. J., Li, H., Nowick, J. S. (2015) X-ray Crystallographic Structures of Oligomers of Peptides Derived from β2-Microglobulin. *J. Am. Chem. Soc. 137*, 6304–6311.

31 Spencer, R. K., Chen, K. H., Manuel, G., Nowick, J. S. (2013) Recipe for β-Sheets: Foldamers Containing Amyloidogenic Peptide Sequences. *Eur. J. Org. Chem*. *2013*, 3523–3528.

32 Nowick, J. S., Brower, J. O. (2003) A new turn structure for the formation of beta-hairpins in peptides. *J. Am. Chem. Soc. 125*, 876–877.

33 Woods, R. J., Brower, J. O., Castellanos, E., Hashemzadeh, M., Khakshoor, O., Russu, W. A., Nowick, J. S. (2007) Cyclic modular beta-sheets. *J. Am. Chem. Soc. 129*, 2548–2558.

34 A homologue of peptide **2** in which the *N*-methyl group is on Gly_{33} and Phe_{19} is mutated to *p*-iodophenylalanine assembles to form a ball-shaped dodecamer. The placement of the *N*-methyl group prevents the formation of a hexamer homologous to that formed by peptide **4.2**. Salveson, P. J., Spencer. R. K., Kreutzer, A. G., Nowick, J. S. (2017) X-ray Crystallographic Structure of a Compact Dodecamer from a Peptide Derived from Aβ16–36. *Org. Lett. 19*. 3462–3465.

35 The $A\beta_{17–36}$ β-hairpin embodied in peptide **4.1** has the same alignment of residues as the affibody-bound Aβ β-hairpin reported in reference 17.

36 In the X-ray crystallographic structure of peptide **4.1**, the triangular trimer also assembles to form a ball-shaped dodecamer.

37 Peptide **4.2** was synthesized as described previously by our laboratory.[26,27,28,29,30] The peptide was synthesized by solid-phase peptide synthesis on 2-chlorotrityl resin, followed by cleavage from the resin, solution-phase cyclization, global deprotection, and purification by reverse-phase HPLC.

38 Dauter, Z., Dauter, M., Rajashankar, K. R. (2000) Novel approach to phasing proteins: derivatization by short cryo-soaking with halides. *Acta. Crystallogr. D Biol. Crystallogr. 56*, 232–237.

39 Spencer, R. K., Nowick, J. S. (2015) A Newcomer's Guide to Peptide Crystallography. *Isr. J. Chem. 55*, 698–710.

40 Liu, Q., Dahmane, T., Zhang, Z., Assur, Z., Brasch, J., Shapiro, L., Mancia, F., Hendrickson, W. A. (2012) Structures from anomalous diffraction of native biological macromolecules. *Science 336*, 1033–1037.

41 Sarma, G. N., Karplus, P. A. (2006) In-house sulfur SAD phasing: a case study of the effects of data quality and resolution cutoffs. *Acta. Crystallogr. D Biol. Crystallogr. 62*, 707–716.

42 Sugita, Y., Okamoto, Y. (1999) Replica-exchange molecular dynamics method for protein folding. *Chem. Phys. Lett. 314*, 141−151.

43 Phillips, J. C., Braun, R., Wang, W., Gumbart, J., Tajkhorshid, E., Villa, E., Chipot, C., Skeel, R. D., Kale, L., Schulten, K. (2005) Scalable molecular dynamics with NAMD. *J. Comput. Chem. 26*, 1781−1802.

44 Lesné, S. E., Sherman, M. A., Grant, M., Kuskowski, M., Schneider, J. A., Bennett D. A., Ashe, K. H. (2013) Brain amyloid-β oligomers in ageing and Alzheimer's disease. *Brain 136*, 1383–1398.

Supporting Information

Table of Contents

Supporting Figures and Tables

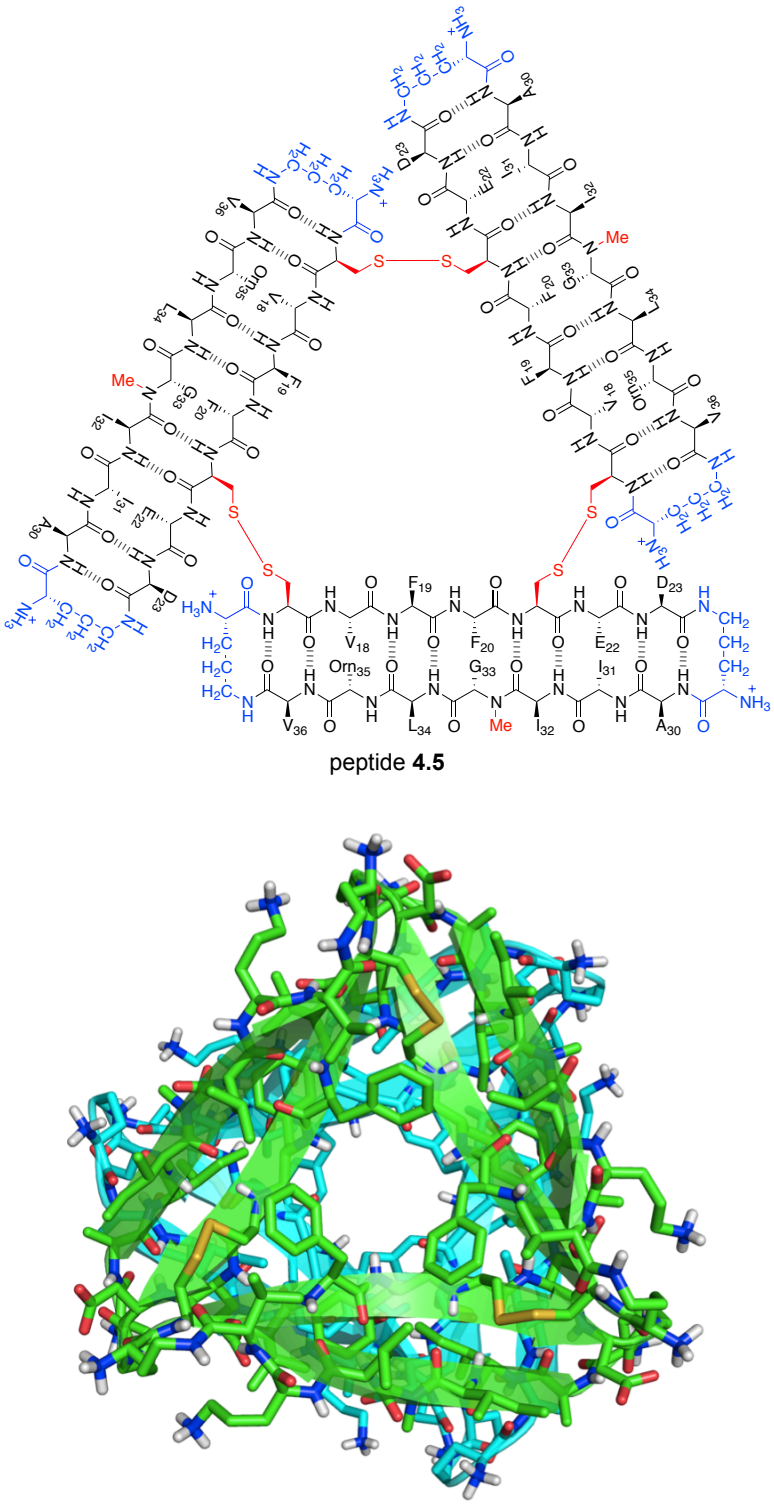

Figure 4.S1. Chemical structure of covalent trimer peptide **4.5** (top). X-ray crystallographic structure of the hexamer formed by covalent trimer peptide **4.5** (PDB 5SUT, bottom).[4]

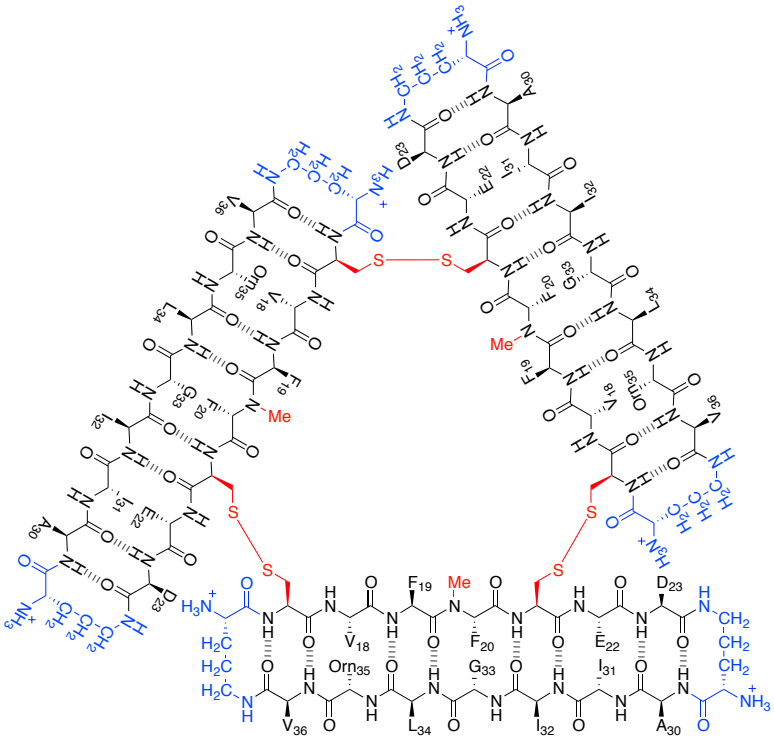

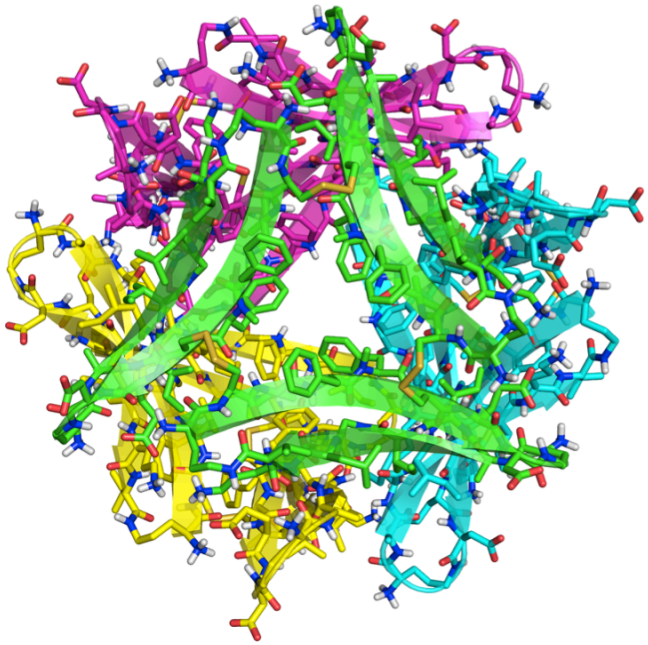

Figure 4.S2. Chemical structure of covalent trimer peptide **4.6** (top). X-ray crystallographic structure of the dodecamer formed by covalent trimer peptide **4.6** (PDB 5SUR, bottom).[4]

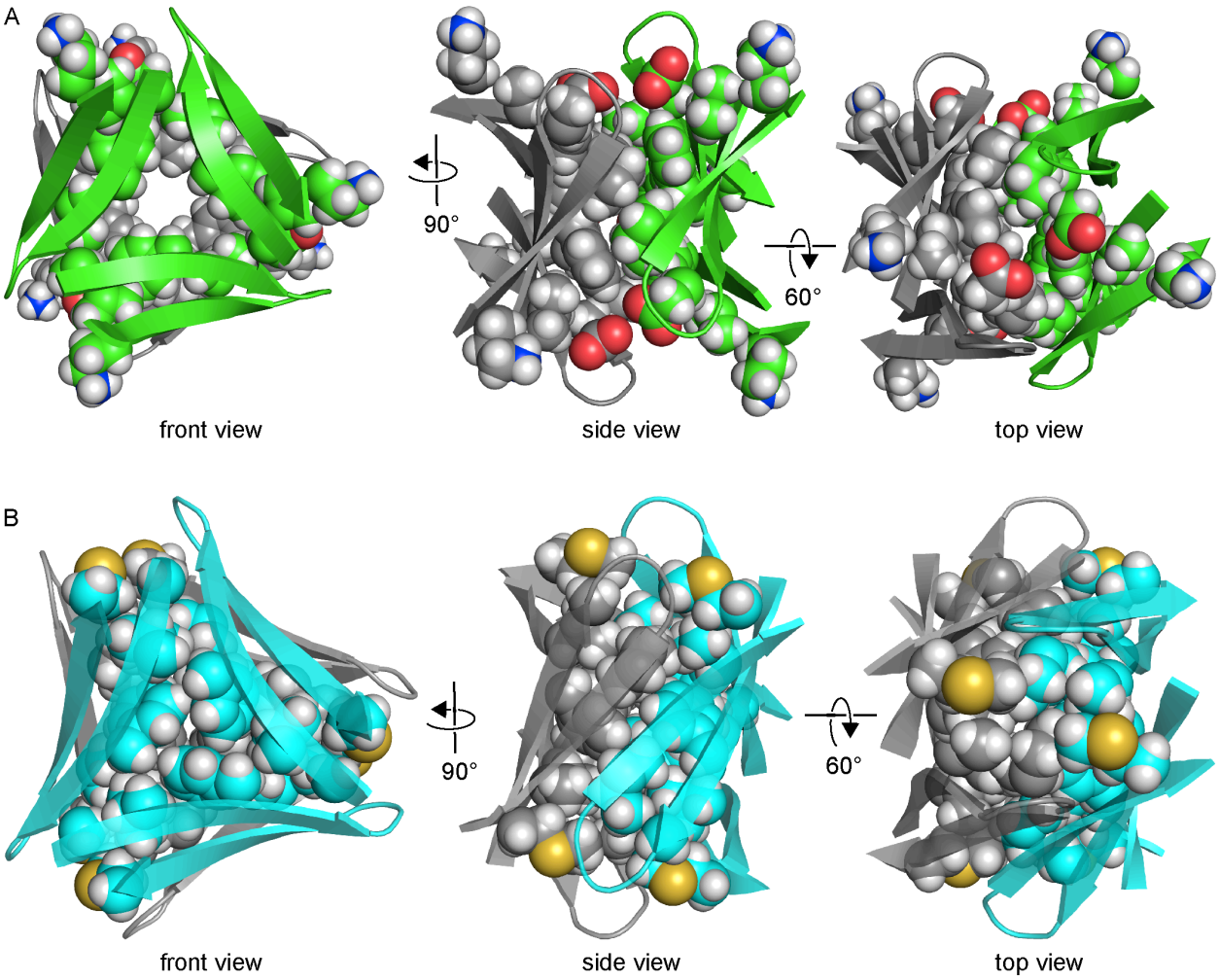

Figure 4.S3. X-ray crystallographic structures of the hexamers formed by peptides **4.1** and **4.2**. The hexamers formed by peptide **4.1** (A) and peptide **4.2** (B) differ in the degree of their hydrogen bonding and hydrophobic packing. The buried surface area of the hexamer formed by peptide **4.1** is 3514 $Å^2$, whereas the buried surface area of the hexamer formed by peptide **4.2** is 5102 $Å^2$.

Table 4.S1. Crystallographic properties, crystallization conditions, and data collection and model refinement statistics for peptide **4.2**.

peptide	peptide **4.2** (synchrotron)	peptide **4.2** (X-ray diffractometer)
PDB ID	5W4H	5W4I
space group	*P*432	*P*432
a, *b*, *c* (Å)	67.53, 67.53, 67.53	67.74, 67.74, 67.74
α, β, λ (°)	90, 90, 90	90, 90, 90
peptides per asymmetric unit	3	3
crystallization conditions	0.1 M HEPES buffer (pH 7.0), 0.25 M magnesium chloride, 34% isopropanol	0.1 M HEPES sodium buffer (pH 7.5), 0.2 M sodium citrate, 22% isopropanol
wavelength (Å)	0.998	1.54
resolution (Å)	67.54–1.718 (1.78–1.718)	19.56–2.026 (2.098–2.026)
total reflections	12043 (1151)	7613 (727)
unique reflections	6026 (580)	3808 (365)
multiplicity	9.5 (6.3)	36.8 (17.2)
completeness (%)	99.34 (97.97)	99.9 (99.8)
mean I/σ	19.79 (1.99)	24.3 (2.1)
Wilson B factor	31.01	24.51
R_{merge}	0.009247 (0.2266)	0.03415 (0.2676)
$R_{measure}$	0.01308 (0.3205)	0.0483 (0.3784)
$CC_{1/2}$	1.000 (0.905)	0.999 (0.867)
CC^*	1.000 (0.975)	1.000 (0.964)
R_{work}	0.2033 (0.3037)	0.2201 (0.3162)
R_{free}	0.2358 (0.3823)	0.2628 (0.3903)
number of non-hydrogen atoms	408	415
RMS_{bonds}	0.015	0.010
RMS_{angles}	1.89	1.24
Ramachandran favored (%)	100	100
outliers (%)	0	0
clashscore	8.06	7.98
average B-factor	40.45	28.68
number of TLS groups	3	3
ligands/ions	N/A	I (5), Cl (3)
water molecules	33	32

Table 4.S2. Crystallographic properties, crystallization conditions, and data collection and model refinement statistics for peptide **4.4**.

peptide	peptide **4.4**
PDB ID	5W4J
space group	$P22_12$
a, *b*, *c* (Å)	30.59, 46.94, 64.30
α, β, λ (°)	90, 90, 90
peptides per asymmetric unit	6
crystallization conditions	0.05 M HEPES buffer (pH 7.5), 0.2 M KCl, 37% pentaerythritol propoxylate (5/4 PO/OH)
wavelength (Å)	1.54
resolution (Å)	32.15–2.08 (2.154–2.08)
total reflections	11904 (1162)
unique reflections	5952 (581)
multiplicity	17.4 (14.5)
completeness (%)	99.82 (100)
mean I/σ	71.11 (28.06)
Wilson B factor	27.69
R_{merge}	0.007097 (0.01986)
$R_{measure}$	0.01004 (0.02809)
$CC_{1/2}$	1.00 (0.999)
CC^*	1.00 (1.00)
R_{work}	0.1969 (0.2194)
R_{free}	0.2410 (0.2892)
number of non-hydrogen atoms	789
RMS_{bonds}	0.011
RMS_{angles}	1.27
Ramachandran favored (%)	100
outliers (%)	0
clashscore	5.65
average B-factor	38.53
number of TLS groups	9
ligands/ions	N/A
water molecules	63

Materials and Methods[1]

General information

All chemicals were used as received unless otherwise noted. Methylene chloride (CH_2Cl_2) was passed through alumina under nitrogen prior to use. Anhydrous, amine-free *N,N*-dimethylformamide (DMF) was purchased from Alfa Aesar. Deionized water (18 MΩ) was obtained from a Barnstead NANOpure Diamond water purification system. Analytical reverse-phase HPLC was performed on an Agilent 1200 instrument equipped with a Phenomonex Aeris PEPTIDE 2.6u XB-C18 column. Preparative reverse-phase HPLC was performed on a Beckman Gold Series P instrument equipped with an Agilent Zorbax SB-C18 column. HPLC grade acetonitrile and deionized water, each containing 0.1% trifluoroacetic acid (TFA), were used for analytical and preparative reverse-phase HPLC. All peptides were prepared and used as the trifluoroacetate salts and were assumed to have one trifluoroacetic acid molecule per amine group on each peptide.

*Synthesis of peptides **4.1**–**4.4**.*

a. *Loading of the resin.* 2-Chlorotrityl chloride resin (300 mg, 1.2 mmol/g) was added to a Bio-Rad Poly-Prep chromatography column (10 mL). The resin was suspended in dry CH_2Cl_2 (10 mL) and allowed to swell for 30 min. The solution was drained from the resin and a solution of Boc-Orn(Fmoc)-OH (0.50 equiv, 82 mg, 0.18 mmol) in 6% (v/v) 2,4,6-collidine in dry CH_2Cl_2 (8 mL) was added immediately and the suspension was gently agitated for 12 h. The solution was then drained and a mixture of CH_2Cl_2/MeOH/*N*,*N*-diisopropylethylamine (DIPEA) (17:2:1, 10 mL) was added immediately. The mixture was gently agitated for 1 h to cap the

unreacted 2-chlorotrityl chloride resin sites. The resin was then washed with dry CH_2Cl_2 (2x) and dried by passing nitrogen through the vessel. This procedure typically yields 0.12–0.15 mmol of loaded resin (0.4–0.5 mmol/g loading).

b. *Peptide coupling.* The Boc-Orn(Fmoc)-2-chlorotrityl resin generated from the previous step was transferred to a microwave-assisted solid-phase peptide synthesizer reaction vessel and submitted to cycles of automated peptide coupling with Fmoc-protected amino acid building blocks using a CEM Liberty 1 Automated Microwave Peptide Synthesizer. The linear peptide was synthesized from the *C*-terminus to the *N*-terminus. Each coupling cycle consisted of i. Fmoc-deprotection with 20% (v/v) piperidine in DMF for 2 min at 50 °C (2x), ii. washing with DMF (3x), iii. coupling of the amino acid (0.75 mmol, 5 equiv) in the presence of HCTU (0.675 mmol, 4.5 equiv) and 20% (v/v) *N*-methylmorpholine (NMM) in DMF for 10 min at 50 °C, iv. washing with DMF (3x). Special coupling conditions were used for the valine that followed the *N*-methylphenylalanine in peptides **4.2** and **4.3** and for the phenylalanine that followed the *N*-methylphenylalanine in peptides **4.1** and **4.4**: The valine or phenylalanine was double coupled (0.75 mmol, 5 equiv.) and allowed to react at ambient temperature for 1 h per coupling with HATU (5 equiv) and HOAt (5 equiv) in 20% (v/v) NMM in DMF. After coupling of the last amino acid, the terminal Fmoc group was removed with 20% (v/v) piperidine in DMF (10 min 50 °C). The resin was transferred from the reaction vessel of the peptide synthesizer to a Bio-Rad Poly-Prep chromatography column.

c. *Cleavage of the peptide from the resin.* The linear peptide was cleaved from the resin by agitating the resin for 1 h with a solution of 1,1,1,3,3,3-hexafluoroisopropanol (HFIP) in CH_2Cl_2 (1:4, 7 mL).[2] The suspension was filtered and the filtrate was collected in a 250-mL round-bottomed flask. The resin was washed with additional HFIP in CH_2Cl_2 (1:4, 7 mL) and

then with CH_2Cl_2 (2×10 mL). The combined filtrates were concentrated by rotary evaporation to give a white solid. The white solid was further dried by vacuum pump to afford the crude protected linear peptide, which was cyclized without further purification.

d. *Cyclization of the linear peptide.* The crude protected linear peptide was dissolved in dry DMF (150 mL). HOBt (114 mg, 0.75 mmol, 5 equiv) and HBTU (317 mg, 0.75 mmol, 5 equiv) were added to the solution. DIPEA (0.33 mL, 1.8 mmol, 12 equiv) was added to the solution and the mixture was stirred under nitrogen for 24 h. The mixture was concentrated under reduced pressure to afford the crude protected cyclic peptide.

e. *Global deprotection of the cyclic peptide.* The protected cyclic peptide was dissolved in TFA/triisopropylsilane (TIPS)/H_2O (18:1:1, 20 mL) in a 250-mL round-bottomed flask equipped with a nitrogen-inlet adaptor. The solution was stirred for 1.5 h. The reaction mixture was then concentrated by rotary evaporation under reduced pressure to afford the crude cyclic peptide as a thin yellow film on the side of the round-bottomed flask. The crude cyclic peptide was immediately subjected to purification by reverse-phase HPLC (RP-HPLC), as described below.

f. *Reverse-phase HPLC purification.* The peptide was dissolved in H_2O and acetonitrile (7:3, 10 mL), and the solution was filtered through a 0.2 μm syringe filter and purified by RP-HPLC (gradient elution with 20–50% CH_3CN over 50 min). Pure fractions were concentrated by rotary evaporation and lyophilized. Typical syntheses yielded ~55 mg of the peptide as the TFA salt.

SDS-PAGE and silver staining.

The oligomerization of peptides **4.1**–**4.4** was studied by Tricine SDS-PAGE. Reagents and gels for Tricine SDS-PAGE were prepared according to recipes and procedures detailed in Schägger, H. *Nat. Protoc.* **2006**, *1*, 16–22.[3] The migration of peptides **4.1**–**4.4** was compared with a molecular weight protein ladder (Spectra™ Multicolor Low Range Protein Ladder, ThermoFisher Scientific, catalog #: 26628) and with previously reported peptides **4.5** and **4.6**.[4]

Sample preparation. Each peptide was dissolved in deionized water to a concentration of 10 mg/mL. Aliquots of the 10-mg/mL solutions were diluted with deionized water to create 0.30-mg/mL solutions of peptides **4.1**–**4.4** and 0.10-mg/mL solutions of peptides **4.5** and **4.6**. The 0.30-mg/mL solutions of peptides **4.1**–**4.4** and 0.10-mg/mL solutions of peptides **4.5** and **4.6** were further diluted with 2X SDS-PAGE loading buffer (100 mM Tris buffer at pH 6.8, 20% (v/v) glycerol, and 4% SDS) to create 0.15-mg/mL working solutions of peptides **4.1**–**4.4** and 0.05-mg/mL working solutions of peptides **4.5** and **4.6**. A 5.0-μL aliquot of each working solution was run on a 16% polyacrylamide gel with a 4% stacking polyacrylamide gel. The gels were run at a constant 80 volts.

Staining with silver nitrate was used to visualize peptides **4.1**–**4.4** and peptides **4.5** and **4.6** in the SDS-PAGE gel. Reagents for silver staining were prepared according to procedures detailed in Simpson, R. J. *CSH Protoc.* **2007**.[5] [The sodium thiosulfate solution, silver nitrate solution, and developing solution were prepared fresh each time silver staining was performed]. Briefly, the gel was removed from the casting glass and rocked in fixing solution (50% (v/v) methanol and 5% (v/v) acetic acid in deionized water) for 20 min. Next, the fixing solution was discarded and the gel was rocked in 50% (v/v) aqueous methanol for 10 min. Next, the 50% methanol was discarded and the gel was rocked in deionized water for 10 min. Next, the water

was discarded and the gel was rocked in 0.02% (w/v) sodium thiosulfate in deionized water for 1 min. The sodium thiosulfate was discarded and the gel was rinsed with deionized water for 1 min (2X). After the last rinse, the gel was submerged in chilled 0.1% (w/v) silver nitrate in deionized water and rocked at 4 °C for 20 min. Next, the silver nitrate solution was discarded and the gel was rinsed with deionized water for 1 min (2X). To develop the gel, the gel was incubated in developing solution (2% (w/v) sodium carbonate, 0.04% (w/v) formaldehyde until the desired intensity of staining was reached (~1–3 min). When the desired intensity of staining was reached, the development was stopped by discarding the developing solution and submerging the gel in 5% aqueous acetic acid.

Size exclusion chromatography.

The oligomerization of peptides **4.1**–**4.4** was studied by size exclusion chromatography (SEC) at 4 °C in TBS (50 mM Tris buffer (pH 7.5) and 100 mM NaCl) as follows: Each peptide was dissolved in deionized water to a concentration of 10 mg/mL. The peptide solutions were then diluted to 1 mg/mL by adding 80 μL of the 10-mg/mL solutions to 720 μL of TBS. The peptide solutions were centrifuged at 13,500 RPM for 30 seconds and then loaded onto a GE Superdex 75 10/300 GL column at 0.5 mL/min over 1 min. After loading, the samples were run with TBS at 1 mL/min Chromatograms were recorded at 214 nm and normalized to the highest absorbance value. Standards (cytochrome C, aprotinin, and vitamin B12) were run in the same fashion.

*Crystallization procedure for peptides **4.2** and **4.4**.*

Initial crystallization conditions for peptides **4.2** and **4.4** were determined using the hanging-drop vapor-diffusion method. Crystallization conditions were screened using three crystallization kits in a 96-well plate format (Hampton Index, PEG/Ion, and Crystal Screen). Three 150 nL hanging drops that differed in the ratio of peptide to well solution were made per condition in each 96-well plate for a total of 864 experiments. Hanging drops were made by combining an appropriate volume of peptide **4.2** or **4.4** (10 mg/mL in deionized water) with an appropriate volume of well solution to create three 150-nL hanging drops with 1:1, 1:2, and 2:1 peptide:well solution. The hanging drops were made using a TTP LabTech Mosquito nanodisperse instrument. Crystals of peptide **4.2** grew in ~72 h in a solution of 0.1 M HEPES buffer (pH 7.0), 0.25 M $MgCl_2$, and 30% isopropanol, as well as in a solution containing 0.1 M HEPES sodium buffer (pH 7.0), 0.2 M sodium citrate, and 30% isopropanol. Crystals of peptide **4.4** grew in ~72 h in a solution of 0.1 M HEPES buffer (pH 7.5), 0.2 M KCl, and 30% pentaerythritol propoxylate.

Crystallization conditions for peptides **4.2** and **4.4** were optimized using a 4x6 matrix Hampton VDX 24-well plate. The HEPES buffer pH was varied in each row in increments of 0.5 pH units (6.5, 7.0, 7.5, and 8.0) and the isopropanol or pentaerythritol propoxylate concentration in each column in increments of 2% (28%, 30%, 32%, 34%, 36%, 38%). The first well in the 4x6 matrix for peptide **4.2** was prepared by combined 100 μL of 1 M HEPES buffer at pH 6.5, 125 μL of 2 M $MgCl_2$, 280 μL of isopropanol, and 495 μL of deionized water. The other wells were prepared in analogous fashion, by combining 100 μL of HEPES buffer of varying pH, 125 μL of 2 M $MgCl_2$, isopropanol in varying amounts, and deionized water for a total volume of 1 mL in each well. Wells for peptide **4.4** were prepared in an analogous fashion.

Three hanging-drops were prepared per borosilicate glass slide by combining a solution of peptide **4.2** or peptide **4.4** (10 mg/mL in deionized water) and the well solution in the following amounts: 1 μL:1 μL, 2 μL:1 μL, and 1 μL:2 μL. Slides were inverted and pressed firmly against the silicone grease surrounding each well. Crystals of peptide **4.2** or of peptide **4.4** suitable for X-ray diffraction grew in ~3 days. Crystallization conditions were further optimized using smaller variations in HEPES buffer pH (in increments of 0.25 pH units) and isopropanol or pentaerythritol propoxylate (in increments of 1%). Crystals were harvested with a nylon loop attached to a copper or steel pin and flash frozen in liquid nitrogen prior to data collection. The optimized crystallization conditions for peptides **4.2** and **4.4** are summarized in Table S1 and Table S2.

*X-ray crystallographic data collection, data processing, and structure determination for peptides **4.2** and **4.4**.*

Diffraction data for peptides **4.2** and **4.4** were collected on a Rigaku Micromax-007HF X-ray diffractometer with a rotating copper anode at 1.54 Å wavelength with 0.5° oscillation. Diffraction data were collected using CrystalClear. Diffraction data were scaled and merged using XDS.[6] Coordinates for the anomalous signals were determined by HySS in the Phenix software suite 1.10.1.[7] Electron density maps were generated using anomalous coordinates determined by HySS as initial positions in Autosol. Molecular manipulation of the model was performed with Coot.[6] Coordinates were refined with phenix.refine.

Diffraction data for peptide **4.2** were also collected at the Advanced Light Source at Lawrence Berkeley National Laboratory with a synchrotron source at 0.998-Å wavelength to achieve higher resolution. Data for peptide **4.2** suitable for refinement at 2.03 Å were obtained

from the diffractometer; data for peptide **4.2** suitable for refinement at 1.72 Å were obtained from the synchrotron. Data for peptide **4.4** suitable for refinement at 2.08 Å were obtained from the diffractometer. Diffraction data were scaled and merged using XDS.[7] The electron density map for peptide **4.2** was generated by molecular replacement using the coordinates from the structure of peptide **4.2** generated by soaking in KI using Phaser in the Phenix software suite 1.10.1.[8] The electron density map for peptide **4.4** was generated by sulfur single-wavelength anomalous diffraction (S-SAD) using the anomalous signal from the six sulfur atoms in methionine in the asymmetric unit using HySS in the Phenix software suite 1.10.1. Molecular manipulation of the peptide **4.2** and peptide **4.4** models was performed with Coot. Coordinates for peptide **4.2** and peptide **4.4** were refined with phenix.refine.

LDH release assays.

The toxicity of peptides **4.1**–**4.4** toward SH-SY5Y cells was assessed by LDH release assays. Cells were incubated in the presence or absence of equivalent concentrations of peptides **4.1**–**4.4** for 72 h in 96-well plates. The LDH release assay was performed using the Pierce LDH Cytotoxicity Assay Kit from Thermo Scientific. Experiments were performed in replicates of five, and an additional 10 wells were used for controls. Cells were cultured in the inner 60 wells (rows B–G, columns 2–11) of the 96-well plate. DMEM:F12 media (100 μL) was added to the outer wells (rows A and H and columns 1 and 12), in order to ensure the greatest reproducibility of data generated from the inner wells.

a. *Preparation of stock solutions of peptides **4.1**–**4.4**.* 10-mg/mL stock solutions of peptides **4.1**–**4.4** were prepared gravimetrically by dissolving 1.0 mg of each compound in 100 μL of deionized water that was either filtered through a 0.2 μm syringe filter or autoclaved. The

stock solution was used to create 500-μM working solutions of peptides **4.1**–**4.4**. The 500-μM working solutions of peptides **4.1**–**4.4** was diluted with deionized water to create 250-μM working solutions of peptides **4.1**–**4.4**.

b. *Preparation of SH-SY5Y cells for LDH release assays.* SH-SY5Y cells were plated in a 96-well plate at 15,000 cells per well. Cells were incubated in 100 μL of a 1:1 mixture of DMEM:F12 media supplemented with 10% fetal bovine serum, 100 U/mL penicillin, and 100 μg/mL streptomycin at 37 °C in a 5% CO_2 atmosphere and allowed to adhere to the bottom of the plate for 24 hours.

c. *Treatment of SH-SY5Y cells with peptides **4.1**–**4.4**.* After 24 hours, the culture media was removed and replaced with 90 μL of serum-free DMEM:F12 media. A 10-μL aliquot of the working solution of peptides **4.1**–**4.4** was added to each well, for well concentrations of 50 μM and 25 μM. Experiments were run in replicates of five. Five wells were used as controls and received 10-μL aliquots of deionized water (vehicle). Another five wells were left untreated, to be subsequently used as controls with lysis buffer for the LDH release assay. Cells were incubated at 37 °C in a 5% CO_2 atmosphere for 72 hours.

d. *LDH release assay.* After 72 hours, 10 μL of 10x lysis buffer—included with the assay kit—was added to the five untreated wells, and the cells were incubated for an additional 45 min. After 45 min, a 50-μL aliquot of the supernatant media from each well was transferred to a new 96-well plate and 50 μL of LDH substrate solution, prepared according to manufacturer's protocol, was added to each well. The treated plates were stored in the dark for 30 min. The absorbance of each well was measured at 490 and 680 nm (A_{490} and A_{680}). Data were processed by calculating the differential absorbance for each well ($A_{490}-A_{680}$) and comparing those values to those of the lysis buffer controls and the untreated controls:

$$\% \text{ cell death} = [(A_{490}-A_{680})_{\text{compound}} - (A_{490}-A_{680})_{\text{vehicle}}] / [(A_{490}-A_{680})_{\text{lysis}} - (A_{490}-A_{680})_{\text{vehicle}}]$$

Replica exchange molecular dynamics (REMD).

A model of an $A\beta_{12-40}$ barrel-like hexamer was generated by replica-exchange molecular dynamics as follows: Starting coordinates for $A\beta_{12-40}$ were generated from the crystallographic coordinates of peptide **4.2**. Symmetry mates of peptide **4.2** were displayed in PyMOL. Six copies of peptide peptide **4.2** corresponding to the barrel-like hexamer were selected and saved to a new PDB file. The two delta-linked ornithine residues were deleted from each macrocycle. Glu_{22} and Ala_{30} were connected with seven alanine residues in PyMOL. Four alanine residues were added to the *N*-terminus of the β-hairpin, and four alanine residues were added to the *C*-terminus. These added residues were minimized in PyMOL using the clean function, ensuring that the crystallographic coordinates of $A\beta_{16-22}$ and $A\beta_{30-36}$ were not perturbed. After this minimization, each added alanine was mutated to its corresponding wild-type residue from Aβ. The mutated residues were again minimized in PyMOL using the clean function. Each *N*-Me-Phe_{19} was replaced with the wild-type Phe_{19}.

The autopsf plugin in VMD was used to prepare the required files for simulation. The coordinates for $A\beta_{16–22}$ and $A\beta_{30–36}$ were fixed throughout the simulation. REMD simulations were run in NAMD with the CHARMM22 force field and generalized Born implicit solvent (GBIS) on 32 replicas. The temperatures for these replicas varied between 300 and 800K. The simulation was performed for 8.5 ns. Representative coordinates were selected uniformly from the last 7.5 ns of the simulation.

References and Notes

1 These procedures follow closely those that our laboratory has previously published. The procedures in this section are adapted from and in some cases taken verbatim from Kreutzer, A. G.; Hamza, I. L.; Spencer, R. K.; Nowick J. S. *J. Am. Chem. Soc.* **2016**, *138*, 4634–4642, Spencer, R. K.; Kreutzer, A. G.; Salveson, P. J.; Li, H.; Nowick, J. S. *J. Am. Chem. Soc. 137*, **2015**, 6304–6311, Spencer, R. K.; Li. H.; Nowick, J. S. *J. Am. Chem. Soc.* **2014**, *136*, 5595–5598, and Kreutzer, A. G.; Yoo, S.; Spencer, R. K.; Nowick, J. S. *J. Am. Chem, Soc.* **2017**, *139*, 966–975.

2 Bollhagen, R.; Schmiedberger, M.; Barlosb, K.; Grell, E. *J. Chem. Soc., Chem. Commun.* **1994**, 2559–2560.

3 Schägger, H. *Nat. Protoc.* **2006**, *1*, 16–22.

4 Kreutzer, A. G.; Yoo, S.; Spencer, R. K.; Nowick, J. S. *J. Am. Chem, Soc.* **2017**, *139*, 966–975.

5 Simpson, R. J. *CSH Protoc.* **2007**, doi: 10.1101/pdb.prot4727.

6 Emsley, P.; Lohkamp, B.; Scott, W. G.; Cowtan, K. *Acta. Cryst.* **2010**, *D66*, 486–501.

7 Kabsch, W. *Acta Cryst.* **2010**, *D66*, 125–132.

8 Adams, P. D.; Afonine, P. V.; Bunkóczi, G.; Chen, V. B.; Davis, I. W.; Echols, N.; Headd, J. J.; Hung, L.-W.; Kapral, G. J.; Grosse-Kunstleve, R. W.; McCoy, A. J.; Moriarty, N. W.; Oeffner, R.; Read, R. J.; Richardson, D. C.; Richardson, J. S.; Terwilliger, T. C.; Zwart., P. H. *Acta Cryst.* **2010**, *D66*, 213–221.

Characterization Data

*Characterization of peptide **4.1***

Analytical HPLC trace of peptide **4.1**.

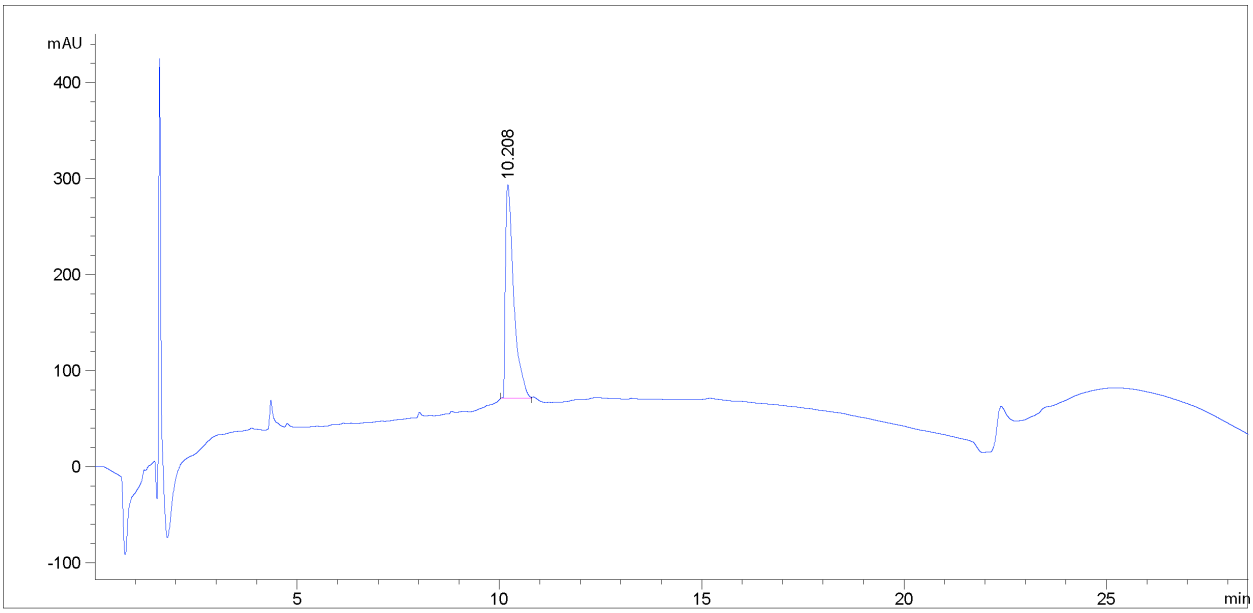

Peak #	RetTime [min]	Type	Width [min]	Area [mAU*s]	Height [mAU]	Area %
1	10.208	MM	0.2374	3173.24780	222.76816	100.0000

High-resolution mass spectrometry of peptide **4.1**.

HRMS (ESI/MeOH) *m/z* calcd for $C_{85}H_{140}N_{19}O_{21}S$ $[M + H]^+$ 1745.0365, found 1745.0377

Mass spectrum and expansions of peptide **4.1**.

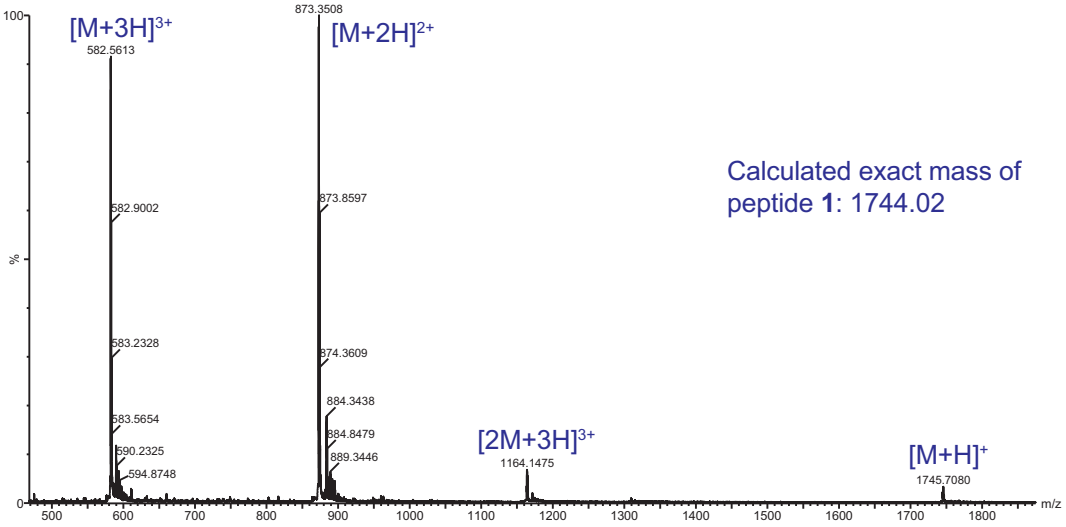

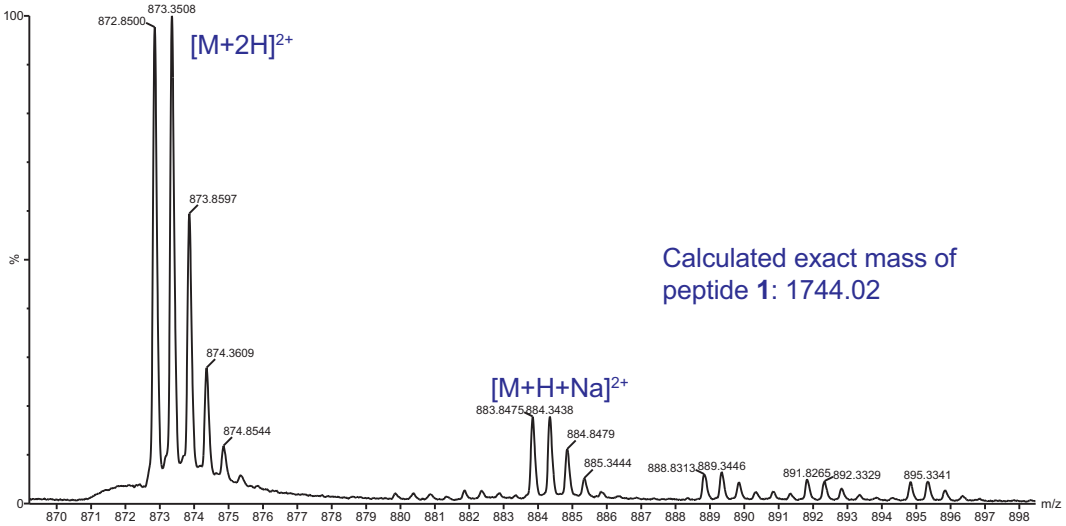

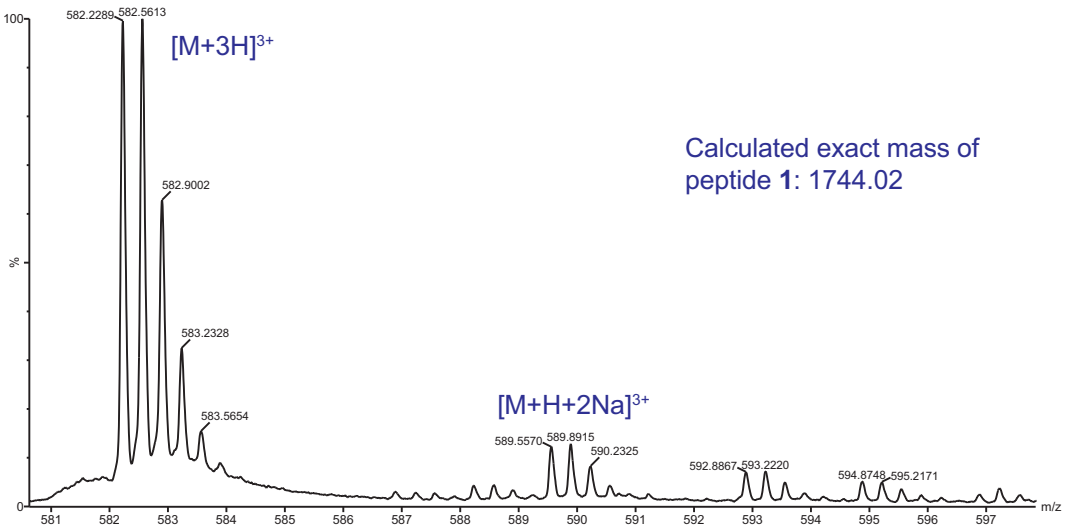
100
%
0
582.2289
582.5613
582.9002
583.2328
583.5654
[M+3H]3+
[M+H+2Na]3+
589.5570
589.8915
590.2325
592.8867
593.2220
594.8748
595.2171
581
582
583
584
585
586
587
588
589
590
591
592
593
594
595
596
597
m/z
Calculated exact mass of
peptide 1: 1744.02

*Characterization of peptide **4.2***

Analytical HPLC trace of peptide **4.2**.

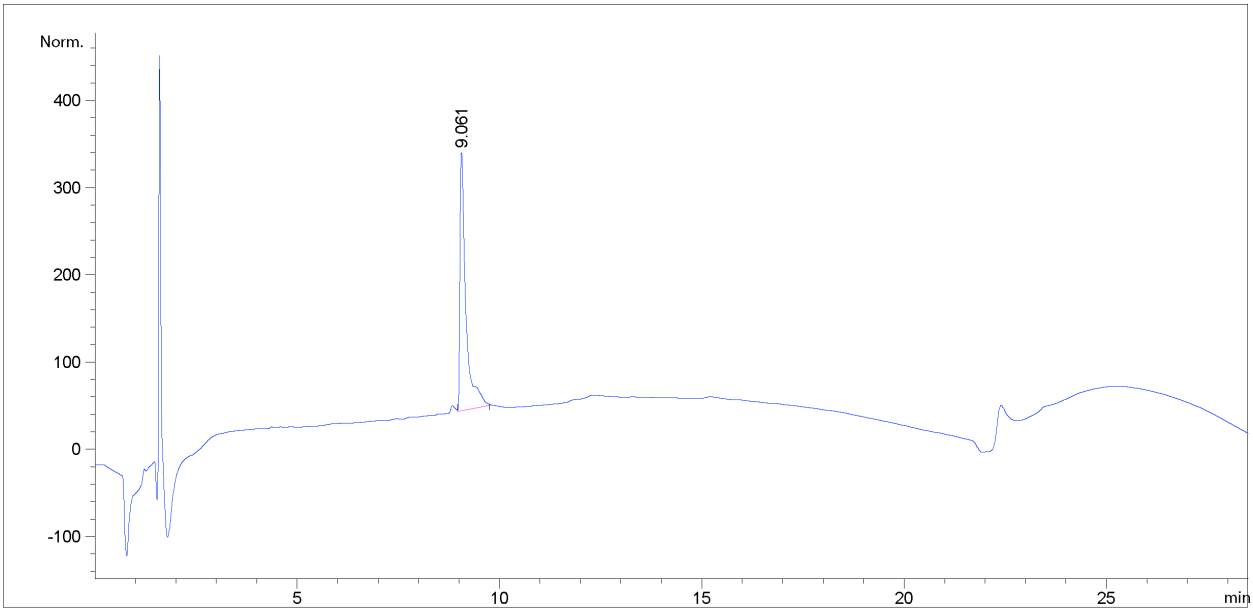

Peak #	RetTime [min]	Type	Width [min]	Area [mAU*s]	Height [mAU]	Area %
1	9.061	MM	0.1679	2686.53735	266.66986	100.0000

High-resolution mass spectrometry of peptide **4.2**.

HRMS (ESI/MeOH) *m/z* calcd for $C_{87}H_{144}N_{19}O_{18}S$ $[M + H]^+$ 1775.0657, found 1775.0638

Mass spectrum and expansions of peptide **4.2**.

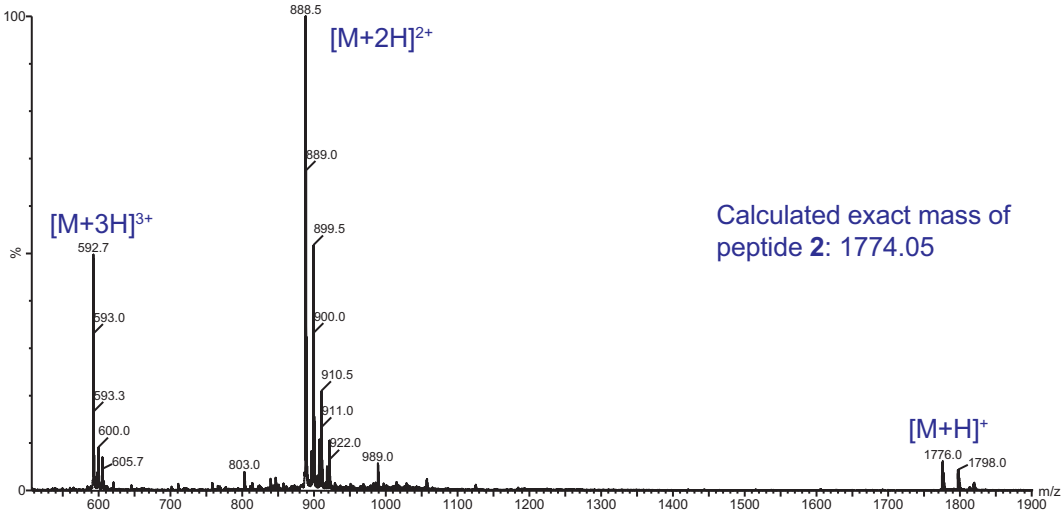

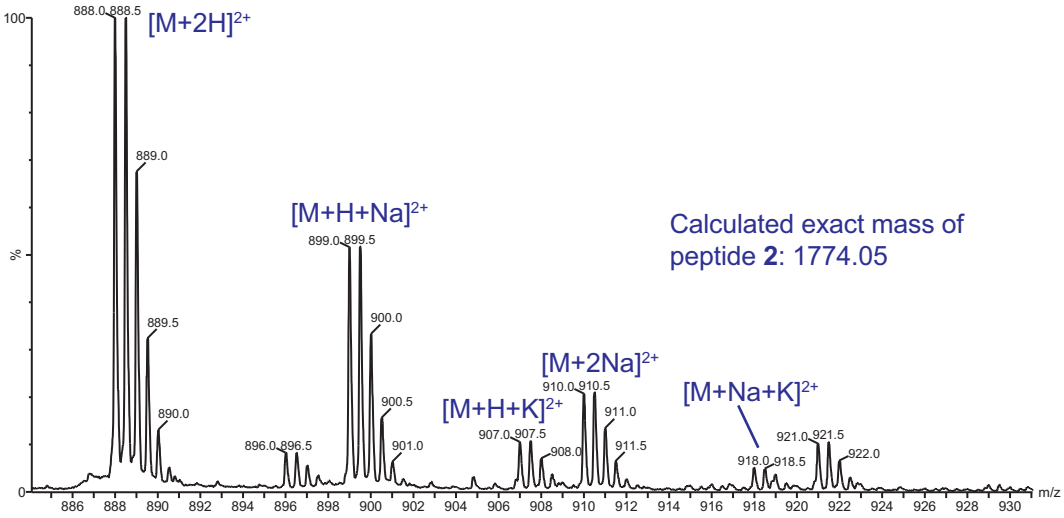

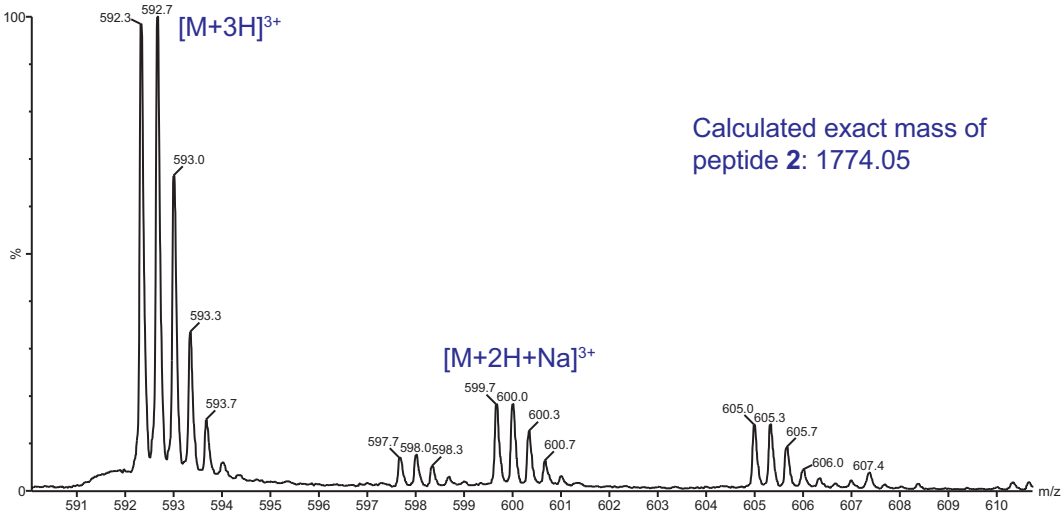

Calculated exact mass of peptide **2**: 1774.05

*Characterization of peptide **4.3***

Analytical HPLC trace of peptide **4.3**.

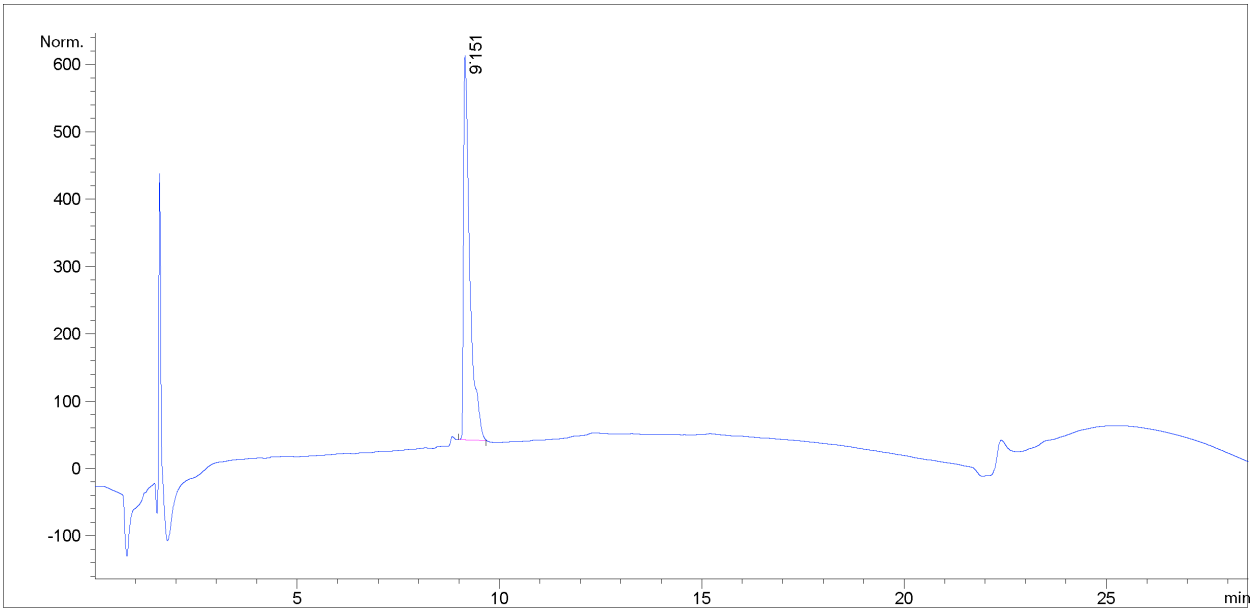

Peak #	RetTime [min]	Type	Width [min]	Area [mAU*s]	Height [mAU]	Area %
1	9.151	MM	0.1788	5522.78467	514.87726	100.0000

High-resolution mass spectrometry of peptide **4.3**.

HRMS (ESI/MeOH) *m/z* calcd for $C_{88}H_{146}N_{19}O_{18}S$ $[M + H]^+$ 1789.0814, found 1789.0822

Mass spectrum and expansions of peptide **4.3**.

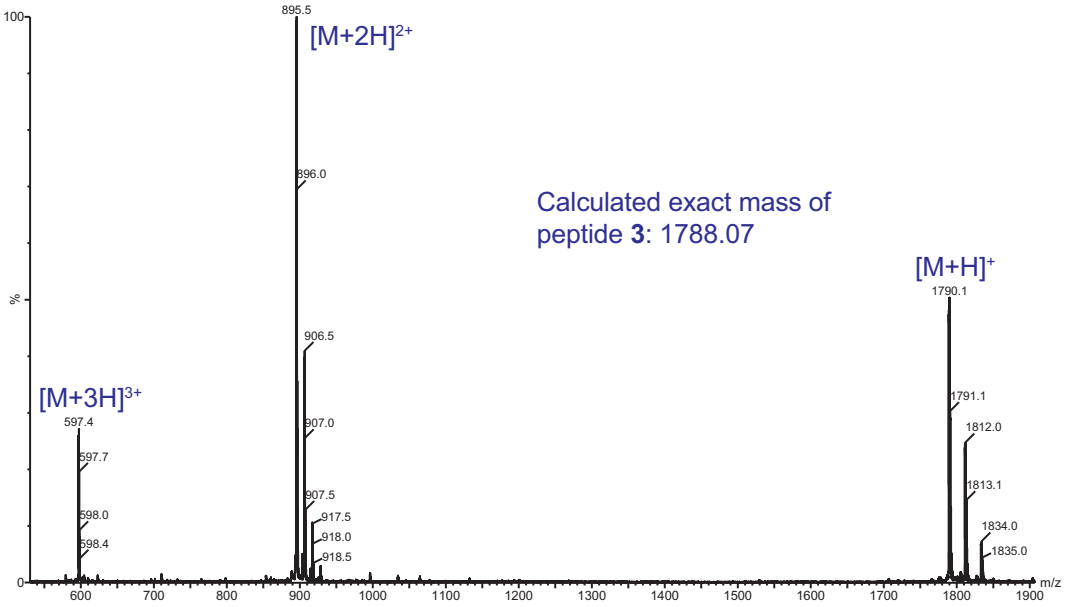

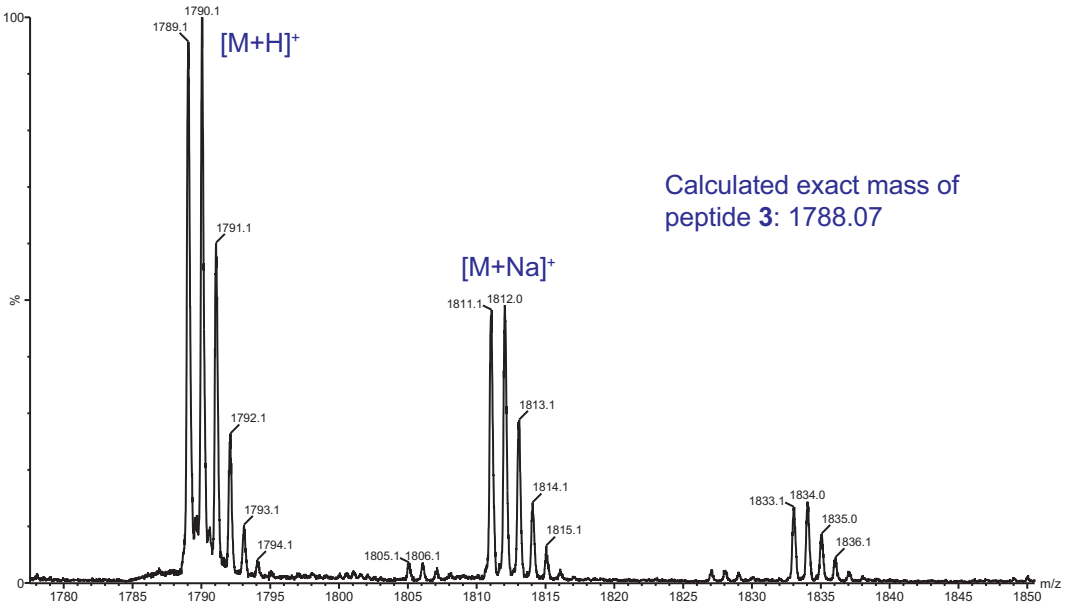

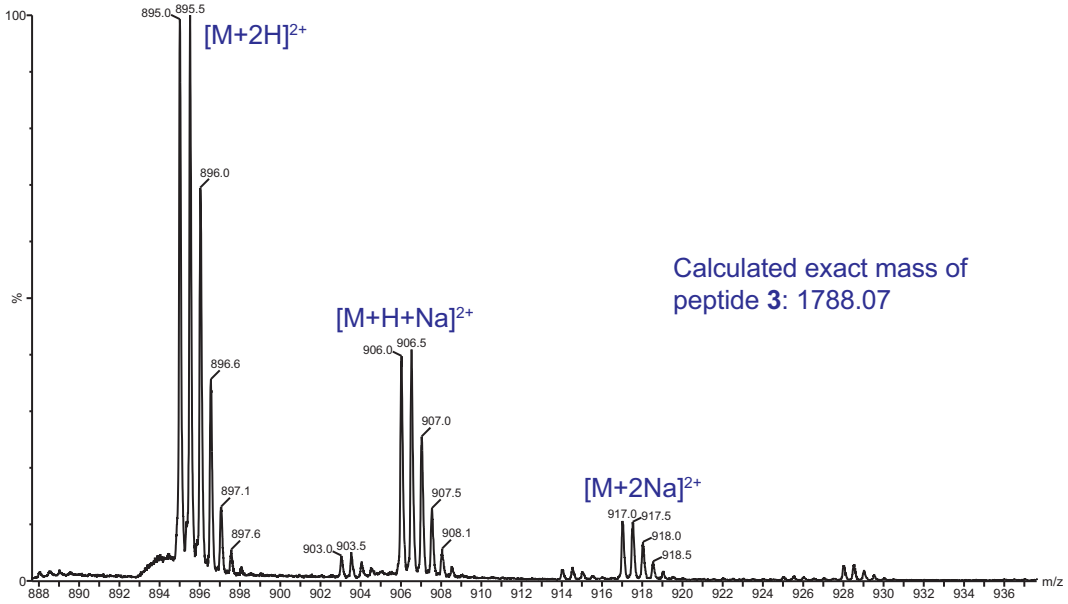

Calculated exact mass of peptide **3**: 1788.07

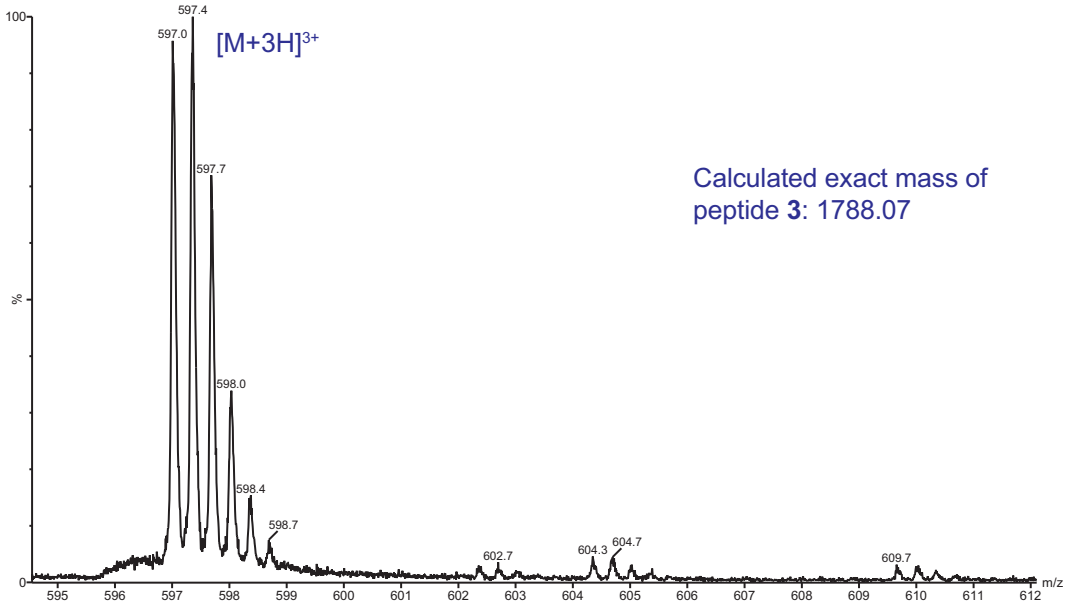

Calculated exact mass of peptide **3**: 1788.07

*Characterization of peptide **4.4***

Analytical HPLC trace of peptide **4.4**.

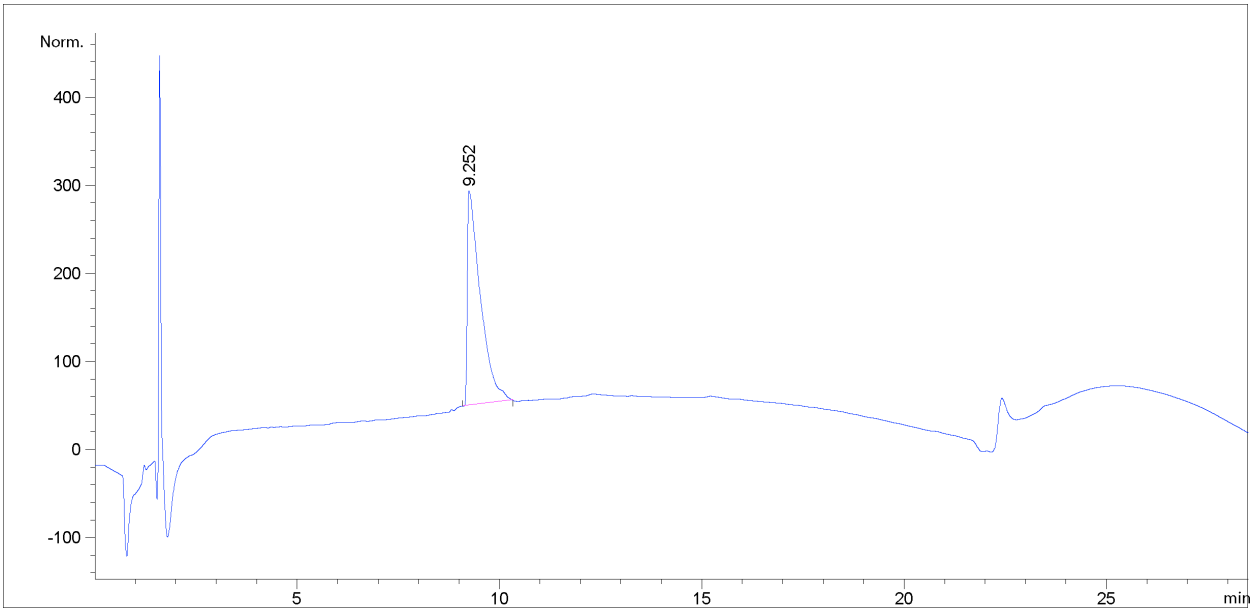

Peak #	RetTime [min]	Type	Width [min]	Area [mAU*s]	Height [mAU]	Area %
1	9.252	MM	0.3742	4923.85791	219.30423	100.0000

High-resolution mass spectrometry of peptide **4.4**.

HRMS (ESI/MeOH) *m/z* calcd for $C_{83}H_{136}N_{19}O_{18}S$ $[M + H]^+$ 1719.0031, found 1719.0042

Mass spectrum and expansions of peptide **4.4**.

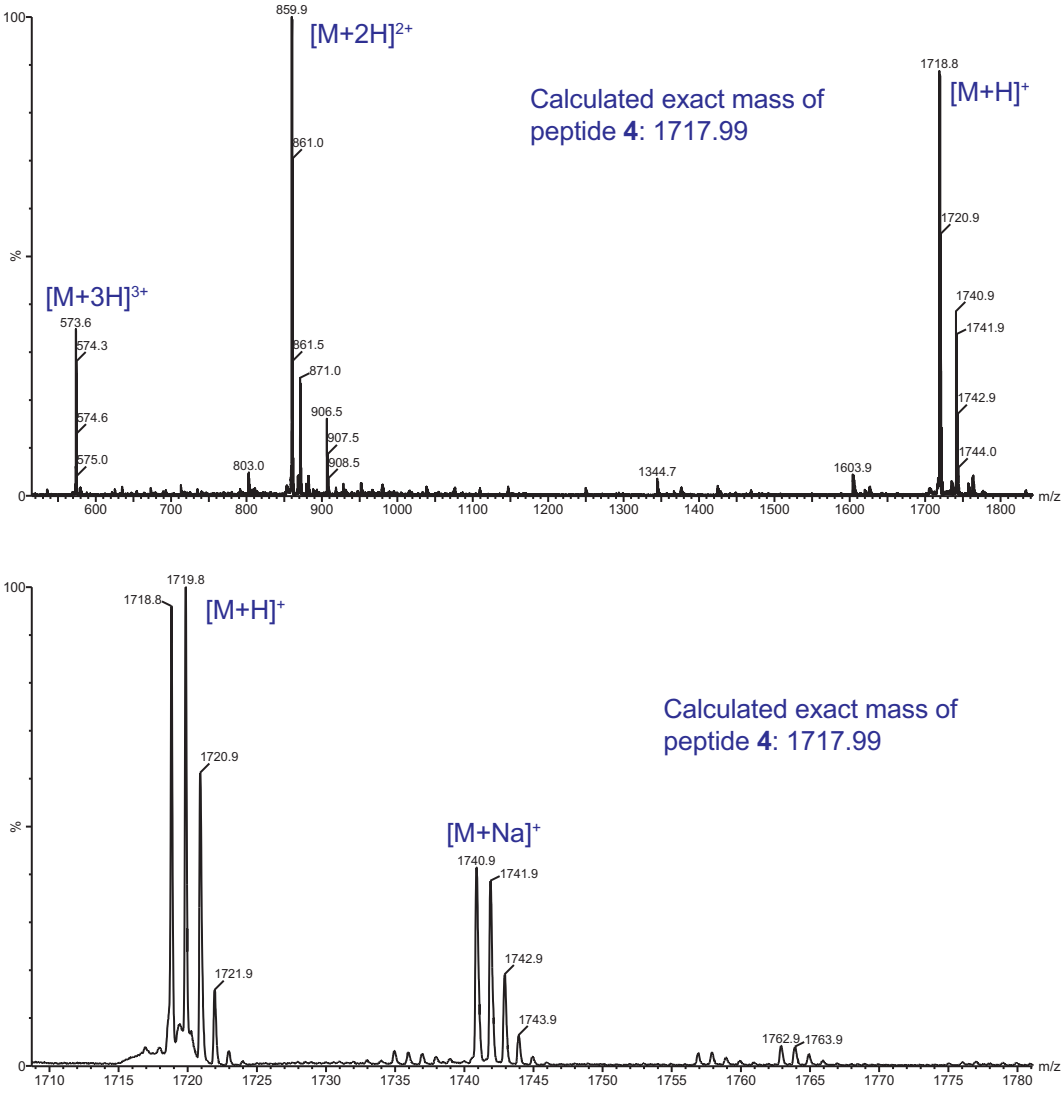

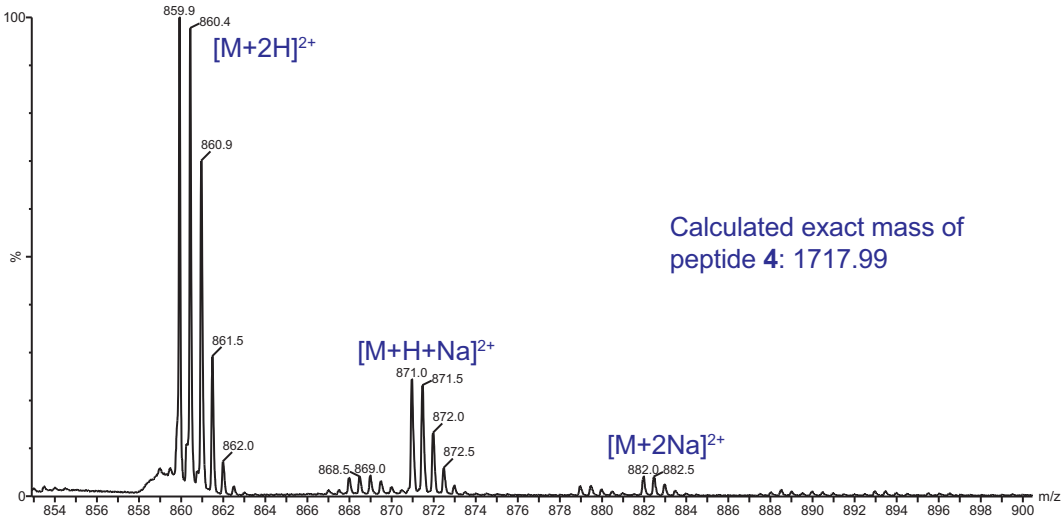
100
%
0
859.9
860.4
[M+2H]2+
860.9
861.5
862.0
[M+H+Na]2+
871.0
871.5
872.0
872.5
868.5
869.0
[M+2Na]2+
882.0
882.5
Calculated exact mass of peptide 4: 1717.99
854 856 858 860 862 864 866 868 870 872 874 876 878 880 882 884 886 888 890 892 894 896 898 900
m/z

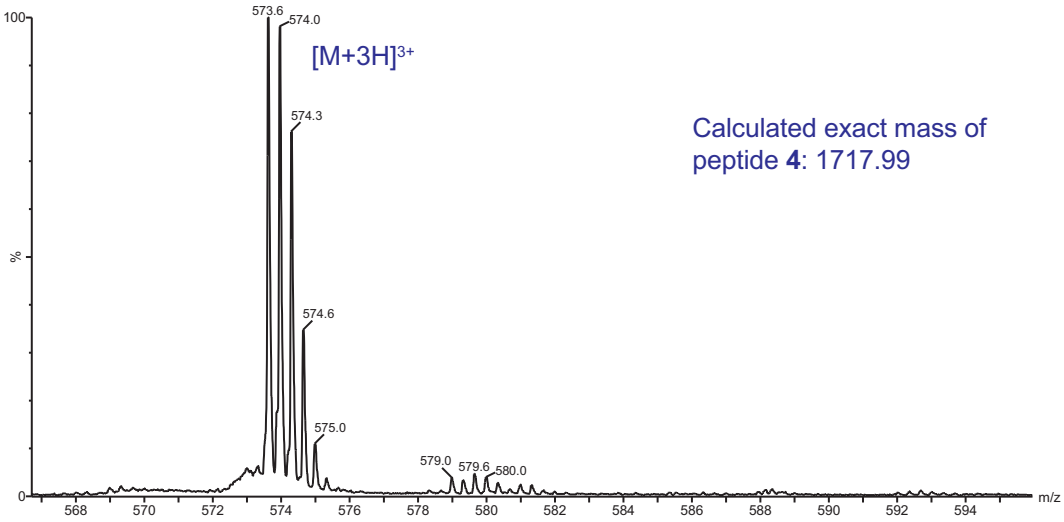
100
%
0
573.6
574.0
[M+3H]3+
574.3
574.6
575.0
579.0
579.6
580.0
Calculated exact mass of peptide 4: 1717.99
568 570 572 574 576 578 580 582 584 586 588 590 592 594
m/z